DE-FG26-07NT43071
Model Predictive Control of Integrated Gasification Combined Cycle Power Plants

Final Report
Reporting Period: January 2007-September 2010

Principal Investigator
B. Wayne Bequette

Graduate Research Associate
Priyadarshi Mahapatra

Department of Chemical and Biological Engineering
Rensselaer Polytechnic Institute

Prepared for:
U.S. Department of Energy
National Energy Technology Laboratory

21 November 2010
Revised 1 February 2011

DISCLAIMER

ABSTRACT

The primary project objectives were to understand how the process design of an integrated gasification combined cycle (IGCC) power plant affects the dynamic operability and controllability of the process. Steady-state and dynamic simulation models were developed to predict the process behavior during typical transients that occur in plant operation. Advanced control strategies were developed to improve the ability of the process to follow changes in the power load demand, and to improve performance during transitions between power levels. Another objective of the proposed work was to educate graduate and undergraduate students in the application of process systems and control to coal technology. Educational materials were developed for use in engineering courses to further broaden this exposure to many students.

ASPENTECH software was used to perform steady-state and dynamic simulations of an IGCC power plant. Linear systems analysis techniques were used to assess the steady-state and dynamic operability of the power plant under various plant operating conditions. Model predictive control (MPC) strategies were developed to improve the dynamic operation of the power plants. MATLAB and SIMULINK software were used for systems analysis and control system design, and the SIMULINK functionality in ASPEN DYNAMICS was used to test the control strategies on the simulated process. Project funds were used to support a Ph.D. student to receive education and training in coal technology and the application of modeling and simulation techniques.

EXECUTIVE SUMMARY

Integrated coal gasification combined cycle (IGCC) power plants have the potential for increased energy efficiency compared with classical coal-fired generating plants, particularly when carbon sequestration is required. An IGCC power plant is an assimilation of operating units or subsections which share characteristics such as tight energy integration, similar process objectives and/or time scales. These subsections closely interact through material and energy flows, which in turn provide a natural hierarchy for high level control structure design. As a first step in this research project, rigorous dynamic process models (implemented in AspenPlus and AspenDynamics software) were developed for individual subsections of the plant; including the Air Separations Unit (ASU), Gasification Island and the Gas Turbine/Compressor (GT) sections. The preliminary "flow-driven" model was extended to a "pressure-driven" simulation model to provide a better understanding of equipment level constraints also able to describe the pressure dynamics responsible for mass-flow fluctuations. The pressure-driven simulation model required that a comprehensive equipment design be performed. It should be noted that most previous IGCC studies have been based on steady-state models, often with only material and energy balances specified, so the detailed equipment design required for our pressure-driven studies represents a substantial contribution to the IGCC model literature.

Initially, simple proportional-integral-derivative (PID) based (single-loop) controllers were implemented for regulating lower-level inventory levels. Later, a multilayer control architecture, where a centralized supervisory layer, based on model predictive control (MPC), keeps track of overall plant performance while coordinating among various subsections, was designed. This is compared and contrasted with a semi-centralized design where each subsection is controlled by a localized MPC strategy where controller pass setpoint information to each other; and a fully decentralized PID controller design where each control loop remains oblivious to the presence of other loops.

The double-column cryogenic ASU is given significant focus in this work due to large operating costs and dynamically slower process time scales. In addition, large material interactions with the gasifier and GT sections and condenser-reboiler heat integration within the system, makes this process both interesting and challenging to control. A rigorous study involving many possible steady-state design configurations within a single flowsheet using optimization and sensitivity tools is presented. Different process flowsheets corresponding to IGCC and non-IGCC scenarios are studied and compared in terms of structural design, energy requirements and process controllability. A rigorous heat-exchanger design is incorporated into the model to study the effect of thermal lags and wrong-way (inverse response) temperature effects due to feed-effuent heat exchange. Further, a model predictive control strategy that handles rate-of-change constraints imposed by the process design of the air separation unit has been studied and compared with performance using decentralized classical PID schemes.

While the research in this report makes significant contributions to both dynamic modeling and advanced control implementation for IGCC power plants, there remain open research issues in this field that suggested for further study, including: (i) temperature-based control of the ASU, (ii) controller design for IGCC power plants with co-production of hydrogen and external steam, (iii) multiple model predictive control for operation over a wider-range of operating conditions, including plant startup and shutdown.

CONTENTS

LIST OF TABLES

LIST OF FIGURES

CHAPTER 1
INTRODUCTION

In recent years, integrated gasification combined cycle (IGCC) technology has attracted significant attention due to demonstrated reliability, higher efficiency, greater fuel and product flexibility as well as ability to meet requirements for future CO_2 trading and stringent environmental regulations (e.g. NO_x, SO_2 and mercury emissions) compared to pulverized coal combustion power plants. Increased and fluctuating demand of electricity from coal-based power plants requires optimal operation and better utilization of raw materials (coal, water) and energy, where the key issue is to achieve these objectives without the need of major capital investments. It is well understood that an efficient plantwide control structure can cope with most of the needs for optimal operation. In practice, the problem is usually solved in situ, based on experience and engineering insight, without the use of existing theoretical tools. Most of the base-case power plants operate continuously at maximum output (economically optimized), until a plant shutdown is needed to perform maintenance. In the future vision of the grid-connected system, an IGCC plant may be expected to have a load following response and/or co-production of hydrogen/chemicals depending on market economics/demands. The control strategy needs to be well suited so that a change in this demand can be met without sacrificing the plant efficiency and without violating the environmental limits. The purpose of this technical report, is to explore applicability of advanced control to these plants.

1.1 Background

As a foundation for conducting research, it is important to first understand the current "state of the art" in IGCC technology and its individual subunit operations. In addition, up to date research efforts on plantwide control theory including dynamic modeling and simulation efforts have to be reviewed. A detailed literature survey is conducted to determine what research is already done and published, and even more importantly, what gaps and voids exist in the open literature.

1.1.1 Integrated Gasification Combined Cycle Overview

In a world with a rapidly expanding appetite for energy and rising concentrations of greenhouse gases, the use of coal as a primary energy source engenders both heightened interest and concern. Coal is the most abundant and least expensive fossil fuel, but also the most carbon intensive. In 2003, coal-fired plants accounted for 53% of electricity generation in the United States, while nuclear accounted for 21%, natural gas 15%, hydroelectricity 7%, oil 3%, geothermal and "other" 1% [1]. With coal likely to remain the primary fuel for the nation's electric power supply for the foreseeable future, there is need for further development of clean coal technology [2]. Coal gasification is a promising clean coal technology used in producing coal gas and recently used in Integrated Gasification Combined Cycle (IGCC) for power generation. IGCC is an innovative power generation technology combining with coal gasification and gas turbine combined cycle. At present, conventional coal-fired power generation technology is the pulverized coal (PC) power plant.

An IGCC system includes several major components: gasification island, gas cleanup, gas turbine combined cycle, and, in most cases, an air separation unit (ASU). In an IGCC system, coal or other fuels is partially oxidation in a gasifier to produce syngas, which is combusted and expanded in a gas turbine to produce power. The heat from exhaust gas is recovered in a heat recovery steam generator (HRSG) to produce steam, which is expanded in a steam turbine to produce additional power (hence the term "combined cycle"). In a conventional PC plant, pulverized coal is combusted in a boiler and the combustion heat is transferred to produce high pressure steam, which is expanded in a steam turbine to produce power. Advantages of IGCC systems over conventional pulverized coal (PC) power generation include higher thermal efficiency, lower emissions of key pollutants, and greater fuel flexibility [3, 4, 5, 6, 7].

Although there are many environmental and performance benefits associated with application of IGCC technology, the commercialization of IGCC is still in an early phase and actual technical data and experiences are limited. A potential disadvantage of IGCC that impedes more widespread use is capital cost and also the perception that IGCC plants are more like chemical process plants than the

conventional power plants. As a technology in an early phase of development, IGCC plants generally are not cost competitive and typically are subsidized as part of demonstration programs [8].

As additional development of IGCC systems occur, the capital cost and operation cost are expected to decrease. Therefore, additional research, development, and demonstration (RD&D) is required to identify and evaluate advances in IGCC technology, identify priorities for improvements in IGCC systems over the next decade, provide risk analysis for technology advances, and provide input to decision making regarding selection of technology options in this area. The risks associated with IGCC technology include the technical or cost risks, such as low efficiency, high emissions, and high cost, caused by the uncertainty in process parameters.

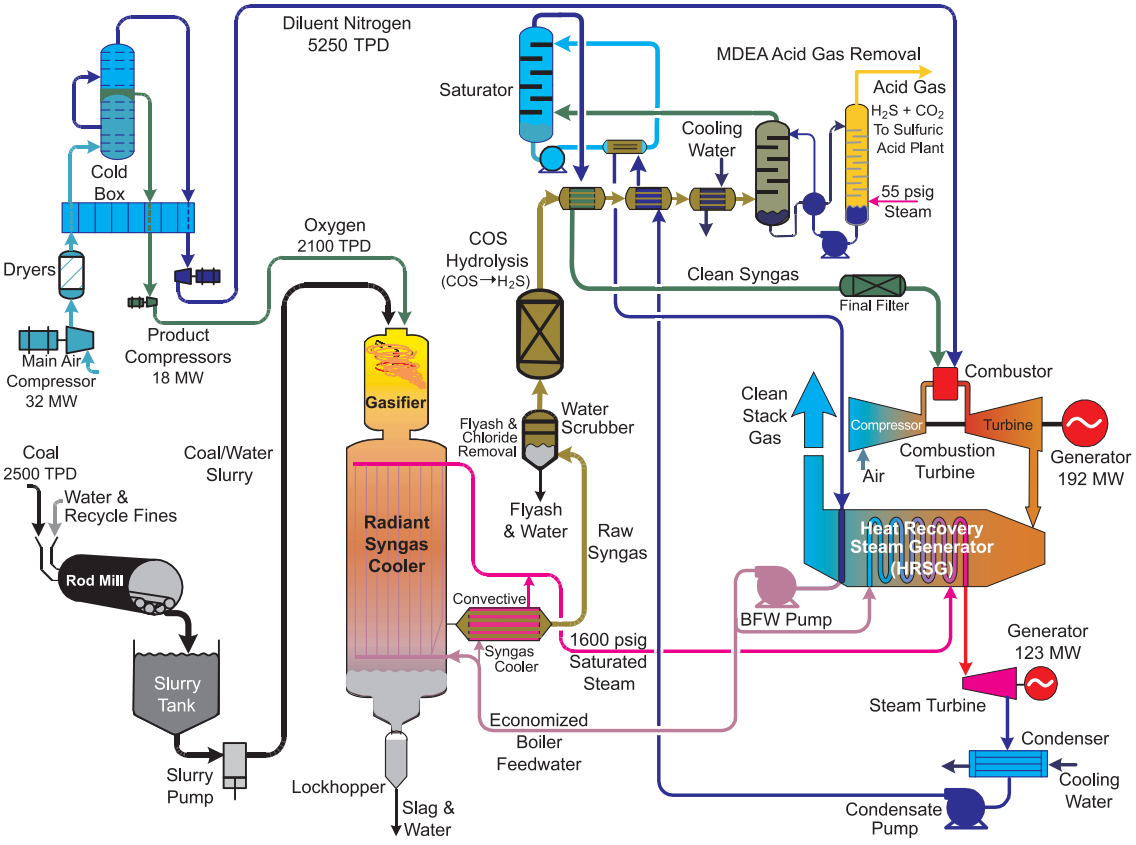

Figure 1.1: Schematic of a typical IGCC power plant [9].

At present, the potential improvements of IGCC technology have taken place in the main components of IGCC systems, including advances in gas turbine combined cycle and integration of different components. The risks associated with advance-

ment in technology need to be evaluated. Therefore, research is required to provide guidelines for improvements in IGCC systems over next decades. Specific areas in which additional progress is needed with regard to IGCC system RD&D include: (a) evaluation of the implications of the use of alternative feedstocks with regard to priorities for system operation; (b) assessment of implications of alternative gas turbine designs on system feasibility; (c) evaluation of the risks associated with performance, emissions, and costs of IGCC technology due to lack of knowledge of technical parameters (d) evaluation the implications of different integration methods between ASU and gas turbine for IGCC system performance. The justification for these specific focus areas is further described in later sections of this chapter.

The first modern IGCC plant began producing electricity in 1984 [10]. Today, several IGCC plants have been constructed for producing power from coal, residual oil, and other low or negative value feedstocks [11]. IGCC systems are an advanced power generation technology with fuel flexibility. In addition to power, IGCC system also can produce steam and hydrogen and other coproducts [11]. Generally, sulfur is produced as a marketable byproduct in an IGCC system. A conceptual diagram of an IGCC system is given in Figure 1.1. In a gasification process, coal or other feedstocks are reacted with a high purity oxidant and steam to produce a syngas rich in carbon monoxide (CO) and hydrogen (H_2). The high purity oxidant is produced in an ASU. The syngas flows through cooling and cleaning steps prior to combustion in a gas turbine combined cycle system. In the combined cycle, the syngas reacts with the compressed air from the compressor. The combustion product is expanded in the turbine and shaft work is produced. The heat from the gas turbine exhaust is used to make steam in a HRSG. The steam is expanded in a steam turbine. Electricity is generated both by the gas turbine and a steam turbine. In the following sections, the details of the technologies used in main components of an IGCC are introduced, including gasification, gas turbine combined cycle, and air separation unit.

1.1.1.1 Gasification Technology

Gasification is a process that produces syngas containing hydrogen and carbon monoxide from coal or other carbonaceous feedstocks. High purity oxidant is fed into

gasifier to partially oxidize fuels. Water or steam is used as a source of hydrolysis in the reactions. Three kinds of gasification technology are generally applied in IGCC systems, including moving-bed, fluidized-bed, and entrained-flow gasifiers.

In a *countercurrent gasifier*, the oxygen and steam are introduced in the lower part of the gasifier and flow vertically upward, while fuel is introduced at the top of the gasifier and flows downward. The fuel is heated as it descends, which drives off the lower molecular weight and more volatile compounds in the fuel. The portions of fuel that reach the bottom of the gasifier are combusted to heat the sygnas that are flowing upward through the gasifier. The heat from the combustion zone provides thermal energy to the endothermic gasification reactions that occur in the middle portion of the gasifier. The generated syngas ascends in a counter-current flow to the fuel. As the hot gas moves upward and contacts the cooler fuel, a relatively large amount of gaseous methane is produced at the low temperature at the top of the gasifier. The outlet temperature of this kind of gasifier is lower than other two kinds of gasifiers. Because of the efficient heat transfer in a counter-current flow method, the oxygen requirement for efficient utilization of fuel is lower than alternative gasifiers [12]. This gasifier is suitable for gasification of large particles of approximately 4 mm to 30 mm due to the feature of countercurrent flow. A typical outlet temperature of the gasifier is about 1,100°F [12]. At this temperature, heavy hydrocarbon compounds, such as tars and oils, will not be cracked. These compounds can condense in the syngas cooling process. Thus, these types of gasifiers typically are associated with the need for a downstream process condensate treatment process.

In a *fluidized-bed gasifier*, the fuel, oxidant or air, and steam are mixed and introduced into the bottom of the gasifier. The reaction bed is fluidized as the fuel gas flow rate increases, in which particles are suspended in a stream of flowing gases. The fuel particles are gasified in the central zone of the gasifier. The ash and char particles flow with the raw gas out of the gasifier and are captured by a cyclone and recycled. The fluidized bed is operated at a nearly constant temperature of 1800°F. This is higher than the operation temperature of BGL gasifier and thus the formation of tars is avoided [13]. Once heated, ash particles in the bed tend to

stick together and agglomerate. The agglomerated ash falls to the bottom of the gasifier where it is cooled by recycled syngas and removed from the reactor. The fluidized bed is suitable for fuel particles in a size range of 0.1 mm to 10 mm. It is restricted to reactive, non-caking fuels for uniform backmixing of fuel and syngas and gasification of the char entering the ash zone. A typical example for fluidized bed gasifier is Kellogg Rust Westinghouse (KRW) gasifier. An air-blown KRW gasifier is used in Pinon Pine IGCC project [13].

The *entrained-flow gasifier* features a plug type reactor and is suitable for gasification of fine fuel particles less than 0.1 mm in diameter. Entrained-flow gasifiers use oxygen as the oxidant and operate at high temperatures well above ash slagging conditions in order to assure reasonable carbon conversion and to provide a mechanism for ash removal [14]. The gasification temperature is above 2300°F. At such a high temperature, low amount of methane is produced and no other hydrocarbon is found in the syngas. The product is a syngas rich in CO and H_2. The entrained-flow gasifier has advantages over other alternative gasifiers in that almost all types of coals can be gasified regardless of coal rank, caking characteristics, and amount of coal fines. The high gasification temperature makes it easy to gasify less reactive fuels that are not efficiently gasified in lower temperature counter-current or fluidized-bed gasifers. Due to the high temperature, the consumption of oxygen during partial combustion in this kind of gasifier is higher than for other gasifiers. A typical example of an entrained-flow gasifier is the Texaco Gasification Process (TGP), now called the GE-Texaco process. The TGP uses coal in a water slurry as the feedstock, in which the water acts as a heat moderator. The TGP gasifier has higher operation pressure than other types of entrained flow gasifiers, which leads to higher syngas production capacity of a gasifier of a given size [14]. The TGP is more widely used than other types of gasifiers for gasification of various fuels, including less reactive feedstocks due to high temperature and high pressure [11]. The TGP is used for conversion of heavy oils, petroleum coke, biomass, and even hazardous wastes, to products including power, steam, hydrogen, ammonia or other chemicals [15, 14].

There are three high-temperature cooling methods used in IGCC system, in-

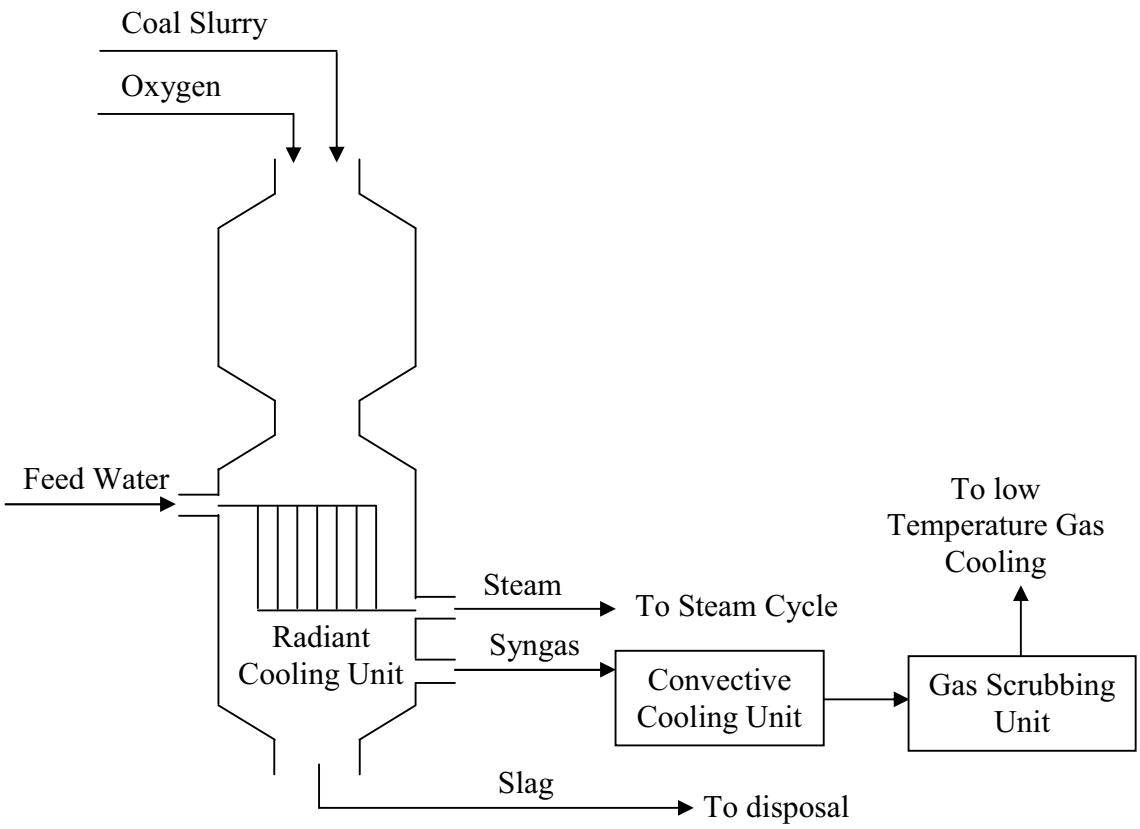

Figure 1.2: Simplified Schematic of a Texaco Gasification Process

cluding radiant and convective cooling design, radiant only design, and total quench design. The IGCC system with radiant and convective cooling design generally has higher efficiency than the IGCC plants with total quench design [16] and radiant only design [17]. Therefore, in this report, the radiant and convective cooling design is selected and simulated. From the reaction chamber of Texaco gasifier, the raw syngas and molten slag flow into the radiant cooling chamber, where the gas is cooled to 1500°F (Figure 1.2). The high temperature steam is generated by the heat recovery from sygnas cooling. The molten ash drops into the water quench pool at the bottom of the radiant cooler. It is cooled and removed. The raw gas is further cooled in the convective cooling unit. The syngas leaves the convective cooler at about 650°F. The raw gas is scrubbed of particulates with recycled process condensate and makeup water and routed to the ammonia separation unit. Virtually all ammonia in the syngas is absorbed into the process water. The scrubbed gas flows to the low-temperature gas cooling unit [17].

The scrubbed syngas flows through various heat exchangers in the low temperature gas cooling process. The syngas is first cooled by heating the circulating saturator water. The syngas is further cooled by exchanging heat to condensate and makeup water. The raw gas is cooled to 105°F in a trim cooled against cooling water. The heat removed from the syngas is recovered to produce low pressure steam by heating condensate and makeup water heat feed water or as a source of heat for fuel gas saturation [17]. The cooled syngas is sent to the shift convertors.

1.1.1.2 Syngas Cleanup and Saturation (Water-Gas Shift, Acid Gas Removal, Sulfur Recovery and Syngas Saturation)

Depending on the amount of carbon-capture and sequestration (CCS) required, the syngas processing may or may not involve shift converters. The Shift reactor converts most of the CO to CO_2 at high pressure using the Water Gas Shift (WGS) reaction.

$$CO + H_2O \rightleftharpoons CO_2 + H_2$$

This reaction is carried out in two stages, stage one a high temperature shift and stage two a low temperature shift. The reaction being slightly exothermic, the heat of reaction is given to intermediate pressure (IP) steam and boiler feed water (BFW). The CO_2 can be extracted/removed by contacting it with amine-based or DEPG (dimethyl ether of polyethelene glycol) solvents, which can selectively remove CO_2 and H_2S from syngas.

The sulfur components in syngas are removed in a Selexol process. In this process, the syngas from the low temperature gas cooling unit flows through an acid gas absorber and is contacted with the Selexol solvent. Most of the hydrogen sulfide (H_2S) is absorbed by the Selexol solvent, typically with 95 to 98 percent removal efficiency. About one-third of carbonyl sulfide and some of carbon dioxide are absorbed producing a low sulfur fuel gas. This solvent has a high molecular weight, high boiling point and can be used at ambient temperatures. The absorbed H_2S, COS, and CO_2 are stripped from the Selexol solvent to form the acid gas. The acid gas is sent to the Claus sulfur plant for element sulfur recovery [18].

In the Claus unit, the acid gas is combusted in a sulfur furnace. The combus-

tion product is sent to a converter to produce elemental sulfur. The tail gas from the Claus process is further treated in a Beavon-Stretford plant. The H_2S is converted to elemental sulfur in the Stretford process. The sulfur is separated, washed, and melted to form a molten sulfur product [17].

The fuel gas from the Selexol unit is saturated with hot water before it enters the gas turbine. The introduction of water is to control the formation of thermal NO_x because the water vapor lowers the peak flame temperatures. The formation of NO_x from nitrogen and oxygen in the inlet air is highly temperature sensitive. Lowering the peak temperature can decrease the formation of the thermal NO_x and hence, lower the NO_x emissions [17]. The fuel gas is saturated in an adiabatic saturator vessel. The hot water at a temperature higher than the syngas is sprayed from the top of the vessel. The saturated gas is heated to a temperature of about 350°F and exits from the saturator from the top of the vessel while the hot water exits from the bottom of the vessel. The heat needed for heating the water is transferred from low temperature gas cooling units and the heat recovery steam generators to the fuel gas saturation unit. The saturated gas is heated by the hot water from HRSG and then fed into the gas turbine combustor [17].

1.1.1.3 Gas Turbine/Compressor

Gas turbines have been widely used for power generation. A typical simple cycle natural gas-fired gas turbine has an efficiency of 35% or greater [19]. Most new power plants also use a heat recovery steam generator (HRSG) and steam turbine in addition to a gas turbine, which is a combined cycle system [20]. In a combined cycle system, the waste heat in the exhaust gas is recovered to generate high temperature steam for a steam turbine [21, 22, 23].

In Figure 1.3, a conceptual diagram of a simple cycle is illustrated. In a simple cycle gas turbine, air enters a compressor. The syngas produced from the gasifier or natural gas is sent to the combustor of a gas turbine. The syngas is combusted with the compressed air. The high pressure hot product gases from the combustor enters the turbine, or expander. In the turbine, the gases are expanded and reduced in pressure, resulting in a corresponding reduction in temperature. The expansion

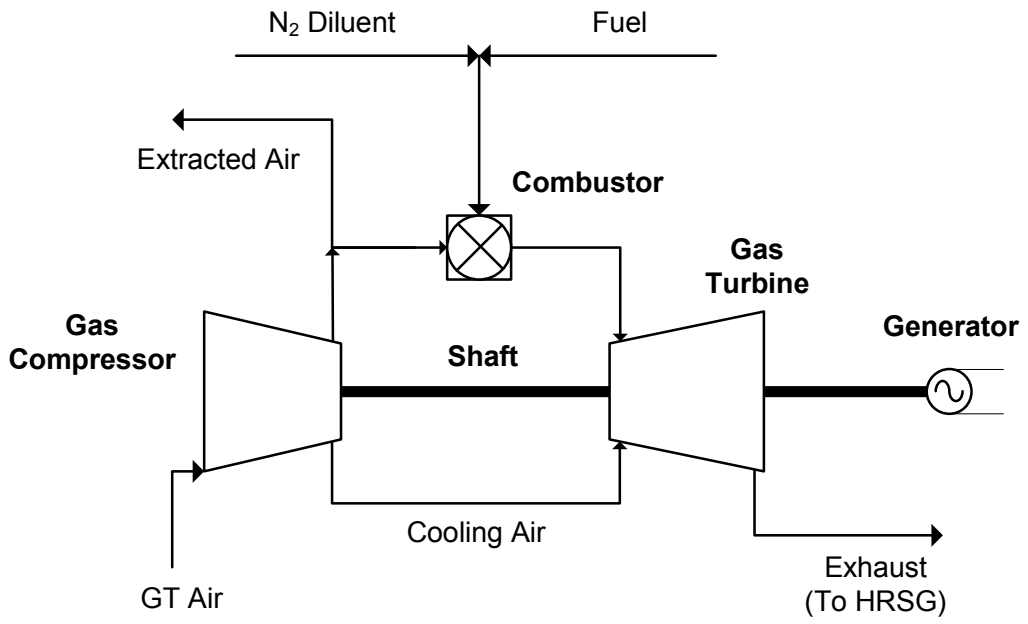

Figure 1.3: Simplified schematic of a Gas Turbine-Compressor unit

and cooling of the hot gases in the turbine results in an energy conversion from the heat of the hot product gases to shaft work and electricity is produced.

Technological advances in gas turbines provide the potential to further improve the efficiency of the overall IGCC system and decrease the cost of electricity. The heavy duty "Frame 7F" design represents current state-of-practice, which has been used in the Tampa IGCC plant and Wabash river IGCC project [24, 9]. The newest steam-cooled "7H" gas turbine is the most advanced recently introduced commercial gas turbine [23]. The Frame 7H gas turbine uses steam rather than air cooling for the hot gas path, thereby enabling higher firing temperatures and efficiency. One of the most referenced mathematical model of gas-turbine is given by Rowen for heavy-duty gas turbines [25] and single shaft gas turbines in mechanical drive service [26].

1.1.1.4 Air Separation Unit

There are three methods used for air separation at present, which are cryogenic separation, pressure swing absorption (PSA) and polymeric membranes [27, 28]. The cryogenic separation technology is the most mature and widely used for medium and very large oxygen production requirements with high purity. It is capable of producing oxygen of purity higher than 99.5% and production ranging from 600

tons per day to over 8000 tons per day [28]. Thus cryogenic separation technology is typically the basis for air separation in IGCC systems.

The PSA is suitable for oxygen production less than 40 tons per day of high purity (about 90%) oxygen in the product gas [27]. The polymeric membrane is not applicable for supplying oxygen to power plants for low oxygen purity, which is less than 50% [28]. Thus, the two technologies are not suitable for used in large IGCC systems.

An emerging breakthrough air separation technology is Oxygen Transport Membrane (OTM). OTM features high operation temperature and thus could enable efficient integration with IGCC. The results of a design study indicate that an IGCC system with OTM would have lower cost and higher efficiency than one with cryogenic air separation. However, commercialization of OTM is not yet realized. A precommercial demonstration was expected to be finished in 2007 [29] Therefore, the cryogenic ASU is still the predominant technology option for air separation applications in IGCC systems.

A cryogenic ASU mainly consists of an air compression system, cryogenic separation units, and an oxygen compression system. Cryogenic ASU designs can be classified into low pressure (LP) and elevated pressure (EP). The LP ASU has a lower cryogenic unit pressure than the EP ASU [30, 31, 32]. The pressure level affects the power consumption of the air compressor, oxygen compressor, and nitrogen compressor. In turn, power consumption of the ASU affects the performance of IGCC system since the ASU is the IGCC process area that typically has the largest auxiliary power consumption [33]. Therefore, selecting a suitable ASU design is important for optimal operation of IGCC systems. A substantial portion of my current work is based on ASU, especially in regards to IGCC plant, and hence detailed description of relevant process units are given in later chapters.

1.1.1.5 Heat Recovery Steam Generator

In most IGCC systems, a Heat Recovery Steam Generator (HRSG) and a steam cycle are combined with a simple cycle gas turbine to form a gas turbine combined cycle (CC). In a combined cycle, the hot exhaust gas is further cooled in

the HRSG. The heat is recovered by producing high temperature and high pressure steam. The steam is expanded in a steam turbine to produce shaft work, which is converted into electricity in a generator. Typically, the steam cycle will have several different pressure levels and the steam turbine will have several corresponding stages (Figure 1.4). A portion of steam may be diverted to the gasifier. Furthermore, some steam may be generated by heat recovered from cooling of hot syngas that exits the gasifier. Thus, there is typically some degree of integration between the steam cycle and other components of an IGCC plant.

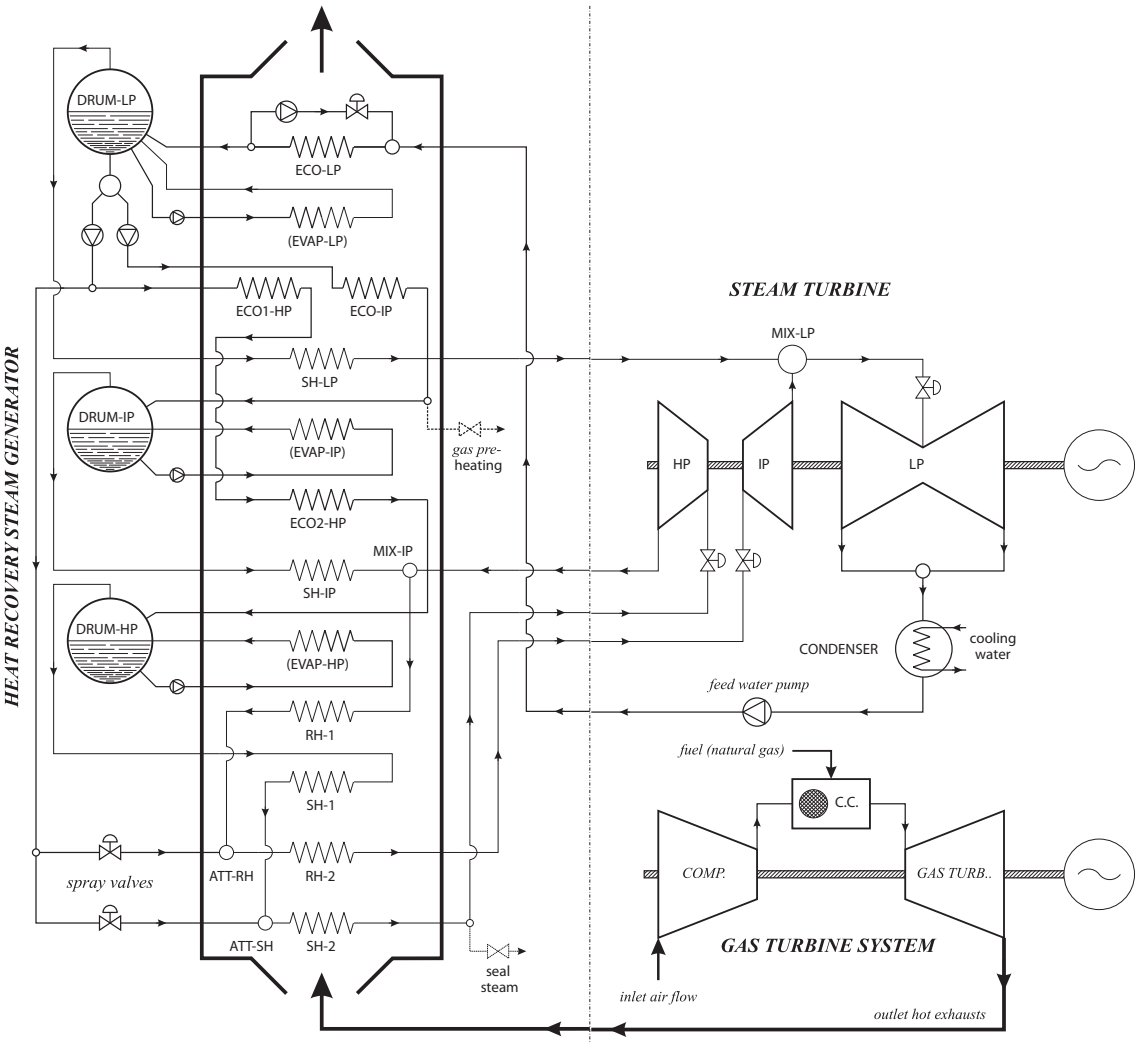

Figure 1.4: Detailed schematic of Combined Cycle and Heat Recovery Units [34]

Since HRSG has been associated with almost every combined cycle power plant

(CCPP) in the world today which involves some form of Rankine Cycle, the modeling and control studies date back to early twentieth century. Some of the recent literature involving dynamic modeling and advanced process control are given here, which serves as the basis for IGCC's HRSG study in this work. A multivariable feedwater control design for drum water-level regulation in a HRSG based on projective output feedback scheme was presented by Younkins and Chow (1988) [35]; the primary design objective being the minimization of drum blowdowns during start-ups. A generalized and simplified model was given by IEEE System Dynamic Performance Subcommittee [36] for a typical steam configuration and gas turbine control system characteristics and response. In addition, a practical expedient model of HRSG and steam turbine was provided which simplified the physics based on lags due to metal heat capacitance and boiler storage time constants. A detailed simulation model of advanced combined cycle with particular application to optimum operation support and start-up scheduling are given by Akiyama et al. [37]. They used an inverse problem approach method and dynamic simulation tool (FODES) for the development and validation of the study. Another study [38] presents a mathematical dynamic model of a combined cycle plant suitable for use in power system stability studies. The model incorporates PID controllers for governor-gas turbine system, speed, temperature and inlet guide vane (IGV) control to improve system dynamic performance. In addition, the models were tested and validated on a simple two-area power system. A group at Delft University [39] used a novel software, SimECS, to model steam cycle of power plants, validated using lab-scale steam cycle setup. The second part of their work [40] describes the development, implementation and validation of the dynamic model (using various small step and ramp disturbances in flue gas mass flow and pump rotational speed) for a small simple Rankine cycle system in a biomass-fired power plant. The model is developed using the same software, implementing physics based equations and some empirical correlations. The authors intend to relate the model to the design of an actual power plant including small biomass fired steam power plants, organic Rankine cycle turbines, large scale steam and combined power plants, co- and trigeneration systems and refrigeration plants.

A study describing specific problem of CCPP control dynamics was given in [41], where various investigations concerning cyclic duty start-ups and operations under grid power and frequency control was conducted. Although not exhaustive, this study gives a good introduction to different transients commonly occurring in a complex CCPP, especially highlighting different transients between a single and a double shafted plant. Nonlinear model predictive control (NMPC) and supervisory/dynamic control optimization studies have been given in [34, 42]. These studies use first principle CCPP models in MATLAB/Simulink which were tuned to mimic a true installation in northern Italy and results of a highly detailed simulator (of the same plant). The main focus of the study was to improve frequency regulation using various methods such as energy storage exploitation and use of HP turbine bypass system. A mathematical model of CCGT (most of the work based on [25, 26, 36, 38]) has been given by [43], to study its response following a frequency disturbance. The study then integrates this into a larger model, representative of the Irish electricity system, and the effects of increasing proportions/load of CCGT generation are examined. In another study [44], the modeling and short-term scheduling optimization in CCPPs is accomplished by exploiting hybrid systems using a mixed logic dynamical (MLD) systems framework. It has also been shown in this work that the optimization of the operation can be recast as an MPC problem that can be solved efficiently by resorting to MILP solvers. An adaptive hybrid predictive controller design and development for optimization of a real CCPP are given in [45]. Here the real plant (Central Interconnected System, Chile) has been modeled as a hybrid system using adaptive fuzzy models for plant start-up, normal operation and shut-down. Thereafter, an adaptive predictive control strategy is used for operational economic optimization of the plant. They show a 3% fuel consumption saving compared to conventional strategies at regulatory level.

A few steady-state studies are available in literature on CCGT systems, which provide some background on specific subsections in the plant. A study focusing on post-combustion carbon capture and sequestration (CCS) [46] using Aspen Plus gives a brief steady-state modeling overview of CCGT, CO_2 removal plant (using monoethanolamine – MEA solvent) and its impact on the CCGT efficiency. In addi-

tion, a parametric study on effect of different MEA temperatures, stripper operating pressures, and MEA flowrate have been given. Another study [47] gives a detailed Aspen Plus flowsheet of the combined cycle cogeneration plant fueled by natural gas and the simulation results were validated with a local cogeneration plant. A steady-state study [48] showing optimal gas turbine cycle for CCPP was given for a 300 MW power plant. This study described and compared four different gas turbine cycles (simple cycle, intercooled cycle, reheated cycle and intercooled/reheated cycle) and concluded that reheated gas cycle showed the highest thermal efficiency and will result in increased savings.

1.1.1.6 IGCC Modeling Efforts

In previous work, the advantages of performance and cost of IGCC systems were investigated [33, 4, 49] and alternative designs of IGCC system were evaluated [10, 50, 51]. The performance and cost models were developed for selected IGCC technologies and probabilistic analysis were developed and applied to evaluate the potential risks of IGCC systems [52, 53, 54]. The work based on Texaco IGCC [16] is one of the most exhaustive models found in the open literature, as it describes many gas purification units. Other works that enhance the flowsheet have been based on it such as [55], which analyses different levels of integration with ASU-CC, and [56], which incorporates CO_2 removal technology. A recent paper by Pérez-Fortes et al. [57] highlights conceptual modeling efforts of IGCC plant using Aspen Hysys^{TM} which was validated with ELCOGAS power plant in Spain.

1.1.2 Model Predictive Control

All of the theoretical predictive control research, along with applications to field of electronics, aeronautical engineering, fuel cells, petrochemical industries etc., involve the use of model predictive control. Model predictive control is an advanced control strategy first developed for use in the petroleum refining industry by Cutler and Ramaker (1980) in the late 1970s.

MPC is based on iterative, finite horizon optimization of a plant model. At time t the current plant state is sampled and a cost minimizing control strategy is computed for a relatively short time horizon (p time steps) in the future. Specifically,

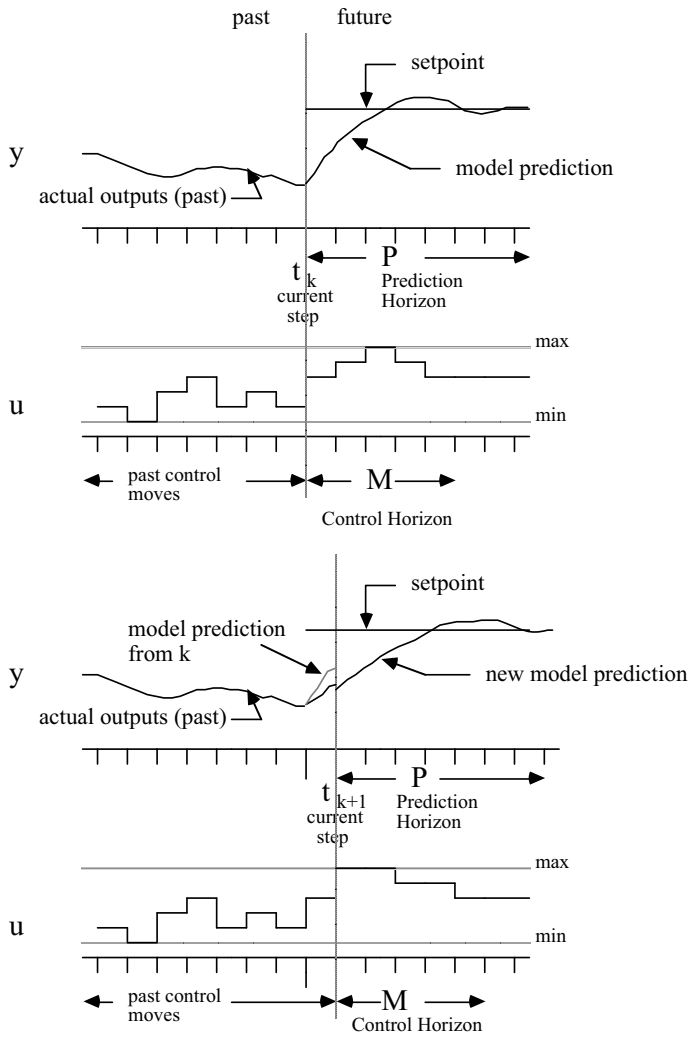

Figure 1.5: Graphical depiction of model predictive control. Taken from Bequette (2003) [58]

textbooks [58, 59, 60, 61].

The model predictive control strategy developed at Shell Oil in the late 1970's and early 1980's by Cutler and Ramaker [62] is known as dynamic matrix control (DMC). One distinguishing feature of DMC is how error and uncertainty are treated over the prediction horizon. Unless the plant being controlled is perfectly modeled, there is an error in predicting the effect of control action on the plant. Disturbances, both measured and unmeasured, add to this error. In DMC, the error measured at the current timestep is assumed to enter the system at the output measurement and maintain a constant value throughout the prediction horizon, an assumption known

as the additive output disturbance assumption. This approach is widely applied in both academic studies and industrial applications.

1.1.3 Plantwide Control

In practice, a plantwide control system is usually decomposed in several layers, separated by time scale (see Figure 1.6). The layers are linked by the control variables, whereby set points computed by the upper layer are implemented by the layer below [63]. This deals with the structural decisions that must be made to design a control structure for a complete chemical plant. The decisions involve the following main tasks:

1. Selection of manipulated variables ("inputs");
2. Selection of controlled variables ("outputs");
3. Selection of (extra) measurements (for control purpose including stabilization);
4. Selection of control configuration i.e. the structure of the overall controller that interconnects the controlled, manipulated and measured variables;
5. Selection of controller type (control law specification, e.g. PID, decoupler, LQG, MPC etc.)

The translation of these tasks into a systematic plantwide procedure for control structure design have been given by Skogestad [63, 64] which focus on a *top-down analysis* and a *bottom-up design* procedure.

1.1.3.1 Regulatory control layer

A lot of research over the past 40 year has been directed into the subject of regulatory control structure design. [65, 66, 67, 68, 69, 70, 71, 72, 73, 74, 75, 76, 77, 78]. A regulatory control layer is defined as a layer in control hierarchy which has operation as its main purpose, and which normally contains the control loops that must be in service in order for the supervisory layer (it may be the operators) to be able to operate the plant in an efficient manner. Here are some highlights of this layer.

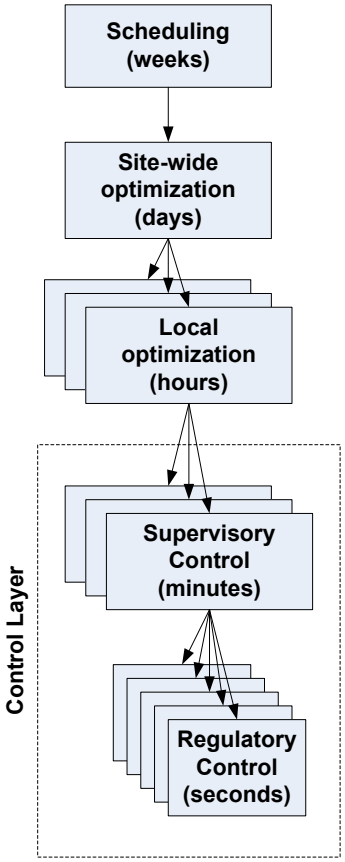

Figure 1.6: Typical control hierarchy in a chemical plant. Taken from Skogestad (2004) [63]

- The main objective of this layer is generally to facilitate smooth operation and not to optimize objectives related to profit, which is done at higher layers.
- This is usually a decentralized control system, which keeps a subset of measurements at a given set point.
- It is usually itself hierarchical, consisting of cascaded loops where the values of the set points of the variables are determined by the upper layers in the control hierarchy.
- If there are unstable modes (RHP-poles) then these are usually stabilized first.
- This layer should also avoid "drift" so the system stays within its linear region which allows the use of linear controllers [79].

- This layer should allow for "fast" control, such that acceptable control is achieved using "slow" control in the layer above.

1.1.3.2 Supervisory control layer

The purpose of the supervisory control layer is to keep the (primary) controlled outputs at their optimal setpoints, using as degrees of freedom the set points in the composition control/regulatory layer and any unused manipulated inputs. This layer can be configured to operate in either multiloop or multivariable (e.g. MPC) control architecture. Both have its own advantages and disadvantages, which will be a focus in one of the later chapters.

1.1.3.3 Optimization layer

Optimization layer identifies the active constraints and recomputes optimal setpoints for controlled variables. It may be based on Real-time Optimization (RTO) where a detailed steady-state model is maintained and continuously updated. In some cases, where the degrees of freedom are small in number, an optimal map or pathway of process variables may be constructed to speed-up computation. If the active constraints do not change and a good set of self-optimizing controlled variables could be found, RTO gives little benefit and should not be used. In this report, we rarely use this strategy and thus the review of optimization layer design has not been done extensively.

1.2 Overview of Methodology

Based on the objective of this study as highlighted in the previous section, detailed steady-state and dynamic models need to be developed for evaluation of advanced controller designs for IGCC plants. In this section, the general methodology used for developing IGCC system models, applying lower inventory layered controllers and implementing supervisory level controller design is described.

1.2.1 Steady-State Process Modeling in AspenPlus™

It has been mentioned earlier that several steady-state simulation models of IGCC have been developed and refined by various sources (including U.S. Depart-

ment of Energy), many of which use AspenPlus™. This is an upgraded simulator based on Aspen, a deterministic steady-state chemical process simulator. The main difference between Aspen and AspenPlus™ is that the latter has a graphical user interface and is regularly updated and maintained by a commercial vendor (Aspen Technology, Inc., 2010). In current study, Aspen Engineering Suite v2006.0 (using Intel Fortran Compiler 9.1 and Microsoft Visual Studio 2005), which provides Aspen Plus User Interface v2006.0 has been used.

In order to simulate a process technology in AspenPlus™, the technology must be described in terms of a flowsheet. In a flowsheet, unit operations are connected via material, heat or work streams. Unit operations are represented by "blocks", which essentially are computer subroutines in the simulator library that perform mass and energy balance calculations for specific unit operations such as heat exchangers, compressors, pumps, reactors, and others. AspenPlus™ includes an extensive thermodynamic database to support energy balance and chemical equilibrium calculations.

AspenPlus™ uses a sequential-modular approach to simulation. In this approach, the simulator progresses from one unit operation block to another in a calculation sequence that can be specified by the user or selected by the simulator. In a large flowsheet such as that for an IGCC system, the simulation results for the input streams to some blocks often depend on results for output streams of other blocks that are calculated later in the sequence. Such streams are often referred to as recycle or tears streams. In such cases, the simulator starts with initial values for such streams and iterates on the flowsheet solution until the simulation values for the inlet of an upstream block and outlet of a downstream block converge.

Another type of iterative solution occurs when the user wishes to specify that the value of a stream or block variable should be varied to achieve a particular design target. This type of iterative calculation is performed using a "design specification" block. This is to facilitate feed-back calculations in a steady state scenario.

Other useful capabilities in AspenPlus™ include *calculator* blocks and *transfer* blocks. A calculator block enables a user to specify their own computer code (in FORTRAN), for instance, for a unit operation not available in the default

AspenPlus™ library. A transfer block enables the values of a block or a stream variable to be transferred to other variables, resulting in a feed-forward type of calculation.

1.2.2 Dynamic Modeling in AspenDynamics™

AspenDynamics™ is a dynamic simulation and optimization tool for chemical processes. Aspen Plus Dynamics extends Aspen Plus steady-state models into dynamic process models, enabling design and verification of process control schemes and, in more recent versions – failure analysis, development of startup–shutdown, rate-change, and grade transition policies. It features conversion of steady-state Aspen Plus models into flow-driven and pressure-driven dynamic models. As in the case in Aspen Plus, physical properties integration with Aspen Properties is done to include a large database of chemical components. It uses an equation-oriented architecture allowing simulation of complex, highly integrated chemical processes.

The Control Design Interface (CDI) in AspenCustomModeler™ enables a linear state space model to be extracted and loaded into MATLAB and used with the Control System Toolbox in designing a process control system. Once the user has designed a control system, they can use the *Simulink Interface*, also included with Aspen Dynamics, to test its performance. The interface enables an Aspen Dynamics process simulation to be used as a block within a Simulink model. This means the user can test the controller performance on the full, rigorous, non-linear dynamic model of the process. Without this interface, the control design can only be tested using the linear dynamic model within MATLAB. This leaves uncertainties about how the controller will perform on the real, non-linear process.

1.2.3 Advanced Controller Design in MATLAB/Simulink

We make extensive use of Control System Toolbox, Simulink and System Identification Toolbox for designing advanced process control (APC) of IGCC. System Identification Toolbox lets us construct mathematical models of dynamic systems from measured input-output data. This data-driven approach helps describe systems that are not easily modeled from first principles or specifications, such as chemical processes and engine dynamics. It also helps simplify detailed first-principle models,

such as the CDI models from ACM, by fitting simpler models to their simulated responses. System Identification Toolbox, a linear and nonlinear models can be fitted to data, a process known as black-box modeling. Available model structures include low-order process models, transfer functions, state-space models, linear models with static nonlinearities at the inputs or outputs, and nonlinear autoregressive models. If a mathematical model of the system dynamics is available, its parameters can be tuned to better match experimental data, a process known as grey-box modeling.

1.3 Structure of the Report

This technical report is divided into nine chapters. In Chapter 2, we first discuss the detailed steady-state design methodology for a low pressure (LP) ASU and an elevated pressure (EP) ASU and highlight a few complexities/challenges that need to be addressed during this design stage. Later, we designed a detailed pressure-driven dynamic model by including various equipment details. We make an operating cost analysis to illustrate the effect of different ASU configurations on the total ASU power consumed and benchmark our model with an existing NETL model.

In Chapter 3, we cover detailed controller design for LP and EP ASU. We start by identifying various control input-output variables and design the structure for regulatory layered control. We later moved into designing a supervisory control layer on top of the regulatory layer using PI, feed-forward/ratio and MPC based methods. We finally compare and discuss the results of these designs.

Chapter 4, 5 and 6 covers the step-by-step approach of building rigorous dynamic models for other important IGCC plant subsections, i.e., the gasifier, gas turbine/compressor and the HRSG respectively. Thereafter, a section-wide controller design for each of them has been provided, again based on a hierarchical control architecture. In each of these subsections, we highlight the complexities and challenges involved during the design stage, the various approximations involved and study their implications on the controller design.

Chapter 7 deals with plantwide controller design, where we move into developing dynamic plantwide process model (by incorporating all the previous models

consisting of the main IGCC power loop) and regulatory layered controller design, initially by conducting pressure swing studies on the entire flowsheet (given in Appendix A.1) to identify various material/energy flow network and conflicting control blocks. Further, we discuss plantwide decentralized and centralized MPC controller design and examine/compare these design for studying controllability of the entire IGCC plant.

In Chapter 8, we perform a detailed operability analysis study on individual sub-units of the IGCC flowsheet to obtain more insights into the possibility and directionality of various input/output pairing within a sub-section.

In Chapter 9, we provide a concise summary of this report and give an outlook for future work by identifying the challenges that remain to extend the current results towards various promising directions.

1.4 Research Contributions

From the literature survey, it is clear that a significant amount of research exists on IGCC, plantwide control and model predictive control. Despite the volume of research, there remain several important gaps in either rigorousness and/or correlation among all of these topics. These limitations fall under following broad categories:

- **Lack of rigorous dynamic models** – Most of the plantwide simulation studies, where scale of problem is as large as a typical IGCC plant, are based on steady-state analysis [16]. Dynamic simulation studies, which require significant amount of equipment details availability (most of which are proprietary) and involve substantial unit-unit interactions are rarely found.

- **Flow-driven mode only operation** – Rigorous dynamic studies found in literature which involve specific sub-units, do not take into account the effect of flow fluctuations due to pressure swings or pressure-driven mode operation, which is commonly found in IGCC systems. Due to this limitation, the results using these models may not be consistent with a real plant especially during load changes or periodic ambient temperature changes.

- **Real-plant–Plant-model mismatch** – Many control studies, based on first-principle plant-models, focus on operability and controllability of a specific portion of the plant, without considering the effect of possible "overall" process mismatch between real-plant–plant-model on control algorithm. For example, there are numerous articles in open literature which show applicability of advanced process control in the study of ASU which involve first-principle, low-order or compartmental modeling of the distillation columns only. Most of these studies fail to account for controllability issues e.g. right-half plane poles [80], arising due to feed-product thermal interactions in the main heat exchanger, which is what is observed in a real plant. Due to this reason, it is essential to have a rigorous dynamic plant-model first (based on a real-plant), before developing a model for control studies.

- **Plant-model–Control-model mismatch** – Another major limitation in control literature, which is generally overlooked, is the assumption that the plant-model is perfectly known. In most simulation studies, due to absence of online plant data, a "surrogate" plant based on the "model" (used in model predictive control formulation) is utilized. Thereafter, some parameters are modified to mimic a real scenario plant. This method (in most cases) does not eliminate structural differences between the surrogate plant-model and the model used for control purposes, leading to unrealistic and "better" control.

In the current study, we utilize the rigorousness of Aspen software to study inherent nonlinearities and interactions in a complex plant such as IGCC, and as a first step towards developing simplified linear model to study controllability for small perturbations around optimized steady-state point. This type of control structure analogy is generally used in industry, where control models are based on real plant data. Much of our efforts has been directed towards study of process design and simulation, flowsheet structure and pressure/flow dynamics. Since Aspen at current stage has stability issues with dynamic optimization and dynamic matrix control (DMC), we try to incorporate advanced controller design in Matlab/Simulink environment with much more flexibility. We admit that a highly complex plant-model (designed using a commercial software), without a first-principles/low-order model,

does not justify using linear MPC. On the other hand, developing such a model might lead to stability/ convergence issues (when multiple units interact via material and energy streams) and high computational time.

CHAPTER 2
DYNAMIC MODELING OF AIR SEPARATIONS UNIT

The partial integration of an air separation unit (ASU) with the combustion turbine, and compressed air available at high pressures (between 200–250 psi), requires high pressure operation of the ASU. Depending on the amount of air integration involved, this operating pressure changes based on fuel-cost, equipment costs, controllability issues and net power generated. Due to decreased separation efficiency at elevated pressures, the design and control of these plants is very challenging. In addition, stringent oxygen demands by the gasifier require drastic variation in production rate while maintaining the purities at desired values. Thus the design and control architecture of a non-IGCC based ASU is different from an ASU integrated with an IGCC plant.

Conventional cryogenic air separation processes, their energy-integration concepts and control technologies have been studied extensively in the past in both open and closed literature. A general review of the current art in ASU and liquefaction systems is given by Castle [81]. The integration of ASU and other energy conversion processes like gas turbines is reviewed by Smith et al. [28, 31]. A dynamic model for low-pressure (LP) stripping and high-pressure rectification columns as part of IGCC power plant has been given by Seliger et al. [82] and Hanke et al. [83]. The approximations involved in these studies, although valid for analysis of single columns, might not capture real pressure dynamics when the coupled case is considered, since multiple material streams connect the HP and LP columns. Apart from the condenser-reboiler heat integration effects, there is also a need to consider subcooler heat interaction effects, which none of the above studies address.

In this chapter, we first discuss the steady-state design for a low pressure (LP) ASU and an elevated pressure (EP) ASU (including the heat-exchanger (HX) design) and highlight a few complexities/challenges that need to be addressed during this design stage. In addition, we present a detailed pressure-driven dynamic design study (in AspenDynamics^{TM}) of pressure, temperature and purity swing effects in-

herent in the ASU due to air-side integration with gas turbine. This chapter of the report is based on the papers presented in [84], [85], [86], [87] and [88].

2.1 Overall Process Description and Design

The basic unit operations of an air separation unit are

- Compression of air,
- Pretreatment to remove CO_2, water and some hydrocarbons,
- Cooling the air down to cryogenic temperatures to allow separation to occur,
- Separation of air into its components,
- Refrigeration to keep the ASU in energy balance, and
- Compression of gaseous products and storage of liquid products.

The cryogenic equipment is all contained in an insulated structure termed as *coldbox* to minimize the impact of heat leak into the process. The simplified process flow diagram (PFD), shown in Figure 2.1, gives the equipment configuration for a simple gaseous oxygen generator. Air is filtered, compressed, and passed through adsorbers to remove CO_2 and water before entering the cryogenic portion of the plant. The air is then cooled to a temperature close to its dew point in the main exchanger by countercurrent heat exchange with oxygen product and a waste stream. The cooled air is then passed to a distillation system comprising of two columns. In the first column (high-pressure column), operating at a pressure slightly lower than that of the air compressor, a rough separation of N_2 from the air occurs. The N_2 being the more volatile component, concentrates, as the vapor passes up the column. A N_2–rich stream generated at the top of the column is condensed, providing reflux for both the high-pressure (HP) column and another column operating at low pressure. In the low-pressure (LP) column the oxygen-rich stream from the bottom of the HP-column is further processed. A higher-purity oxygen stream is produced at the bottom of this LP column, and product oxygen is

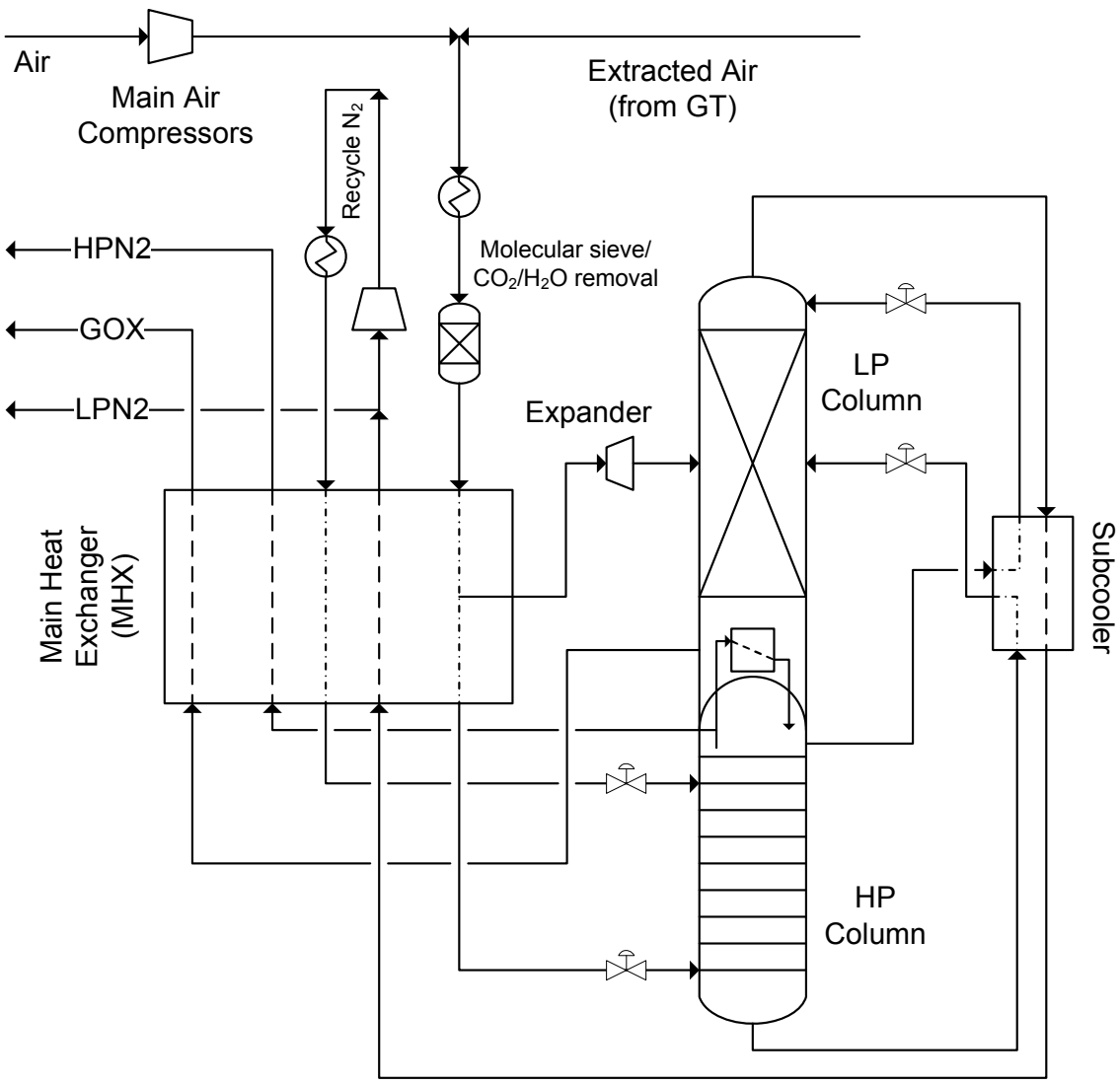

Figure 2.1: Schematic showing a typical ASU process

removed as a vapor and warmed up in the main exchanger. Vapor boil-up for the LP column is generated in a reboiler thermally linked to the HP column.

Liquid reflux for the LP column can be subcooled by cooling against waste vapor from the LP column. This minimizes flash when the reflux stream is dropped to the lower pressure and also warms up the waste stream. A portion of the air stream is removed from the main exchanger and expanded in a turbine to generate refrigeration, and gaseous oxygen product from the main exchanger is compressed to its required delivery pressure. The following subsections give detailed explanation of the processes.

Air compression and pretreatment

The main air compressor (MAC) provides air to the coldbox at pressures ranging from 60 to 270 psia depending on the type of ASU and economic parameters associated with the plant design. For most ASUs, centrifugal compressors are used. The compressed air is intercooled between stages with the final stage heat of compression removed in an aftercooler.

Before entering the adsorbers, the air may be precooled (depending on the adsorber configuration), using direct heat-exchange against boiling freon. Most modern ASUs remove H_2O and CO_2 in a warm-end adsorption system. The adsorbent of choice is 13× molecular sieve (Na Zeolite) [89, 90] and a *temperature swing adsorption* (TSA) process is being used. In current study, we assume the air free of any CO_2 and H_2O, and hence, the pretreatment stage is not modeled.

MAC discharge pressure determination

The discharge pressure required by the main air compressor is determined from individual equipment, line resistances and more importantly, in case of IGCC plants, the amount of gas-turbine (GT) and ASU integration. The degree of air-extraction from GT, in turn, is determined by the overall economic considerations and plant design, for instance, an IGCC plant with is carbon-capture and sequestration (CCS) ready requires lower or no GT-air extraction [31], and hence operating an LP-ASU (lower MAC delivery pressures) is more desirable to avoid operability and controllability issues[1]. If limited nitrogen integration is required (in cases which requires syngas saturation using steam or CO_2), a LP-ASU is always considered. The effect of ASU-GT integration on the choice of ASU has been discussed in detail in the literature [31, 30, 28] and in one of the later chapters.

Typically, for the LP-column of a LP ASU, the top pressure is set by the waste (low-pressure N_2 stream) exit pressure and the resistances in the waste circuit. These consist of piping and heat exchanger frictional losses. The pressure at the bottom of the column includes the resistance of the column itself. The reboiler top approach temperature determines the HP-column pressure. The main

[1] Obviously, the savings in air compression cost will be exploited in increased oxygen and nitrogen compression, due to lower suction pressures

air compressor discharge is the result of this pressure and the resistances in the air circuit.

Heat exchangers

In order to minimize the refrigeration losses from ASU, it is important to have efficient heat exchangers. Heat transfer coefficients for sensible heat exchange between gases are poor and can only be improved at the expense of pressure drop. The ideal heat exchanger for cryogenic ASUs with gas/gas exchange has to have a high ratio of surface area to cross-sectional flow area with low resistance to flow. The standard heat exchanger type used is therefore the *brazed aluminum plate-and-fin*, almost exclusively used for cryogenic gas/gas heat exchange in air separation.

The main heat exchanger (MHX) ensures that the product gases leave the exchanger at a temperature close to that of the air entering the exchanger. The typical average temperature difference between the air and the warming streams is of the order of 8°F (4.4 K)[2]. Typically the MHX contains 10% of the total plant inefficiencies.

The subcoolers are also brazen aluminum heat exchangers with the function of warming the waste stream from the LP column and, in turn, subcooling the reflux streams. It accomplishes two things: firstly it minimizes the flash losses as the refluxes enter the LP column, and, secondly, it transfers heat to the waste stream which in turn allows a warmer airstream leaving the main exchanger.

Refrigeration generation

Losses in refrigeration normally translate into a process inefficiency. The generation of refrigeration to offset losses requires additional power consumption or loss in product recovery. Refrigeration losses in an ASU are typically

1. Heat leak into the coldbox,

2. Warm-end losses in the MHX, and

[2]Modern heat-exchanger manufacturers, like the Linde group specialized in aluminum plate-fin type heat-exchangers for applications in air separation, have been able to reach a minimum temperature approach of 2–3°F

3. Liquid products

4. Products at high pressure (from HP-column)

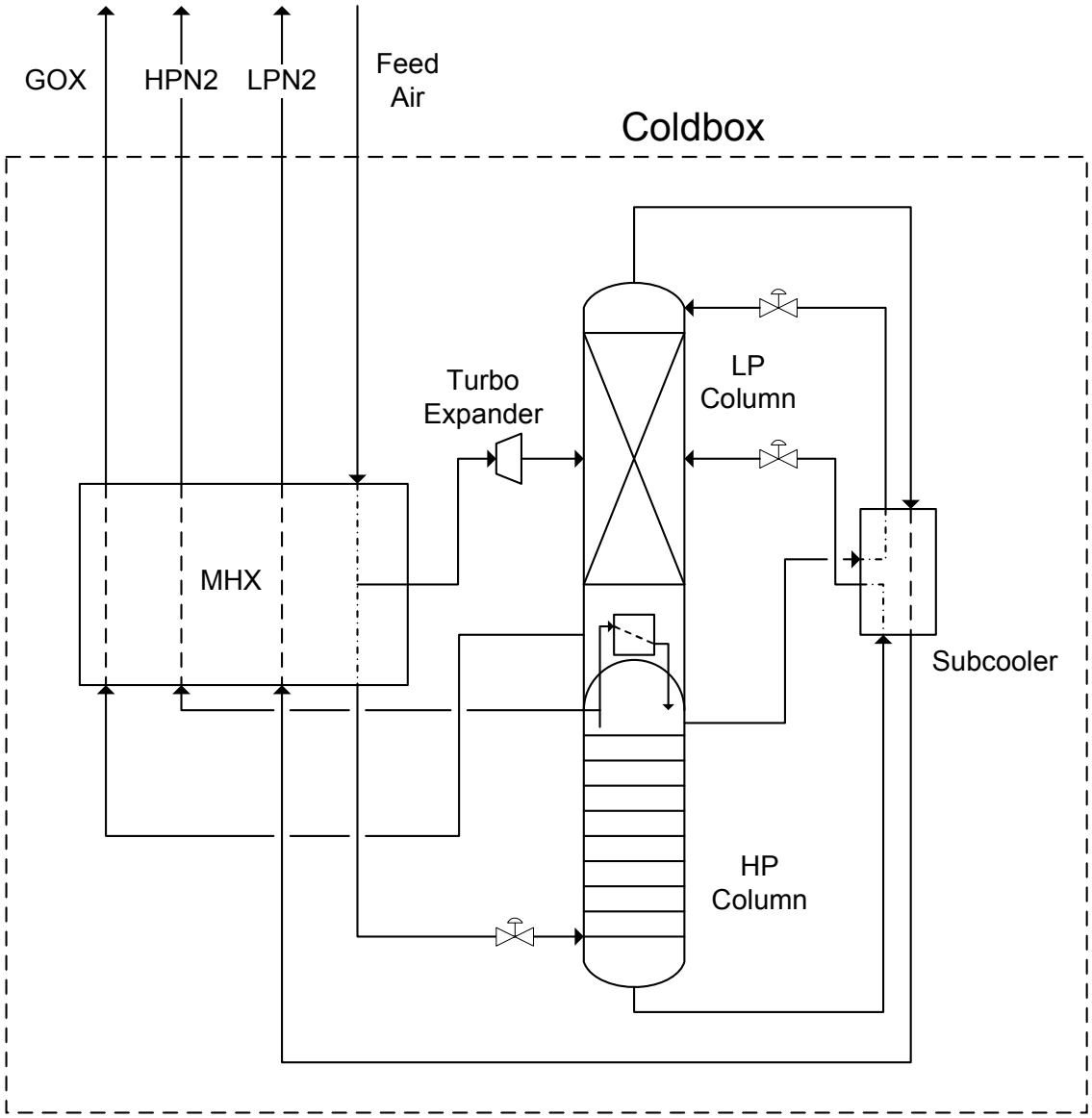

Figure 2.2: Schematic of base-case ASU process for refrigeration requirement studies

This refrigeration is generated by using an expansion engine, typically a turboexpander in ASU. The work extracted from the expanding fluid, may be utilized to generate electricity, compress gas, or just dissipate in an ambient blower or oil friction brake. Figure 2.2 shows a typical application of expander in ASU. Air is

compressed to desired inlet pressure (depending on LP or EP ASU), cooled in the main exchanger, and then a portion of the air is expanded to a lower pressure to generate the necessary refrigeration. The HP and LP airstreams are then passed to the distillation columns. Obviously, as more flow passes through the turbine, less is available to the HP distillation. This impacts distillation efficiency and increases air compressor power. A typical enthalpy balance and refrigeration requirement calculation is shown in Table 2.1. Here we assume a heat leak into the coldbox of 20 Btu/hr per lbmol of incoming air. A typical refrigeration generation capability from the turboexpander (with an isentropic efficiency of 90% and mechanical efficiency of 75%) is approximately 600 Btu/lbmol expander flow (1400 kJ/kgmol), evaluted using steady state calculations in Aspen. Hence, for a required refrigeration, the flow required through the expander can be calculated. For the base-case [3], a refrigeration of 103.2 Btu/hr per lbmol of airflow is needed (calculations shown in Table 2.1), which requires an expander flow of 16.9% of the airflow.

Tables 2.1 and 2.2 show a comparison of the refrigeration requirement for a base-case, with no liquid O_2 (LOX), to a case with large LOX requirement (3 mole% of incoming air). For high-LOX case, where the refrigeration requirement is 268.5 Btu/hr/lbmol-airflow, the required expander flow is 44% of the airflow. In addition, upon closely looking at the component flowrate, the recovery of oxygen has gone down to 65% when producing LOX (as compared to 98.8% recovery for base-case). This shows that the LOX generation, although a small flow, has a significant impact on refrigeration balance and oxygen recovery. This is also a simplistic demonstration of the limitations of ASU to produce liquid, proving the impacts of the high expander flow become prohibitive at high LOX demands. To meet these demands, while still maintaining high oxygen recovery, compressors/expanders specifically needed for liquefaction are added.

Expansion-valve vs. expander – An adiabatic expansion valve does not generate any refrigeration (pure Joule Thompson expansion), unless a booster compressor is used on the expanded-air stream. Table 2.4 show results of a LP-ASU

[3]The base-case (Figure 2.2), is taken as a simple low-pressure ASU producing 95% pure gaseous O_2 (GOX), 99.5% pure high-pressure gaseous N_2 and low-pressure gaseous N_2-rich stream (also termed as 'waste' stream).

Table 2.1: Refrigeration balance for base-case LP-ASU (Basis: 1.0 lbmol/hr feed air)

	Pressure	Temp	Enthalpy	Component Flow (lbmol/h)			Total Flow	Enthalpy
	psia	°F	Btu/lbmol	N_2	O_2	Ar	lbmol/h	Btu/h
Air to coldbox	120.0	100	133.9	0.7811	0.2096	0.0093	1.0000	133.9
GOX from coldbox	18.8	85	50.5	0.0043	0.2072	0.0066	0.2181	11.0
LOX from coldbox	18.9	-294	-5462.0	0.0000	0.0000	0.0000	0.0000	-0.1
LPN2 from coldbox	14.7	85	52.4	0.7023	0.0024	0.0024	0.7070	37.0
HPN2 from coldbox	90.2	85	36.0	0.0745	0.0001	0.0003	0.0749	2.7
Heat leak into coldbox								20.0
Required refrigeration/Turboexpander			609.6				**0.1693**	**103.2**

Table 2.2: Refrigeration balance for LP-ASU with high liquid production

	Pressure	Temp	Enthalpy	Component Flow (lbmol/h)			Total Flow	Enthalpy
	psia	°F	Btu/lbmol	N_2	O_2	Ar	lbmol/h	Btu/h
Air to coldbox	120.0	100	133.9	0.7811	0.2096	0.0093	1.0000	133.9
GOX from coldbox	18.8	85	50.5	0.0023	0.1066	0.0033	0.1123	5.7
LOX from coldbox	18.9	-294	-5462.6	0.0002	0.0292	0.0006	0.0300	-163.9
LPN2 from coldbox	14.7	85	52.3	0.7041	0.0737	0.0051	0.7828	40.9
HPN2 from coldbox	90.2	85	36.0	0.0745	0.0001	0.0003	0.0749	2.7
Heat leak into coldbox								20.0
Required refrigeration/Turboexpander			609.6				**0.4404**	**268.5**

Table 2.3: Refrigeration balance for LP-ASU with high HP-nitrogen production

	Pressure	Temp	Enthalpy	Component Flow (lbmol/h)			Total Flow	Enthalpy
	psia	°F	Btu/lbmol	N_2	O_2	Ar	lbmol/h	Btu/h
Air to coldbox	120.0	100	133.9	0.7811	0.2096	0.0093	1.0000	133.9
GOX from coldbox	18.8	85	50.6	0.0045	0.1886	0.0054	0.1986	10.0
LOX from coldbox	18.9	-294	-5462.0	0.0000	0.0000	0.0000	0.0000	-0.1
LPN2 from coldbox	14.7	85	52.3	0.6275	0.0208	0.0033	0.6516	34.1
HPN2 from coldbox	90.2	85	36.0	0.1491	0.0001	0.0006	0.1498	5.4
Heat leak into coldbox								20.0
Required refrigeration/Turboexpander			609.6				**0.1713**	**104.4**

system where refrigeration is being generated without an expander engine (using an adiabatic expansion valve only). For the expander air which is compressed to 2000 psi, we do not obtain too much refrigeration advantage ($\Delta H = -320$ Btu/lbmol of feed air), while the compression cost is large (0.67 hp/lbmol-air for a single-stage booster compressor). This can be compared directly to the performance of an ASU utilizing a turboexpander (Table 2.1), with a refrigeration generation, ΔH, of -610 Btu/lbmol-air, without any compression cost involved (on the contrary, we can extract some work from the expander).

Distillation

The distillation columns are the heart of an ASU. The boiling points (or volatility) of nitrogen, argon, and oxygen are different enough to allow separation by distillation. The double column is by far the most common column configuration used in ASUs. Air at a temperature close to its dew point is fed to the bottom of the HP column. This column consists of only a rectification section; thus, a nitrogen-rich stream can be generated at the top of the column. The reflux for this column is generated in the reboiler–condenser. The fact that the HP-column does not have a stripping section means that the liquid leaving the bottom of the column is no richer in oxygen than the liquid in equilibrium with the air vapor. This oxygen-rich reflux, thus having the same purity irrespective of the separation achieved in HP-column, is then subcooled against warming low-pressure nitrogen exiting LP column top[4] and flashed into the LP-column. This column has both stripping and rectification sections. Reflux for the rectification stream is provided from the top of the HP-column. This reflux is also subcooled against the low-pressure nitrogen stream. The rectification section produces a nitrogen-rich stream allowing oxygen recovery to be significantly higher than that of a single column ASU design. The stripping section produces a bottoms product richer in oxygen. The purity of this product vapor stream is a function of the number of distillation stages available and the boilup generated in the reboiler. The recovery of oxygen is a function of total

[4]The primary purpose of the subcooler is to subcool the reflux nitrogen stream to the LP-column top; subcooling of oxygen stream is only done if additional refrigeration is available from the cold stream, depending on the hot-end temperature approach

Table 2.4: Calculation for amount of expanded air needed (see fig. below). Basis: 1.0 lbmol/hr feed air

	Pressure	Temp	Enthalpy	Mole Fraction			Total Flow	Enthalpy
	psia	°F	Btu/lbmol	N_2	O_2	Ar	lbmol/h	Btu/h
Air to HP-column	120.0	100	133.9	0.7811	0.2096	0.0093	$(1-x)$	$133.9\,(1-x)$
Air to LP-column	2000.0	100	-185.0	0.7811	0.2096	0.0093	x	$-185.0x$
GOX from coldbox	18.8	85	53.6	0.0161	0.9500	0.0339	0.218	11.7
LOX from coldbox	18.9	-294	-5462.0	0.0054	0.9734	0.0212	0.000	-0.1
LPN2 from coldbox	14.7	85	55.4	0.9972	0.0007	0.0021	0.707	39.2
HPN2 from coldbox	90.2	85	36.4	0.9951	0.0003	0.0046	0.075	2.7
Heat leak into coldbox								20.0
Total							0	$100.4 - 318.9x = 0$
								$\boldsymbol{x = 0.315}$

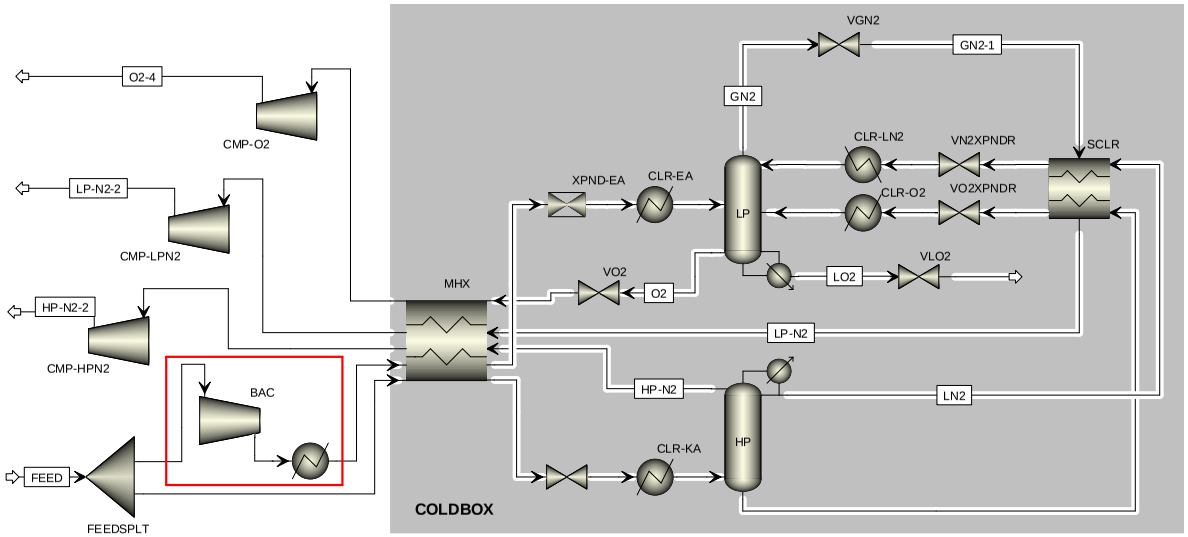

distillation stages, boilup and reflux availability.

In previous section, the production of small quantities of liquid product was discussed. Increasing the need for liquid production requires increased expansion turbine flow. Referring to the PFD of a typical ASU cycle (Figure 2.2), as expander flow is increased, less air is available for the HP column. This air generates boil-up and reflux from the HP column. Therefore, as less reflux and boil-up is available in the LP column, oxygen recovery is reduced. This is similar to the case where high HP-nitrogen is produced. A large amount of nitrogen is extracted before it can be utilized for boil-up. This also leads to a drastic reduction of reflux to the LP-column. The refrigeration balance for this case is given in Table 2.3, which shows that, although the refrigeration requirement remains similar to base-case, we encounter a huge recovery loss.

Condenser-Reboiler Integration

The reboiler-condenser equipment serves as the thermal link between the HP column and the LP column. It provides vapor boil-up for the LP column and reflux for the HP column by condensing a nitrogen stream and boiling an oxygen stream. In this study, a *thermo-syphon reboiler* has been used as shown in Figure 2.3, which is submerged in a pool of liquid oxygen at the bottom of the LP column. The nitrogen passages are contained in a high pressure circuit. The oxygen passages, however are open at the top and the bottom so LOX is free to flow into and out of the reboiler. As oxygen is boiled within the open side of the heat exchanger, it flows upwards.

In principle, any hydrocarbon entering the coldbox will migrate to the bottom of the LP column and, hence, the LOX in the reboiler. It is important that hydrocarbons should not be allowed to concentrate and a constant liquid purge is necessary. Again, in this study we do not model any contaminants with the air. It is also important to maintain high liquid levels and recirculation rates through the reboiler to eliminate dry boiling zones. It is recommended that the reboiler level be maintained at the top of a thermosyphon reboiler.

Other types of reboiler commonly found in practice is termed as the *downflow*

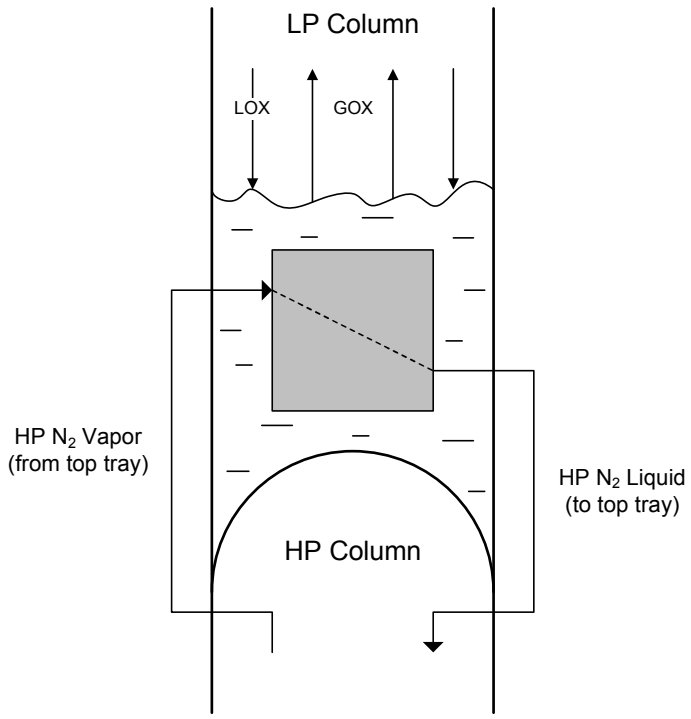

Figure 2.3: Schematic showing the integrated condenser–reboiler arrangement in a typical double-column ASU

reboiler due to the fact that LOX enters at the top of the core and flows down. Vapor and liquid exits at the base of the core. The exit stream should have sufficient liquid flow to wash contaminants from the core and prevent dry boiling. A constant purge is still needed, however, from the column sump.

Product Compression

Pressurizing the product streams for delivery is accomplished by gas compression, liquid pumping or combinations of pumping followed by compression[5]. Product storage can be provided as backup or for "peaking" duty, supplying higher than design rates of product delivery for short periods of time. We do not consider

[5]Pumped LOX cycles are also typically used, where the oxygen compression cost is reduced significantly at the expense of additional air compression in the booster air compressor. The major difference is that oxygen is produced from the LP-column as a liquid, pumped to the required pressure, and then vaporized in the MAC. Typically, the power consumption of LOX and LP cycles is comparable. At large oxygen delivery pressure requirement or lower efficiency of oxygen compressor (compared to the air-booster), LOX cycles might prove advantageous. This pressure is not significantly large in IGCC systems and LOX cycles will not prove advantageous, and hence, has not been considered in current study

storage/backup operations as part of current study and has not been included in this technical report.

2.2 Low-Pressure ASU

2.2.1 Steady State Design

Setting up a steady-state simulation requires identifying the main requirements and bottlenecks in the process. The feed-air is available, after removal of water, CO_2 and other impurities, in upstream process. A MAC after-cooler outlet temperature of 100°F, i.e. equal to feed-air temperature, has been assumed. This can provide operational flexibility for a hot summer day. The important specifications/requirements are identified below

- Desired composition of oxygen stream is 95.0 mole% with a molar flowrate of atleast 14460 lbmol/hr (to be used in gasifier and Claus units)
- 5000 lbmol/hr of high-pressure nitrogen (99.5 mole% pure) from the HP-column must be made available to the plant
- The HP-condensor and LP-reboiler heat duties must match
- Minimum temperature approach for integrated condensor–reboiler heat exchanger is 9°F
- Minimum temperature approach for the main heat exchanger is 9°F
- Minimum temperature approach for the subcooler is 5°F
- Heat leak into the system of magnitude 20 Btu/hr per lbmol of feed-air

Figure 2.4 gives the steady-state AspenPlus^{TM} flowsheet of the LP-ASU studied in this report.

Determining the operating pressures

For a LP-ASU, where some or all of LP-N_2 may be vented out, the LP-column top pressure is set close to atmospheric pressure. This obviously requires additional

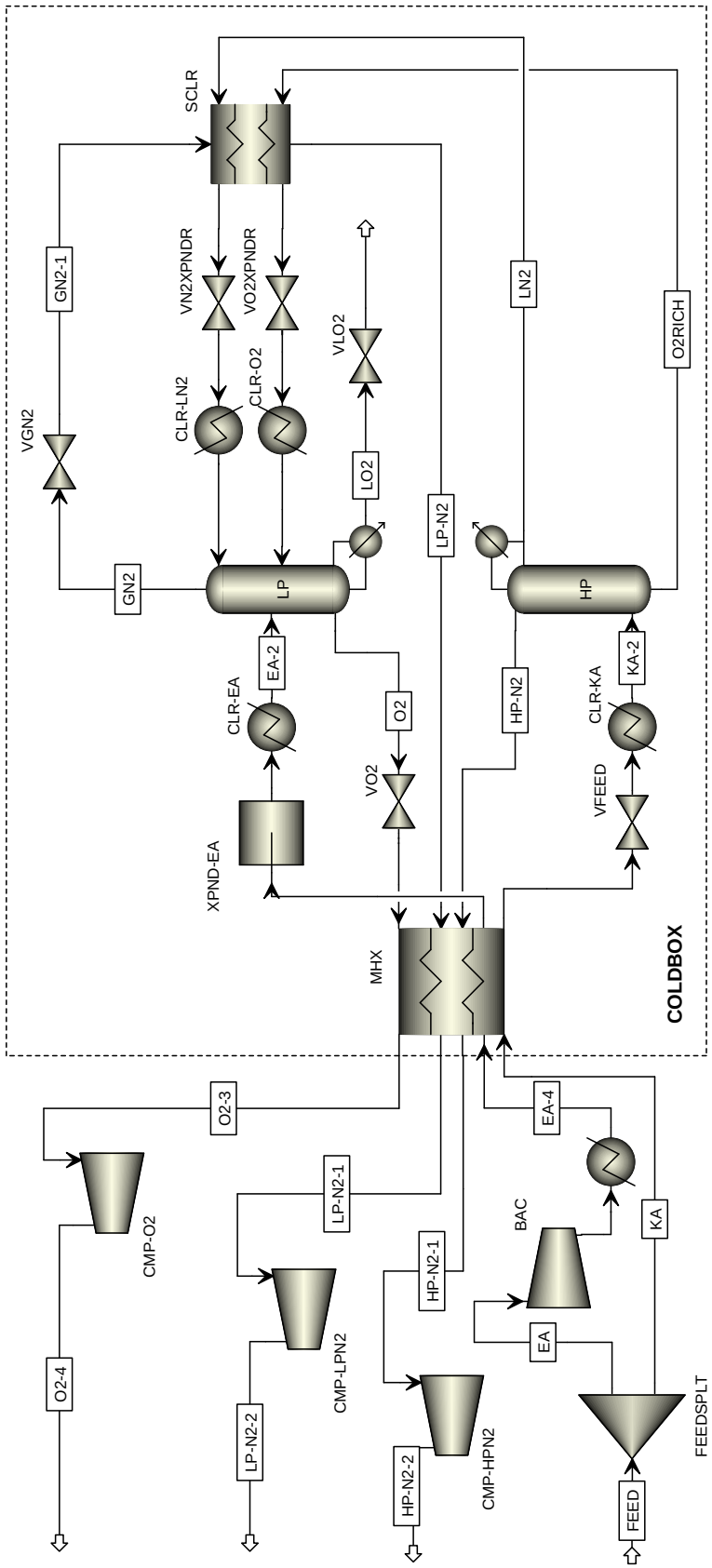

Figure 2.4: Process flowsheet showing low–pressure double-column ASU in AspenPlus™

pressure head for resistances in the waste/LP-N_2 circuit, which constitute of pressure drops in the subcooler (0.5 psi), frictional resistances in the MHX (1.5 psi) and (optionally) in the adsorber regenerating units (1–2 psi). General pipeline resistances have been modeled using a simple valve block (VGN2 in Figure 2.4). This gives a LP-column top pressure of 19.2 psi. The determination of HP-column top pressure requires initial assumptions and subsequent iterations. We assume that the LP-column pressure drop of the order of 0.5–0.7 psi (since the bed consists of structured packing, which has substantial low pressure drop). At 20 psi, we get the bubble-point of 95 mole% pure oxygen (assuming 3 mole% argon and 2% nitrogen) as $-293.5°$F (evaluated using AspenProperties^{TM} taking Peng-Robinson method for base-case thermodynamic property calculation). We take a 9°F temperature approach between the LP reboiler and HP condensor, which although low, is typical for cryogenic applications amounting to a HP-column top temperature of $-284.5°$F. This gives a dew-point pressure as 91.8 psi for 99.5 mole% nitrogen (assuming 0.4 mole% argon and 0.1% oxygen), which is the pressure at the top of HP-column. We assume a pressure drop of 2–4 psi for the HP-column which typically contains 10–35 sieve-trays. This gives 97 psi as an approximate entry pressure for the feed-air stream to the HP-column bottom. Adding pressure heads for pipeline resistances (0.5 psi) and frictional pressure drops in MHX (2 psi), we can assume 100 psi, as a conservative figure, for feed-air pressure when it enters the cold-box. It must be noted that the main air compressor (MAC), which is further upstream, has a higher discharge pressure. This takes into account the pressure drop in adsorbers (for CO_2 and H_2O removal), coolers and other equipment resistances.

Distillation Columns

The LP and HP column is modeled using a rigorous distillation (RADFRAC) block in AspenPlus^{TM}. The number of trays and feed entry trays, as a starting point, are taken from literature [83, 82, 91]. Most of the feed–product stream connectivity are similar to the base-case schematic shown in Figure 2.2. For the HP-column, high pressure nitrogen (HPN2) is specified as a product stream leaving stage–2 (top-most physical stage, excluding the condenser) of the HP-column. High pressure liquid-

nitrogen (LN2) leaves stage–1 (condenser) and eventually enters as a feed stream to stage–1 of the LP-column. It must be noted that HP-column (top), in reality, does not include a separate condenser vessel. It is a continuous stream/pipe which passes through the condenser-reboiler heat exchanger (see Figure 2.3), where a total condensation takes place. Thereafter, a part of the nitrogen-rich liquid stream is extracted, to serve as a reflux to the LP-column. The rest is refluxed back to the HP-column. This kind of equipment model is not available as a part of rigorous distillation module in Aspen, and hence as an admissible approximation, we include a "fictitious" condenser in our study. The oxygen-rich stream (O2RICH) exiting stage–N_{HP} (bottom-most stage) of the HP-column[6], enters the LP-column at a tray located approximately two-thirds from the column top. The expanded air feed stream (EA) also enters a couple of trays below the oxygen feed stream. The column pressure-drop, number of trays and feed tray are refined/optimized as we go into more detailed design of the columns, prior to moving into dynamic simulations, highlighted in next section.

The LP-column has three product streams. Gaseous nitrogen (GN2) leaving stage–1[7], after warming the feed/intermediate streams, is compressed, stored or vented, depending on the process specifications. The gaseous oxygen stream (O2), which is the main ASU product, is specified as a product exiting the reboiler or the bottom-most stage, N_{LP}, in vapor form. A "required" liquid oxygen stream (LO2) leaving the reboiler is also specified. Since, neither any liquid-oxygen ASU product nor pumped LOX cycles are considered here, this flowrate is specified a value close to zero[8], i.e., 1.0 lbmol/hr.

Two "Design Spec/Vary" functions are defined for meeting the purity requirements.

1. Varying the HP-column distillate rate (or the flowrate of LP-column reflux) to bring the mole-fraction of nitrogen in HP-nitrogen (HPN2) stream to the

[6]No reboiler is specified for the HP-column

[7]LP-column does not have a condenser and hence, stage–1 denotes the top-most physical stage (in this case, *equivalent* physical stage for a packed column)

[8]The simulator does not accept exact zero values for liquid products leaving the reboiler. In addition, forcing a zero flow through the valve on this line (VLO2), may lead to singularity issues in dynamic simulations

design-value of 0.995 ± 0.0001

2. Varying the LP-column gaseous-oxygen (GO2) product flowrate to bring the mole-fraction of oxygen in this stream to the design-value of 0.95 ± 0.0001

At this stage, we do not specify the detailed hydraulics, equipment details and "link" the condensor-reboiler. The pressure at the column-top and the pressure drop for each column is specified by the estimated figures from the analysis earlier. Later as we go into more detailed design, the column pressure drops will be calculated depending on the packing/tray equipment specifications and rigorous hydraulics, and will require iterations to meet the desired minimum temperature approach in the condenser-reboiler heat exchanger.

Heat Exchangers

Two heat exchangers, i.e, the MHX and the subcooler, are specified as multistream counter-current heat exchanger (MHeatX[9]) blocks in AspenPlus^{TM}. A temperature approach of 15°F on the hot-side of the MHX, gives a temperature outlet specification of 85°F for the product streams. The outlet condition specification of the hot streams (KA and EA), requires a more deeper analysis. It is known that having a high EA temperature exiting the MHX, will give more refrigeration across the expander (due to greater expander-work that can be extracted per lbmol feed-air). Figure 2.5 shows the adverse effect of this temperature below −160°F on oxygen production. At higher temperatures, although we get a marginal improvement in GOX production, we see a consistent decrease in expanded-air flowrate. This significantly decreases the booster-compression cost, if used.

The downside of not limiting the upper-limit of EA-exit temperature is that the minimum temperature approach in the MHX decreases (as shown in the figure), leading to a higher heat-exchange area and equipment cost. In addition, since the HP-column feed air temperature (and the vapor fraction) decreases, less boil-up and reflux is available from the HP-column. This does not affect the overall recovery but

[9]In a MHeatX block, the outlet specification for each stream on one side of the heat exchanger must be provided. The other-side must have atleast one unspecified stream. MHeatX block assumes that all unspecified streams have the same outlet temperature. An overall energy balance determines the temperature of any unspecified stream(s)

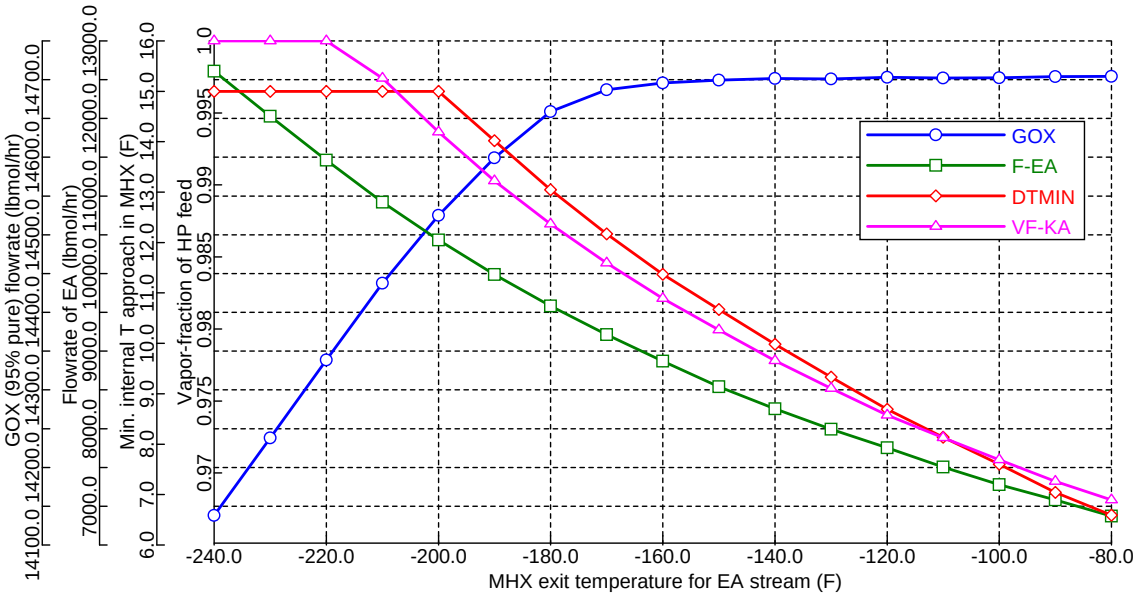

Figure 2.5: Sensitivity plot showing effect of expanded-air temperature (from MHX) on LP-ASU

might lead to equipment modifications due to higher liquid overhead, such as control-valves, HP-column trays and sump. Here, the EA stream exit temperature is chosen as -140°F, which gives a balance between a minimum temperature approach ≥ 10°F and high oxygen recovery (see Figure 2.5). The KA stream cold-side temperature is left unspecified and is calculated by Aspen from an overall energy balance. A heat leakage amount of 1.335×10^6 Btu/hr (i.e. 20 Btu/hr per lbmol of feed-air) is provided in the MHX block.

The subcooler (SCLR) uses a similar MHeatX model block. The cold side outlet temperature for liquid nitrogen stream is specified based on a temperature approach of 5°F. Hence, a *cold inlet – hot outlet temperature difference* specification of this amount to the block is given. For the oxygen stream, ideally the exit temperature should be specified such that the hot side temperature approach should be close to 9°F. Here, for brevity sake, the oxygen stream is not cooled ($Q_{cooled} = 100$ Btu/hr). The refrigeration saved by this approach is anyhow transferred in cooling the inlet air streams in the MHX, hence showing no significant degradation in ASU performance due to this approximation.

One might also note additional heater/cooler blocks on the flowsheet shown

in Figure 2.4, labeled as CLR-KA, CLR-EA, CLR-LN2 and CLR-O2. These are dummy equipments, where a zero heat-duty has been specified in steady-state simulations. These have been placed for additional sensitivity studies and in preventing open-loop instability in dynamic simulations (since this is an energy-recycle system and may lead to *cumulative causation* or *positive feedback*). It must be noted that, if there is any cooling involved in these kind of equipments, it would require expensive refrigerants and must be strictly avoided.

Compressors and Expanders

One of the most important units in the entire ASU process is the expander installed on the EA-air stream, immediately following the MHX. This unit has been specified as a turbine/compressor block in AspenPlus^{TM}. Since expansion may involve 2-phase flow at the outlet, the *check valid phases at outlet* has been disabled. The discharge pressure has been provided as the feed stage-pressure to the LP-column (plus some pressure head, i.e. 0.2 psi, for pipeline resistances). The booster air compressor (BAC) acts as a dummy compressor, with $\Delta P = 1$ psi, at steady-state, but is installed to provide an additional degree of freedom for refrigeration[10], during large deviation from SS operations.

Matching condenser-reboiler heat duty

This is also called "neat" operation, since we do not require any external refrigeration/boilup for the column's condenser and reboiler. The pressures of both the column are maintained such that the corresponding dew/bubble-points have a appropriate temperature difference feasible for heat-transfer from the condensing system (operating at higher temperature) to the evaporating system (lower temperature). Table 2.1 had given calculations for a base-case LP-ASU, showing that for a certain EA-flowrate, the coldbox enthalpy balance is completely satisfied, without the need to incorporate additional coolers/heaters. For the current steady-state flowsheet, the sensitivity of condenser–reboiler heat balance to EA-flowate has been

[10]EA/KA split-ratio is an input variable that can be manipulated to control the amount of refrigeration. This drastically affects the boilup/reflux amount in the columns, leading to recovery fluctuations

shown in Figure 2.6, where a perfect balance is obtained at approximately 8250 lbmol/hr EA flow. The derogatory effect of increasing this flow beyond a certain value, on oxygen-recovery, is also clear from this figure, due to lowering of available boilup and reflux (even when the operation is not "neat").

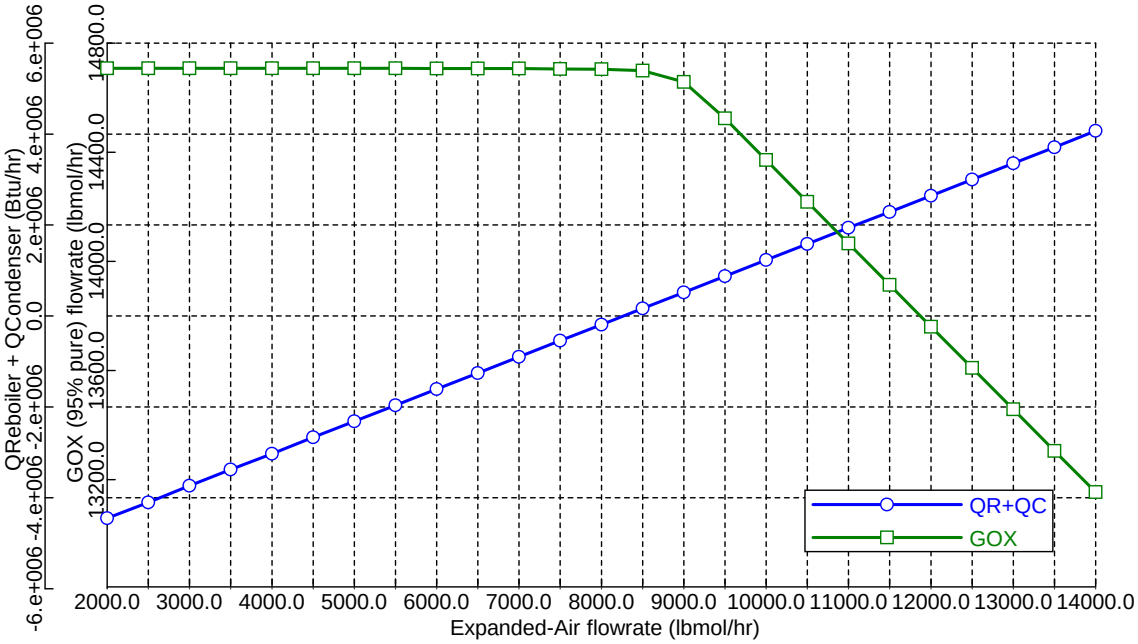

Figure 2.6: Sensitivity plot showing effect of EA flowrate on condenser-reboiler heat balance

For steady-state simulations in AspenPlus™, we specify this balance by defining a "Design Spec/Vary" function, where the EA molar flowrate, specified in the feed splitter (FEEDSPLT), is varied to match the reboiler-condenser heat duties, i.e, $Q_{reboiler} + Q_{condenser} = 0$. The tolerance is specified a marginal value of 1000 Btu/hr (for the first run) and 10 Btu/hr for refining the results in subsequent runs. This amount of precision is very important in lowering the deviation[11] of steady state values obtained from AspenPlus™ and AspenDynamics™.

[11] AspenPlus™ uses a sequential modular approach, whereas AspenDynamics™ uses an equation-oriented approach

Solver options and other specifications

For a required specification of 14460 lbmol/hr of GOX, the required amount of feed-air to be provided is given by

$$\mathrm{F_{FEEDAIR}} = \frac{14460 \times 0.95}{0.21 \times 0.98} \cong 66750 \text{ lbmol/hr}$$

assuming a 98% oxygen recovery. The components selected are nitrogen, oxygen and argon of type "conventional" using Legacy Property Databanks. The base property method for thermodynamic calculations was chosen as Peng–Robinson, which is suitable for air separation processes [91, 92, 82]. The convergence method chosen are Wengtein for tear convergence and Broyden for design-spec convergence. The current system, having no material recycle stream, converges fast without any additional tear-stream specification. With all the simulation requirement in place, the steady-state simulation is run to satisfy four solver specifications (1 overall balance, 3 design-specs). The convergence takes longer (computational time of $\sim$45 sec) after the first initialization, and significantly less time ($\sim$10 sec) for subsequent runs. The following subsection goes into moving the flowsheet (discussed till this step) to a more rigorous pressure-driven dynamic model by incorporating various equipment details.

2.2.2 Dynamic Model

Setting up a rigorous pressure-driven dynamic model, ready to be implemented in Aspen-Dynamics^{TM} requires realistic equipment sizing/rating, matching pressure of the streams to the equipment, providing pressure changers (valves, pumps, compressors) for flow and pressure controllability etc. Similar to previous sub-section, these details are explained equipment by equipment.

2.2.2.1 Distillation Columns

Distillation column design involves decision(s) related to the type of column (tray, packed), column geometry (including condenser, reboiler, sump), tray design (geometry, spacing, weir height, etc.), structure and material for packing (if any), optimizing the number of (equivalent) trays & feed-tray location, flooding consideration etc. An attempt has been made to add as much detail as possible for the model to mimic a real plant. Including every minute detail is beyond the scope of this study (due to software limitations and/or due to limited access to proprietary information) and allowable approximations are sometimes made.

Equipment sizing and rating Rigorous hydraulic calculations are enabled for both HP and LP columns. The column rating/sizing specifications are given in Table 2.5 and 2.6. The data for packed LP-column have obtained by searching for typical packed structures suitable for cryogenic applications [93, 94] and thereafter, visiting the vendor's (Sulzer Chemtech.) catalog/website for specific structured packing. Most of the packing characteristics (surface area, void fraction) are available in AspenPlus^{TM} database.

Table 2.5: LP-column pack rating specifications

Column type	Structured Packing
Packing material	Mellapak^{TM} Plus
Vendor	Sulzer Chemtech.
Dimension	252Y
Sheet thickness (in)	0.006
Section diameter (ft)	17
HETP (in)	14

The section/tray diameter plays a very important role in the overall pressure drop and flooding characteristic through the column. This parameter has been adjusted based on typical pressure drops, maximum flooding factor (preferred value $\leq 80\%$) and liquid holdups in the columns. Parameters such as sieve hole diameter, fraction of total sieve hole area to active area, tray spacing and deck thickness has been chosen based on typical trays used in distillation columns.

Table 2.6: HP-column tray rating specifications

Column type	Tray
Tray type	Sieve
Number of passes	1
Tray diameter (ft)	22
Deck thickness	10 GAUGE
Tray spacing (ft)	2
Sieve hole diameter (in)	0.5
Sieve hole area to active area fraction	0.12

It must be noted that by incorporating rigorous hydraulic calculations, the pressure drop inside the column is now dependent on the vapor-liquid flows (the pressure drop specified during initial design is overwritten). After choosing suitable number of stages and optimum feed-tray locations[12] (shown later in this section), we obtain the sizing/rating results shown in Table 2.7 and 2.8.

Table 2.7: LP-columns sizing/rating results

Section starting stage:	1
Section ending stage:	35
Column diameter (ft):	17
Maximum fractional capacity:	0.929
Maximum capacity factor (ft/sec):	0.379
Section pressure drop (psi):	0.632
Maximum stage liquid holdup (ft^2/ft^3):	12.176
Max liquid superficial velocity (ft/sec):	0.028
Surface area (ft^2/ft^3):	75.89612
Void fraction:	0.9889

[12]This requires iterations which change the stage diameters, for each run, such that the pressure drops and flooding factors are brought back to acceptable values

Table 2.8: HP-columns sizing/rating results

Section starting stage:	2
Section ending stage:	41
Column diameter (ft):	22
Maximum flooding factor:	0.771
Stage:	2
Section pressure drop (psi):	4.104
Maximum backup / Tray spacing:	0.613
Backup (ft):	1.225
Velocity (ft/sec):	0.161

Feed tray location The feed to the HP-column is given at the bottom-most stage of the column, since there is no reboiler present in the HP-column. The HP feed stream, being in vapor phase, is responsible for the all the required boilup in the column. Similarly, for the LP-column, we need to provide a reflux stream to the top. This is fulfilled by the liquid nitrogen stream, commonly extracted from the top portion of the HP-column. It is highly desirable to have the vapor fraction close to zero (or feed quality, $q \cong 1$). The amount of liquid available in this steam (reflux), significantly affects the ASU oxygen recovery capability.

Table 2.9: Table for determining the optimum feed stages

EA feed stage	O2RICH feed stage	GOX flowrate (lbmol/hr)
28	24	14700.50
29	24	14700.53
30	24	14700.21
28	25	14700.66
29	**25**	**14700.96**
30	25	14700.27
28	26	14700.72
29	26	14700.25
30	26	14700.55
28	27	14694.98
29	27	14696.86
30	27	14697.27

Apart from the reflux stream to the top, there are two feed streams (EA and O2RICH) for which we need to determine optimum tray locations. This gives two

degrees of freedom, for maximizing the amount of oxygen recovery. This is done by a trial and error approach[13], shown in Table 2.9. These simulations suggest an optimum value for oxygen-feed input stage as 25 and expanded-air feed stage as 28, for ASU having 35 and 40 total stages for LP-column and HP-column respectively. A comment must be made on the physical effect of oxygen feed stage being too low in the column. In such a case, the nitrogen and argon components in the oxygen-rich stream, do not get sufficient equilibration time to vaporize/separate from the "heavier" oxygen component and get entrained out to the stage below, along the liquid stream. This effect is substantial for oxygen feed below 27^{th} stage.

Table 2.10: Table for determining total column stages

Total LP stages	Total HP stages	GOX Flowrate (lbmol/hr)
30	35	14656
35	35	14679
40	35	14683
45	35	14685
30	40	14687
35	**40**	**14701**
40	40	14703
45	40	14705
30	45	14694
35	45	14702
40	45	14704
45	45	14705
30	50	14699
35	50	14703
40	50	14705
45	50	14705

Number of trays Deciding the number of stages requires an economic tradeoff between the extent of oxygen recovery and capital-cost involved in adding more stages. In this case, there are two highly interacting columns, whose total number of stages must be determined. The correlation between the number of stages in each column can be established by the fact that similar oxygen recovery can be obtained

[13] AspenPlus™ has an inbuilt optimization capability using SQP convergence method, although the current version (v2006.0) does not support operations involving flowsheet structural changes, which include attempts to change the feed stages #

by simultaneously increasing the number of trays in HP-column and decreasing the number of equivalent-stages in LP-column. Evaluating the number of stages in these column calls for a rigorous cost analysis of a single HP-column tray vs. material cost estimation of structured-packings in a single "equivalent" LP-column stage. For simplicity, we assume the cost of each stage to be similar for both the columns. Table 2.10 gives oxygen flowrate corresponding to different number of trays in HP and LP columns. It must be noted that the feed-stage (which had been established earlier) is adjusted to keep the fraction of stages above and below the feed-stage constant, for each iteration. It can be clearly seen that LP–HP total stages corresponding to 35 & 40 give substantial recovery with the lowest number of stages. Adding further stages, marginally improves the oxygen production (by a maximum of 4 lbmol/hr), whereas lowering this number shows a significant degradation.

Sizing reflux-drum and column-base Using the heuristics of 10 minutes total holdup, the volume (V) in the reflux drum and in the column base can be calculated, assuming a cylindrical equipment with flat ends having length/height, L, and diameter, D:

$$V = \frac{\pi D^2}{4}\left(\frac{L}{D}\right)D$$

For the reflux drum, where a $\frac{L}{D}$ value of 2 is assumed,

$$D = \sqrt[3]{\frac{4V}{\pi\left(\frac{L}{D}\right)}}$$

$$L = \left(\frac{L}{D}\right)D$$

For the column base, the tray diameter values shown in Table 2.7 and 2.8 have been used,

$$L = \frac{4V}{\pi D^2}$$

These calculations are shown in Table 2.11. Bracketed dimensions show the rounded-off values used in actual design. The column base geometry is modeled as vertical

vessel with flat head[14]. The HP-column reflux drum is modeled as a horizontal cylindrical vessel, again with flat head type.

Table 2.11: Equipment sizing for LP-ASU

Column	**HP**	**LP**
Volumeric flowrate for reflux-drum (ft^3/min)	593.264	
Volumeric flowrate for column-base (ft^3/min)	312.898	302.258
Volume of reflux-drum for 10 min holdup (ft^3)	5932.64	
Volume of column-base for 10 min holdup (ft^3)	3128.98	3022.58
Diameter for reflux-drum (ft)	**15.57**	
	(15.5)	
Length for reflux-drum (ft)	**31.14**	
	(31)	
Diameter for column-base (ft)	**22**	**17**
Length for column-base (ft)	**8.23**	**13.32**
	(8.5)	(14)

2.2.2.2 Heat Exchangers

A rigorous internal zone analysis is used to calculate the internal pinch points for both the exchangers (main heat exchanger and subcooler). One zone is added for dynamic model corresponding to stream entry point (for feed stream at different temperature), stream exit point (for product streams at different temperature), phase change points (if a phase change occurs internally). Additional zones are also added adaptively by the simulator to account for nonlinearities in zone-profiles. The internal zone analysis is used to determine

- Internal pinch points
- UA (Overall heat-transfer coefficient × Area) and LMTD (Log Mean Temperature Difference) for each zone
- Total UA of the exchanger
- Overall average LMTD

[14]Other available head types include elliptical and hemispherical. Here a flat-type is chosen for brevity sake

Property calculations are done by the *flashing at each point* method[15]. Very detailed analysis like film coefficients and pressure drop calculations are not included in the MHeatX model. This is a major but allowable approximation to the dynamic calculations.

The subcooler (SCLR) block, unlike the main heat exchanger (MHX), involves gas-liquid heat exchange and hence, demands modification in various equipment design. We assume that these changes can be captured by correctly specifying the pipeline/ equipment volume and heat transfer coefficients between different phases. Fortunately, the averaged value of these coefficients is evaluated by Aspen depending on the zone-profiles generated in steady-state simulation.

Typical heat transfer surface area for high performance brazed aluminum plate-fin heat exchangers is given by 300–450 ft^2 per cubic feet of exchanger volume. For both the heat exchangers, each of the stream volumes are specified to be 100 ft^3. For modeling equipment heat capacity, an equipment mass of 1000 lb (per stream) and a specific heat of 0.22 Btu/lb-R, corresponding to brazed-aluminum, is specified.

2.2.2.3 Valves and compressors

All of the valves, except the expansion valves, VN2XPNDR and VO2XPNDR, represent pipeline losses on the flow line, and hence, pressure drop of the order of 0.1–0.2 psi are defined for each of them. None of these valves are attached to actuators for control purpose. The expansion/throttle valves, on the other hand, have a huge pressure drop. In this work, we use this valve for actuation purpose as well, to control the flowrate or pressure of the respective stream (LN2 and O2RICH). For brevity sake, we use a simple adiabatic 2-phase flash calculation for evaluating characteristics of these valves. Since the pressure-drop is significant, we can safely assume that valve-saturation will not occur at drastic load changes.

The booster air compressor is based on an isentropic centrifugal compressor model using ASME method, with an isentropic efficiency of 0.9 and mechanical

[15]Another method includes interpolating from flash tables, which leads to faster calculation in dynamic simulations. For temperature sensitive systems such as ASU, the rigorousness is prioritized over computation cost, and hence this method has not been used.

efficiency of 0.8. The product compressors have a typical compression ratio of 2, and are used for controlling the flowrate of product streams by manipulating the brake power[16]. These units have very fast dynamics and hence the *instantaneous* dynamic mode is chosen and does not include problems such as surge protection in real applications.

2.2.3 Steady-State Results

The steady-state profiles for HP and LP columns have been shown in Figure 2.7. It can be seen that the wave profiles for both nitrogen and oxygen are well balanced in the entire HP and LP-columns, proving high component recoveries. The detailed steady-state block and stream results are shown in Table 2.13 and 2.12 respectively. We move further to study an elevated-pressure ASU, which is more commonly utilized in an IGCC plant.

[16]The three basic ways to control flow through a compressor are suction throttling, bypassing (spill-back) or varying speed. The last is the most energy-efficient, but requires a variable-speed drive. In dynamic simulations, the compressor variable-speed operation can be approximated by having the output signal from a controller (F, P, T, etc.) adjust the work (brake-power) to the compressor.

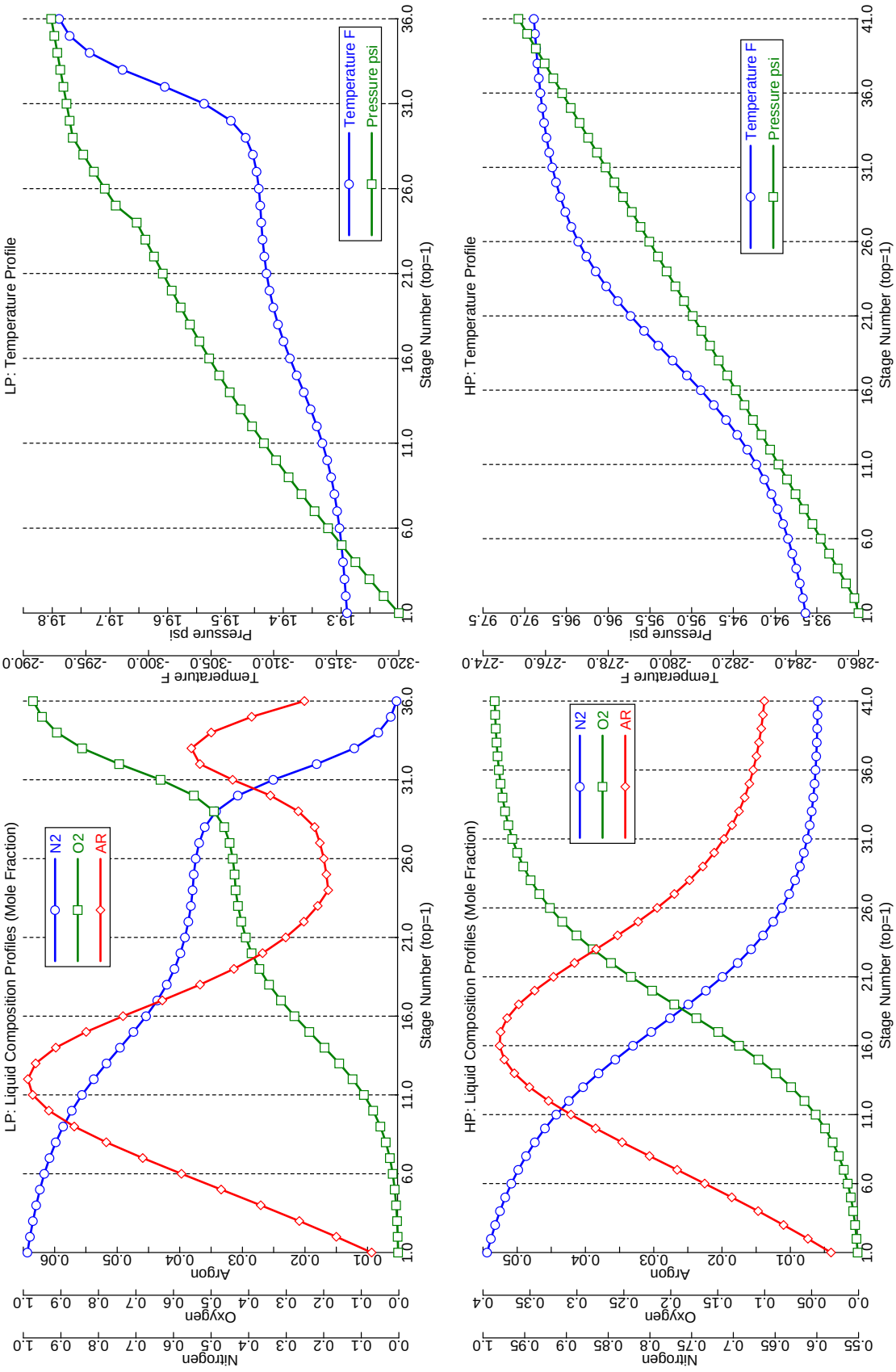

Figure 2.7: Steady-state (LP-ASU) profiles for LP-column (top) and HP-column (bottom)

Table 2.12: AspenPlus™ steady-state stream results for low-pressure ASU (see Figure 2.4)

Stream Name	**FEED**	**KA**	**EA-4**	**KA-2**	**EA-2**	**O2RICH**	**LN2**	**O2**	**O2-3**
Temperature (°F)	100.0	100.0	100.0	-275.8	-247.7	-275.8	-284.3	-292.8	85.0
Pressure (psia)	100.0	100.0	100.0	97.0	19.8	97.0	93.0	19.8	18.2
Vapor Fraction	1	1	1	0.977719	1	0	0	1	1
Mole Flow (lbmol/hr)	**66750.0**	58473.0	8277.0	58473.0	8277.0	32273.2	21199.8	14701.4	**14701.4**
Mass Flow (lb/hr)	1933066	1693365	239701	1693365	239701	958070	594971	472748	472748
Enthalpy (MMBtu/hr)	9.223	8.079	1.144	-154.337	-18.818	-155.330	-99.252	-37.979	0.745
Mole Flow (lbmol/hr)									
N_2	52138.4	45673.2	6465.2	45673.2	6465.2	19604.8	21093.5	295.6	295.6
O_2	13990.8	12255.9	1734.9	12255.9	1734.9	12228.4	22.3	13966.0	13966.0
AR	620.8	543.8	77.0	543.8	77.0	440.0	84.0	439.9	439.9
Mole Frac									
N_2	0.781	0.781	0.781	0.781	0.781	0.607	0.995	0.020	0.020
O_2	0.210	0.210	0.210	0.210	0.210	0.379	0.001	0.950	**0.950**
AR	0.009	0.009	0.009	0.009	0.009	0.014	0.004	0.030	0.030

Stream Name	**GN2**	**LP-N2**	**LP-N2-1**	**HP-N2**	**HP-N2-1**
Temperature (°F)	-315.9	-292.1	85.0	-284.2	85.0
Pressure (psia)	19.2	18.6	17.1	93.1	**91.6**
Vapor Fraction	1	1	1	1	1
Mole Flow (lbmol/hr)	47047.6	47047.6	47047.6	5000.0	**5000.0**
Mass Flow (lb/hr)	1319962	1319962	1319962	140325	140325
Enthalpy (MMBtu/hr)	-130.040	-121.903	2.440	-13.268	0.178
Mole Flow (lbmol/hr)					
N_2	46867.9	46867.9	46867.9	4974.9	4974.9
O_2	18.6	18.6	18.6	5.3	5.3
AR	161.1	161.1	161.1	19.8	19.8
Mole Frac					
N_2	0.996	0.996	0.996	0.995	**0.995**
O_2	0.000	0.000	0.000	0.001	0.001
AR	0.003	0.003	0.003	0.004	0.004

Table 2.13: AspenPlus™ steady-state block results for low-pressure ASU (see Figure 2.4)

Distillation Columns

Block Name	**LP**	**HP**
Top-stage Temperature (°F)	-315.88	**-284.30**
Condenser Heat Duty (Btu/hr)		**-113512339**
Condenser Medium Temperature (°F)		**-292.83**
Distillate Rate (lbmol/hr)	47047.55	21199.76
Reflux Rate (lbmol/hr)	20562.89	34770.17
Reflux Ratio	0.437	1.640
Bottom-stage Temperature (°F)	**-292.83**	-275.82
Reboiler Heat Duty (Btu/hr)	**113512351**	
Bottoms Rate (lbmol/hr)	1.00	32273.19
Boilup Rate	24986.32	57166.71
Boilup Ratio	24986.32	1.77

Expanders/Compressors

Block Name	**XPND-EA**	**BAC**
Indicated Horsepower (hp)	-2307.6	39.9
Net work required (hp)	-1846.1	49.9
Isentropic Efficiency	0.9	0.9
Mechanical Efficiency	0.8	0.8
Outlet pressure (psia)	19.98532	101
Outlet temperature (°F)	-247.66	101.77
Isentropic outlet temperature (°F)	-258.78	101.60
Vapor fraction	1	1

Heat Exchangers

Block Name	**MHX**	**SCLR**
Duty (Btu/hr)	-1.77×10^8	8.14×10^6
UA (Btu/hr-R)	11810148	1305546
LMTD (°F)	14.9	6.2
Min Temp Approach (°F)	10.0	4.9
Hot-end temp approach (°F)	15.0	16.3
Cold-end temp approach (°F)	11.4	4.9
Hot NTU	25.5	5.6
Cold NTU	25.3	3.8

2.3 Elevated-Pressure ASU

In the previous section it was seen that low pressure (LP) ASU cycles are based on compressing the feed air only to the pressure required to reject the majority of the nitrogen byproduct at atmospheric pressure. Feed air pressures typically vary between 65 to 105 psia (3.5 to 6 barg) depending on the oxygen purity and the level of energy efficiency desired. Elevated pressure (EP) ASU cycles produce all product and byproduct streams at pressures well above atmospheric pressures. An EP cycle is chosen when all or nearly all of the nitrogen byproduct will be compressed as a product stream. The air pressure of an EP cycle is optimized based on the tradeoffs between increased air compression power versus decreased product compression power. Or, the pressure may be set by air extracted from a gas turbine and supplied to the ASU. This has been discussed in a later section (Section 2.4) on operating cost analysis.

Most of the steady-state and dynamic design procedure is similar to low-pressure ASU, discussed at length earlier in this chapter. Hence, only a brief process description highlighting the changes in EP-ASU design have been given here.

2.3.1 Steady-State Design

The plant configuration in terms of operating pressures and flowrates for ASU are based on Case #2 reported in a recent NETL study [3]. The Aspen Plus steady-state flowsheet showing the major equipments for this study has been given in Figure 2.8. The steady-state design involves two columns operating at two different pressures so that the condensor for the high-pressure (high-temperature) column can be used as the reboiler in the low-pressure (low-temperature) column. To achieve the required temperature differential driving force (15°F) in the condenser/reboiler, the pressure of the LP-column is appropriately selected (sump pressure of 60.5 psi). The compressed feed stream, after air-pretreatment steps (not shown), is cooled using the product streams in a multistream heat exchanger (MHX), enters the HP-column bottom stage slightly above dew-point condition. We use a recycle stream, which compresses part of the gaseous nitrogen from top of LP-column and sends it back as an additional reflux to HP-column. This acts as the “heat-pump” for this

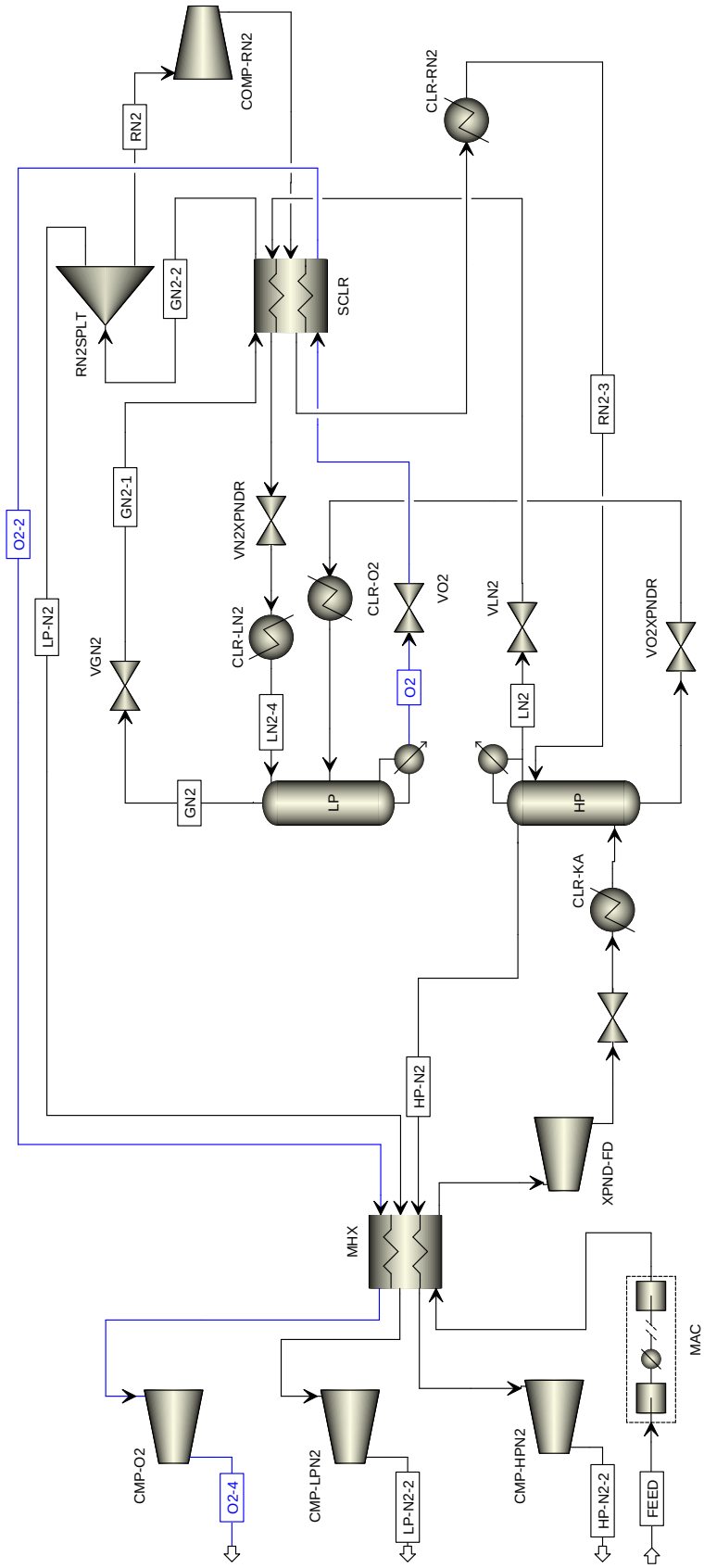

Figure 2.8: Process flowsheet showing elevated–pressure double-column ASU in AspenPlus™

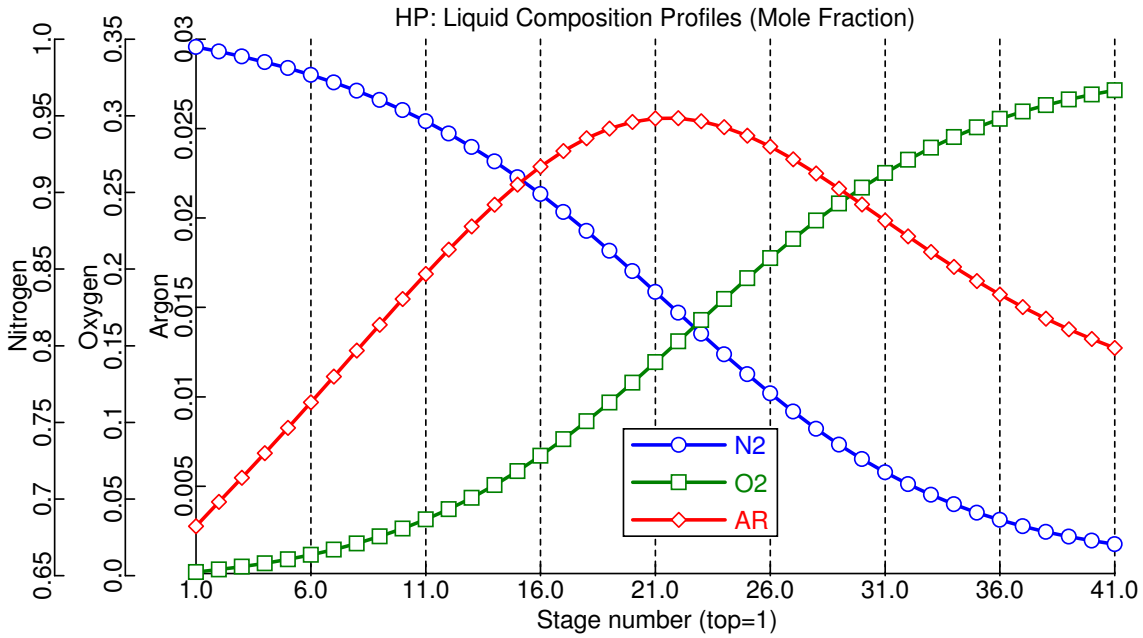

(a)

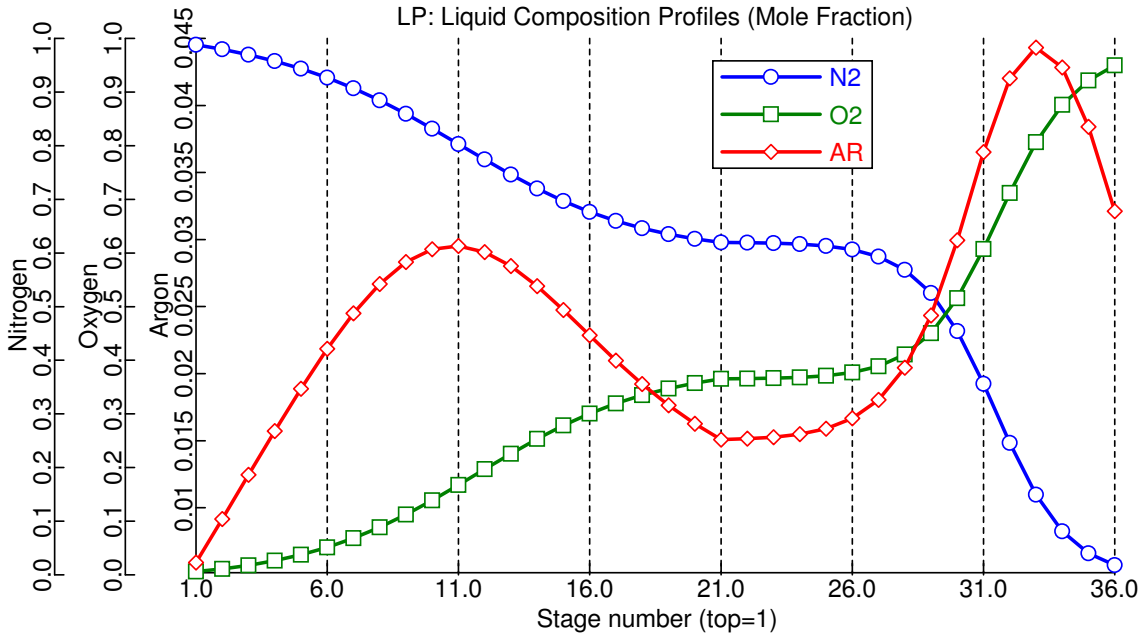

(b)

Figure 2.9: EP-ASU steady-state liquid phase composition profile of (a) high pressure column and (b) low pressure column

system and hence additional refrigeration in form of expanded air feed split to LP-column has not been used. Environment heat losses (or refrigeration losses) have, in general, been neglected. A subcooler (SCLR) is used to decrease the liquid nitrogen reflux (to the LP-column) temperature below dew-point before undergoing adiabatic expansion in valve VN2XPNDR, using the exiting gaseous nitrogen (GN2) and liquid oxygen (O2) streams as heat exchanger cold streams. Additionally, the temperature of the recycled-nitrogen stream (RN2), which stepped up due to heat generated in the recycled-nitrogen compressor (COMP-RN2), is brought down to a near bubble-point in the subcooler. Auxiliary coolers (CLR-KA, CLR-EA, CLR-LN2, CLR-O2) have been installed on relevant streams, prior to entering distillation unit. They have been assigned zero heat-duty values in the steady-state simulations, but could be used for providing additional refrigeration (at the cost of external refrigerants) and/or studying controllabity, switchability and testing purposes during dynamic operation.

The steady-state profiles for HP and LP columns have been shown in Figure 2.9a and Figure 2.9b respectively. The wave profiles for both nitrogen and oxygen are well balanced in the entire HP-column, LP-column rectifying part (stages 1-20) and LP-column stripping part (stages 21-35). For a fixed value of feed air flowrate and oxygen flowrates, we observe a certain liquid nitrogen (LN2) flowrate value where the oxygen mole-fraction (or molar flow) reaches a maximum. This behavior is shown in Figure 2.10. This value can be expressed as a function of oxygen flowrate (oxygen demand setpoint from a supervisory control layer) as:

$$F_{LN_2}^{Optimum} = f\left(F_{O_2}^{setpoint}\right) \tag{2.1}$$

Due to floating pressure arrangement, this relationship is non-linear; although a good linear-fit can be applied to Equation (2.1). A linear relation $F_{LN_2}^{Optimum} = 2.2266 F_{O_2}^{setpoint}$ has been used in our control study as a feed-forward/ratio control.

2.3.2 Dynamic Model

A simple packing and simple tray hydraulics has been assumed for LP-column and HP-column respectively. The main heat exchanger (MHX) and subcooler heat

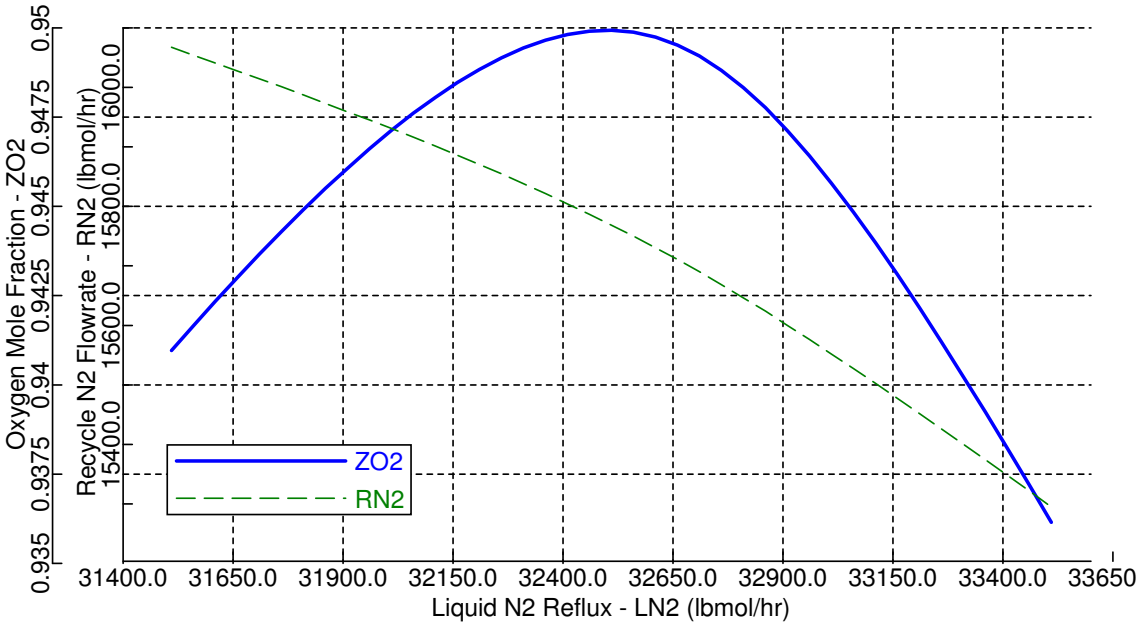

Figure 2.10: Graph showing optimal operating point at 100% load ($\mathbf{F_{air}}$ = 66750 lbmol-hr^{-1}, $\mathbf{F_{oxygen}}$ = 14600 lbmol-hr^{-1} and $\mathbf{F_{HP\text{-}N_2}}$ = 6000 lbmol-hr^{-1}. Note: Recycled nitrogen (RN2) flowrate varies to balance out reboiler-condensor heat duties.

exchanger (SCLR) have been modeled using detailed heat exchanger design (Hetran+) Aspen package which includes heat curve generation and zone analysis for multiphase HX calculations. All equipment heat storage capacity has been modeled for proper dynamic behavior when interacting with streams having different temperature and with the environment. Typical values of equipment mass, volume and heat-capacity values have been used from available literature. [93, 94, 95].

Similar to the LP-ASU, the condenser-reboiler heat duty is calculated dynamically using Equation (3.1). The details on how this is specified in dynamic simulations is given in the next chapter. Internal PI-based controllers are installed after the AspenPlus^{TM} file is exported to AspenDynamics^{TM} as a pressure-driven simulation. This has been discussed in the next chapter on controller design for EP-ASU. The dynamic simulation of this block involves 9,800 equations solved by an equation oriented approach using a variable step Gear's method.

2.4 Operating Cost Analysis

There are many different configurations in which an ASU may be operated, including the type of cycles (LP-cycles, pumped LOX cycles and recycled-N2 cycles) within the coldbox itself. Here we focused on double column LP-cycles only (it has been verified in our previous studies that pumped LOX cycles do not give significant advantages, especially for small air-integration).

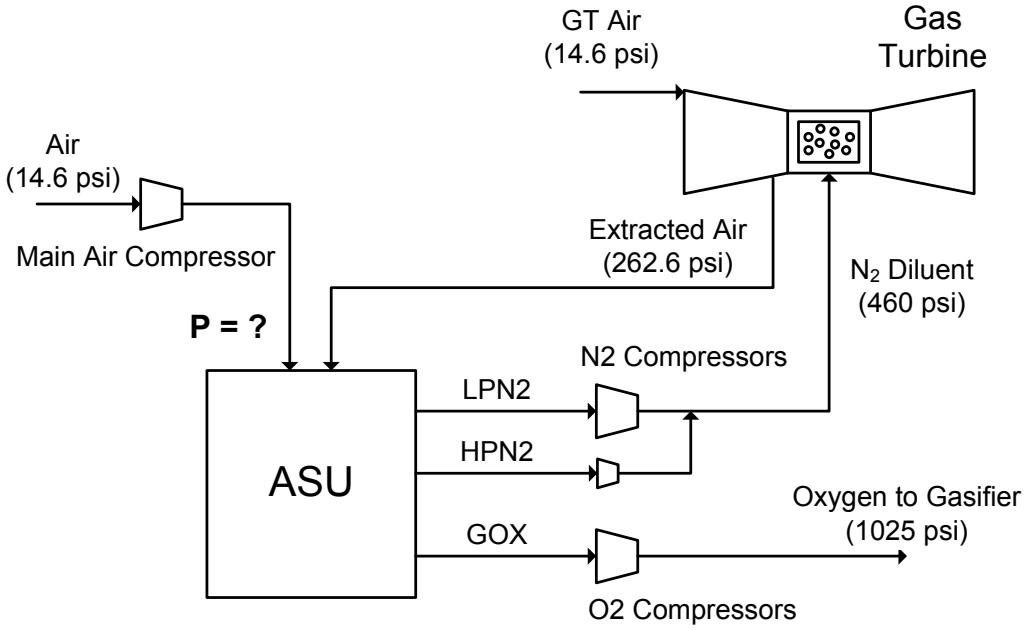

Figure 2.11: Schematic used for determining the optimal ASU operating pressure

In general, the optimal ASU configuration is determined by

- Oxygen and nitrogen supply pressure - this is vendor specified (1025 and 460 psi, respectively, in our case)
- Air extraction rate - this is a limit imposed by dynamic operability and controllability of the plant. In addition, the amount of desired air-cooling also determines this rate (for example, in IGCC CCS equipped plants, the proposed H2-based GT model requires high air-cooling rate and no air-extraction to ASU is done)
- Gas-turbine/compressor operating pressure (this is again vendor specified, 16.1:1 pressure-ratio in our case)

- Amount of nitrogen injection (full nitrogen injection, in our case)

We ran some optimization tests for three different air-integration cases, i.e., 0%, 15% and 30%. These involved the following assumptions

1. Desired oxygen flowrate is kept fixed (14200 lbmol/hr, 95% pure)
2. Molar flowrate of high-pressure nitrogen (HPN2 in Figure 2.11) equals 50% that of desired oxygen flowrate
3. No additional booster compressor is used inside the ASU unit, even at low pressures
4. Air expander is used to reduce the pressure of the major portion of feed air

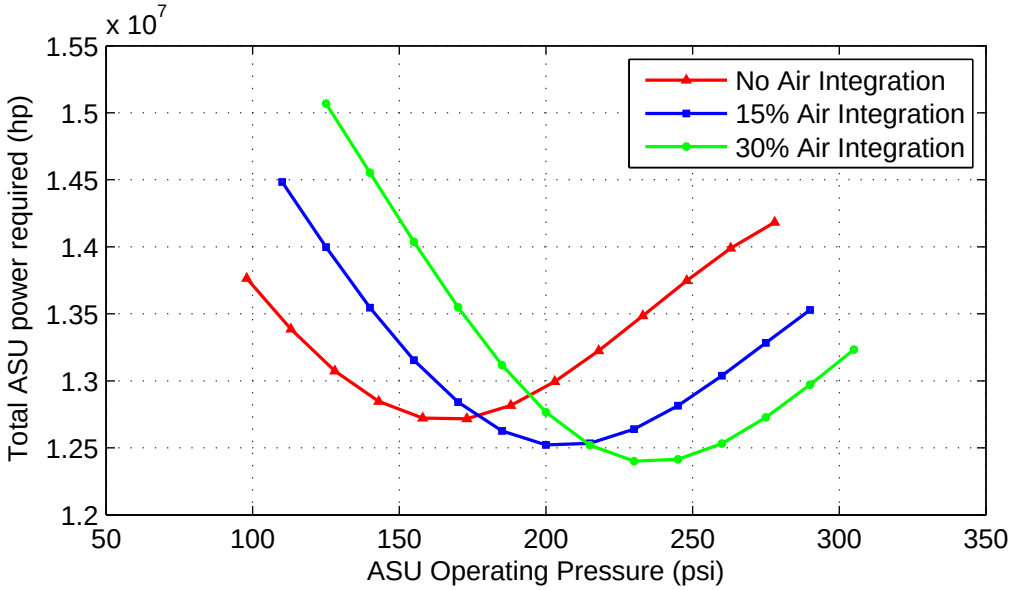

Figure 2.12: Plots showing optimum ASU pressure for three different extracted-air amounts

Here, the total ASU power is defined by sum of power required in air compressors (MAC), oxygen and nitrogen compressors, and portion of gas-compressor work utilized in air-extraction (minus a small amount of work extracted from the expander). The low total ASU power for higher air-integration clearly shows higher gas turbine-compressor efficiency compared to conventional centrifugal MAC (incorporating capital costs into cost/energy optimization will move this further in favor

of higher pressure ASUs). In addition, the plots show an optimum ASU operating pressure for each air-extraction level. At high ASU pressures, the decrease in separation efficiency (and hence, higher feed-air requirement to meet the same oxygen demand) outweighs the increasing product compressor suction pressures as shown in Figure 2.12.

In term of ASU design, we had the Parson's IGCC flowsheet where the ASU block (operating at 230 psi), was modeled as a component separator block and hence presented an "idealized" scenario. Since the separation efficiency inherently decreases at high pressures (governed by thermodynamic limitation), it is never possible to attain this level of efficiency using cryogenic distillation. Using nitrogen-recycle, high level of oxygen recovery can be attained (also a part of our previous study) at the cost of additional recycle energy (and controllability issues).

We had obtained a cryogenic ASU process model developed by Reaction Engineering International (DOE Cooperative Agreement No: DE-FC26-05NT42444), which used a three-column ASU and pumped LOX (where liquid oxygen is pumped to a higher pressure before vaporizing in main heat exchanger, at the cost of compressing feed-air to a very high value for generating liquid air), specifically designed for implementation into Parson's IGCC (Case #1) flowsheet. Table 2.14 lists the comparison between the REI version and our version (modified for IGCC Case #1) for performance comparison.

We see a much higher yield for ASU with recycled-N2 (98.8% recovery) compared to REI model (86.5% recovery). The recovery with LP-cycle is 92.3%. If nitrogen is not required at high purity, LP-cycles are far better as the compression costs are substantially less. Note that due to lower oxygen recovery, the need for inlet feed air flowrate are higher leading to an increase in compression cost. It has been shown that even with this increase in compression cost, the total energy requirement remain lower than that in a recycled-N2 system. In addition, the equipment cost increases in other two cases due to an additional pump (in pumped LOX) or a compressor (recycled N2).

In addition, there are many unrealistic discrepancies in the REI/DOE model (for example, flow from a low pressure to high pressure) which might substantially

Table 2.14: Comparison showing REI model with the previous studied model (both LP-cycle and recycle N2

	REI Model LOX cycle	**Current** LP-cycle	**Current** Recycle N2
No. of Distillation Columns	3	2	2
No. of (equiv.) stages	39, 32, 56	40, 35	40,35
Feed Streams			
Mole flow rate (lbmol/hr)	60500	60500	60500
Temperature (°F)	200	200	200
Pressure (psi)	190	190	190
Oxygen Product Stream			
Mole flow rate (lbmol/hr)	**11219.2**	**12342**	**13200**
Temperature (°F)	90	90	90
Pressure (psi)	125	125	125
Purity (mole fraction)	**0.979**	**0.95**	**0.95**
HP Nitrogen Stream			
Mole flow rate (lbmol/hr)	6627	6627	6627
Temperature (°F)	50	50	50
Pressure (psi)	182	182	182
Purity (mole fraction)	0.9778	0.987	0.995
Dil. Nitrogen Stream			
Mole flow rate (lbmol/hr)	42031.7	41530	40673
Temperature (°F)	90	90	90
Pressure (psi)	56.4	52	52
Purity (mole fraction)	0.975	0.974	0.999
Power Supplied (kW)			
AIR Compressor-1	1238.82	5635	3652
AIR Compressor-2	21722.72		
Oxygen Compressor		8459	6120
Recycle Compressor			11802

increase the operating costs. The model being not "plant-ready" and operating at steady-state "instantaneous" mode, cannot be used to analyze pressure drops at different flows and hence do not give accurate operating costs with load changes.

2.5 Discussion and Conclusion

This chapter focuses on the steady-state design of low pressure (LP) and elevated pressure (EP) ASU. These steady-state models have been developed in AspenPlus^{TM} software with the sole objective of them serving as a good or "realistic" candidates for control studies in terms of generating linearized control-models.

In absence of a real plant, each Aspen-model thus designed may also serve as a "surrogate" non-linear plant-model to test the controller performance on, and thus provide certain credibility to the designed controller scheme. With this motivation in mind, every minute equipment detail of the ASU, which can be evaluated by Aspen (in its current version), has been provided based on available open and semi-closed literature. In addition, many optimization studies which involved decision for number of stages, feed-entry stage and various internal flowrates were done, to ensure maximum oxygen-recovery for a given feed-air flowrate (leading to a minimization in operating cost). Pursuing the path of developing a "realistic" model, various valves, pumps and compressors have been incorporated to make the flowsheet fully pressure-driven (or having the ability of handling pressure dependent flows), similar to a real plant. The chapter was closed by providing an operating cost analysis, specifically for determining the optimal ASU pressure, when integrated with the gas-turbine. This study was done for different GT-air extraction (or percentage of air-integration amount) and it was concluded that higher air-integration lead to a larger optimal ASU pressure (and a lower ASU power at this optimum pressure) compared to lower air-integration. In addition, a comparison of different elevated-pressure designs and a previously developed NETL-REI steady-state ASU model has been given to validate and justify the work given in this chapter. In the next chapter, we identify various non-linearities and control challenges involved in the ASU and provide different control schemes based on the models developed in this chapter.

CHAPTER 3
CONTROLLER DESIGN OF AIR SEPARATIONS UNIT

This chapter describes the design of a control structure for the air separation plant-model developed in Chapter 2. Most of the literature related to this subject are limited to patented or "closed" studies as early as 1950s, predominantly for high purity ASUs operating as separate plants producing compressed liquid oxygen, nitrogen and/or argon. As gasification technology gained prominence, especially in the purview of power generation, ASUs that were able to cope up with elevated pressure operation, high throughput and rapid fluctuation of product demand needed to be developed. These stringent operating conditions required highly efficient control structure and numerous studies were made available in open and closed literature during early 1990s. Some of these studies are mentioned below.

A review article on air separation control technology by Vinson [96] gives a general overview of some of the many control challenges involved. Many studies have been pursued on dynamic modeling and multivariable control of ASU using first-principle models [91, 97] and nonlinear wave models [98, 92]. These studies, along with the work cited in previous chapters, were done with significant assumptions that might diminish energy-integration effects on dynamics and controllability of the entire plant. None of these studies consider the possibility of positive feedback effect due to feed-product heat integration in the main heat exchanger (also mentioned in previous chapter). Additionally, the condenser-reboiler heat effects have been decoupled and the behavior of one of the columns is investigated independently from the rest of the ASU process, by usually considering just a single variable (temperature) effect on the other column as an input variable. These studies show a significant void in open literature for "realistic" plantwide control of ASU and motivate further work in this area. In this chapter we attempt to study some of the controllability issues and propose different control layouts for efficient oxygen flowrate setpoint tracking.

In this chapter, we present a detailed dynamic study (in Aspen Dynamics) of

pressure, temperature and purity swing effects inherent in the ASU due to air-side integration with gas turbine. We further try to understand the variable (material and/or energy) perturbation or control move necessary to maintain the desired product purity and flowrate along with its physical significance. This chapter (along with the previous chapter) of the report is based on the papers presented in [84], [85], [86], [87] and [88]. Furthermore, in this thesis work, only a direct composition control scheme has been used, in contrast to temperature control scheme (both conventional and differential) [99]. Other possibilities include controlling three or even four compositions, or inferential temperature control instead of, or in combination with, composition control. Studying these structure has been discussed within the scope of future work.

3.1 Moving to Dynamic Simulation in AspenDynamics™

In Chapter 2, the condenser-reboiler balance is met by varying the feed-air splitter (FEEDSPLT in Figure 2.4) using a "Design Spec/Vary" function. In addition, the *medium* temperature of the condenser is made equal to the reboiler temperature as shown in Table 2.13. In principle, the heat duty is dependent on the condenser-reboiler temperature difference as given in Equation(3.1).

$$Q_{reb} = -Q_{cond} = UA\,(T_{top,\ HP} - T_{bottom,\ LP}) \tag{3.1}$$

where Q_{reb} and Q_{cond} are LP-column reboiler and HP-column condenser heat duties respectively. $T_{top,\ HP}$ is the temperature at the top of the HP-column and $T_{bottom,\ LP}$ is the temperature at the bottom of LP-column. UA is the product of overall heat transfer coefficient and effective heat transfer area, which is automatically evaluated during steady-state calculations.

When moving to dynamics mode, this balance is imposed by the following Fortran statements within AspenDynamics™(AD),

```
Blocks('LP').QRebR = -Blocks('HP').Condenser(1).Q;
Blocks('HP').Condenser(1).Tmed = Blocks('LP').TReb;
```

This mathematically specifies the reboiling liquid in the LP-column as the condens-

ing medium for the HP-column and that the heat transfer between the column is driven by the temperature difference between the two. For having this in AD, we make the reboiler heat duty `Blocks('LP').QRebR` and condenser cooling-medium temperature `Blocks('HP').Condenser(1).Tmed`, "free" or unspecified. As a simplified assumption, the ability to store energy in the heat-transferring wall is neglected. Internal PI-based controllers are installed after the AspenPlus^{TM} file is exported to AspenDynamics^{TM} as a pressure-driven simulation. This has been discussed in the next section. The dynamic simulation of this flowsheet involves 10,700 equations and 410 states, solved by an equation oriented approach using a variable step Gear's method (maximum order of 5). The details of the regulatory layered and higher layered controller design are given in the following section(s).

3.2 Controller Design for Low-Pressure ASU

For LP-ASU with a simple LP-cycle, we identify the controlled variables (all measured) shown by various indicators in Figure 3.1. All of the manipulated variables are indicated by dashed arrows signifying flowrate changes on the corresponding streams. These changes, in reality, are attained by direct valve-actuation or manipulating brake power of the downstream compressor (not shown) using a simple PI-based flow controller at the inner-most loop (discussed later). The *overall* controllable variables and manipulable inputs, along with their nominal steady-state values, are shown in Table 3.1

Table 3.1: List of control input/output variables for LP-ASU

Inputs			**Outputs**		
Variable	**Nominal**	**Units**	**Variable**	**Nominal**	**Units**
F_airASU	66742	lbmol/hr	Z_O2	0.95	lbmol/lbmol
F_EA	8280	lbmol/hr	Z_HPN2	0.995	lbmol/lbmol
F_HPN2	5000	lbmol/hr	Z_LPN2	0.997	lbmol/lbmol
F_O2	14700	lbmol/hr	P_LPTop	19.2	psi
F_LN2	21765	lbmol/hr	L_LPBot	7	ft
F_O2Rich	31695	lbmol/hr	L_HPBot	4.25	ft
F_GN2	47042	lbmol/hr	L_HPTop	7.75	ft
F_Reflux	1009236	lb/hr			

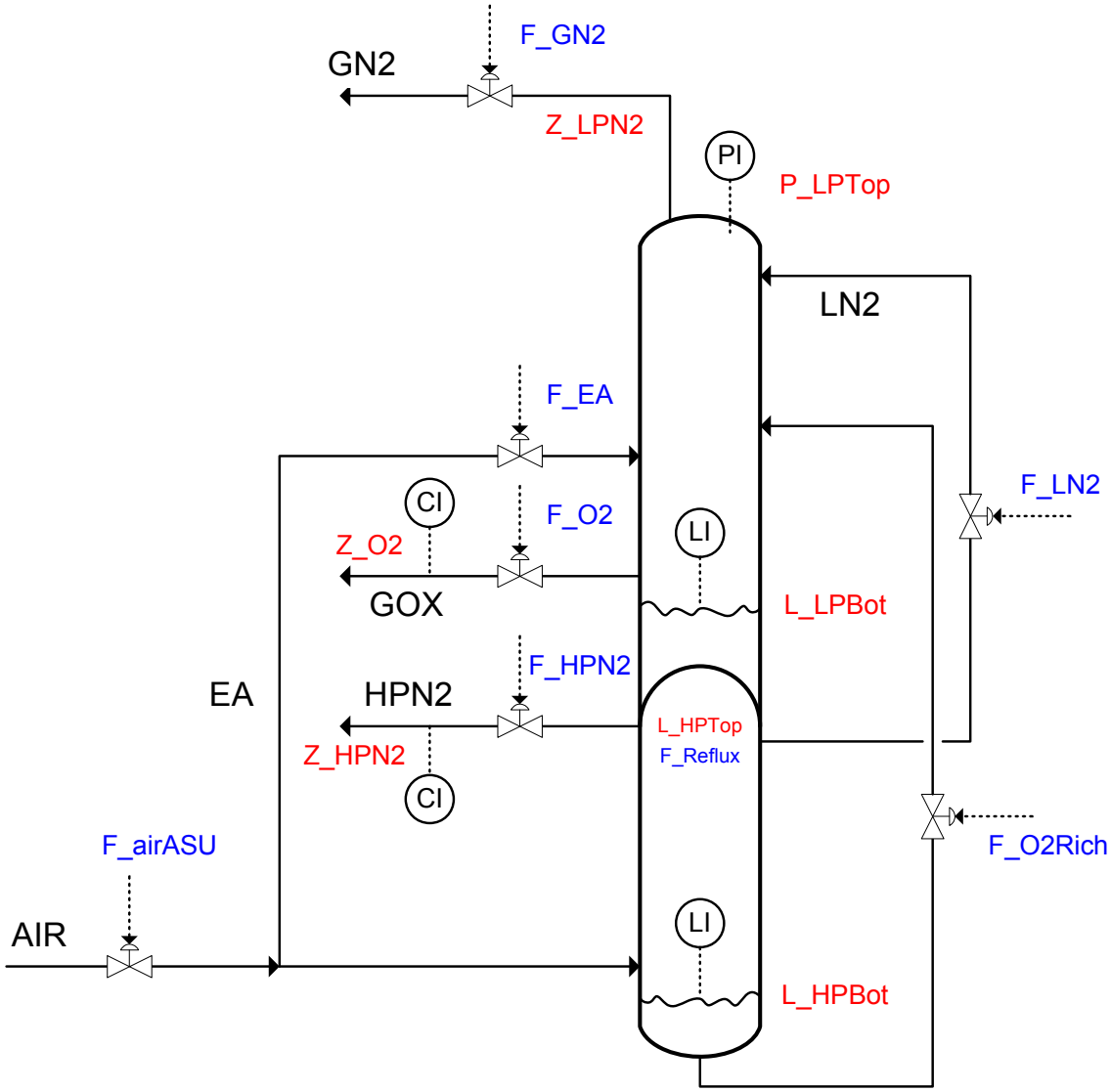

Figure 3.1: The proposed PID control structure for ASU in Aspen Dynamics.

As mentioned in Chapter 2, the HP-column condenser is *fictitious*[17] and is, in reality, a continuous pipe passing through the condenser-reboiler HX, where the condensing heat duty affects the refluxed-flowrate directly rather than the condenser drum liquid-level. This phenomenon is mimicked in the current study by pairing F_Reflux with L_HPTop using a high-gain P-only level controller, which instantly directs any condensing-duty and/or pressure disturbances towards the column through refluxed liquid flowrate, effectively making it a similar to a continuous stream/pipe

[17]Hence, the output variable L_HPTop (Figure 3.1) has no physical meaning

without any intermediate holdup.

3.2.1 Structure of Regulatory Control Layer

The main objective of this layer is to provide sufficient quality of control to enable a trained operator to keep the plant running safely without the use of higher layers in the control system. The regulatory control layer should be designed such that it is independent of the mode of operation.

Flow control loops To reduce drift caused by pressure changes and to avoid nonlinearity in control valves, we use flow controllers on various streams

- Feed flow control is achieved indirectly by making the upstream pressure "free" and the feed flowrate "fixed". This is a very simplified approach, where we let the simulator to determine the upstream pressure to generate a certain given feed flowrate (F_airASU).

- High-pressure nitrogen flow controller (FCHPN2) changes the nitrogen compressor (CMP-HPN2) brake-power or suction-side pressure to control flowrate (F_HPN2). The setpoint is generally sent as a fixed ratio of oxygen demand (see page 83).

- Gaseous oxygen flow controller (FCGOX) changes the oxygen compressor (CMP-O2) brake-power or suction-side pressure to control flowrate (F_O2). The setpoint is either provided by a higher-level controller or as a direct throughput manipulation.

- Liquid nitrogen reflux flow controller (FCLN2) adjusts a valve (VLN2) for liquid nitrogen flowrate (F_LN2) control. Setpoint is provided by a higher-level controller.

- Expanded air flow controller (FCEA) manipulates the turboexpander (XPND-EA) brake-power to control expanded air flowrate (F_EA). The setpoint is provided by a higher-level controller.

Pressure control loops In addition to stabilizing unstable modes (discussed below), the regulatory layer has a primary objective to prevent the plant from drifting away from its desired operating point on the short time scale. Pressure dynamics are generally too fast, so pressure drift is avoided by controlling pressure at selected locations in the plant. Generally, the pressures in the distillation columns either use condenser heat-duty or distillate rate (vapor) as manipulated variables. For the LP-column, the pressure at the column top (P_LPTop) is maintained using a pressure controller (PCLP) by changing the nitrogen compressor (CMP-LN2) brakepower (which in turn changes the suction side pressure and hence the flowrate, F_GN2).

For the HP-column, the integration of condenser-reboiler, where the heat-duty cannot be independently manipulated, makes up loose the ability to control the HP-column top pressure. In essence, keeping the pressure of HP-column floating is desirable due to following reasons:

1. In a floating/sliding pressure arrangement, as the HP-column top pressure varies with load-changes, the equilibrium temperature changes as well. This changes the reboiler-condenser temperature differential and hence the corresponding heat-duty. This in turn brings back the pressure to a new operating steady state. Since the system is self-stabilizing, we do not need to worry about regulating this pressure.

2. In case of gas turbine/compressor integration, the sliding pressure ASU is much more energy-efficient as the need for a flow control valve is eliminated, avoiding significant pressure drops across throttle.

3. This arrangement also permits higher range of upstream/downstream flow rates without reaching operating constraints.

Other alternate arrangements include pressure control using high-pressure nitrogen stream (F_HPN2) or even feed air stream. These cases have been studied in the past and have proved very inefficient, considering both energy-usage and oxygen-production, in spite of the operability and controllability being easier. These studies have not been included in this thesis.

Another interesting thought relates to the operating pressure of the low pressure column. The setpoint signal to the pressure controller (PCLP) can be used as an additional manipulated input for our process. The dual distillation columns, similar to double-column ASU, can be modeled using a "spring" analogy as given by Koggersbøl et al., 1996 [80]. We reasoned that one end of the "spring" needs to be fixed, to avoid large conflicting swings in both the column pressures, making controllability extremely difficult. In reality, the LP-column operating pressure should be determined by the higher optimization layer taking overall plant economics (including cost of nitrogen compression, nitrogen integration, GT integration etc.) into consideration. Hence, in this technical report, we limit our study to fixed LP-column top pressure.

Temperature control loops Temperature measurements are fast and reliable, so temperature loops are frequently closed to avoid drift. In current flowsheet, we hardly see any operational heater/coolers, since that would involve either generation or loss of expensive refrigeration. It must be noted that the Aspen heater/cooler blocks inside the cryogenic region in Figure 2.4 are for testing purpose only and have been assigned a zero heat-duty. A temperature controller (TCBACClr) is installed on the booster compressor (BAC) aftercooler for preventing temperature drifts with varying flowrates.

Stabilization of unstable modes (including liquid levels) Before moving to performing step-tests for the process and design regulatory/supervisory control layer, we need to ensure that the system is open-loop stable by eliminating all RHP-poles in the process. This requires closing the corresponding unstable nodes through a feedback controller. The manipulated variable used depends on the physical proximity to the node and/or is chosen among the ones which leads to the instability.

The level in the HP-column sump is a highly unstable node, where initial simulations revealed that the sump liquid completely drained or over-flooded out with slight disturbances in reboiler-condenser heat duty or column pressure. Without any controller, this behavior is exacerbated, in terms of run-away rate from steady-state, due to pairing of HP-column reflux-flowrate with the condenser drum level,

transferring column-top disturbances to the bottom through the reflux liquid. Since the throughput manipulator is at the feed, we use the liquid flow out of the column bottom (F_O2Rich) to control the sump-level (L_HPBot). An alternate pairing uses feed-flow to control the sump-level which, in our case, leads to slower responses due to pure vapor feed[18].

The control of liquid level in the "virtual" HP-column condenser was discussed earlier (page 71). After closing both the pressure, flow and HP-column level loops, we analyze the sump-level in LP-column drum (L_LPBot) for instability and, in addition, to determine its sensitivity to different manipulated inputs for evaluating best possible pairing. Figure 3.2 gives the control output step responses to various manipulated inputs listed in Table 3.1. Figure 3.3 and 3.4 give the responses of various heat-duty/work and column temperature/pressure to similar manipulated input step changes respectively. Upon closely observing Figure 3.2, we find that the LP-column sump level fails to attain new steady-state value for step changes in expanded-air flow, oxygen flow and high-pressure nitrogen flow, proving our system still contains RHP eigenvalues. These three inputs also serve as good stabilizing-controller candidates for the integrating level responses. We chose expanded-air flowrate (F_EA) as the manipulated input to be paired with LP-column sump-level due to following reasons

1. F_EA has the highest sensitivity towards the sump-level in terms of reaching instability.

2. Expanded air feed tray (stage 29) has the close proximity to LP-column sump (stage 36).

3. The other two "sensitive" inputs serve as a throughput manipulator to the system and may not be available for pairing for all possible plantwide controller designs.

Summary of the regulatory control layer Table 3.2 gives a summary of the regulatory loops we decided to "close" for our study, along with the controller tuning

[18]Sump-level changes, in this case, occurs indirectly though flashing of vapor, due to direct effect of feed flowrate on column pressure

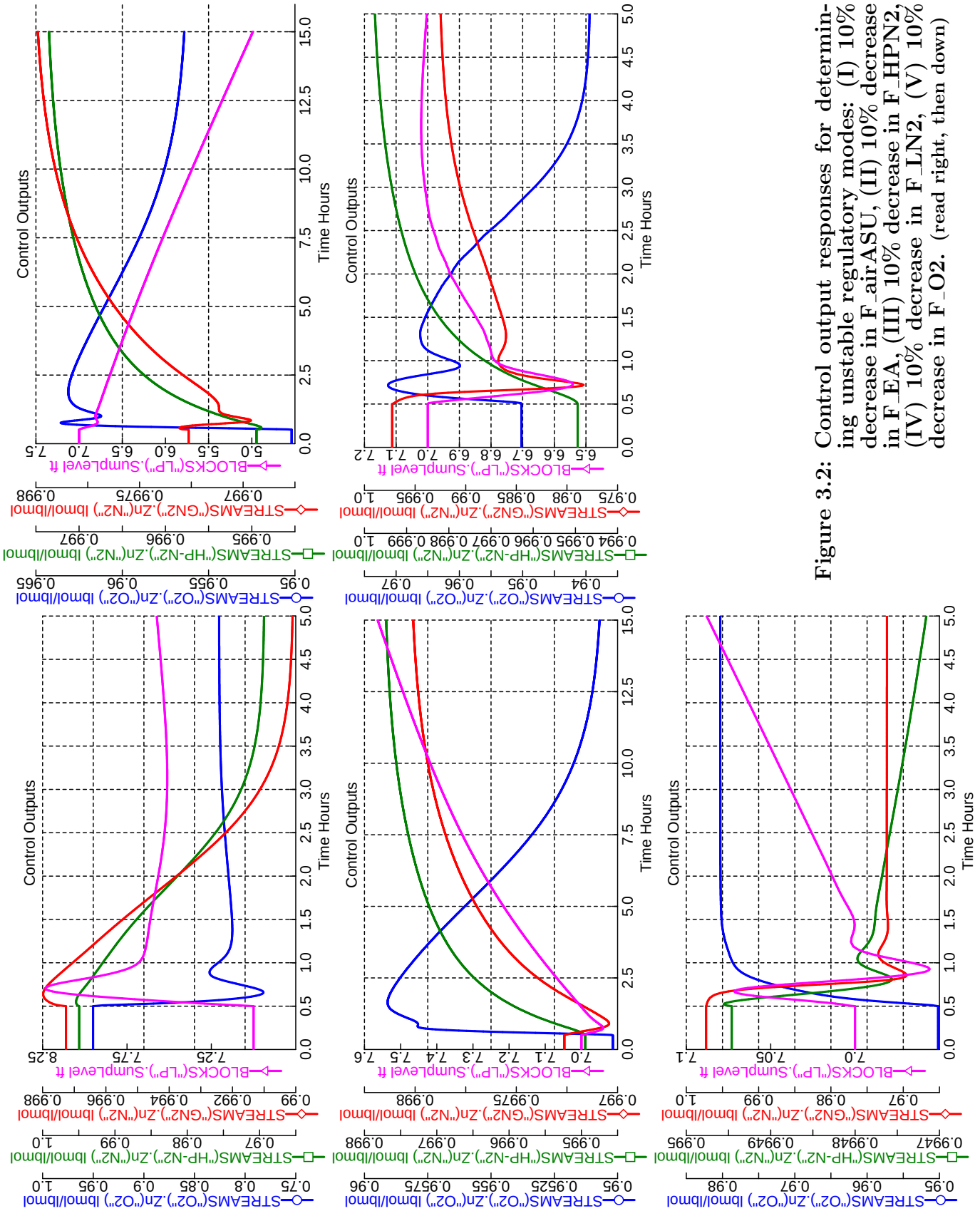

Figure 3.2: Control output responses for determining unstable regulatory modes: (I) 10% decrease in F_airASU, (II) 10% decrease in F_HPN2, (III) 10% decrease in F_EA, (IV) 10% decrease in F_LN2, (V) 10% decrease in F_O2. (read right, then down)

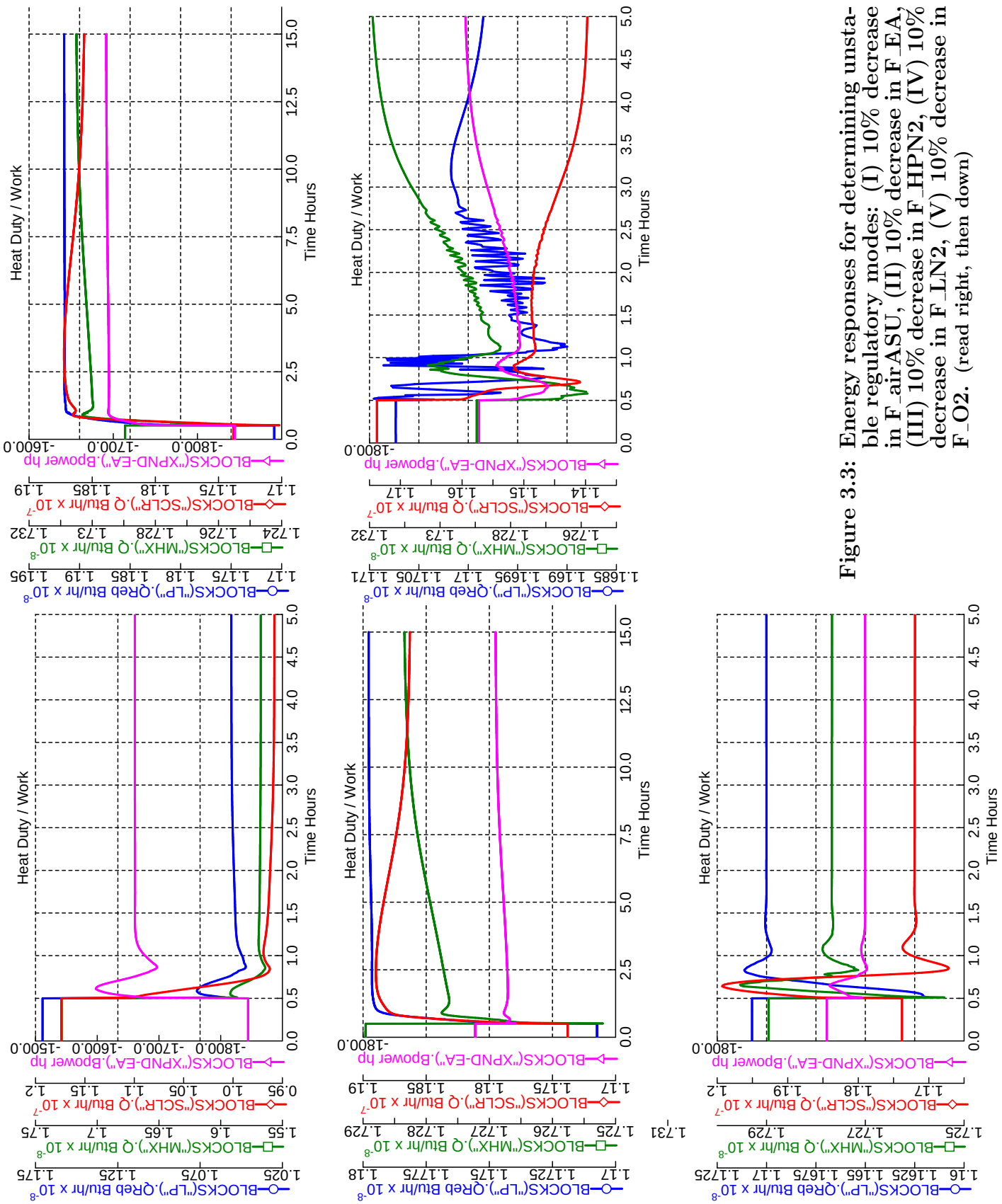

Figure 3.3: Energy responses for determining unstable regulatory modes: (I) 10% decrease in F_airASU, (II) 10% decrease in F_EA, (III) 10% decrease in F_HPN2, (IV) 10% decrease in F_LN2, (V) 10% decrease in F_O2. (read right, then down)

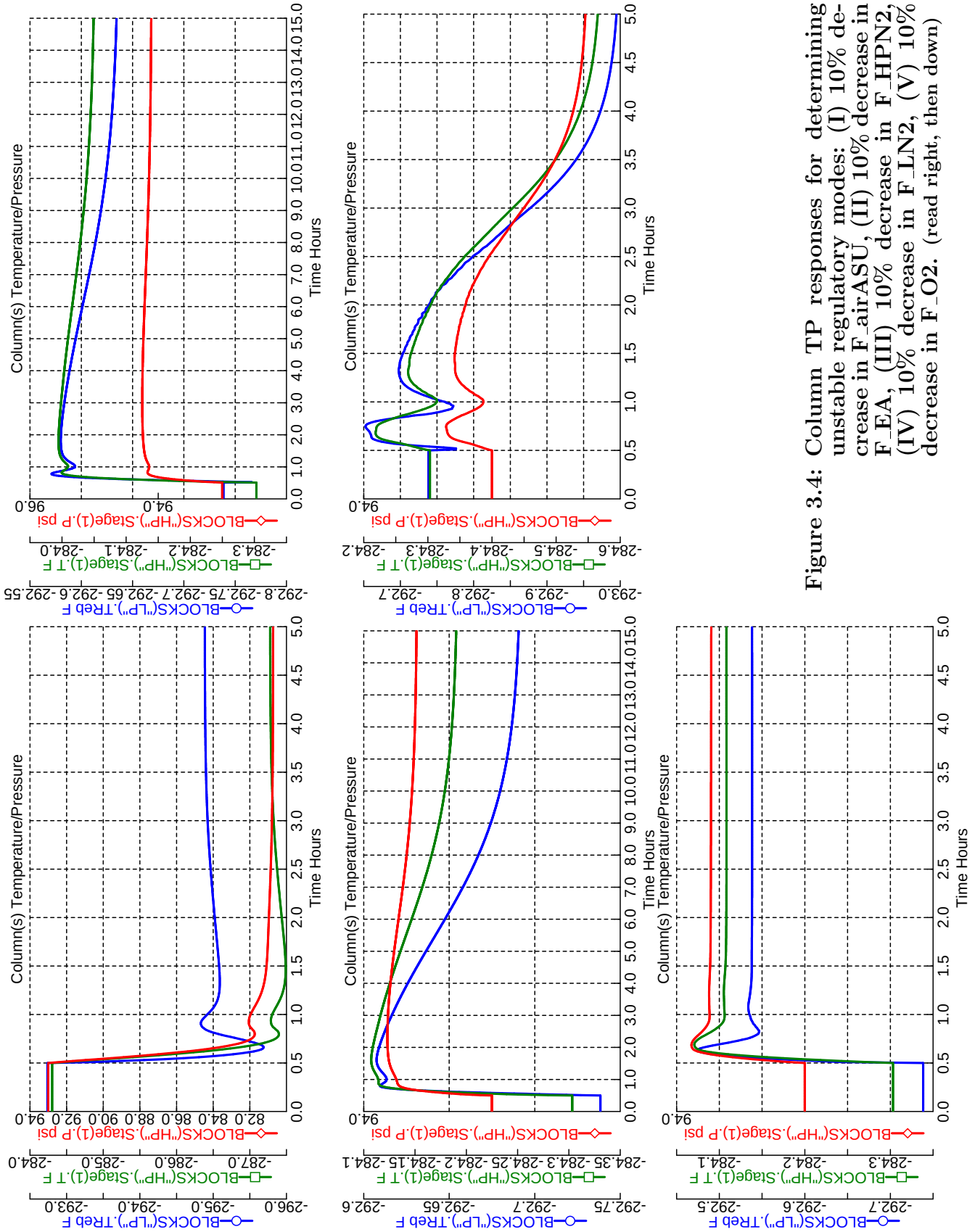

Figure 3.4: Column TP responses for determining unstable regulatory modes: (I) 10% decrease in F_airASU, (II) 10% decrease in F_EA, (III) 10% decrease in F_HPN2, (IV) 10% decrease in F_LN2, (V) 10% decrease in F_O2. (read right, then down)

parameters. It must be noted that all of the level controllers are P-only controllers leading to slight offset with setpoints changes/disturbances, but reducing phase-shifts. For flow and pressure controllers, where we do not desire any offset, PI controllers have been used. Since these are all very fast loops, the tuning parameters have been selected based on heuristics and/or recommended default values. The AspenDynamics^{TM} flowsheet with regulatory controller in place has been given in Figure 3.5. The composition control loops (CCZO2, CCZN2, CCZGN2) have not been closed yet. This will be discussed in the next section.

Table 3.2: List of regulatory controllers for LP-ASU

Controller	**Process Variable**	**Manipulated Input**	K_c (%/%)	τ_I (min)
FCHPN2	F_HPN2	CMP-HPN2 (Brake Power)	2	5
FCGOX	F_O2	CMP-O2 (Brake Power)	2	5
FCLN2	F_LN2	VLN2 (Valve Position)	2	5
FCEA	F_EA	XPND-EA (Brake Power)	-2	5
PCLP	P_LPTop	CMP-LN2 (Brake Power) / F_GN2	-6	12
TCBACClr	T_EA	CLR-BAC (Heat Duty)	5	10
LCHPBot	L_HPBot	VO2XPNDR (Valve Position) / F_O2Rich	-20	
LCHPTop	L_HPTop	F_Reflux (Reflux Mass Flow)	-20	
LCLPBot	L_LPBot	F_EA	20	

3.2.2 Structure of Supervisory Control Layer

With the regulatory control in place, there are still three composition loops to be closed, and we will proceed with a more detailed multiloop SISO control design based on RGA methods and later, a multivariable MPC design. It can be seen from Figure 3.5 that we have included dead-time / time-delay blocks (with 10 min delay) in the path of every composition measurement to mimic slow composition detectors/analyzers seen in a real plant.

3.2.2.1 Proportional-Integral-Derivative (PID-based) Control

The control objectives are to maintain stable on-specification operation in the face of disturbances in throughput and feed composition and to minimize energy consumption. We limit our study to conventional PID control structures in this

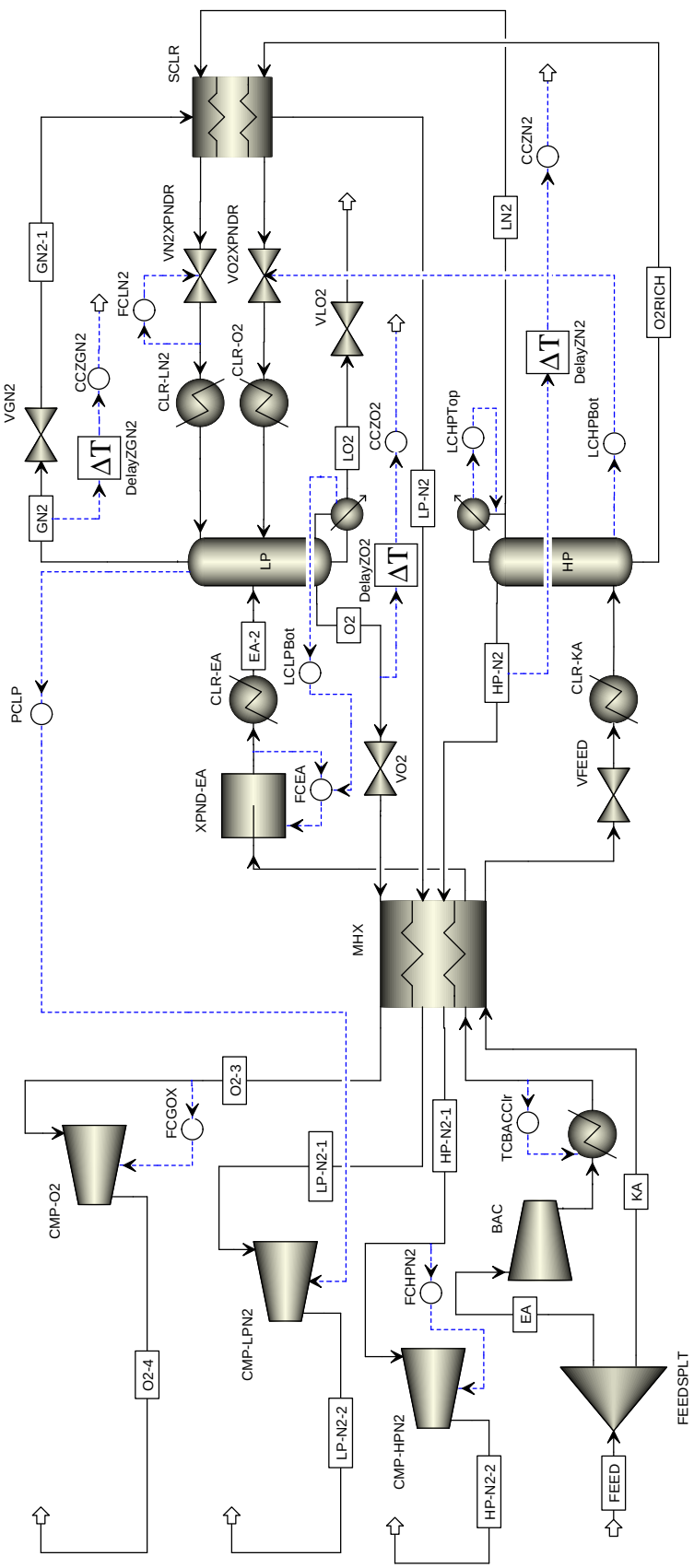

Figure 3.5: Process flowsheet showing low–pressure double-column ASU in AspenDynamics^{TM} with regulatory layer control installed

subsection. Conventional distillation control wisdom says that it is usually more effective to control impurity levels than to control purity levels. The use of impurity instead of purity is a standard process control principle because one wants to control a variable that is sensitive to the manipulated variable. A change in impurity from 1 to 1.5 mol % is much greater (on a relative basis) than the corresponding change in purity from 99 to 89.5 mol %. The principle is particularly important in distillation control where changes in trace amounts of other nonkey components can make it impossible to maintain a key-component purity, but maintaining an impurity of the other key component is still possible.

Modes of operation While designing a control layer for a plant which serves as sub-process to a bigger plant, we often have to consider our main plant objectives. A standalone ASU plant, would likely operate in a way to maximize production rate. As the feedrate is increased, we reach a point where some flow/pressure variable[19]

[19]In an ASU, this variable may be the vapor flowrate inside the column (constrained by flooding) or pressure in the HP-column (constrained by equipment pressure withstanding capacity)

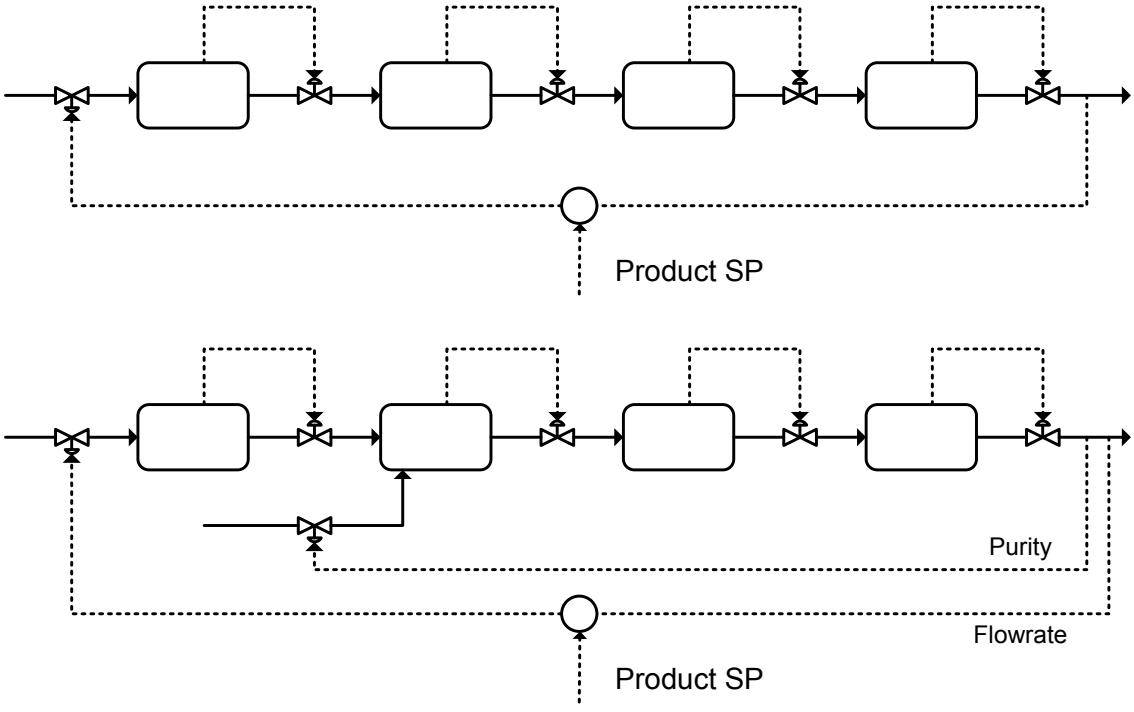

Figure 3.6: Examples of inventory control designed for a *given feed rate* with production rate as the through-put variable

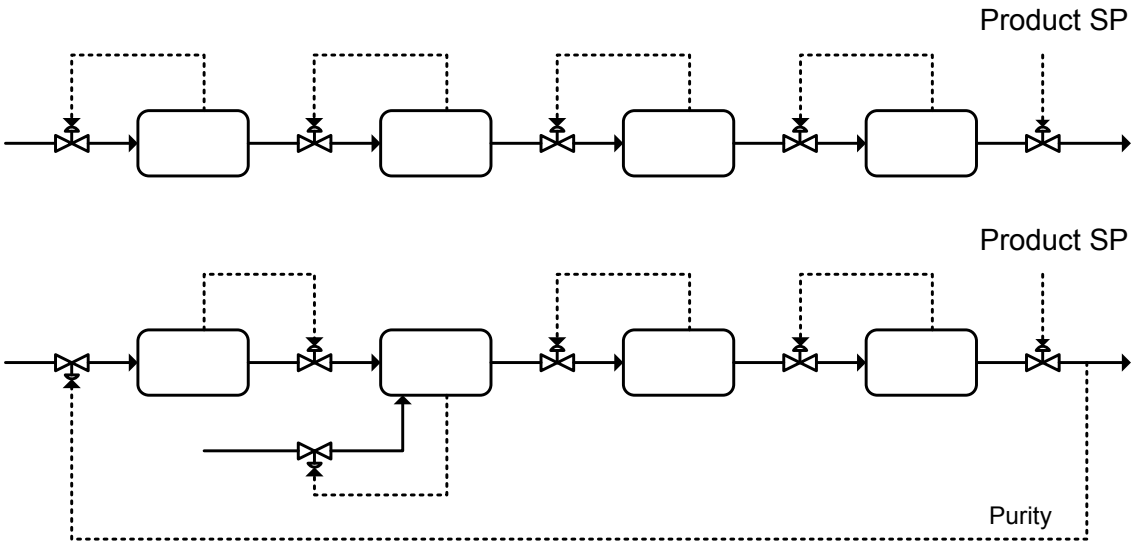

Figure 3.7: Examples of inventory control designed for a *given production rate* with production rate as the through-put variable

internally in the plant reaches its constraint and becomes a *bottleneck* for further increase in production. For an ASU operating as part of an IGCC power plant, the main objective is to meet the gasifier oxygen demand in a dynamically "best" possible way. Since the ASU is designed at a 100% plant load (in terms of electricity demand), we select the oxygen production rate as the through-put manipulator. Figure 3.6 and 3.7 show two examples each of inventory control designs where control structure decisions are based on fixed feed rate and production rate. Based on our selection of through-put variable, we would prefer the second design(s), since the first set of design i.e., using feedrate as a manipulated variable for controlling the through-put variable, will give a very "slow" loop dynamically because of long physical distance.

Identifying relevant control inputs/outputs Figure 3.8 gives us responses of the three product purities to step changes in "remaining" input variables. It is clear from the graphs that the oxygen product purity is strongly dependent on feed-air flowrate. To ensure this, we construct the RGA matrix, when $u =$

$\begin{bmatrix} \mathrm{F_{airASU}} & \mathrm{F_{HPN2}} & \mathrm{F_{LN2}} \end{bmatrix}$ and $y = \begin{bmatrix} \mathrm{Z_{O2}} & \mathrm{Z_{HPN2}} & \mathrm{Z_{LPN2}} \end{bmatrix}$ as

$$\Lambda = \begin{bmatrix} \underline{1.0944} & -0.0856 & -0.0088 \\ 0.0480 & 0.7284 & 0.2237 \\ -0.1423 & 0.3573 & 0.7851 \end{bmatrix}$$

which shows that Z_O2–F_airASU is one of the MV-SISO loops we need to close.

The high-pressure nitrogen flowrate setpoint is a higher "optimization" layered or "vendor" supplied quantity, and is generally provided as a fixed ratio to the oxygen production rate. Hence, while designing the supervisory control layer, we will eliminate this as a manipulated input. This leaves us either of nitrogen purities (HP-column top or LP-column top) to be controlled by the only remaining manipulated input, i.e. flowrate of liquid-nitrogen (F_LN2). We chose to control HP-column top nitrogen concentration (Z_HPN2) using this input due to following reasons:

- Controlling the concentration at HP-column top ensures "balanced" wave profile inside the HP-column at all times, leading to a near-constant oxygen composition in the oxygen-rich stream (O2RICH). Since this stream serves as the main feed to the LP-column, it leads to low fluctuations in LP-column wave profiles as well.

- The responses of Z_HPN2 to step changes in F_LN2 follow a simple first order + dead time representation (Figure 3.8), making the design of controller much robust.

- It is well known from industrial and patent literature that the oxygen recovery losses in ASU, appear as purity deterioration in the dilute-nitrogen stream or waste stream (and hence the term "waste").

Controller tuning The supervisory layer loops selected above are closed and tuned one at a time in a sequential manner (starting with the faster loop, i.e., Z_O2–F_airASU). AspenDynamics$^{\mathrm{TM}}$ has an open loop test capability that was used to determine a first order plus time delay model from u to y. Based on the model

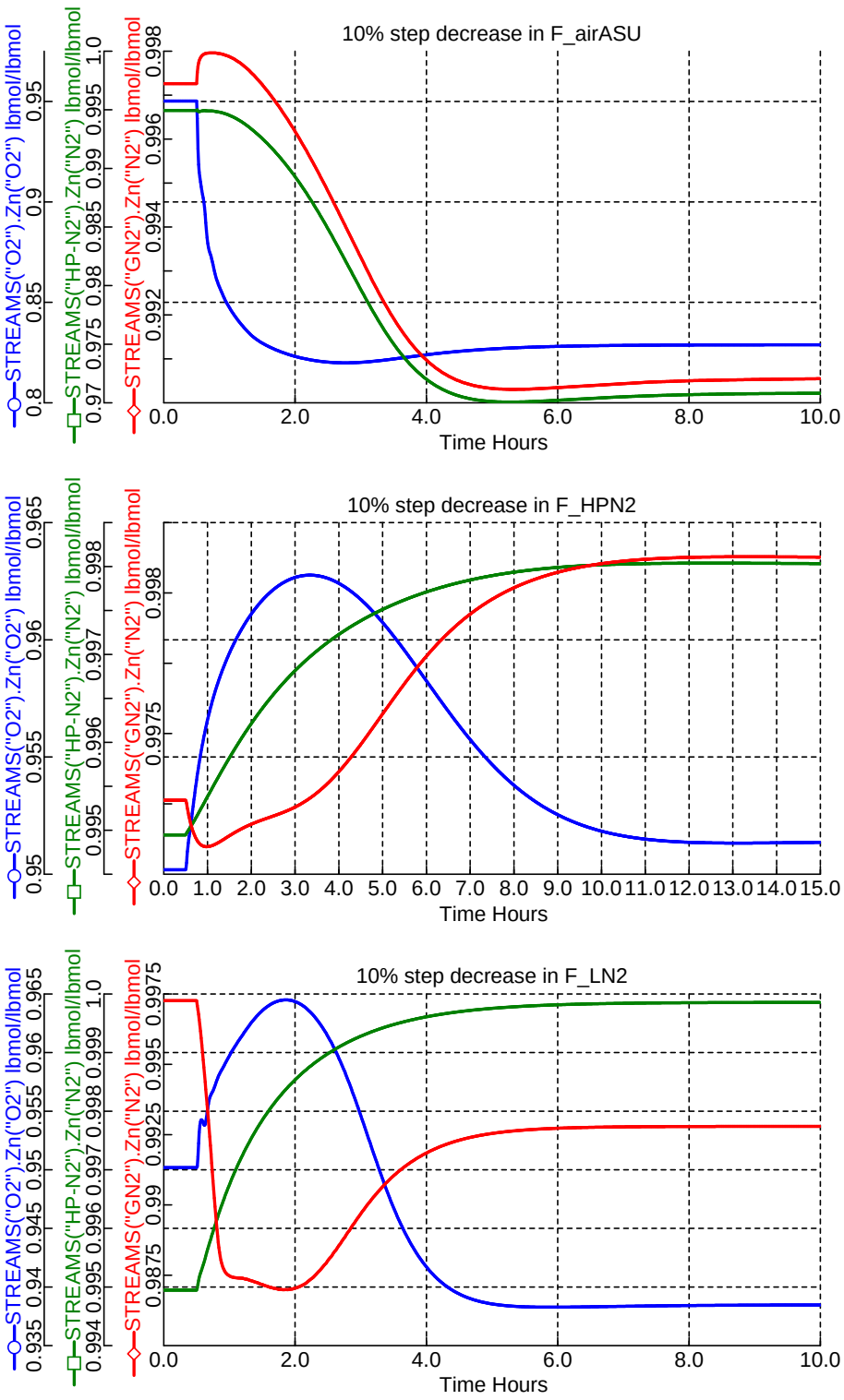

Figure 3.8: Control output (composition) responses to (I) 10% step decrease in F_airASU, (II) 10% step decrease in F_HPN2, (III) 10% step decrease in F_LN2. All input step changes given at t = 20 min

parameters, we used the SISO-IMC tuning rules [58] to design the PI-controllers with controller gain (K_c) and integral time-constant (τ_I) as

$$K_c = \frac{\tau_p + \frac{\theta}{2}}{k_p \lambda}, \quad \tau_I = \tau_p + \frac{\theta}{2} \tag{3.2}$$

where, k_p, τ_p and θ are the process gain, time constant and effective time delay respectively. In our case, we choose the minimum recommended value of tuning parameter, $\lambda = \max[0.2\tau_p, 1.7\theta]$ to give smooth control with acceptable performance in terms of disturbance rejection. Table 3.3 gives the model and PID tuning parameters[20] for the supervisory control layer.

Table 3.3: List of PI-based supervisory controllers for LP-ASU

ID	**PV**	**OP**	K_p (%/%)	τ_p (min)	θ (min)	λ (min)	K_c (%/%)	τ_I (min)
CCZO2	Z_O2	F_airASU	1.28	5.72	5.86	9.96	0.675	8.644
CCZN2	Z_HPN2	F_LN2	-0.049	47.79	5.84	9.93	-104	50.706
CCZGN2	–	–	–	–	–	–	–	–

Controller responses Figure 3.9 gives the supervisory control layer implementation in AspenDynamics^{TM}. It must be noted that the high-pressure nitrogen flowrate (F_HPN2) is ratio-ed with the oxygen production rate through a multiplier block, HPN2/GOX. The controller responses to load changes (variation in oxygen production rate) are given in Figure 3.10. The multiloop SISO based PID controller performs well for drastic load changes (step change in oxygen demand of 25%). During turn-down conditions, it can be seen that expanded-air is not required (mainly due to rise of liquid-level in LP-column sump). This is due to the thermal mass (or the refrigeration enthalpy) contained in the liquid overheads. Looking at the low purity plots of low-pressure nitrogen during initial transients, we can also infer a shift in oxygen wave profile towards the left, which implies energy imbalance between columns during transients. This is mainly due to pressure and temperature fluctuations with changes in feed air flowrate.

[20]Nomenclature – PV: Process Variable, OP: Controller Output, ID: Controller Tag (see Figure 3.9)

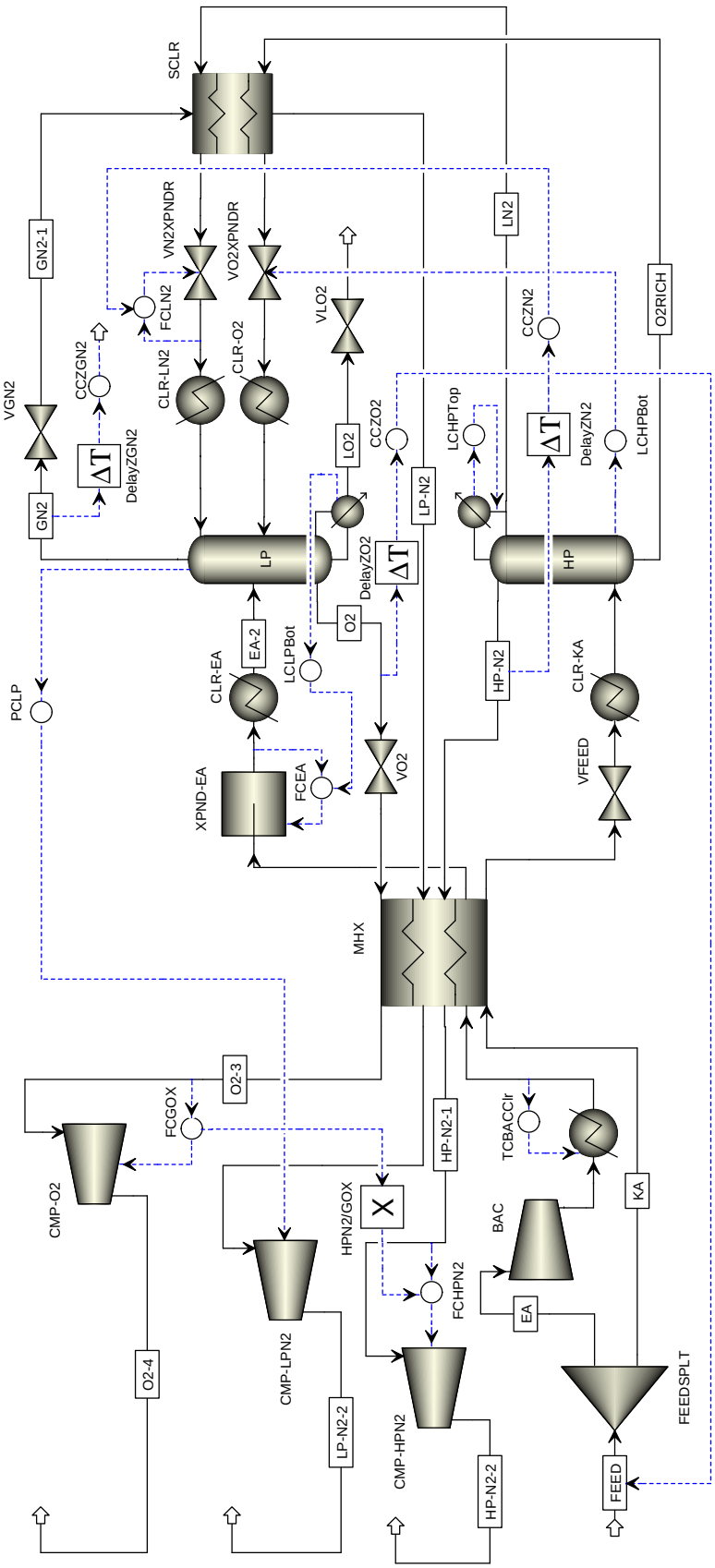

Figure 3.9: Process flowsheet showing low–pressure double-column ASU in AspenDynamics^{TM} with PID-based supervisory layer control

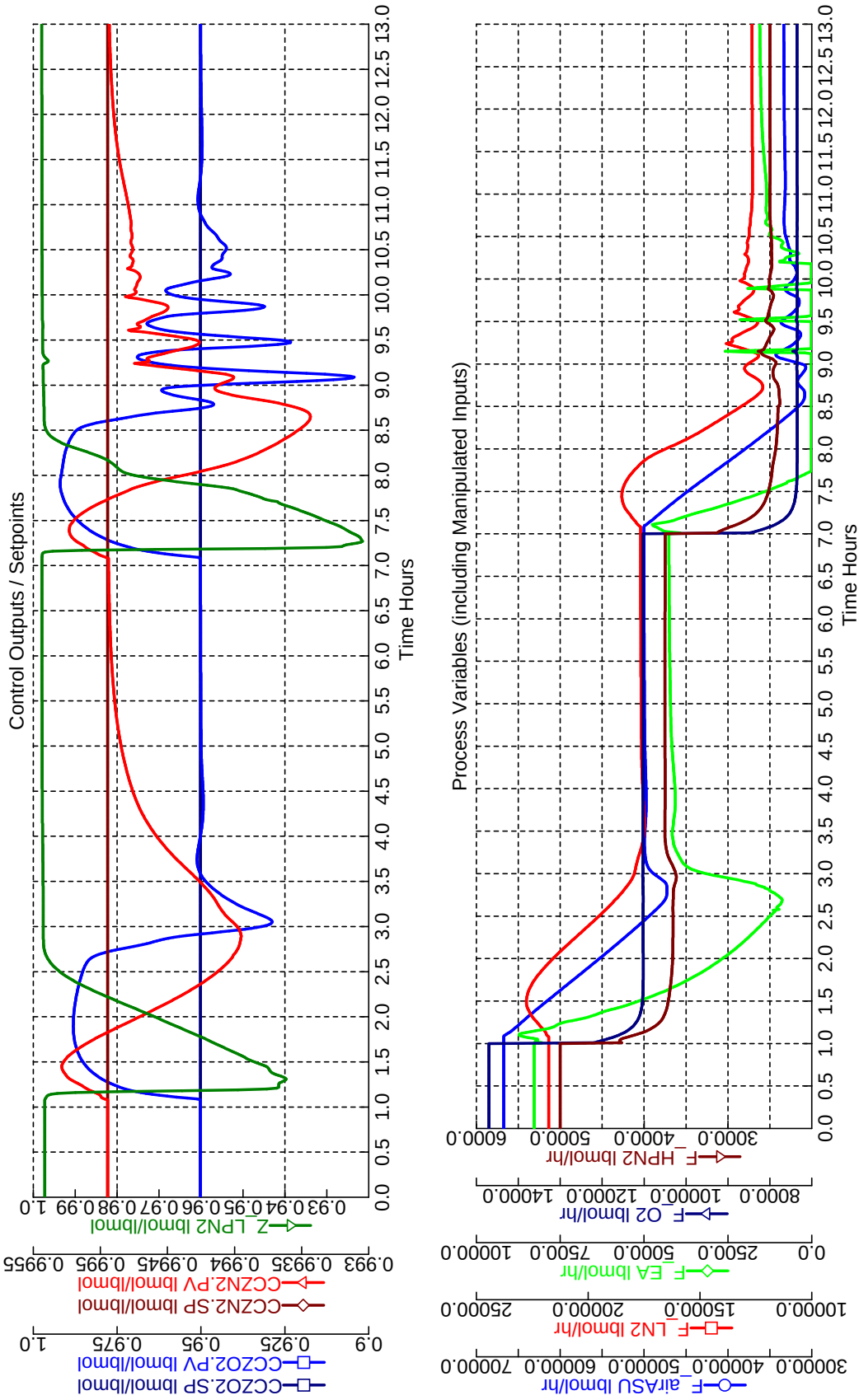

Figure 3.10: LP-ASU PID-based multiloop supervisory controller (see Figure 3.9) response to (I) 25% step decrease in oxygen production rate (F_O2) setpoint at t = 1 hr, (II) 50% step decrease at t = 7 hr.

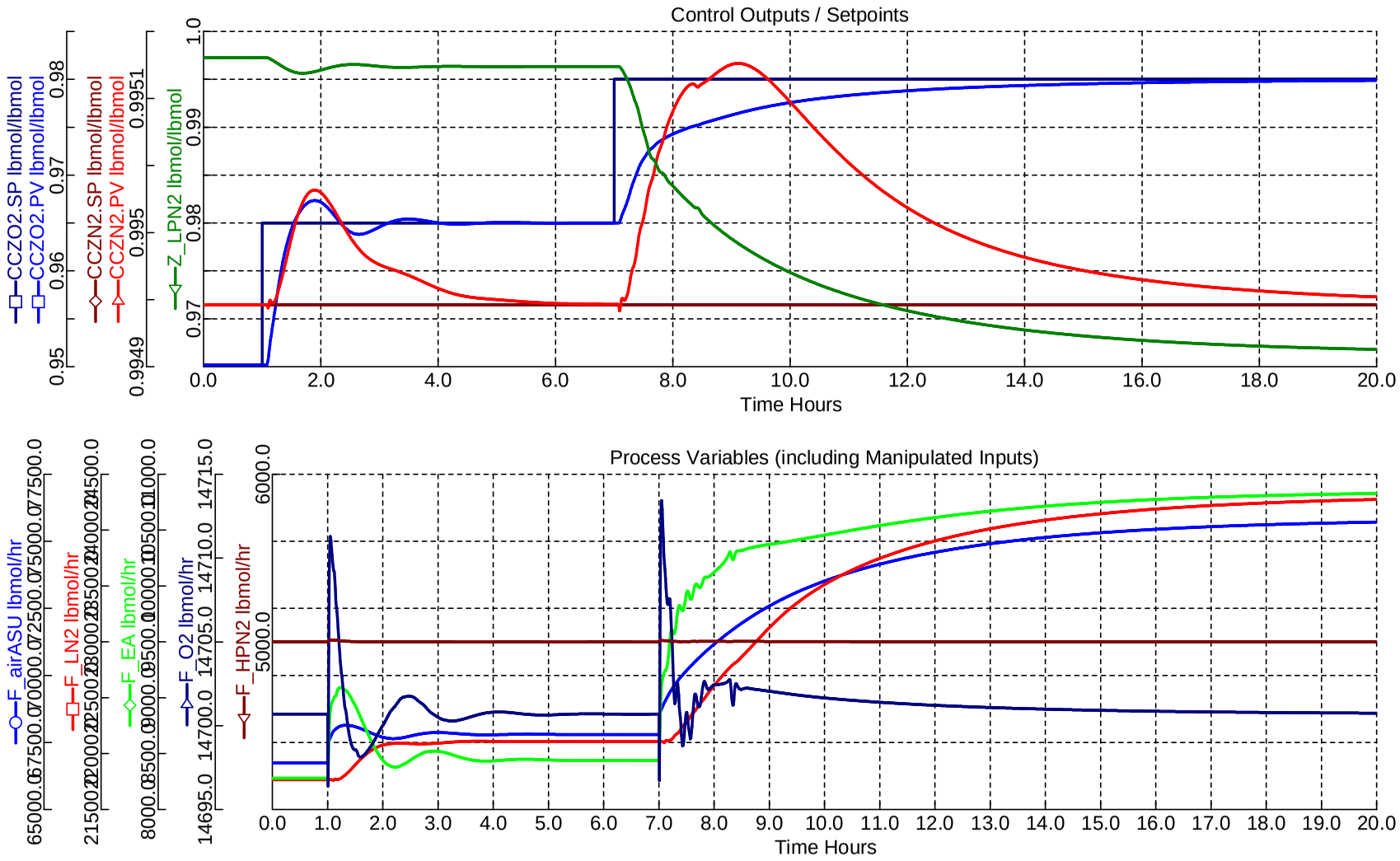

Figure 3.11: LP-ASU PID-based multiloop supervisory controller (see Figure 3.9) response to (I) step setpoint increase in oxygen molar composition (Z_O2) to 96.5% at t = 1 hr, (II) step setpoint increase in Z_O2 to 98% at t = 7 hr hr.

Further dropping the load from 25% to 50%, saturates the expanded air flowrate to zero. In absence of external refrigeration, the columns interact among each other (via the integrated condenser-reboiler) to self stabilize the pressure and temperature variations showing oscillations in product purities before meeting the setpoint. In spite of sudden step change in loads, the purities fluctuate for brief amount of time and finally get back to the setpoints within 6 hours. This is in general admissible mainly due to (a) in real applications, we provide a ramp change in oxygen-demand; in our case, the setpoint tracking is almost perfect (not shown), with nearly no purity oscillations, and (b)unlike dedicated ASUs for generating high purity oxygen for industrial needs, gasification applications can sustain purity fluctuations for small period of time. It will also be interesting to note that low-pressure or "waste" nitrogen stream maintains similar purity at the new steady state, even though no purity control has been used. The effectiveness of the controller design can be appreciated when we look at the oxygen recovery at 50% load. It was seen that there is no loss of recovery at all; in fact, on the contrary the recovery increased by 0.2% (which is intuitive, since the pressure involved decreases at lower loads making the separation factor higher).

We can further test the robustness of our controller scheme by giving purity setpoint changes. This is a very challenging task in a system where condenser and reboiler heat duties cannot be independently changed and brings the system refrigeration and heat balances to an extreme limit. In worst case, the purity and flowrate demands can be met but at the cost of a significant recovery loss. This can be seen in Figure 3.11 where a step setpoint change from 95% to 96.5% purity is provided. The oxygen flowrate initially spikes up due to increased feed-air flowrate and later falls back to the original rate. For this purity increase, the recovery is still maintained at 99.6%. For higher purity step setpoint changes, the tracking is very slow. The deviation of nitrogen purity in HPN2 stream is very less, although a major change occurs in the purity level of LPN2 stream. The reason for this is the high expanded air flowrate required for additional refrigeration (needed for high purity), which decreases the fraction of air available to the HP-column and hence generating low boilup in that column. This in turn generates low reflux to the

LP-column leading to a much lower oxygen recovery (only 90.6% at 98% setpoint).

3.2.2.2 Model Predictive Control

Model predictive control, or receding horizon control, is an advanced control technique that takes advantage of the models inherent ability to predict system behavior into the future. At each time step, an optimization problem is formulated and solved. The objective function is to minimize control action over p time steps, where p is known as the prediction horizon. The decision variables are m control moves, where m is the control horizon. Only the first control move is applied to the system, the model is updated, and the entire process is repeated at the next time step. A number of different types of models are used as the model $\hat{y}_{k+i}$ in a model predictive control framework. Among the most popular are step response, impulse response and state space models [58]. We use both step response and state space models in this research. This has been discussed in the next heading.

MPC: System Identification

For overall supervisory layer system identification study, we first need to identify the relevant process input and output variables, including input disturbances, for developing the control model. These variables can be both measured or unmeasured. For the LP-ASU process, apart from the manipulated input and measured output variables listed earlier (page 82), the measured disturbance plays a very important role for implementing feedforward type control. This is specifically relevant when a localized supervisory control is implemented on a single plant subsection and these individual subsection controllers need to pass setpoint (demand) information among each other. For instance, the demand for oxygen set by the gasification island is sent to the ASU, which is immediately met by the regulatory oxygen flow controller by manipulating the valve or compressor-power on the oxygen line. This leads to a change in purity levels and a feedback signal, either in form of purity or tray temperature, is sent to the ASU's local supervisory controller which manipulates the feed-air flowrate (and liquid nitrogen flowrate) to bring the purity back to the desired level. A more robust controller can be designed, especially in purview of MPC, if the oxygen flowrate signal (or demands set external to the plant) is sent

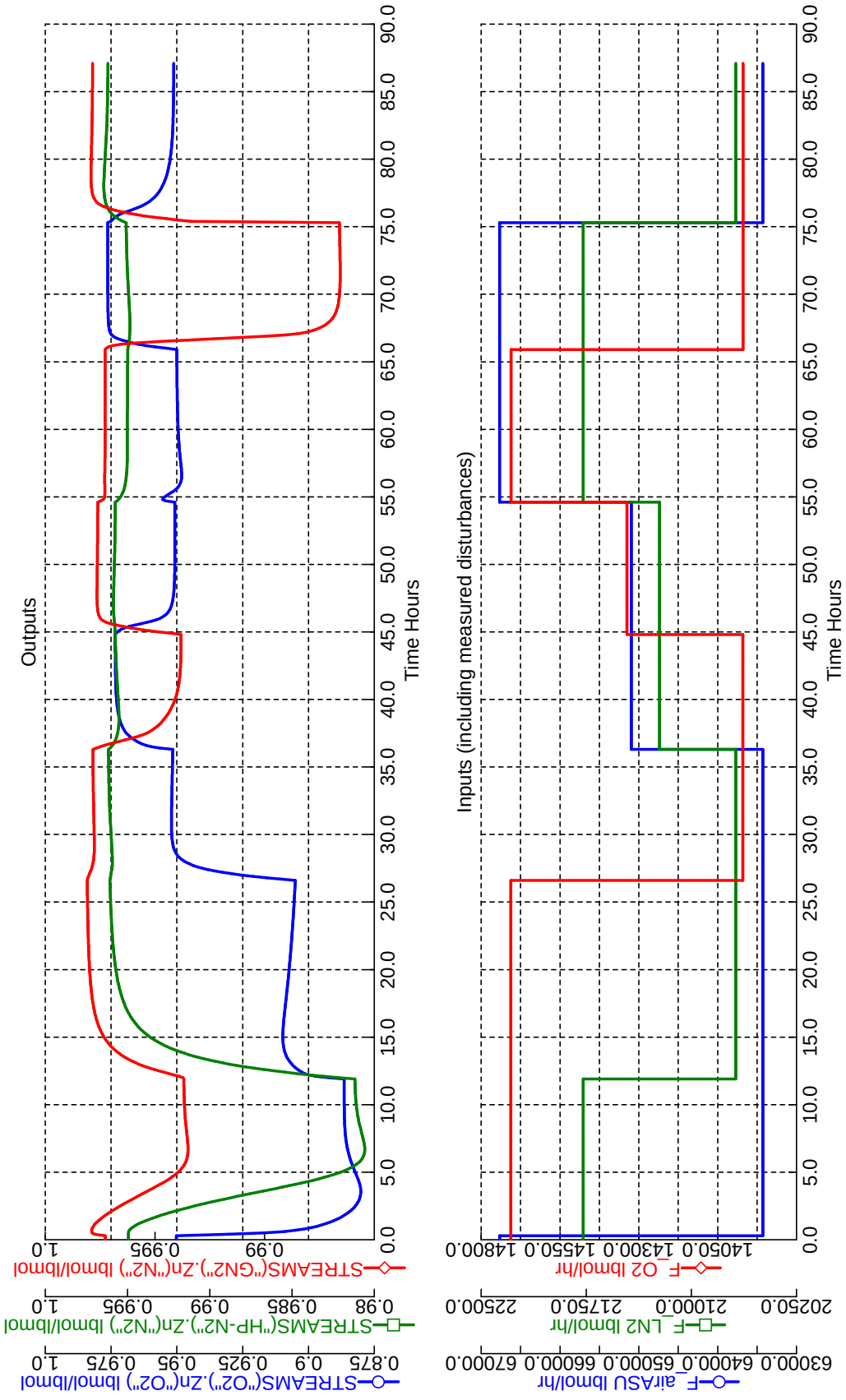

Figure 3.12: LP-ASU responses to various supervisory-layered step-inputs (including measured disturbance, F_O2) for system-identification. The steps (relative to nominal in %) are provided in the following sequence for (F_airASU,F_LN2,F_O2): (95,100,100) (95,95,100) (95,95,95) (97.5,97.5,95) (97.5,97.5,97.5) (100,100,100) (100,100,95) (95,95,95)

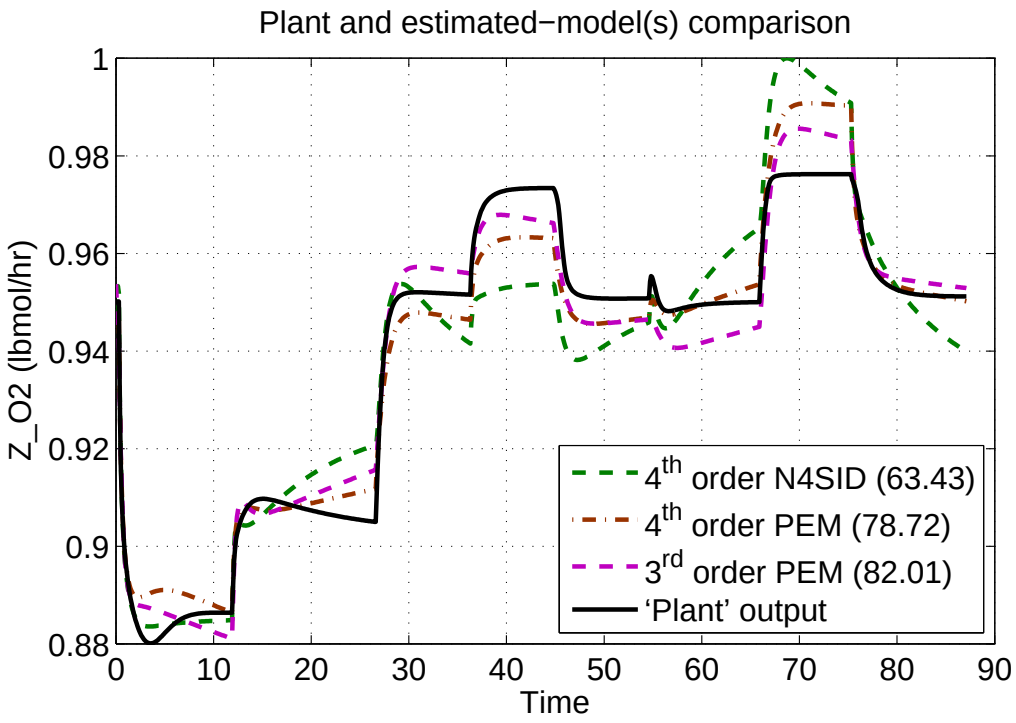

Figure 3.13: Comparison of system-identified step-response models to simulator 'surrogate-plant' data (with step-responses given in Figure 3.12)

to the controller directly in a feedforward fashion, which can thereafter exploit this information to rapidly adjust the feed-air flowrate rather than base them on feedback purity signals only. By incorporating the measured disturbance inputs (i.e., the oxygen flowrate in this example) in the model, MPC can predict their effect on measured output (or oxygen purity) and adjust the manipulated input (or feed-air flowrate) accordingly.

Figure 3.12 gives the simulator (a 'surrogate plant' or 'plant-model') responses to different combination of step excitations in the manipulated inputs (F_airASU, F_LN2) and measured disturbances (F_O2). These input-output data in form of a time-series data is used for determining an approximate linear 'control-model' for MPC studies. This is done using MATLAB's System Identification GUI Tool, where different algorithms and model-order are used on a trial-and-error basis, to determine the best fit to the 'plant' data (details provided in Appendix C). Figure 3.12

gives a comparison of different system-identified models, along with *fit* magnitude[21]. Although quantitatively PEM 3-state model gives the best fit, we choose to use PEM 4-state model since it seems to capture the initial dynamics (corresponding to pressure-dynamics) better. The following state-space values and other details are reported by MATLAB, for u≡[F_airASU F_LN2 F_O2]' and y≡[Z_O2 Z_HPN2]'.

```
State-space model:  x(t+Ts) = A x(t) + B u(t) + K e(t)
                       y(t) = C x(t) + D u(t) + e(t)
A =
                x1          x2          x3          x4
     x1      0.72265     0.20356     0.31602     0.63555
     x2      0.29286     0.58965    -0.51479    -1.1539
     x3     -0.33686     0.31345      1.4495      1.1805
     x4      0.10291    -0.097572   -0.13868     0.68138
B =
                u1          u2          u3
     x1   0.00057967  -0.00085294  -0.00016611
     x2  -0.00098753   0.0014486   0.00024015
     x3   0.00099502  -0.0014453  -0.00027609
     x4  -0.00027553   0.00040353  7.3678e-005
C =
                x1          x2          x3          x4
     y1      0.11878     0.10519     0.011109    -0.10401
     y2   -0.0087904   -0.0085191   -0.031008    -0.10261
D =
                u1          u2          u3
     y1          0           0           0
     y2          0           0           0
K =
                y1          y2
```

[21]This is the percentage of output variations that is produced by the model and is defined by $Fit = \left(1 - \frac{\|y - \hat{y}\|}{\|y - \bar{y}\|}\right) \times 100$, where y is the measured output, $\hat{y}$ is the simulated/predicted model output and $\bar{y}$ is the mean of y. A higher number depicts a better model.

```
            x1            0            0
            x2            0            0
            x3            0            0
            x4            0            0
x(0) =
            x1       25.565
            x2      -44.091
            x3       39.853
            x4      -20.366

Estimated using PEM using SearchMethod = Auto from data set z
Loss function 5.84211e-010 and FPE 6.1637e-010
Sampling interval: 0.1
```

For examining predictive control methods and perform step tests, we interface the relevant control input-output variable from Aspen Dynamics into Matlab/Simulink programming environment. Input/output noise blocks were added to simulate/mimic a real plant scenario. This modified block now acts as a surrogate plant for MPC studies. For consistency and qualitative comparison with PID responses, we have ignored the input/output noises in the current study. This approach is then used to develop a MPC control layer for the ASU block (described in next subsection). Examples of the primary manipulated input variables and controller outputs in Simulink have been shown later in Figure 3.18 and 4.8.

MPC: Methodology

The objective function J used in this work is a sum of squares, given as

$$J = \sum_{i=1}^{p} \left(r_{k+i|k} - \hat{y}_{k+i|k}\right)^T W^y \left(r_{k+i|k} - \hat{y}_{k+i|k}\right) + \sum_{i=0}^{m-1} \Delta u_{k+i}^T W^u \Delta u_{k+i}^T \qquad (3.3)$$

where, $r_{k+i|k}$ is the setpoint, u_k is the control action and $\hat{y}_{k+i|k}$ is the model prediction at $(k+i)^{th}$ time-step (given the plant output till k^{th} time-step). The objective function is of the sum-of-squared errors form, where the first term represents the error across the prediction horizon and the second term is a penalization of ex-

cessive control actions whose purpose is to minimize potentially expensive control actions. In a constrained MPC formulation, we minimize the objective function along with the input constraints, input-rate constraints and output constraints as given in Equation (3.4).

$$\begin{aligned} u_{\min} \leq u_{k+i} \leq u_{\max} \\ \Delta u_{\min} \leq \Delta u_{k+i} \leq \Delta u_{\max} \\ y_{\min} \leq \hat{y}_{k+i|k} \leq y_{\max} \end{aligned} \tag{3.4}$$

Before moving to detailed system identification studies, we briefly take a look into the model formulation. The simplest and most frequently used model is the additive output disturbance model. In our studies, most of the inputs enter as "measured" disturbances or demands. These variables serve as feed-forward input state in the corresponding state space model. This is given in following form

$$\begin{aligned} x_{k+1} &= \Phi x_k + \Gamma u_k + \Gamma^F d_k^F \\ d_{k+1} &= d_k + \omega_k \\ y_{k+1} &= C x_{k+1} + D u_k + d_{k+1} + \nu_{k+1} \end{aligned} \tag{3.5}$$

where, ω_k term is the process noise associated with the disturbance estimation, ν_{k+1} term is the measurement noise. Using matrix-vector notation, the augmented model is rewritten in terms of predictor-correction equations as follows

Prediction Step

$$\begin{aligned} \begin{bmatrix} \hat{x}_{k+1|k} \\ \hat{d}_{k+1|k} \end{bmatrix} &= \underbrace{\begin{bmatrix} \Phi & 0 \\ 0 & I \end{bmatrix}}_{\Phi^a} \underbrace{\begin{bmatrix} \hat{x}_{k|k} \\ \hat{d}_{k|k} \end{bmatrix}}_{\hat{x}^a_{k|k}} + \underbrace{\begin{bmatrix} \Gamma \\ 0 \end{bmatrix}}_{\Gamma^a} u_k + \underbrace{\begin{bmatrix} \Gamma^F \\ 0 \end{bmatrix}}_{\Gamma^{F,a}} d_k^F \\ \hat{y}_{k+1|k} &= \underbrace{\begin{bmatrix} C & I \end{bmatrix}}_{C^a} \begin{bmatrix} \hat{x}_{k+1|k} \\ \hat{d}_{k+1|k} \end{bmatrix} + D u_k \end{aligned} \tag{3.6}$$

Table 3.4: Input variable constraints used in MPC formulation for LP-ASU

Variable	u_{ss}	u_{min}	u_{max}	Δu_-	Δu_+
F_airASU (lbmol hr^{-1})	66742	30000	70000	15000	15000
F_LN2 (lbmol hr^{-1})	21765	10000	25000	2000	2000

Correction Step

$$\begin{bmatrix} \hat{x}_{k+1|k+1} \\ \hat{d}_{k+1|k+1} \end{bmatrix} = \begin{bmatrix} \hat{x}_{k+1|k} \\ \hat{d}_{k+1|k} \end{bmatrix} + \underbrace{\begin{bmatrix} 0 \\ I \end{bmatrix}}_{L^a} \left(y_{k+1} - \hat{y}_{k+1|k} \right)$$

$$\hat{y}_{k+1|k+1} = \begin{bmatrix} C & I \end{bmatrix} \begin{bmatrix} \hat{x}_{k+1|k+1} \\ \hat{d}_{k+1|k+1} \end{bmatrix} + Du_k \tag{3.7}$$

The predicted output vector (over p time steps) are given in terms of "free" or "unforced" response and "forced" response as

$$\begin{bmatrix} \hat{y}_{k+1|k} \\ \hat{y}_{k+2|k} \\ \vdots \\ \hat{y}_{k+p|k} \end{bmatrix} = \begin{bmatrix} C\Phi \\ C\Phi^2 \\ \vdots \\ C\Phi^p \end{bmatrix} \hat{x}_{k|k} + \begin{bmatrix} C\Gamma + D \\ C\Phi\Gamma + C\Gamma + D \\ \vdots \\ \sum_{i=1}^{p} C\Phi^{i-1}\Gamma + D \end{bmatrix} u_{k-1} + \begin{bmatrix} C\Gamma^F + D \\ C\Phi\Gamma^F + C\Gamma^F + D \\ \vdots \\ \sum_{i=1}^{p} C\Phi^{i-1}\Gamma^F + D \end{bmatrix} d_k^F$$
$$+ \begin{bmatrix} I \\ I \\ \vdots \\ I \end{bmatrix} \hat{d}_{k|k} + \begin{bmatrix} C\Gamma + D & 0 & 0 & \cdots & 0 \\ C\Phi\Gamma + C\Gamma + D & C\Gamma + D & 0 & \cdots & 0 \\ \vdots & \vdots & \vdots & & \\ \sum_{i=1}^{p} C\Phi^{i-1}\Gamma + D & \sum_{i=1}^{p-1} C\Phi^{i-1}\Gamma + D & & \cdots & \end{bmatrix} \begin{bmatrix} \Delta u_k \\ \Delta u_{k+1} \\ \\ \Delta u_{k+m-1} \end{bmatrix} \tag{3.8}$$

For examining predictive control methods, we interface the relevant control input-output variable from AspenDynamics^{TM} into MATLAB/Simulink programming environment similar to that shown Figure 3.18. Input/output noise blocks

were added to simulate/mimic a real plant scenario. This modified block now acts as a surrogate plant for MPC studies. For consistency and qualitative comparison with continuous PID responses, we have ignored the input/output noises in the current study. Simplified linear step-response models have been used (as highlighted in steps above) which allows us to control solely the states associated with the measured output. An additive output disturbance assumption (similar to dynamic matrix control) in appended-state formulation is utilized in the linear constrained MPC study. Inputs contraints used in the study have been given in Table 3.4. The sample time is 0.1 hr. A control horizon (m) of 3 and prediction horizon (p) of 30 was chosen.

3.2.2.3 FeedForward Control

A pure feedforward design (Figure 3.14) has also been analyzed for comparison purpose. If noted carefully there is no feedback involved in any of the primary control outputs, and hence load and disturbance changes might lead to an offset in these outputs. This design takes advantage of the instantaneous known oxygen flowrate demand signal (from the gasifier controller) to make adjustments in air feed rate, without relying on delayed purity measurements to take action. This is very advantageous when the measurement dead-time is comparable to the process time constant, and slight offsets in product purity is admissible. This has been shown in some of the simulations results later in the section. It should be noted that this method is very ineffective in handing process disturbance and large offsets in control-outputs will always be seen.

3.2.3 Simulation Results

A performance comparison between the two controller designs, mentioned in the previous section, has been done by step decreasing the oxygen demand by 10% (i.e., giving a step setpoint change to the FCGOX controller). These responses have been shown in Figure 3.15. In practice, this is done in a ramp fashion, where the rate of demand change can be adjusted. Here, we do it to maintain consistency between pure Aspen (PID design) and Aspen + Matlab (MPC design) simulation results. We see a marked difference between the PID and the MPC reponses. The

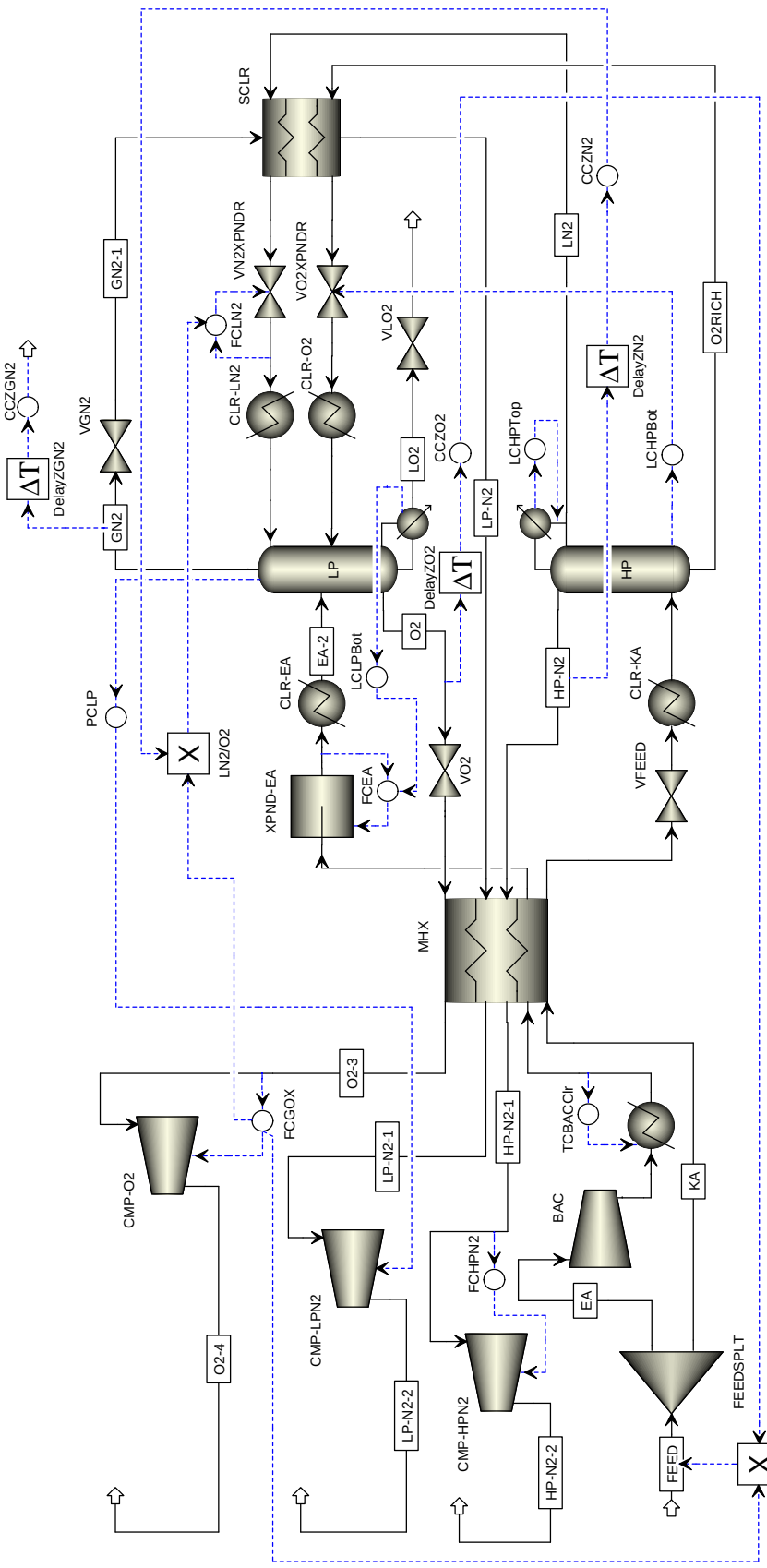

Figure 3.14: Process flowsheet showing low–pressure double-column ASU in AspenDynamics^{TM} with pure feedforward control

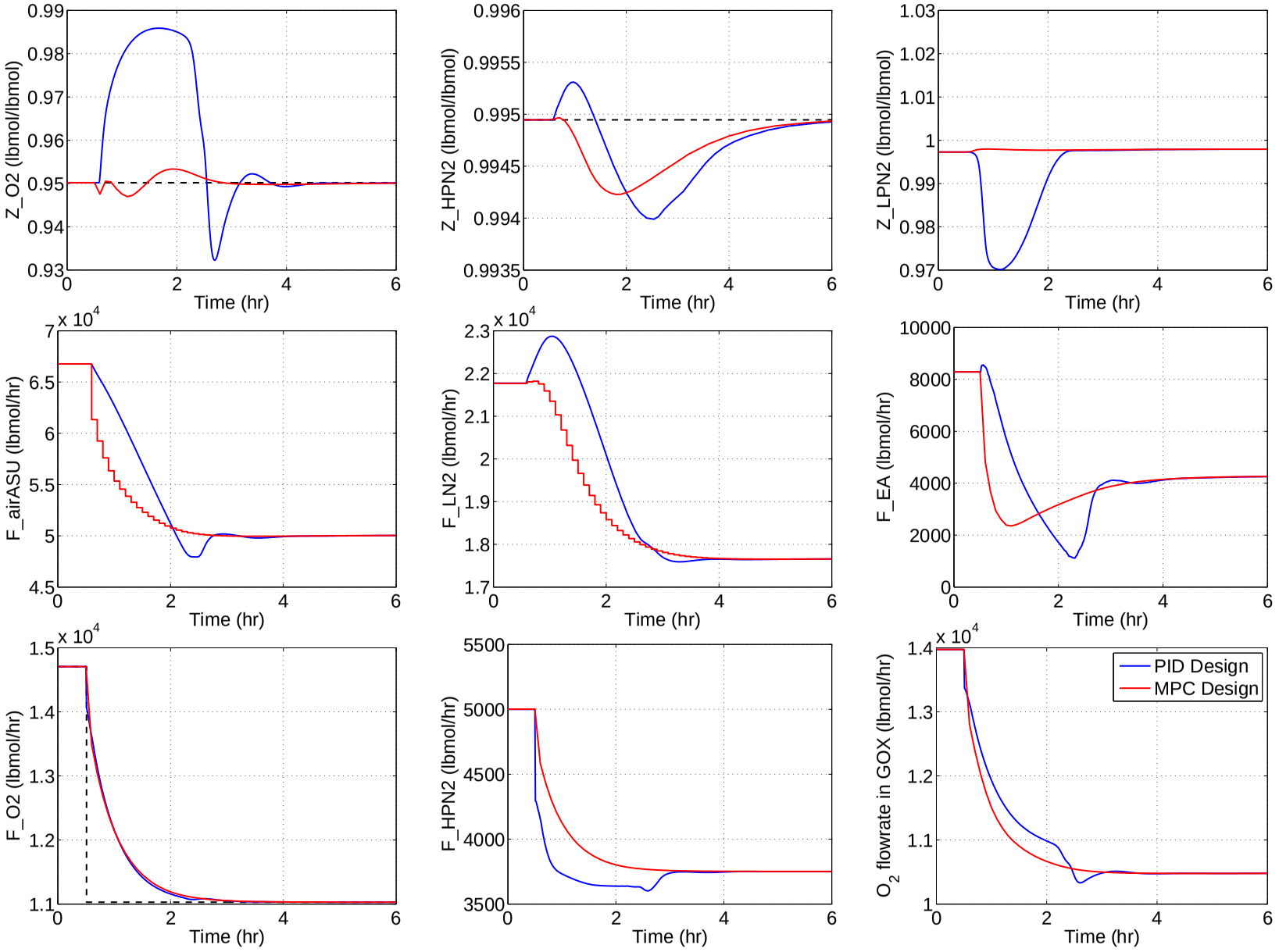

Figure 3.15: Simulation results showing PID vs. MPC controller responses for 10% decrease in oxygen demand. Outputs are shown in top row, inputs in bottom row

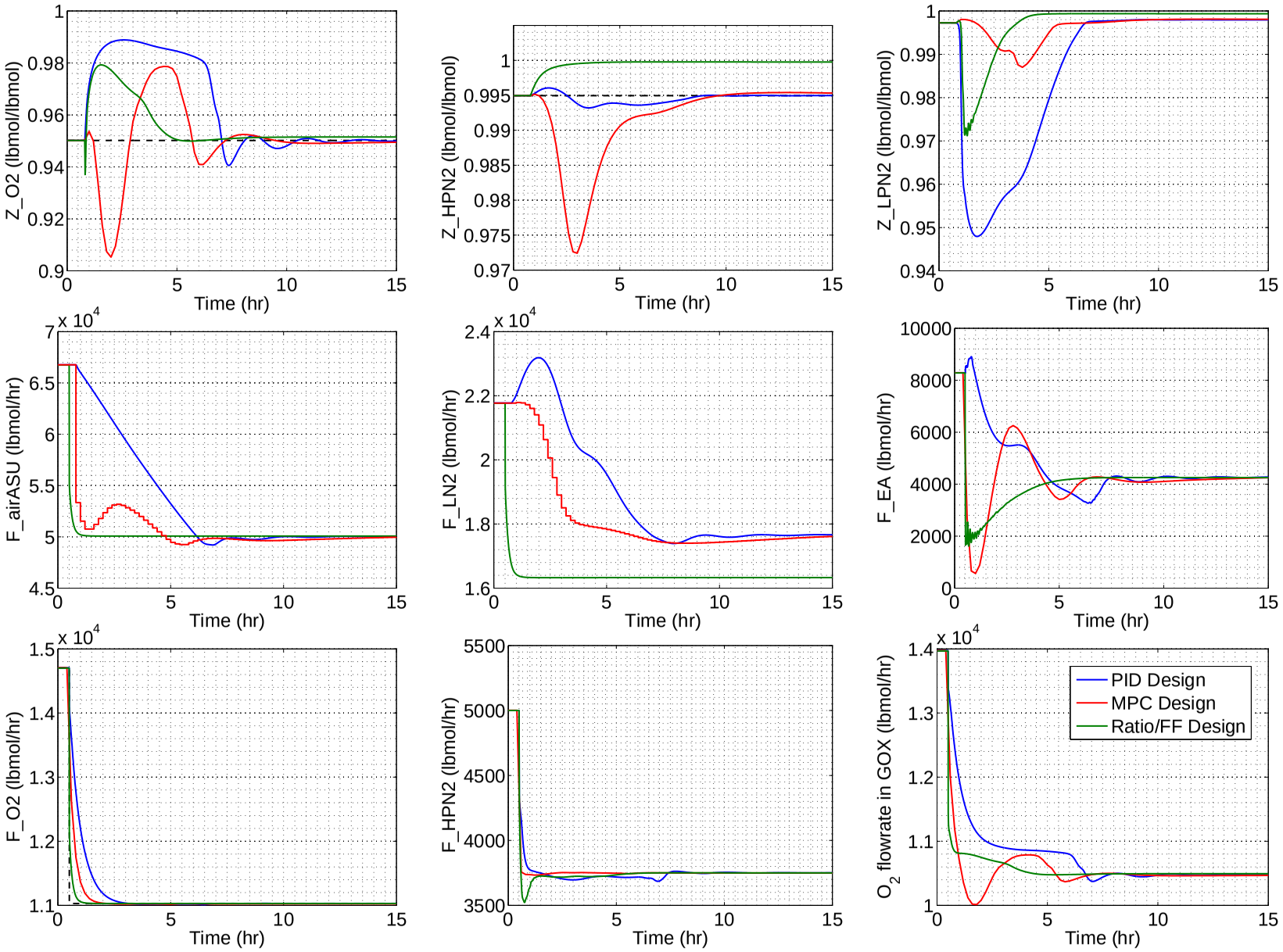

Figure 3.16: Simulation results showing PID, MPC and feed-forward controller responses for 10% decrease in oxygen demand *for slower and delayed sampling*. Outputs are shown in top row, inputs in bottom row.

PID responses show significant purity deviations (upto 98.5% purity) for initial 2 hours. This can be seen in the oxygen component flowrate in the GOX stream as well. The dip in nitrogen purity during that time (showing oxygen escaping from the LP-column top) signifies insufficient refrigeration during the transient phase for the amount of air holdup already inside the system.

It must be noted that the above analysis was for a sample time of 6 min and a composition measurement delay, for all three streams, of 5 min. To study the robustness of MPC controller, we studied the system for a sample time of 12 min and a dead-time of 18 min. It can be seen from the responses given in Figure 3.16 that MPC controller performs poorly in this case, although it still outperforms the continuous PID. Furthermore, it is interesting to realize that a pure feed-forward design meets the oxygen demand almost instantaneously with much lower purity deviations compared to other two designs at the cost of minor offset in product purities.

3.3 Controller Design for Elevated-Pressure ASU

Due to feed-product energy interaction, the resulting dynamic state equations do not converge to a single operating point. In absence of any reboiler and condenser for the HP-column and LP-column respectively, along with a condenser-reboiler integration, we loose four degrees of freedom. The columns have to operate at floating pressure arrangement (self-stabilizing), due to lack of any manipulated variable to control pressure. This arrangement also permits higher range of upstream/downstream flowrates without reaching operating constraints. Initial stabilizing level-control loops were installed. Simulations revealed that small disturbances to the energy balance initiated run-away of the ASU. This suggested presence of right-half-plane eigenvalues which remained to be moved to the left-half-plane in order to eliminate the instability. A pre-feed temperature controller (maintaining constant inlet temperature) was used, and no further run-aways from steady state were observed. The details of the controllers including variable-actuator pairing have been given in the following sub-section.

3.3.1 Regulatory Control Layer

The regulatory control structure has the following features (Figure 3.17):

Stabilizing level-control loops

- The reflux flow rate is used for level control (HP_DrumLC) in the HP-column condensor, instead of the distillate (LN2) flowrate.
- The LP-column bottom flow (O2) is used for LP-column sump level control (LP_SumpLC)

Flow control loops

- Feed flow controller (FCFeed) which changes the compressor (MAC) brake-power or outlet pressure to control air flowrate. The setpoint (SP) is provided by higher-level controller.

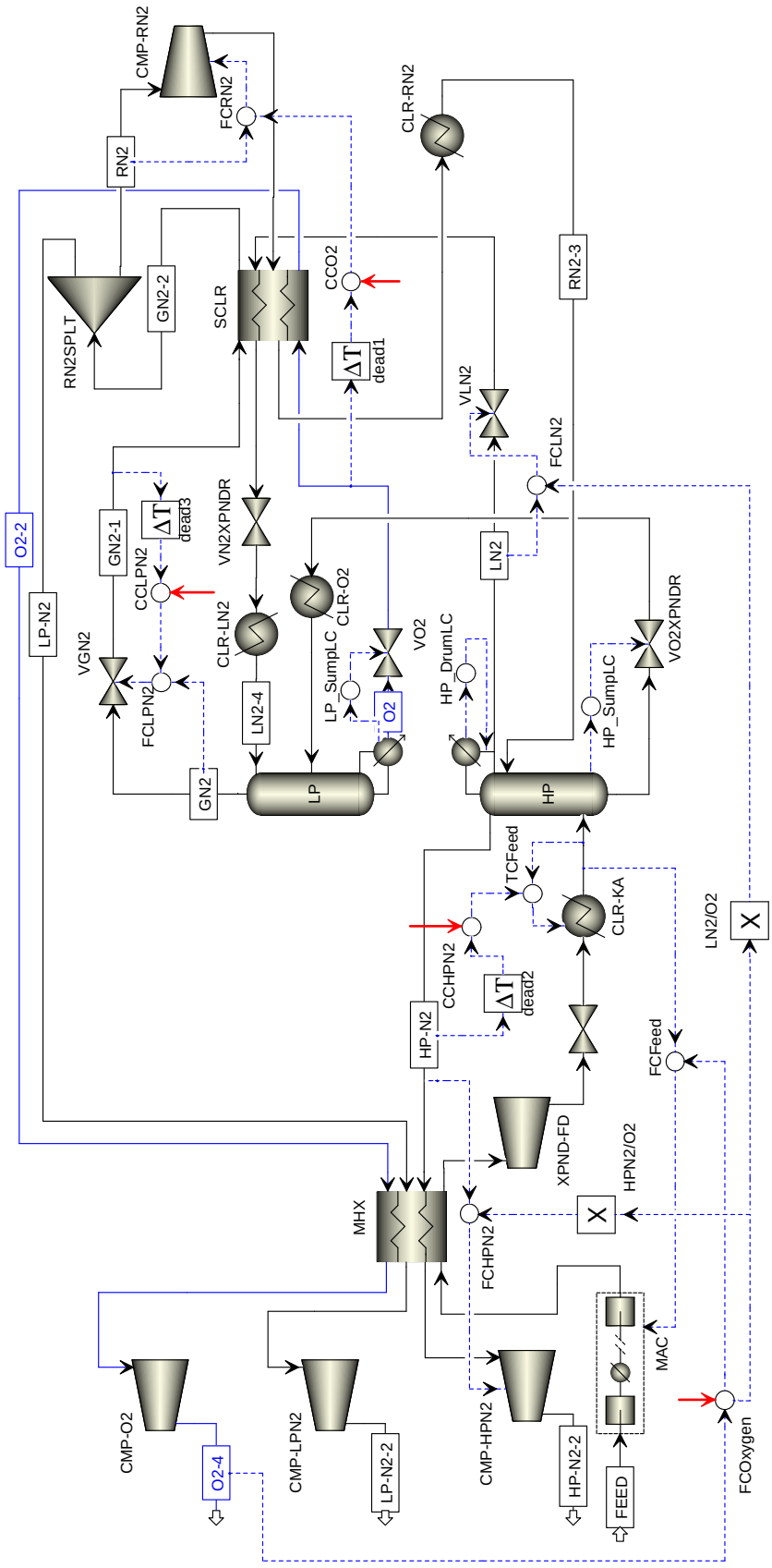

Figure 3.17: The proposed PID control structure for EP-ASU in Aspen Dynamics. (↗) denotes setpoint signals from a supervisory control layer

- High-pressure nitrogen flow controller (FCHPN2) changes the nitrogen compressor (CMP-HPN2) brake-power or suction-side pressure to control flowrate. The setpoint is sent as a fixed ratio of oxygen demand.

- Liquid nitrogen reflux flow controller (FCLN2) adjusts a valve (VLN2) for flowrate control. Setpoint is provided as a fixed ratio of oxygen demand (Equation (2.1)).

- Recycled nitrogen flow controller (FCRN2) changes the recycle compressor (CMP-RN2) brake-power or suction to control F_RN2. The setpoint is provided by higher-level controller.

- Low-pressure nitrogen flowrate exiting LP-column top is controlled (FCLPN2) using a control valve (VGN2). Again, SP is provided by upper level controllers.

Temperature control loop

- The controller (TCFeed) controls the open-loop instability by providing additional refrigeration (for circumventing heat losses and purity control). Refrigeration can be varied by changing heat-exchange bypass amount. For brevity sake, refrigeration heat-duty of CLR-KA has been manipulated here.

3.3.2 Primary/Supervisory Control Layer

Based on the above analysis, we propose a PI-based control structure for the cryogenic heat-integrated ASU, as shown in Figure 3.17. The control structure has the following pairing. For sake of brevity, the RGA analysis and controller tuning methodology (similar to that for LP-ASU) have not been given here.

- Oxygen flow controller (FCOxygen) controls the flowrate of oxygen to a supervisory/plant determined setpoint value (shown as red arrow in Figure 3.17) by giving feed flowrate setpoint signal to the cascaded FCFeed controller.

- Oxygen purity controller (CCO2) controls purity by manipulating recycled-nitrogen flowrate. Output is sent as setpoint signal to flow controller FCRN2.

Setpoint is obtained from supervisory computer and is fixed at 0.95 mole fraction of oxygen.

- High-pressure nitrogen composition controller (CCHPN2) adjusts the HP-column pre-feed temperature to maintain composition of HP-N2 stream. Set-point is set from supervisory layer and fixed at 0.991 nitrogen mole fraction.

- Low-pressure nitrogen composition controller (CCLPN2) controls purity by manipulating flowrate of low-pressure nitrogen exiting LP-column top. Again, SP is provided by supervisory level controllers and fixed at 0.991 mole fraction of nitrogen.

Upon carefully observing the regulatory control architecture for EP-ASU, the reader can distinguish this structure from that of LP-ASU. The control of low-pressure column was earlier regulated by using the expanded air. Here, in absence of this stream, we are bind to use the oxygen product stream to level control. Hence this variable cannot be manipulated directly to set the production rate. This is a typical case of a controller design for a given feed rate where production rate is a through-put variable (Figure 3.6).

3.3.2.1 Model Predictive Control

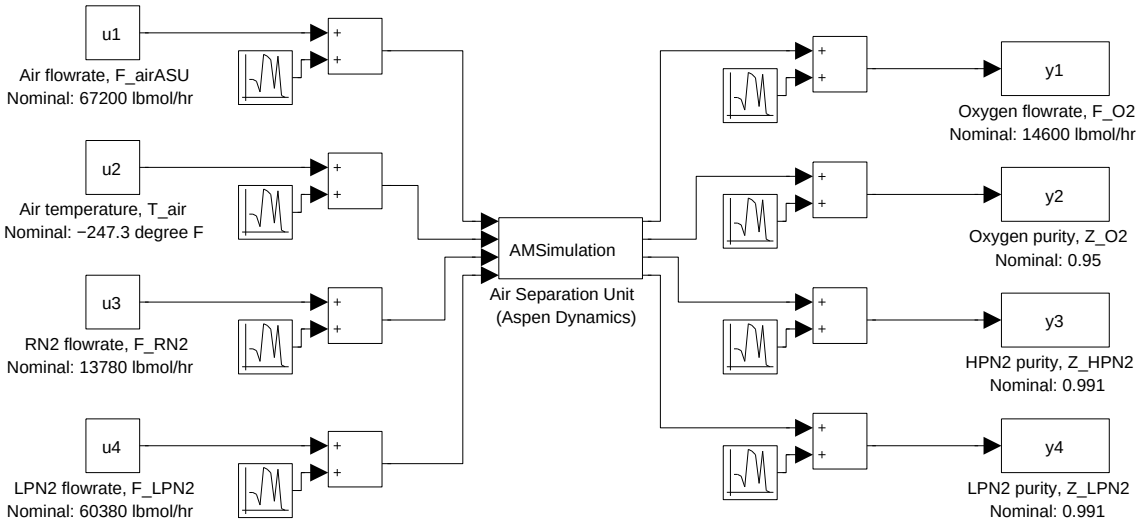

Figure 3.18: Simulink block diagram showing interfacing with Aspen Dynamics for EP-ASU

Table 3.5: Input variable constraints used in MPC formulation for EP-ASU

Variable	u_{ss}	u_{min}	u_{max}	Δu_-	Δu_+
F_airASU (lbmol hr^{-1})	67200	33600	73920	672	672
T_air (°F)	-247.3	-255	-240	0.5	0.5
F_RN2 (lbmol hr^{-1})	13780	6890	15158	137.8	137.8
F_LPN2 (lbmol hr^{-1})	60380	30190	66418	6038	6038

For examining predictive control methods, we interface the relevant control input-output variable from Aspen Dynamics into Matlab/Simulink programming environment. This approach is then used to develop a supervisory control layer for the ASU block. The primary manipulated input variables and controller outputs have been shown in Figure 3.18. Input/output noise blocks were added to simulate/mimic a real plant scenario. This modified block now acts as a surrogate plant for MPC studies. For consistency and qualitative comparison with PID responses, we have ignored the input/output noises in the current study. Simplified linear step-response models have been used which allows us to control solely the states associated with the measured output. An additive output disturbance assumption (similar to dynamic matrix control) in appended-state formulation is utilized in the linear constrained MPC study. Inputs contraints used in the study have been given in Table 3.5. The sample time is 0.1 hr. A control horizon of 3 and prediction horizon of 30 was chosen.

3.3.3 Simulation Results

A performance comparison between the two controller designs, mentioned in the previous section, has been done by step decreasing the oxygen demand by 10%. These responses have been shown in Figure 3.19. In practice, this is done in a ramp fashion, where the rate of demand change can be adjusted. Here, we do it to maintain consistency between pure Aspen (PID design) and Aspen + Matlab (MPC design) simulation results. Both controllers give robust performance and purity deviations remains within ±1% during transient state. A steep change in response immediate following the demand change shows the fast-acting pressure-

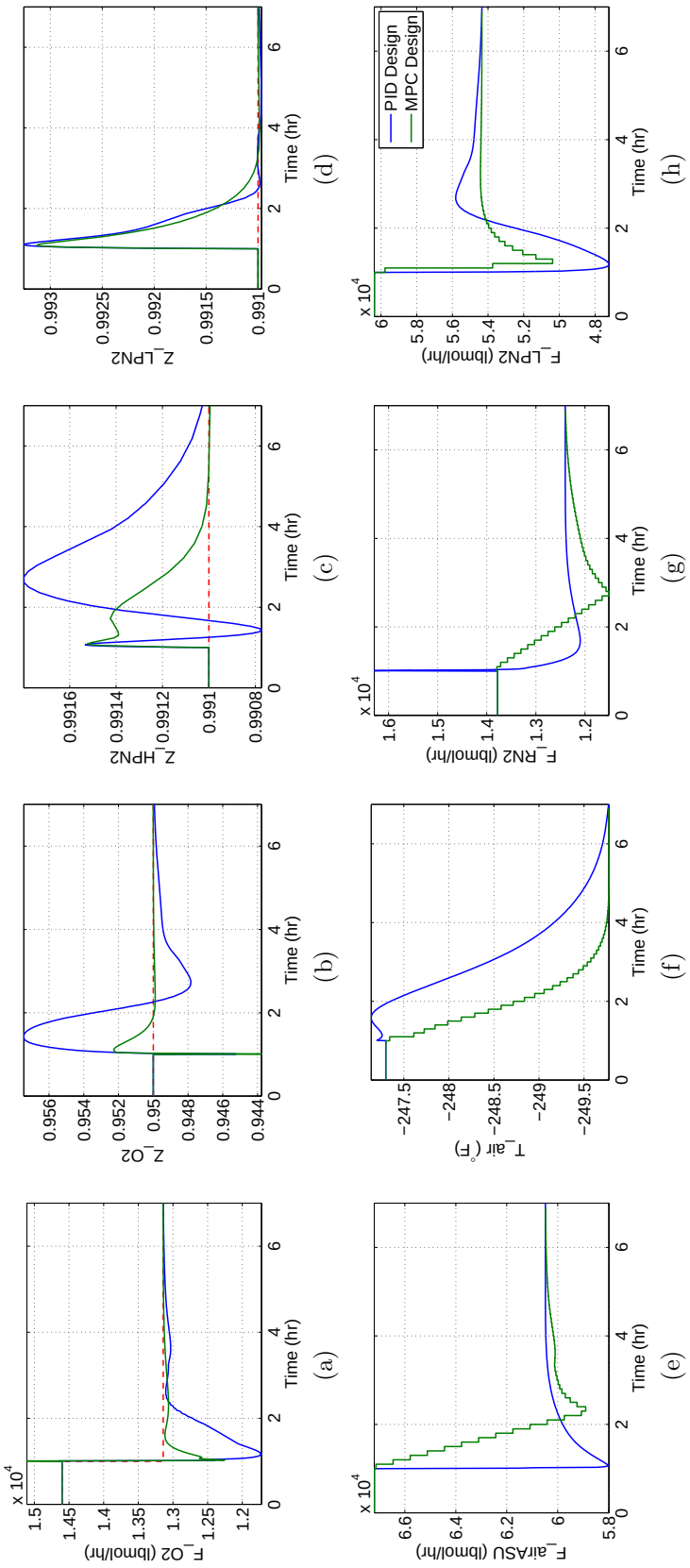

Figure 3.19: Simulation results showing EP-ASU PID vs. MPC controller responses for 10% decrease in oxygen demand. Outputs are shown in top row, inputs in bottom row

dynamics. The transients in oxygen flowrate is seen for one hour, during which the product quantity dips to a minimum of 80% value, with an increased purity. This behavior is not desirable when the product stream is linked with another plant sub-unit such as a gasifier, and hence the entire plant is ramped to desired load condition.

Upon close observation of responses, we also find that all the PID controller moves, except T_air, are aggressive but still fail to attain new setpoint values in a shorter time than the MPC controller. The key difference here is the rate at which refrigeration is provided, which in case of MPC design, brings back oxygen purity to steady value within one hour. This indirectly actuates condensation/flashing of the vapor due to rapid pressure changes induced by flowrate perturbations. Many units provide this refrigeration in form of an additional expander unit which connects part of the feed air to the LP-column. In some other systems, a nitrogen liquification tank (in the path of LN2 streams) is maintained which provides liquid nitrogen as refrigeration during transient states [100]. In addition, multiloop PID scenario presents a high loop-loop interaction and additional control moves are made to annul the effect of control moves made by another loop. Multivariable MPC determines the best possible combination of all control moves, by solving a least-square optimization problem at each time-step, to meet the requirement in a best possible way.

3.4 Discussion and Conclusion

In Chapter 2, a pressure-driven dynamic model of an ASU is built using rigorous Aspen simulation. This ASU unit to be installed as part of IGCC power plant, must have unique characteristics of fast load following depending on gasifier oxygen demand. In this chapter, initially a PID-based controller scheme having a two-layered hierarchical structure is proposed to maximize the dynamic yield of oxygen based on optimum value of reflux liquid nitrogen sent to LP-column. Later, a linear model predictive control strategy with absolute and rate-of-change constraints is designed using the supervisory-layer input/outputs to compare and investigate any performance benefits compared to the previous PID-based design. Simulation studies based on both of these designs give an attainment of desired flowrate and purity

levels up to acceptable limits within 5-6 hrs of a 10% step change in load-demand. A linear MPC scheme outperforms the PID-based controller even with absolute and rate-of-change constraints. It is also found that with significant composition-measurement delays, a feedforward/ratio scheme without any feedback, leads to meeting the set-point quickly with an acceptable level of offset.

"Interim analysis" shows that the ASU dynamics change rapidly when a multistream feed-product heat-exchanger is incorporated in the model leading to open-loop unstable operation. To stabilize and control this behavior, refrigeration either in form of pre-feed cooler or turboexpander work is provided to the columns which can be seen from rapid heat-removal (fast decrease of T_air in Figure 3.19f) during transient states. From the controller responses, it is also realized that this refrigeration amount is responsible for determining the rate at which oxygen purity and flowrate meets desired setpoint. The same refrigeration is provided in form of liquid nitrogen extracted from a storage vessel (in path of liquid nitrogen reflux stream) or by using external refrigerants during transient states. This study also justifies the engineering effort required for controller development/maintenance for IGCC integrated ASU.

The MPC scheme used in this chapter involves a linear step-response model built around the dynamic non-linear ASU plant-model (developed in Chapter 2). A future direction of research might focus on exploiting better system identification tools such as multisine input signal to improve model quality for ASU control. In addition, to capture non-linearities, the Aspen model may be linearized at multiple operating-loads to design and implement a multiple model predictive control (MMPC) strategy. A key limitation of this study is the use of direct composition measurements for controlling purity. To best "mimic" the composition measurement lag involved in real plants, dead-time blocks associated with these measurements are used in our simulations. Alternatively, using relatively "faster" temperature measurements (or differential tray-temperature measurements) for controlling the ASU process may lead to a better and robust performance. All of these are discussed within the scope of future research directions in Chapter 9.

CHAPTER 4
DYNAMIC MODELING AND CONTROL OF GASIFICATION ISLAND

In chapters 2 and 3, a rigorous model for the air separation unit (ASU) was designed. This unit consumes about 15–25% of the IGCC gross power produced and is one of the IGCC subsections with very slow dynamics, serving as a major bottleneck to the entire process. In this chapter, we focus on dynamic modeling and control of the heart of an IGCC power plant – the "gasification island". The gasification island, in general, includes the coal distribution system, the GE–Texaco based gasifier with 'radiant-only' cooling, the syngas quench, water-gas shift reactors (CCS only), syngas-cooling, sulphur-removal and CO_2-removal stages (CCS only). This subunit can be categorized relating to two kind of IGCC plants: (1) plants without carbon capture and sequestration (CCS) based on Parson's IGCC Case#1 flowsheet, and (2) plants equipped with CCS based on Parson's IGCC Case#2 flowsheet. The first section of this chapter gives a detailed dynamic modeling and control procedure for the gasification island in plants *without CO_2 capture*, before moving to those *with CO_2 capture* in the subsequent section.

4.1 Gasification Island (without CO_2 capture)

Most of the literature deals exclusively with steady-state conditions and design of the gasifier without much focus on its dynamics and control aspect. In addition, model details, equipment sizes and parameter values are hardly specified or made available. Steady-state analysis involving solids using Aspen Plus is possible [101] but export to Aspen Dynamics is currently not supported. An approximate workaround using high molecular weight hydrocarbon, $C_{18}H_{20}$, as a pseudofuel has been used based on the AspenPlus^{TM}/AspenDynamics^{TM} model by Robinson and Luyben (2008) [102]. In this article, a 99% conversion of carbon has been assumed based on Tampa Electric Company (TECO) report [9].

Another method employed as a workaround for solid handling in AD involves

treating non-conventional (NC) solids as electrolytic-salts and use electrolytic NRTL property method for thermodynamic calculations. This method has been used as a 'pseudo' coal in the plantwide dynamic simulator study by NETL [103], and results have been validated with Parson's flowsheet using NC-solids.

4.1.1 Steady-State and Dynamic Design

On carefully reviewing NETL IGCC Parson's flowsheet and tabulating the gasifier input/output stream results (Table 4.1)[22], we find that coal has lot of ash component in it. This component does not take part in the reactions and from material balance point of view is converted to slag (at high gasification) temperature according to the following equation

$$0 \cdot 8834\,\mathrm{ASH} + 0 \cdot 009708\,\mathrm{C} \longrightarrow \mathrm{SLAG}$$

Table 4.1: Relevant gasifier input-output stream results of IGCC (Parson's) flowsheet

	COAL	WATER	OXIDANT	PRODUCTS
Mole Flow lbmol/hr				
H_2O	3088.62	11410.11		7490.60
Ar			416.48	416.49
CO_2				7920.14
O_2	1077.14		12364.47	0.00
N_2	276.24		234.27	467.17
CH_4				51.77
CO				18041.15
COS				9.91
H_2	11163.25			17556.60
H_2S				381.21
NH_3				86.68
C	26556.19			0.00
S	391.12			0.00
Mass Flow lb/hr				
SLAG	0.00			54925.24
ASH	48520.96			0.00

[22]This is applicable to both Case#1 and Case#2, since we are focusing on the balance around gasifier-only (excluding the shift, cleanup units, etc.)

This 'pseudo' reaction consumes some small quantity of "active" carbon in coal which now becomes unavailable for the gasification reactions. On calculation[23] this quantity amounts to 2% of total carbon content in coal. In our new model, we need to incorporate this loss of active carbon as unburnt fuel which amounts to $0.02 \times 1447 = 28.94$ lbmol/hr of unburnt $C_{18}H_{20}$ (which is the new hydrocarbon equivalent of coal). This is specified as a "Design Spec" in Aspen flowsheet where the oxygen flowrate is varied to determine the amount of unburnt hydrocarbon.

The gasifier operates at 2500°F and 800°F psi. The partial oxidation zone in a real coal gasifier operates adiabatically, with just enough oxygen fed to raise the temperature to the desired level for high conversion of the coal. The partial oxidation zone in the approximate gasifier model studied/used here does not operate adiabatically. A small heat removal term is directly related to the heat of dissociation corresponding to any hydrocarbon, C_nH_m.

$$C_nH_m + \tfrac{1}{2}nO_2 \longrightarrow nCO + \tfrac{1}{2}mH_2$$

It has been demonstrated in the above-mentioned article that moving from $C_{10}H_{10}$ fuel to a $C_{18}H_{20}$ fuel requires less heat to be removed from the partial oxidation zone of the gasifier and the amount of oxygen is adjusted for any type of fuel to consume 99% of the fuel. Here in our study, instead of 99%, we match the consumed fuel to Parson's flowsheet as has been mentioned in details above.

Sulfur removal is achieved by converting hydrogen sulfide to elemental sulfur using an Aspen "RGibbs" reactor block (CLAUS in Figure 4.3) which uses overall Claus reaction equation (without thermal and catalytic steps):

$$H_2S + \tfrac{1}{2}O_2 \longrightarrow S + H_2O$$

with a "forced" complete conversion of H_2S. The 95% pure oxygen for this reaction is provided by a separate stream and is not extracted from the air separation unit for this study. Further downstream, a simple flash drum (SourSep in Figure 4.3) operating at 120°F, separates unburnt fuel ($C_{18}H_{20}$), sulfur and most of the water from desired syngas stream. Table 4.2 gives the inlet-outlet stream results from the AspenPlus™ simulation for the gasification island sub-section.

[23] Amount of carbon unreacted = 54925.24 (mass of SLAG in gasifier product) – 48520.96 (mass of ASH in gasifier feed) = 6404.28 lb/hr. Hence, percentage of unburnt carbon = $\frac{6404.28}{26556.19 \times 12} \times 100 = 2$

Table 4.2: Steady-state stream results for Gasification-Island (Case#1) model

	Fuel	Water	Oxygen	Syngas	Waste
Flowrate (lbmol hr^{-1})	2087	14502	14356	46205	25843
Temperature (°F)	141	141	206	119.8	117
Pressure (psi)	1000	1000	1000	748	748
Mole Fractions					
H_2				0.418	0
CO				0.394	0
CO_2				0.165	192 ppm
H_2O		1		0.003	0.984
O_2			0.95	0	0
N_2	0.115		0.018	0.011	0
Ar			0.032	0.01	0
$C_{18}H_{20}$	0.693			0	470 ppm
H_2S				0	0
SO_2	0.192			0	0
S				0	0.015

Table 4.3 compares the final syngas (sent to the gas turbine) composition for Parson's IGCC Case#1 gasifier model vs. current gasifier model. In the Parson's Case#1 flowsheet we have two syngas streams extracted from Selexol #1 and Selexol #2 stages. These gases are eventually mixed before igniting it in a turbine. It can be found that the specific properties including molar composition, molar enthalpy, density and average MW (weighted with respect to respective flowrates of Selexol #1 and Selexol #2) closely matches with the current version of syngas. The total flowrate quantity is very similar i.e. 44584 lbmol/hr and 46205 lbmol/hr for Parson's and new flowsheet respectively.

Most of the equipment specifications (estimated volumes and metal weights) have been modified for twice the throughput as that specified in Luyben's article (as the designs are based on a single gasifier, whereas in NETL design we operate two gasifiers in parallel). The dynamic simulation for this block involves 4,600 equations solved by an equation oriented approach using a variable step Gear's method. It is assumed that the dynamic model, in spite of substantial simplification in gasification-block downstream units (AGR, Claus, tail-gas cleaning), should adequately capture the macroscale thermal, pressure, flow and composition dynamics of the gas-phase gasifier.

Table 4.3: Comparison showing syngas (post cleanup) streams details between Parson's and current flowsheet for Case#1

	Parson's IGCC #1		CURRENT
	Selexol #1	**Selexol #2**	
Mole Flow lbmol/hr			
H_2O	35.79	0.00	115.51
Ar	393.95	20.96	459.35
CO_2	5743.49	2150.22	7605.56
O_2	0.00	0.00	0.00
N_2	446.40	1155.25	498.40
SO_2	0.00	0.00	0.00
CH_4	47.88	83.03	0.09
CO	17058.99	323.55	18217.83
COS	0.15	0.00	
H_2	16911.69	211.19	19308.44
H_2S	0.50	0.54	
C/ $C_{10}H_{20}$	0.00	0.00	0.02
S	0.00	0.00	0.00
Mole Frac			
H_2O	0.0009	0.0000	0.0025
Ar	0.0097	0.0053	0.0099
CO_2	0.1413	0.5451	0.1646
O_2	0.0000	0.0000	0.0000
N_2	0.0110	0.2929	0.0108
SO_2	0.0000	0.0000	0.0000
CH_4	0.0012	0.0210	0.0000
CO	0.4198	0.0820	0.3943
COS	0.0000	0.0000	
H_2	0.4161	0.0535	0.4179
H_2S	0.0000	0.0001	0.0000
C/ $C_{10}H_{20}$	0.0000	0.0000	0.0000
S	0.0000	0.0000	0.0000
Total Flow lbmol/hr	40638.84	3944.72	46204.64
Total Flow lb/hr	7.94E+05	1.39E+05	918318.8
Total Flow cuft/hr	3.47E+05	56159.47	383963.6
Temperature °F	112.23	150.5804	119.8335
Pressure psi	719	460	748
Vapor Frac	1	1	1
Liquid Frac	0	0	0
Solid Frac	0	0	0
Enthalpy Btu/lbmol	-43733.1	-96189.3	-46638.7
Enthalpy Btu/lb	-2237.32	-2736.3	-2346.6
Enthalpy Btu/hr	-1.78E+09	-3.80E+08	-2.16E+09
Entropy Btu/lbmol-R	3.963125	-1.75967	3.331143
Entropy Btu/lb-R	0.202747	-0.05006	0.167604
Density lbmol/cuft	0.117153	0.070241	0.120336
Density lb/cuft	2.289998	2.469202	2.391682
Average MW	19.54713	35.15308	19.87503
Liq Vol 60°F cuft/hr	34844.26	3384.229	39573.95

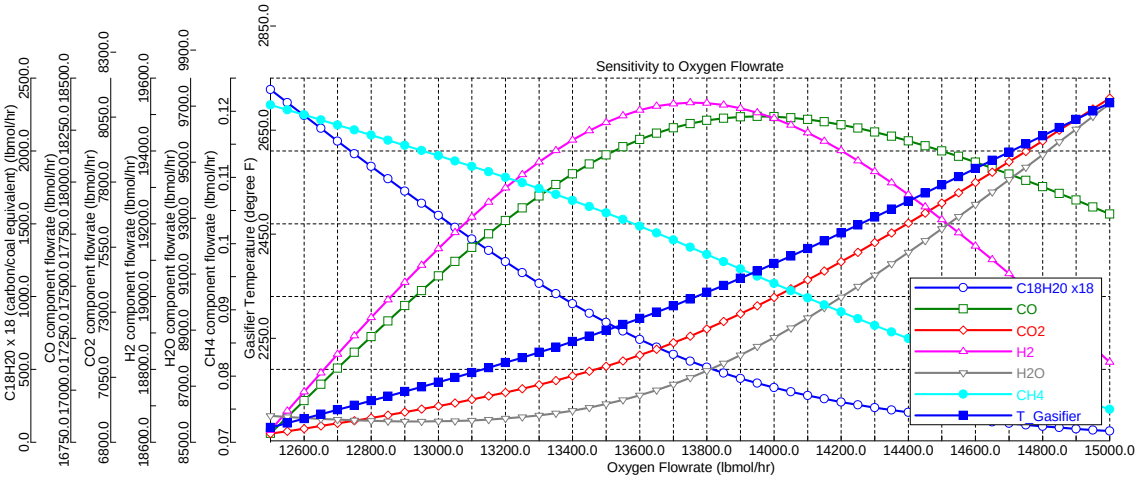

Figure 4.1: Gasifier sensitivity to oxygen flow

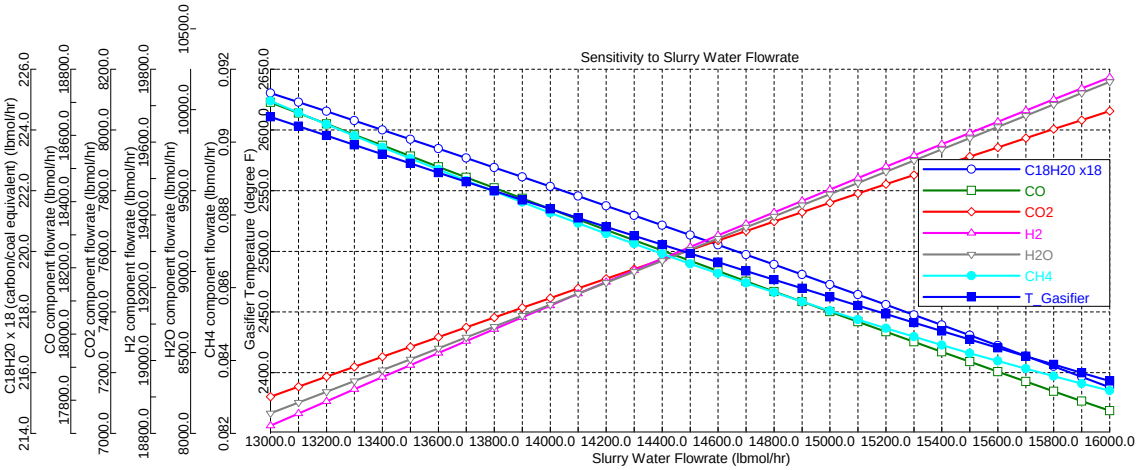

Figure 4.2: Gasifier sensitivity to slurry-water flow

4.1.1.1 Gasifier Sensitivity studies

Figure 4.1 and 4.2 show the sensitivity of gasifier temperature and molar flowrate of various components in the gasifier product stream[24] to different oxygen and slurry-water flowrates respectively. We observe that for a certain range of oxygen flowrates, H_2 and CO reach the maximum production rate. Decreasing the oxygen flow, reduces the fuel conversion, shifting the COAL $\longleftrightarrow$ SLAG kinetics towards the left, whereas increasing it lead the reaction towards full oxidation, producing more CO_2 and H_2O. It can also be observed that the gasifier temperature

[24]Note: The flowrates correspond to "internal" gasifier stream immediately before the water quench. The temperature representing the *highest core temperature* is right after the partial oxidation stage (first reactor)

increases monotonously with increasing oxygen flow. For a fixed flow of oxygen, if the slurry-water feed is changed, we observe a reverse response in H_2 and CO production, which shows that the H2/CO ratio is a strong function of slurry-water flowrate. These qualitative results will be further quantified when we calculate the RGA matrix for supervisory control layer, later in the section.

4.1.2 Regulatory Control Layer

Here, we look at the dynamics and controllability of the gasifier section, independent of the air separation unit, discussed previously. This signifies that, during the study, the controller assumed that the oxygen demand by the gasifier is readily/instantaneously met by the ASU without any purity fluctuations. Later in the report, when we will club all these sub-section and perform a plantwide assay, the oxygen stream dynamics start playing an important role.

Figure 4.3 shows the Aspen Dynamic flowsheet with relevant internal controllers installed. The flowrate of fuel, water and oxygen are flow controlled. The controller (prefixed with FC) manipulates the corresponding upstream valve to attain the desired flowrate. Pressure in the gasifier is controlled by the control valve "VOUT" on the gas stream after the quench (PC). The temperatures of the gas leaving the first two parts of the radiant cooler are controlled by manipulating the corresponding coolant temperatures (TCRX1 and TCRX2). Physically this corresponds to changing steam pressure. The temperature of the gas leaving the radiant cooler is controlled by manipulating heat removal (TCRadCool). The temperature of the gas leaving the quench is controlled by manipulating quench water flowrate valve (TCquench). The Claus reactor is considered adiabatic and there are no temperature controllers installed. Instead a feed-forward ratio control (shown the figure as O2/H2S multiplier block) is used which measures the H_2S molar flowrate in the main feed stream (to the Claus Reactor) and manipulates the molar flowrate of O2 to the reactor. The flash drum (Sour_Sep) has the basic inventory pressure and level controllers. The flash temperature is controlled by manipulating the heat duty to the flash vessel (TCSep).

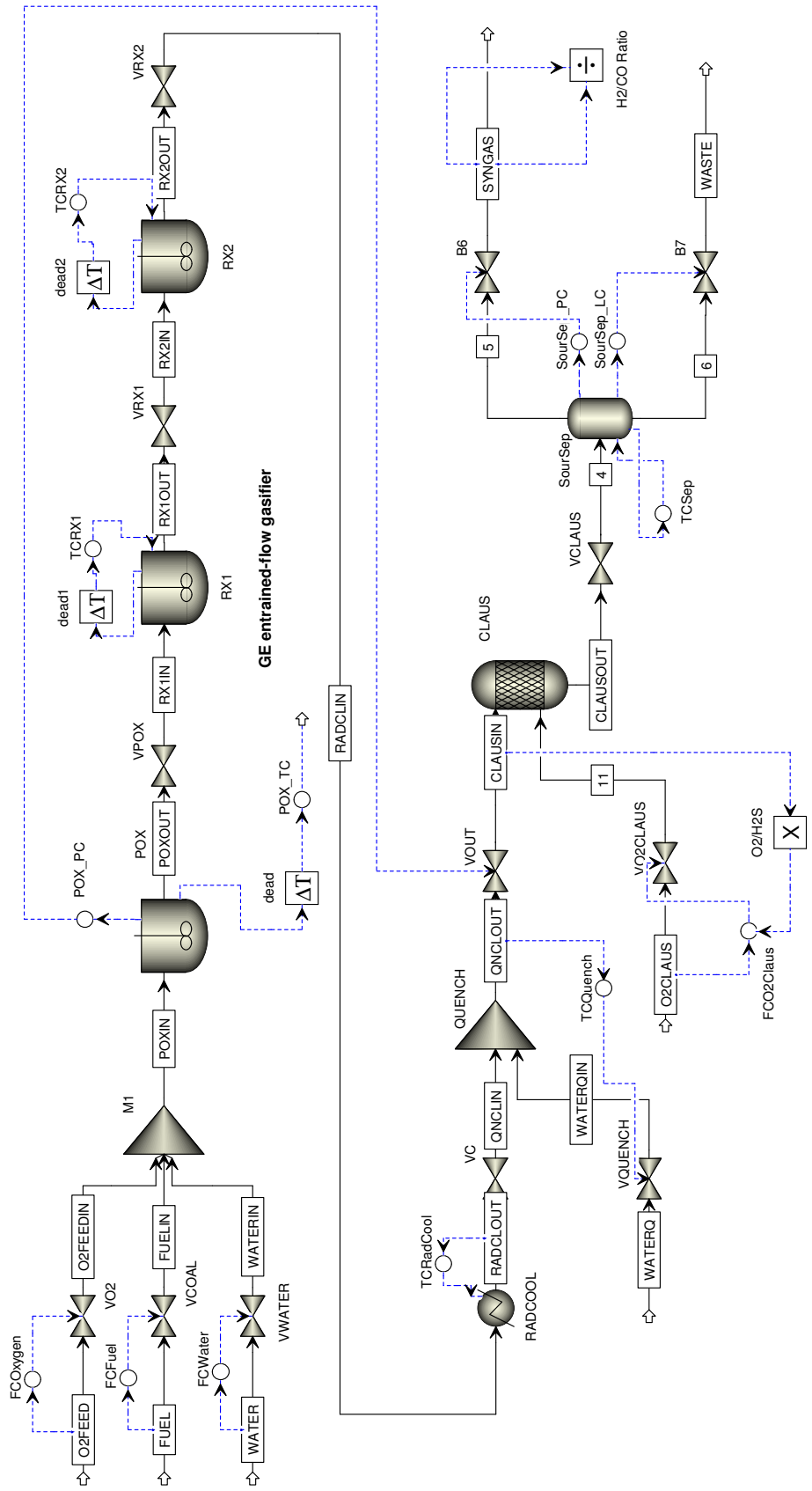

Figure 4.3: Process flowsheet showing gasification-island (Case#1) in AspenDynamics™ with regulatory layer control installed

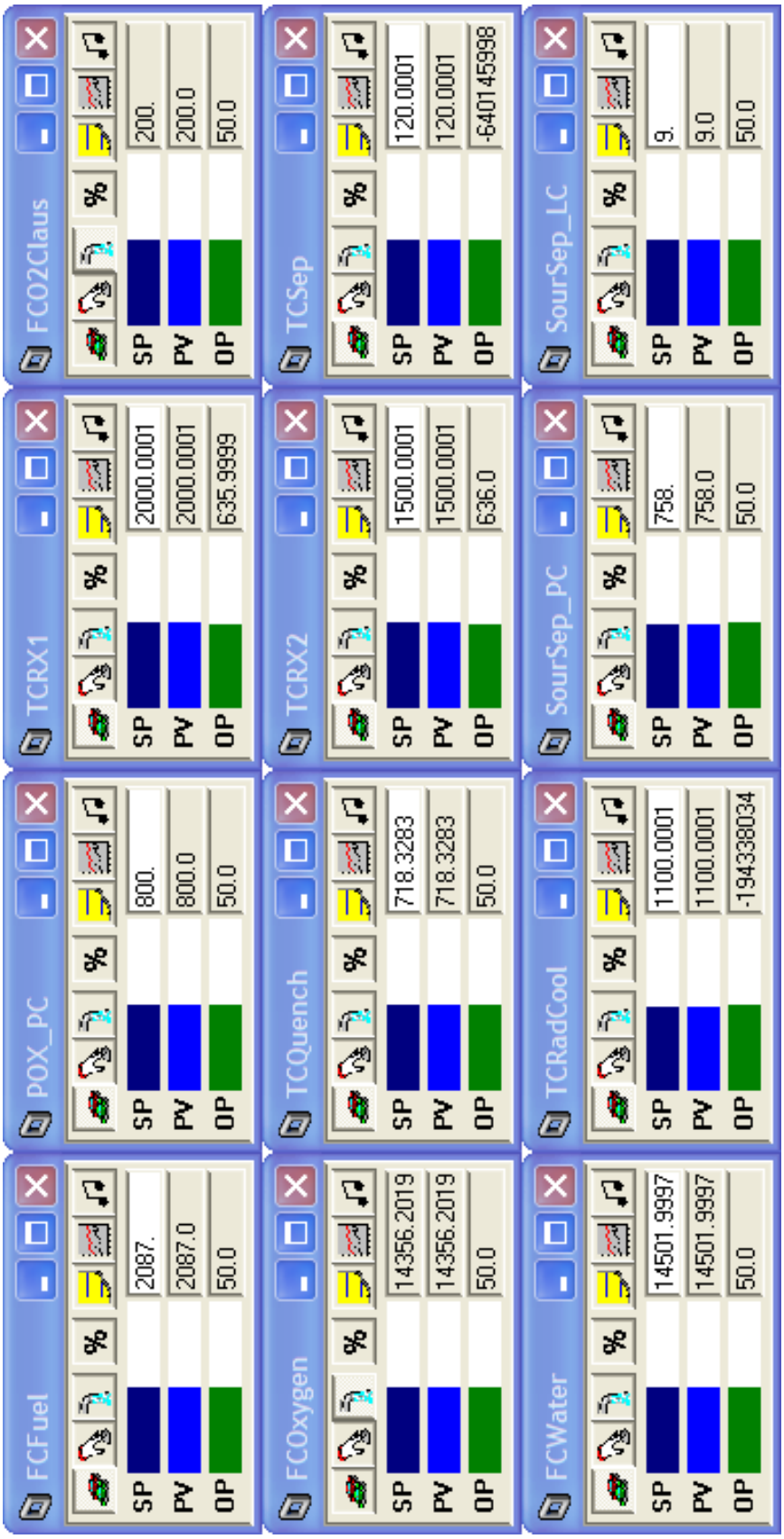

Figure 4.4: AspenDynamics™ regulatory layer controller faceplates for gasification island (Case#1)

Table 4.4: List of primary control I/O variables for Gasification Island (Case#1)

Variable	Description	Nominal
Inputs		
F_fuel	Fuel (coal equivalent/$C_{18}H_{20}$) flowrate	2087 lbmol hr^{-1}
F_water	Slurry-water flowrate to gasifier	14502 lbmol hr^{-1}
F_O2	Oxygen (95% purity, from ASU) to gasifier	14356 lbmol hr^{-1}
Outputs		
F_syngas	Pure syngas product flowrate (entering GT)	46204.6 lbmol hr^{-1}
r_H2/CO	Hydrogen to CO ratio in syngas (measure of syngas enthalpy)	1.06 lbmol/lbmol
T_gasifier	Gasifier temperature (post partial-oxidation stage)	2500°F
Disturbances		
	Coal quality	
Z_O2	Oxygen purity	0.95 lbmol/lbmol
	Gasifier pressure (partial-oxidation stage)	800 psi

4.1.3 Supervisory Control Layer

In this subsection, we discuss about the step responses to various gasifier's control input-output variables and design a PID-based multiloop controller. Multivariable control using MPC has not been studied here and will be discussed later while designing a plantwide MPC. The overall gasification island input-outputs are identified, as given in Table 4.4.

PID-based MV-SISO Design

Figure 4.5 gives us responses of the syngas flowrate, H_2/CO ratio (measure of syngas enthalpy) and gasifier temperature to 10% step changes in input variables. The process is open-loop stable for large operating conditions showing robust regulatory-layer design. The temperature of the gasifier has the fastest open-loop response and reaches the new steady state value in 10 min. In contrast, the H_2/CO takes a much longer time. It can also be seen that gasifier temperature is strongly dependent on all three input variables. H_2/CO output variable is a strong function of slurry water flowrate, suggesting this pairing for multiloop design. For determining the MV-SISO pairing, we construct the RGA matrix, when

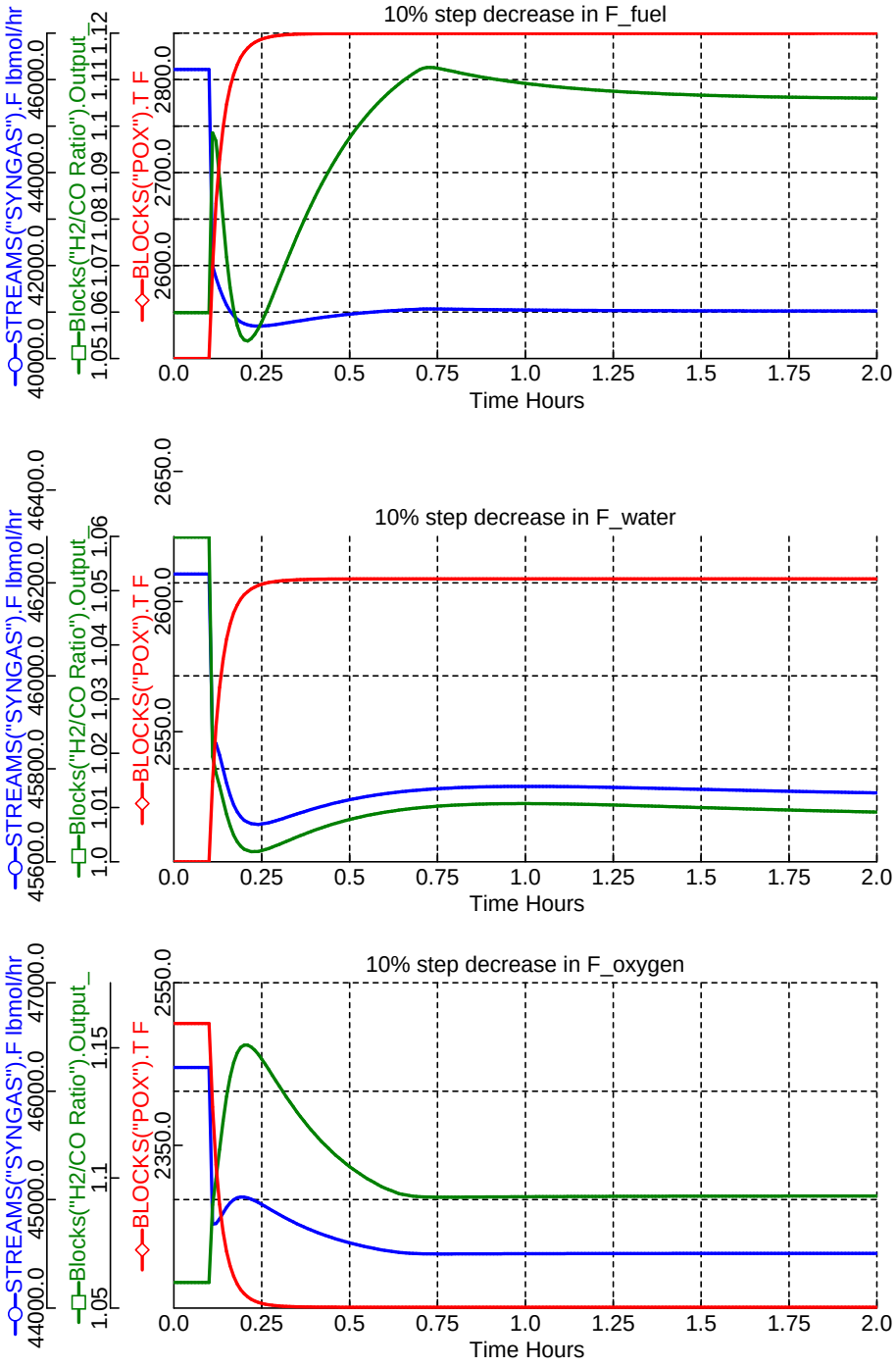

Figure 4.5: Control output responses to (I) 10% step decrease in F_fuel, (II) 10% step decrease in F_water, (III) 10% step decrease in F_O2. All input step changes given at t = 0.1 hr

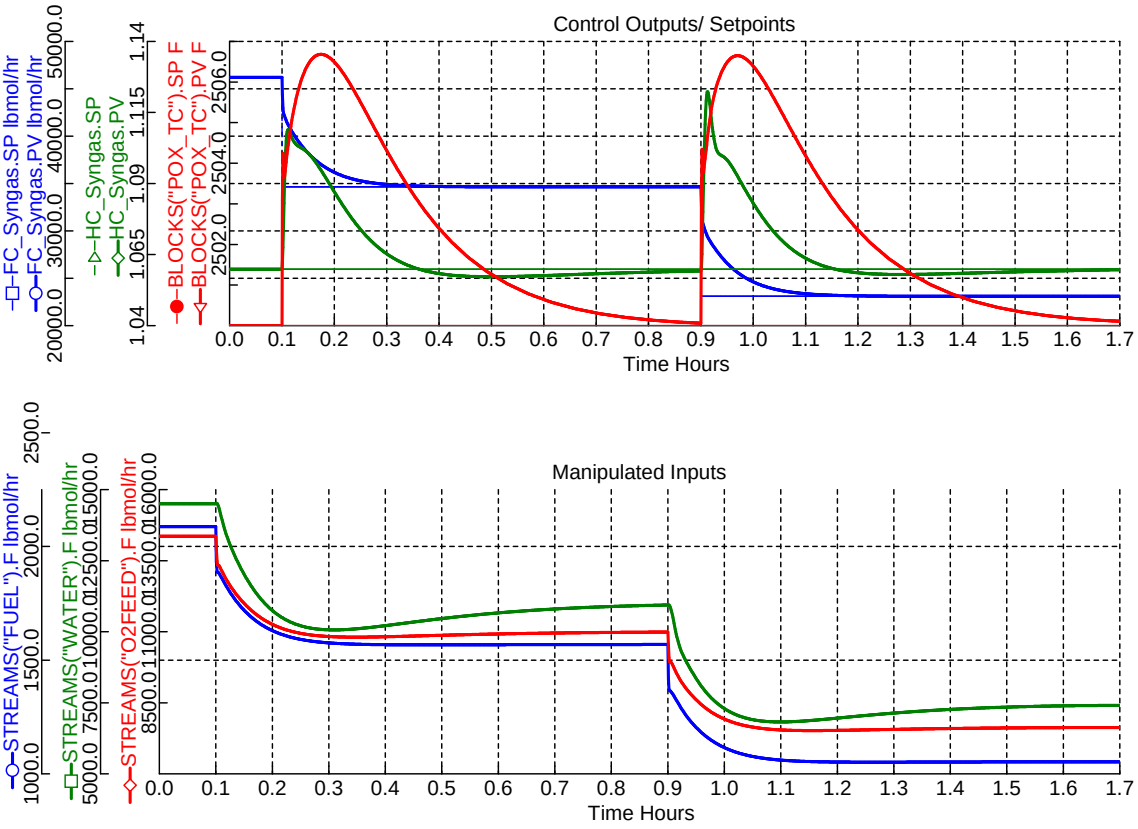

Figure 4.6: Gasifier PID-based multiloop supervisory controller response to (I) 25% step decrease in syngas production rate (F_syngas) setpoint at t = 0.1 hr, (II) 50% step decrease at t = 0.7 hr.

$u = \begin{bmatrix} \mathrm{F_{fuel}} & \mathrm{F_{water}} & \mathrm{F_{oxygen}} \end{bmatrix}$ and $y = \begin{bmatrix} \mathrm{F_{syngas}} & \mathrm{R_{H2/CO}} & \mathrm{T_{gasifier}} \end{bmatrix}$ as

$$\Lambda = \begin{bmatrix} \underline{0.576} & 0.102 & 0.322 \\ 0.129 & \underline{0.973} & -0.102 \\ 0.295 & -0.075 & \underline{0.780} \end{bmatrix}$$

which shows that F_syngas–F_fuel, r_H2/CO–F_water and T_gasifier–F_O2 are the MV-SISO loops we need to close.

Controller tuning is based on sequentially closing and tuning one loop at a time, starting with the fastest of the loops. As mentioned in previous chapter, we use the AspenDynamics^{TM} open loop test capability to determine a first order plus time delay model from u to y. Based on the model parameters, we used the SISO-IMC tuning rules [58] to design the PI-controllers.

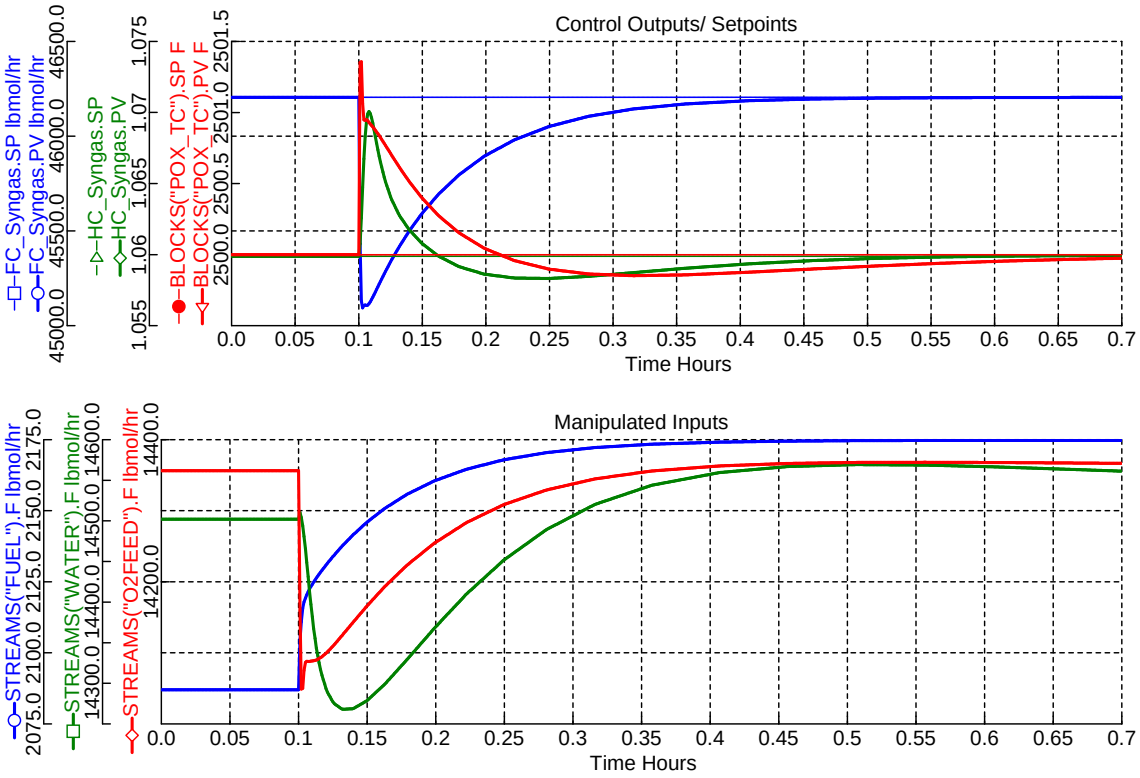

Figure 4.7: Gasifier PID-based multiloop supervisory controller response to disturbance in feed quality (50 lbmol/hr increase in CO, 40 lbmol/hr increase in H_2S and 2 lbmol/hr decrease in $C_{18}H_{20}$) at t = 0.1 hr

It can seen from the responses given in Figure 4.6, that the controller is very robust and can handle large range of step-changes in setpoints (load changes). It is also interesting to note that the control input responses, where a simultaneous rate of change for each controller output can be seen. This suggest incorporating a feed-forward/ratio controller, where the ratioed value can be set by a feedback controller, as discussed here. In addition, Figure 4.7 shows the controller ability to handle large disturbance in coal quality by changing a small elemental composition percentage of sulfur, carbon and hydrogen in the fuel.

Forming the "plant" model for MPC studies

The overall block is now interfaced with Matlab/Simulink for developing a supervisory MPC control layer for gasification-island block. The Simulink block diagram showing the primary manipulated input variables and primary controller

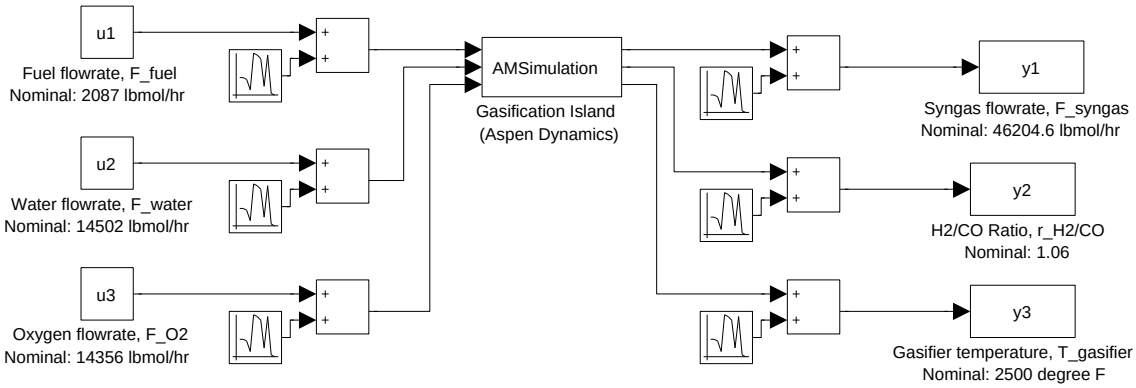

Figure 4.8: Simulink block diagram interfacing gasification island with AspenDynamics™

outputs has been given in Figure 4.8. The modified Aspen Dynamic block (with input/output noises) now acts as a surrogate plant for our centralized/decentralized control studies. The noises are Gaussian distributed with a 0.1% standard deviation of corresponding input/output steady state value.

4.2 Gasification Island (with CO_2 capture)

We extend our study on modeling and control of gasification island to IGCC plants equipped with carbon-capture and sequestration. This study is based on NETL IGCC Case#2 flowsheet developed by Parsons Corporation (Aspen filename – `igcc005.bkp`) which models an advanced IGCC system based on the General Electric (GE) Energy gasifier; Syngas desulfurization is provided by a Selexol Acid Gas Removal (AGR) system and a two-bed Claus Unit with Tail Gas Recycle to Selexol; 95% CO2 Capture is accomplished in the Selexol system, and the product is compressed to 2200 psig. The following subsection gives details of a steady-state and dynamic gasification-island design which incorporates many dynamically-relevant equipment-level modifications absent in the Parson's flowsheet, followed by regulatory and supervisory control implementation of this pressure-driven subsection model.

4.2.1 Steady-State and Dynamic Design

Similar to the modeling procedure given earlier (no CO_2 capture), the choice of pseudo-fuel for coal and the gasifier design are based on reference [102]. Most of the design procedure, relevant approximations and other flowsheeting-options, such as various design-specs, remain similar to the previous-case (see page 111). The resultant raw-syngas product is then shifted, cooled, cleaned-up of acid-gases and CO_2, and again warmed before combusting in GT. Design and modeling involved in these steps, which were not part of Case#1, are discussed next.

4.2.1.1 Water Gas Shift

In most hydrocarbon processors, the water gas shift reactor is the biggest and heaviest component because the reaction is relatively slow compared to the other reactions and is inhibited at higher temperatures by thermodynamics. Therefore, reducing the size of the water gas shift reactor is an important issue. To capture the dynamics and design these reactors using process simulation and optimization, WGS reaction kinetics are a required and key component.

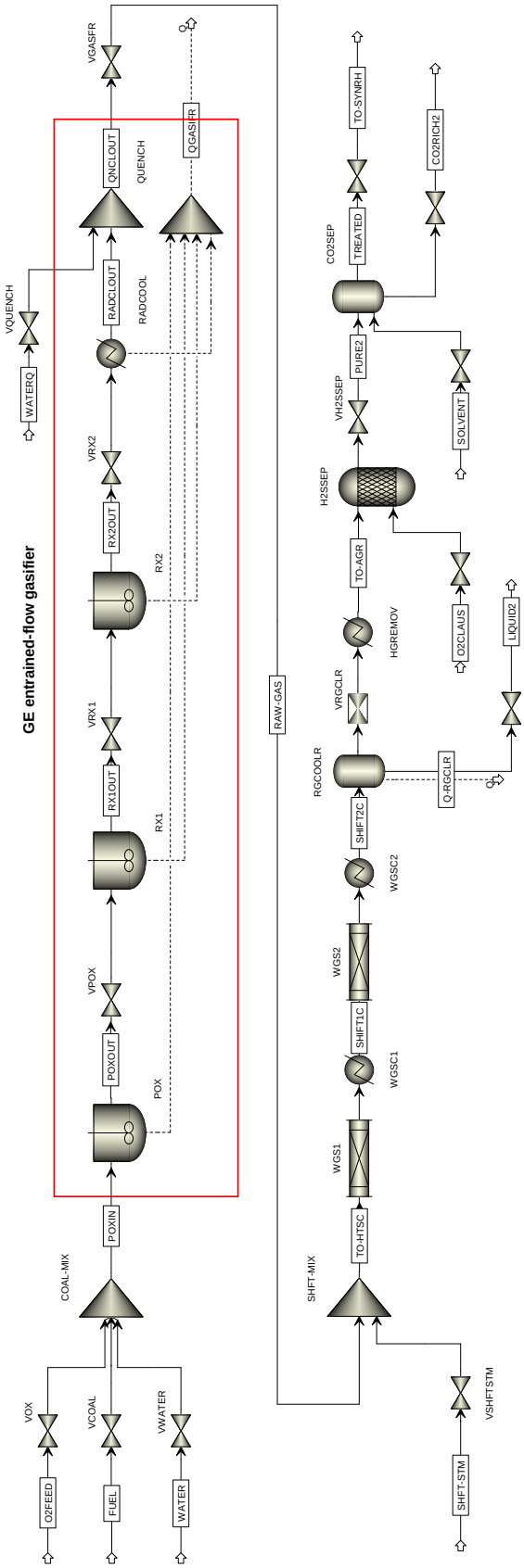

Figure 4.9: Process flowsheet showing gasification island (Case#2) in AspenPlus™

Table 4.5: AspenPlus™ steady-state stream results for Gasification Island (Case#2) (see Figure 4.9) - I

Stream Name	FUEL	WATER	O2FEED	POXIN	POXOUT	RX1OUT	RX2OUT	RADCLOUT	WATERQ	RAW-GAS
Total Flow (lbmol/hr)	2087.00	14502.00	13798.26	30387.26	55151.93	55168.88	55168.76	55168.76	16000.00	71168.76
Total Flow (lb/hr)	3.74E+05	2.61E+05	4.44E+05	1.08E+06	1.08E+06	1.08E+06	1.08E+06	1.08E+06	2.88E+05	1.37E+06
Temperature (°F)	141.0	141.0	206.0	4.3	2500.0	2000.0	1500.0	1100.0	200.0	422.5
Pressure (psia)	1000.0	1000.0	1000.0	800.0	800.0	799.8	799.6	799.0	1000.0	798.0
Vapor Fraction	0.039	0	1	0.450	1	1	1	1	0	1
Enthalpy (Btu/lb)	18.9	-6794.8	22.7	-1628.3	-1672.1	-1928.2	-2189.3	-2367.8	-6730.8	-3287.2
Mole Flow (lbmol/hr)										
H_2O		14502.00		14502.00	12362.34	11044.21	8756.27	8756.27	16000.00	24756.27
Ar			441.54	441.54	441.54	441.54	441.54	441.54		441.54
CO_2				0.00	3622.91	4947.79	7235.83	7235.83		7235.83
O_2			13108.35	13108.35	10.47	0.01	0.00	0.00		0.00
N_2	240.00		248.37	488.37	488.37	488.37	488.37	488.37		488.37
SO_2	400.00			400.00	3.11	0.02	0.00	0.00		0.00
CH_4				0.00	0.00	0.03	0.09	0.09		0.09
CO				0.00	21883.38	20578.84	18290.76	18290.76		18290.76
H_2				0.00	15912.92	17239.22	19527.04	19527.04		19527.04
H_2S				0.00	396.89	399.98	400.00	400.00		400.00
$C_{18}H_{20}$	1447.00			1447.00	29.98	28.85	28.85	28.85		28.85
S				0.00	0.00	0.00	0.00	0.00		0.00
MEA				0.00	0.00	0.00	0.00	0.00		0.00
MEA^+				0.00	0.00	0.00	0.00	0.00		0.00
$MEACOO^-$				0.00	0.00	0.00	0.00	0.00		0.00
Mole Frac										
H_2O		1.000		0.477	0.224	0.200	0.159	0.159	1.000	0.348
Ar			0.032	0.015	0.008	0.008	0.008	0.008		0.006
CO_2				0.000	0.066	0.090	0.131	0.131		0.102
O_2			0.950	0.431	0.000	0.000	0.000	0.000		0.000
N_2	0.115		0.018	0.016	0.009	0.009	0.009	0.009		0.007
SO_2	0.192			0.013	0.000	0.000	0.000	0.000		0.000
CH_4				0.000	0.000	0.000	0.000	0.000		0.000
CO				0.000	0.397	0.373	0.332	0.332		0.257
H_2				0.000	0.289	0.312	0.354	0.354		0.274
H_2S				0.000	0.007	0.007	0.007	0.007		0.006
$C_{18}H_{20}$	0.693			0.048	0.001	0.001	0.001	0.001		0.000
S				0.000	0.000	0.000	0.000	0.000		0.000
MEA				0.000	0.000	0.000	0.000	0.000		0.000
MEA^+				0.000	0.000	0.000	0.000	0.000		0.000
$MEACOO^-$				0.000	0.000	0.000	0.000	0.000		0.000

Table 4.6: AspenPlus™ steady-state stream results for Gasification Island (Case#2) (see Figure 4.9) - II

Stream Name	SHFT-STM	TO-HTSC	SHIFT1C	SHIFT2C	LIQUID2	TO-AGR	O2CLAUS	SOLVENT	TO-SYNRH	CO2RICH2
Total Flow (lbmol/hr)	11825.26	82994.02	82994.02	82994.02	18979.27	64014.75	208.16	42059.81	40537.33	65943.06
Total Flow (lb/hr)	2.13E+05	1.58E+06	1.58E+06	1.58E+06	3.49E+05	1.23E+06	6699.018	2.57E+06	2.06E+05	3.60E+06
Temperature (°F)	615.0	449.2	450.0	450.0	90.0	98.7	200.0	100.0	101.6	-335.2
Pressure (psia)	800.0	798.0	787.5	777.0	767.0	727.0	800.0	780.0	696.2	702.5
Vapor Fraction	1	1	1	1	0	1	1	0	1	0
Enthalpy (Btu/lb)	-5573.3	-3595.2	-3745.9	-3776.3	-6694.2	-3441.0	22.3	-1844.6	-1618.0	-2656.8
Mole Flow (lbmol/hr)										
H_2O	11825.26	36581.53	21947.62	19021.53	18928.69	92.80			0.29	487.83
Ar		441.54	441.54	441.54	0.06	441.49	6.66		437.73	10.42
CO_2		7235.83	21869.74	24795.83	18.10	24777.75			1803.85	22973.90
O_2		0.00	0.00	0.00	0.00	0.00	197.76		0.10	0.00
N_2		488.37	488.37	488.37	0.03	488.34	3.75		487.15	4.94
SO_2		0.00	0.00	0.00	0.00	0.00			0.00	0.00
CH_4		0.09	0.09	0.09	0.00	0.09			0.09	0.01
CO		18290.76	3656.85	730.77	0.04	730.73			721.26	9.47
H_2		19527.04	34160.95	37087.03	0.83	37086.23			37086.23	0.00
H_2S		400.00	400.00	400.00	2.70	397.30			0.63	1.36
$C_{18}H_{20}$		28.85	28.85	28.85	28.84	0.01			0.00	0.01
S		0.00	0.00	0.00	0.00	0.00			0.00	395.31
MEA		0.00	0.00	0.00	0.00	0.00		42059.81	0.00	42059.81
MEA^+		0.00	0.00	0.00	0.00	0.00			0.00	0.00
$MEACOO^-$		0.00	0.00	0.00	0.00	0.00			0.00	0.00
Mole Frac										
H_2O	1.000	0.441	0.264	0.229	0.997	0.001			0.000	0.007
Ar		0.005	0.005	0.005	0.000	0.007	0.032		0.011	0.000
CO_2		0.087	0.264	0.299	0.001	0.387			0.044	0.348
O_2		0.000	0.000	0.000	0.000	0.000	0.950		0.000	0.000
N_2		0.006	0.006	0.006	0.000	0.008	0.018		0.012	0.000
SO_2		0.000	0.000	0.000	0.000	0.000			0.000	0.000
CH_4		0.000	0.000	0.000	0.000	0.000			0.000	0.000
CO		0.220	0.044	0.009	0.000	0.011			0.018	0.000
H_2		0.235	0.412	0.447	0.000	0.579			0.915	0.000
H_2S		0.005	0.005	0.005	0.000	0.006			0.000	0.000
$C_{18}H_{20}$		0.000	0.000	0.000	0.002	0.000			0.000	0.000
S		0.000	0.000	0.000	0.000	0.000			0.000	0.006
MEA		0.000	0.000	0.000	0.000	0.000		1.000	0.000	0.638
MEA^+		0.000	0.000	0.000	0.000	0.000			0.000	0.000
$MEACOO^-$		0.000	0.000	0.000	0.000	0.000			0.000	0.000

$$CO + H_2O \rightleftharpoons CO_2 + H_2 \qquad \Delta H^{\circ}_{298} = -41.1\text{kJ/mol} \tag{4.1}$$

In this study, we focus on conditions most likely involved in the WGS reaction at high temperature and pressure, along with large concentration of sulfur. We use the heterogeneous kinetics reported by Choi and Stenger [104] for a sulfur tolerant Sud-Chemie $Cu/ZnO/Al_2O_3$ commercial catalyst. Since the reactor(s) operate adiabatically, to ensure proper kinetics, we need the dependence of the equilibrium constant on temperature. This is given by the following equation

$$\ln(K_{\text{eq}}) = -13.148 + \frac{5693.5}{T} + 1.077 \ln T + 5.44 \times 10^{-4} T \tag{4.2}$$

where $K_{\text{eq}} \cong \dfrac{P_{CO_2} P_{H_2}}{P_{H_2O} P_{CO}}$. The reaction is slightly exothermic and its equilibrium constant decreases with increasing temperature. The units of the overall reaction rates given in the cited paper are mol g^{-1} hr^{-1}, and the pressures are in atm. These parameters must be converted into required Aspen units of kmol s^{-1} m^{-3} and Pa. The converted parameter values are given below. Overall reaction rate for WGS is given by

$$r_{CO} = k_F \exp\left(-\frac{E_F}{RT}\right)\left(P_{CO} P_{H_2O} - \frac{P_{CO_2} P_{H_2}}{K_{\text{eq}}}\right) \tag{4.3}$$

where r_{CO} is rate of reaction (kmol s^{-1} m^{-3}), k_F is forward pre-exponential factor $= 1.612 \times 10^{-5}$ (kmol s^{-1} m^{-3} Pa^{-2}), E_F is the forward activation energy $= 47400$ (kJ/kmol), P_j is partial pressure of component j (Pa).

This kinetic reactions given by Equations (4.2) & (4.3) are defined in Aspen using a generalized Langmuir–Hinshelwood–Hougen–Watson (LHHW) model. This needs rearrangement of Equation (4.3) into the following form

$$r_{CO} = k_F \exp\left(-\frac{E_F}{RT}\right)\left(\frac{K_{\text{eq}} P_{CO} P_{H_2O} - P_{CO_2} P_{H_2}}{K_{\text{eq}}}\right) \tag{4.4}$$

where the numerator term, $K_{\text{eq}} P_{CO} P_{H_2O} - P_{CO_2} P_{H_2}$, represents the driving force expression. The driving force constant in the first term of this expression has coefficient given by Equation (4.2), whereas the second term constant is -1.

The denominator term, K_{eq}, represents the adsorption expression with adsorption constant (and coefficients) given again by Equation (4.2).

In our current IGCC study, the raw syngas, after the quench stages, is mixed with high pressure steam (SHIFT-STM in Figure 4.9) to raise the shift-reactor inlet H_2O/CO molar ratio to 2. This is done in steady-state simulations using a "Design Spec" which varies the flowrate of SHIFT-STM to attain this ratio. The resultant mixture is passed through two reactor stages, i.e., a high temperature shift followed by a low temperature shift. After each of these reactor stages (shown by WGS1 and WGS2 in Figure 4.9), the gas is cooled back to 450°F in inter-stage coolers labeled as WGSC1 and WGSC2 in Figure 4.9. The heat from the first cooler (∼250 million Btu/hr) is used to generate IP-steam (2SHIFTB in Figure 6.9) Figure 6.9) from pumped IP-water in a boiler (RGCLR1 in , most of which is sent back to the shift-reactor section as shift-steam (SHIFT-STM). The heat from the second cooler (∼45 million Btu/hr) is used to generate IP-steam[25] and is eventually utilized in IP-steam turbine.

The size of each reactor is based on the conversion of CO in the product streams. This conversion is set at 80% and 96% (based on inlet to high-temperature reactor, TO-HTSC stream in Figure 4.9) at the end of high-temperature shift (HTS) and low-temperature shift (LTS) reactors respectively. "Design Specs" have been used in steady-state simulations, which varies the reactor length given a fixed reactor diameter[26]. A catalyst void fraction of 0.3 is assumed and pressure drop calculations are based on Beggs-Brill frictional pressure drop correlation, assuming a pressure drop scaling factor of 1 and roughness of 0.00015 ft.

Figure 4.10 gives the composition, temperature and pressure profiles for both the shift-reactors. It can be seen that the HTS has faster kinetics (and hence a lower equipment size) compared to the LTS. LTS has the advantage of having a higher equilibrium constant (at low temperature) and hence conversion as high as 98% can be obtained which otherwise cannot be attained using HTS alone.

[25]This steam (stream labeled 'WGS1' in Figure 6.9) is mixed with HP steam-turbine exhaust stream, just before the IP-steam reheater

[26]This diameter is also changed, on a trial-and-error basis, to obtain a L/D ratio close to 2

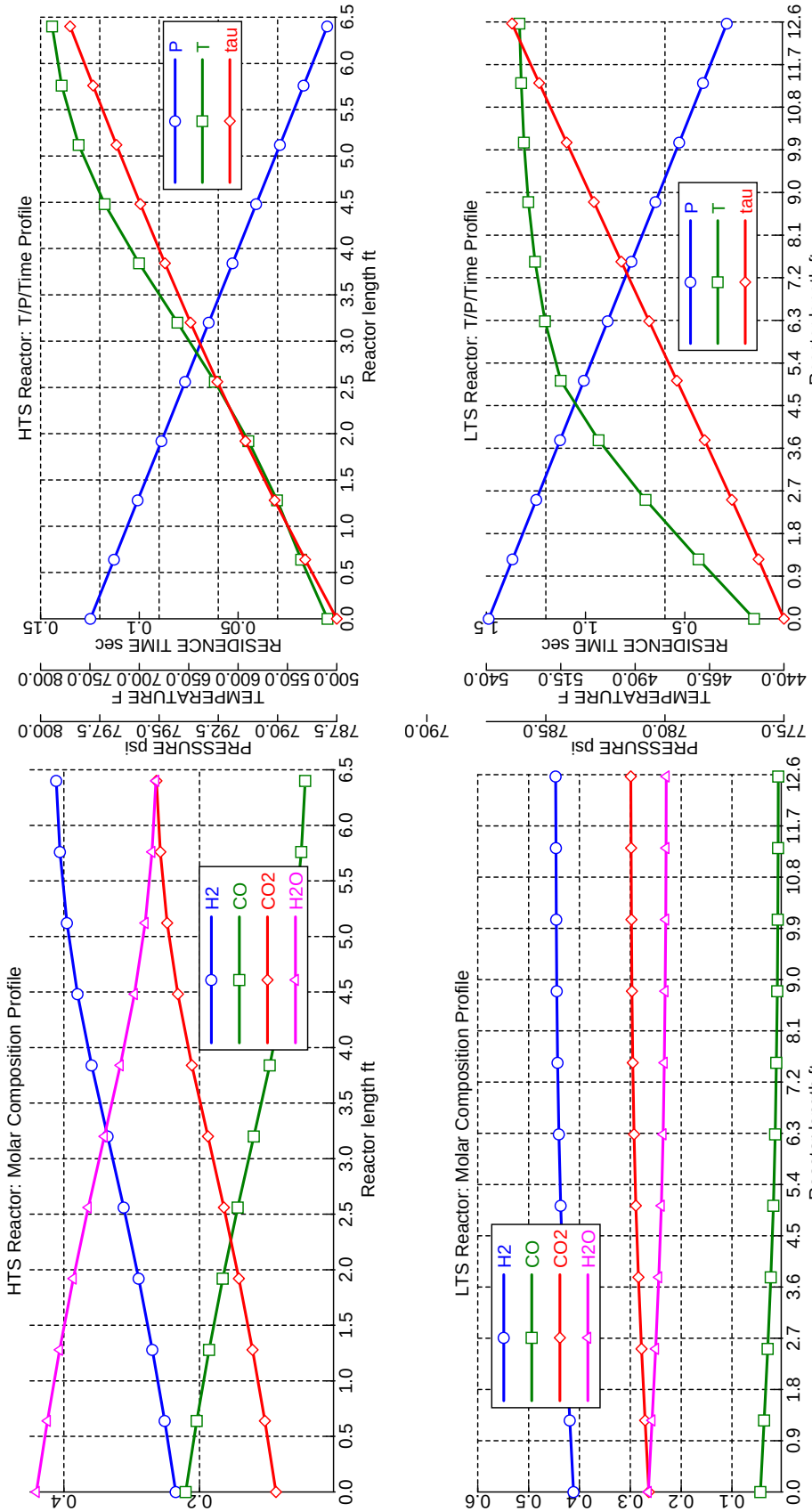

Figure 4.10: Steady-state profiles for High-Temperature Shift Reactor (top) and Low-Temperature Shift Reactor (bottom)

4.2.1.2 Acid Gas Removal

The shift reactor products are cooled to 100°F using a series of radiant-gas coolers. Part of the heat (available at 450°) is provided to the LP-boiler/evaporator. Remaining heat is used to preheat the HRSG feedwater/scrubber and coal-slurry water. In our simulation, we use a single flash-drum (RGCOOLR in Figure 4.9), with valid phases specified as vapor–liquid–liquid (V–L–L), which separates most of the "unburnt coal" (in our case – unreacted $C_{18}H_{20}$) and water from the product mixture. Each of these radiant-gas coolers, in reality, also involves large pressure drop (∼10 psi each) in the process stream. We combine all of these pressure drops into a single throttle valve (VRGCLR) with a pressure drop of 40 psi.

Sulfur Removal Moving further, we simulate the H_2S removal using a stoichiometric reactor (H2SSEP), where hydrogen sulfide is converted to elemental sulfur using an Aspen "RStoic" reactor block which uses overall Claus reaction equation (without thermal and catalytic steps):

$$H_2S + \tfrac{1}{2}O_2 \longrightarrow S + H_2O$$

with a "forced" 99.5% conversion[27] of H_2S. This is a major approximation where complex adsorption/desorption AGR steps in a Selexol/Rectisol/Sulfinol based separator is over-simplified using overall mass-energy balances. This assumption is justified by the fast dynamics involved in these adsorption/desorption units. The 95% pure oxygen for the above reaction is provided by an oxidant stream (O2CLAUS) and is not (currently) extracted from the ASU[28]. Dynamically, this implies that the oxygen demanded by the "approximated Claus" unit is being met instantly. Again, this is a valid approximation since the Claus units are, in reality, placed downstream of AGR units and does not affect the dynamics of treated–syngas stream. The flowrate of oxidant stream is calculated at runtime using a "Design Spec" such that there is negligible unreacted oxygen in the product stream.

[27]This number is obtained, on a trial and error basis, to match with that of IGCC Case #2 flowsheet. In real plant, some remnants of sulfur would be observed, and hence, providing a 100% conversion is impractical

[28]This is from the purview of studying dynamics and control of gasification island separately. In later chapters on plantwide control, this linkage has been established

CO_2 Removal We use an amine-based solvent to selectively react the carbon dioxide in the sulfur–treated syngas stream. The following electrolytic reaction chemistry is defined, with a significantly high equilibrium constant.

$$2\,\mathrm{MEA} + \mathrm{CO_2} \longleftrightarrow \mathrm{MEA^+} + \mathrm{MEACOO^-}$$

where, K_{eq} (mole-fraction basis) $= \dfrac{[\mathrm{MEA^+}][\mathrm{MEACOO^-}]}{[\mathrm{MEA}]^2[\mathrm{CO_2}]} = 25$ at 100°F and ∼700 psi.

The equilibration (and subsequent phase separation) takes place in a flash-drum (CO2SEP) where the remaining "heavy" components (which include MEA, traces of unburnt coal and "dirty" water) are separated from the "pure" syngas stream (TO-SYNRH). This flash-drum uses the Electrolyte NRTL model with Redlich-Kwong equation of state to adequately capture the thermodynamics involving amide-ions at high pressures. The flowrate of solvent stream (SOLVENT) is adjusted at runtime using a "Design Spec" such that the equilibrium concentration of CO_2 in the treated syngas matches that with Parson's IGCC Case#2 results.

Again, this model involves significant simplification in terms of process units and can be justified by the fast dynamics involved, in comparison to bottleneck processes such as ASU and gasifier. Additionally, detailed dynamic modeling of every single process units in a full-blown IGCC plant is beyond the scope of this project and "allowable" engineering approximations have to be made.

Table 4.7 compares the final syngas (sent to the gas turbine) composition for Parson's IGCC Case#2 gasifier model vs. current gasifier model. We can observe a very close match for most of the intrinsic thermodynamic properties including the specific enthalpy. Figure 4.9 shows the AspenPlus$^{\mathrm{TM}}$ flowsheet and Tables 4.5 & 4.6 give the steady-state stream results.

4.2.2 Regulatory Control Layer

Figure 4.11 shows the Aspen Dynamic flowsheet for Case#2 with relevant internal controllers installed. The flowrate of fuel, water and oxygen are flow controlled. The controller (prefixed with FC) manipulates the corresponding upstream valve to attain the desired flowrate. The setpoints to water and oxygen controllers

Table 4.7: Comparison showing syngas (post cleanup) streams details between Parson's and current flowsheet for Case#2

	Parson's IGCC #2	CURRENT
Mole Flow lbmol/hr		
H_2O	1.62	0.29
Ar	424.20	437.73
CO_2	1717.65	1803.72
O_2	0.00	0.10
N_2	513.52	487.15
SO_2	0.00	0.00
CH_4	84.31	0.09
CO	727.51	721.90
COS	0.28	
H_2	34853.29	37085.68
H_2S	0.60	0.63
NH_3	0.00	
C/ $C_{18}H_{20}$	0.00	0.00
S	0.00	0.00
Mole Frac		
H_2O	0.0000	0.0000
Ar	0.0111	0.0108
CO_2	0.0448	0.0445
O_2	0.0000	0.0000
N_2	0.0134	0.0120
SO_2	0.0000	0.0000
CH_4	0.0022	0.0000
CO	0.0190	0.0178
COS	0.0000	
H_2	0.9095	0.9149
H_2S	0.0000	0.0000
NH_3	0.0000	
C/ $C_{10}H_{20}$	0.0000	0.0000
S	0.0000	0.0000
Total Flow lbmol/hr	38322.98	40537.29
Total Flow lb/hr	198982	205526.7
Total Flow cuft/hr	330804	357971.4
Temperature °F	100.3318	101.5717
Pressure psi	696.2	696.2
Enthalpy Btu/lbmol	-8397.79	-8203.03
Enthalpy Btu/lb	-1617.38	-1617.93
Enthalpy Btu/hr	-3.22E+08	-3.33E+08
Entropy Btu/lbmol-R	-6.13	-6.20
Entropy Btu/lb-R	-1.18	-1.22
Density lbmol/cuft	0.116	0.113
Density lb/cuft	0.602	0.574
Average MW	5.19	5.07
Liq Vol 60°F cuft/hr	32876.88	34777.33

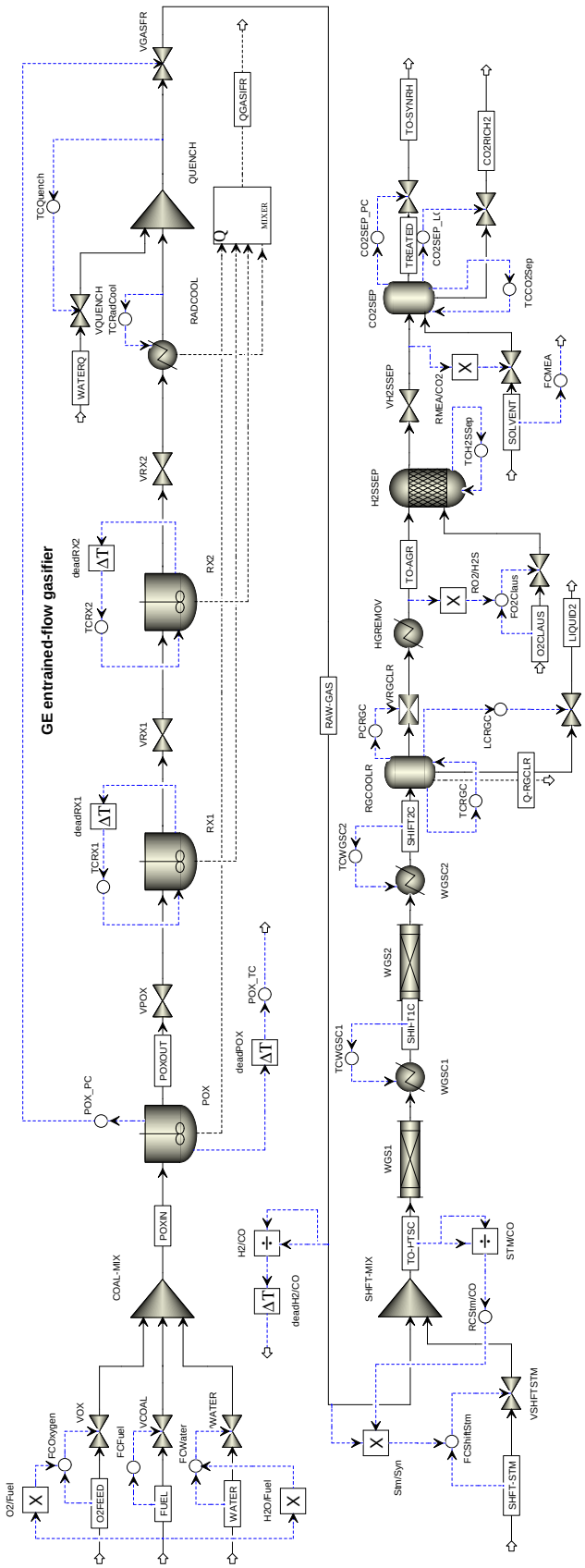

Figure 4.11: Process flowsheet showing gasification-island (Case#2) in AspenDynamics^{TM} with regulatory layer control installed

are ratioed with fuel flowrate, hence acting as a feed-forward control to fuel flow fluctuations. As in Case#1, gasifier-pressure, temperature of various gasifier reactor stages (RX1, RX2), radiant-cooler (RADCOOL) temperature and quench temperature are controlled using various pressure and temperature controllers. Relevant information within this is the direct manipulation of heat-duties for the temperature control, which sum-up and appear as total gasifier extracted heat (Q-GASIFR). It must be noted that direct manipulation of heat-duties in a real physical system is not possible since it depends on the temperature differential to the sink (HP evaporator-drum). Direct temperature manipulation of the sink/boiler is also difficult to attain[29]. Hence some kind of bypass system (either on the source or the sink side) exists which indirectly manipulates the heat-transfer coefficient to achieve this control. In our case, a simple transfer of heat, as an approximation, is done (as QGASIFR stream) to the boiler, which appears as an external heat-source (Q-GSFR in Figure 6.14) to the unit, without any temperature dependence.

Moving further downstream, the flow controller (FCShiftStm) maintains the shift-steam at desired flowrate. The setpoint to this controller is ratioed, using the Stm/Syn block, to the raw-syngas, hence acting as an 'indirect' feed-forward control to raw-syngas flow fluctuations. A ratio controller (RCStm/CO) has been used to control the steam-to-CO ratio in the shift reactor feed (TO-HTSC). This controller manipulates the ratio given to the Stm/Syn block (serving as an indirect manipulation to the amount of shift-steam). The outlet of shift-coolers (WGSC1 and WGSC2) are temperature controlled again by manipulating the heat-duties of the cooler blocks directly. The heat is given to the generate IP steam in two separator boilers (corresponding to the two coolers), shown as RGCLR1 and RGCLR2S blocks in Figures 6.9, 6.10 and 6.14. Similar to the gasifier heat, this heat transfer is approximated as a simple 'virtual' heat-stream in Aspen, without any temperature dependence.

The radiant syngas cooler, RGCOOLR, modeled as a simple flash drum has level, pressure and temperature controllers installed, manipulating the liquid-flow,

[29]This depends on the equilibrium drum-pressure; the pressure swings and limitations are generally based on the turbine operation mode and not on desired gasifier (source) operation. These concepts have been discussed extensively in Chapter 6

vapor-flow and vessel heat-duty respectively. Again, the heat is transferred as a virtual stream to the LP-boiler (IPSCBRG in Figures 6.9 and 6.10). The amount of oxygen (O2CLAUS) sent to the sulfur removal block (H2SSEP) is ratioed to the incoming syngas line (TO-AGR) using a ratio block (RO2/H2S). This unit is also temperature controlled (TCH2SSep). Further downstream, the CO2SEP flash drum is level, pressure and temperature controlled. The MEA-feed (SOLVENT) flowrate is ratio-controlled to the incoming syngas feed[30]. In the next subsection, we first identify the overall input/outputs for this island and later implement a supervisory layered control, sitting on top of this regulatory control layer.

4.2.3 Supervisory Control Layer

In this subsection, we discuss about the step responses to various gasifier's control input-output variables and design a PID-based multiloop controller. Multivariable control using MPC has not been studied here and will be discussed later while designing a plantwide MPC. The overall gasification island input-outputs are identified, as given in Table 4.8.

PID-based MV-SISO Design

Figure 4.12 gives us responses of the syngas flowrate, H_2/CO ratio (measure of syngas enthalpy) and gasifier temperature to 10% step changes in input variables. The process is open-loop stable for large operating conditions showing robust regulatory-layer design. The temperature of the gasifier has the fastest open-loop response and reaches the new steady state value in 10 min. In contrast, the H_2/CO takes a much longer time. It can also be seen that gasifier temperature is strongly dependent on all three input variables. H_2/CO output variable is a strong function of slurry water flowrate, suggesting this pairing for multiloop design. For determining the MV-SISO pairing, we construct the RGA matrix, when

[30]Due to some unexplained reason, a flow-controller on the MEA-feed led to strange oscillatory behavior at regular intervals. This maybe due to a bug in Aspen calculations when using Electrolytic NRTL property method. Manipulating the valve directly on this stream, in response to the ratio block (RMEA/CO2), solved this problem

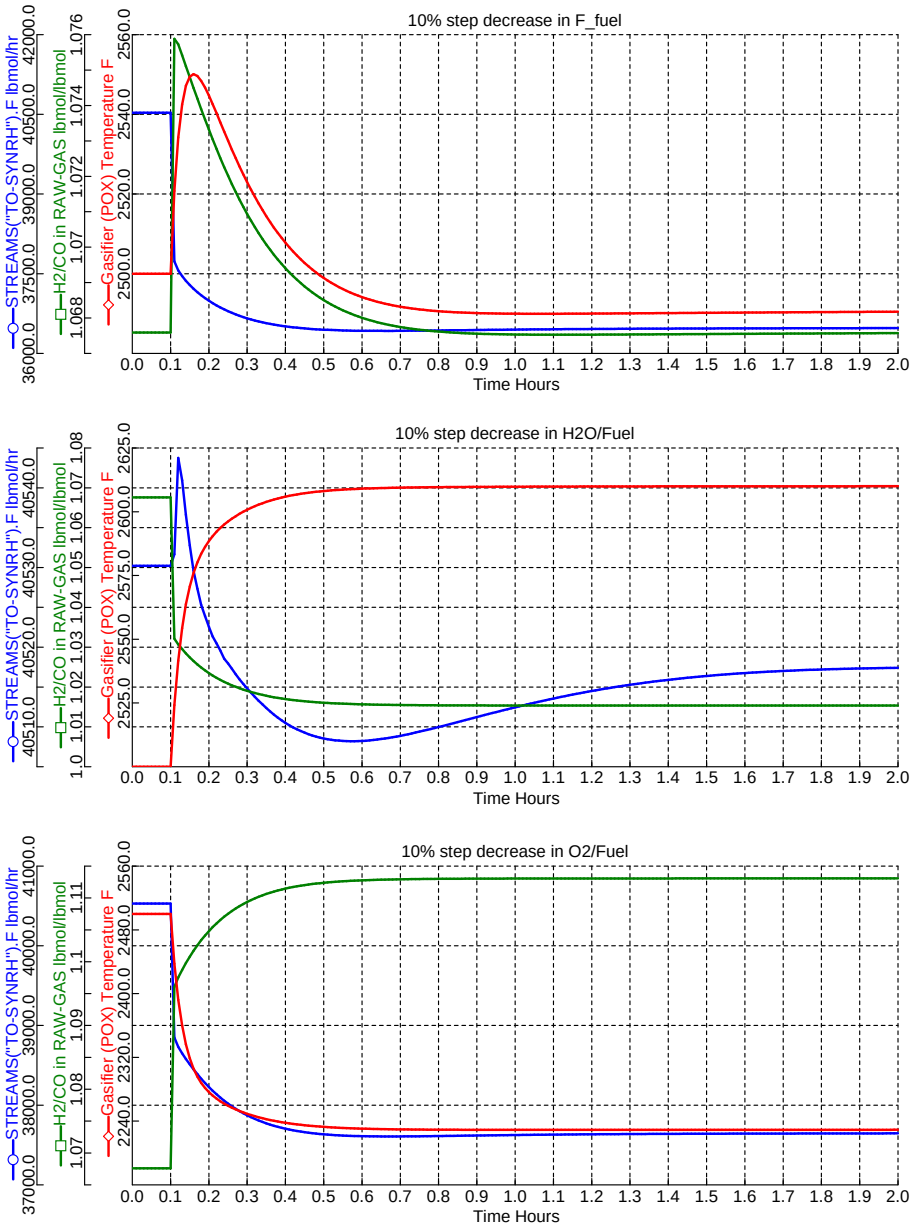

Figure 4.12: Control output responses to (I) 10% step decrease in F_fuel, (II) 10% step decrease in H2O/Fuel, (III) 10% step decrease in O2/Fuel. All input step changes given at t = 0.1 hr

Table 4.8: List of primary control I/O variables for Gasification Island (Case#2)

Variable	Description	Nominal
Inputs		
F_fuel	Fuel (coal equivalent/$C_{18}H_{20}$) flowrate	2087 lbmol hr^{-1}
H2O/Fuel	Slurry-water flowrate to gasifier	6.95 lbmol/lbmol
O2/Fuel	Oxygen (95% purity, from ASU) to gasifier	6.61 lbmol/lbmol
Outputs		
F_syngas	H_2-enriched syngas (TO-SYNRH) flowrate to GT	40530.2 lbmol hr^{-1}
H2/CO	Hydrogen to CO ratio in raw syngas, RAW-GAS (measure of syngas enthalpy)	1.0676 lbmol/lbmol
T_gasifier	Gasifier temperature (post partial-oxidation stage, POX)	2500°F
Disturbances		
	Coal quality	
Z_O2	Oxygen purity	0.95 lbmol/lbmol
	Gasifier pressure (partial-oxidation stage)	800 psi

$u = \begin{bmatrix} \mathrm{F_{fuel}} & \mathrm{H_2O/Fuel} & \mathrm{O_2/Fuel} \end{bmatrix}$ and $y = \begin{bmatrix} \mathrm{F_{syngas}} & \mathrm{H_2/CO} & \mathrm{T_{gasifier}} \end{bmatrix}$ as

$$K(\%/\%) = \begin{bmatrix} 0.9989 & 0.0032 & 0.7097 \\ 0 & 0.4889 & -0.4262 \\ 0.0368 & -0.4400 & 1.0831 \end{bmatrix}$$

$$\Lambda = \begin{bmatrix} \underline{1.0390} & -0.0002 & -0.0389 \\ 0 & \underline{1.5698} & -0.5698 \\ -0.0390 & -0.5697 & \underline{1.6087} \end{bmatrix}$$

which shows that F_syngas–F_fuel, H2/CO–H2O/Fuel and T_gasifier–O2/Fuel is the only possible MV-SISO pairing set. It denotes low interaction (coupling) among the input/output variables.

Controller tuning is based on sequentially closing and tuning one loop at a time, starting with the fastest of the loops. As mentioned in previous chapter, we use the AspenDynamics^{TM} open loop test capability to determine a first order plus time delay model from u to y. Based on the model parameters, we used the SISO-IMC tuning rules [58] to design the PI-controllers.

It can seen from the responses given in Figure 4.13, that the controller is

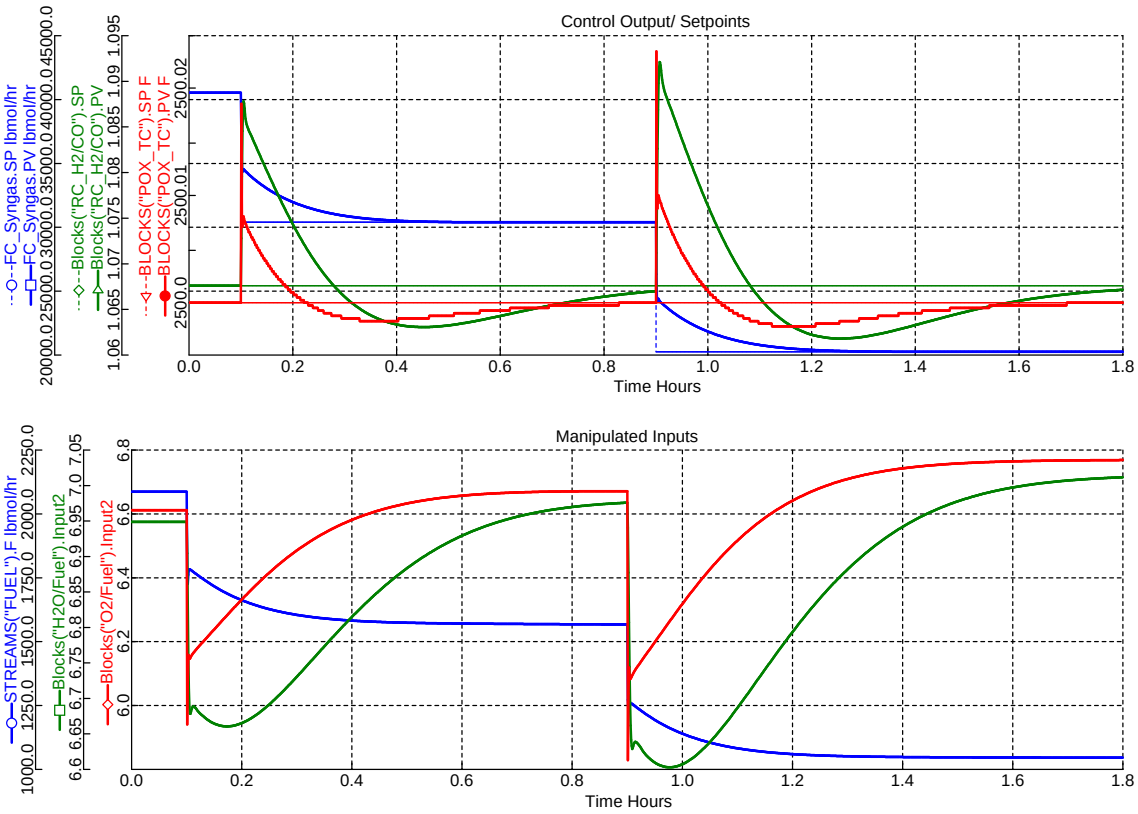

Figure 4.13: Gasifier (Case#2) PID-based multiloop supervisory controller response to (I) 25% step decrease in syngas production rate (F_syngas) setpoint at t = 0.1 hr, (II) 50% step decrease at t = 0.7 hr.

very robust and can handle large range of step-changes in setpoints (load changes). As expected in case of pure load change (without any disturbance), the water/fuel and oxygen/fuel ratio returns back to the nominal value. Hence implementing a ratio/feedforward block (along with a feedback loop) for water and oxygen flowrate is a more robust and a fail-tolerant way of designing the controller. The advantage of adding a feedback loop for oxygen and water flowrate can be better appreciated by comparing Figure 4.12 and 4.13 closely, where the gasifier temperature rises by about 50°F in case of open-loop (pure feedforward) whereas practically no deviation is observed in case of oxygen feedback due to initial/early feedback control action. As observed in Chapter 3, feedforward/ratio controller plays a vital role in case of measurement delays (for instance, deadPOX and deadH2/CO delay blocks have large dead time) or known disturbances (fuel flowrate). In addition, Figure 4.14

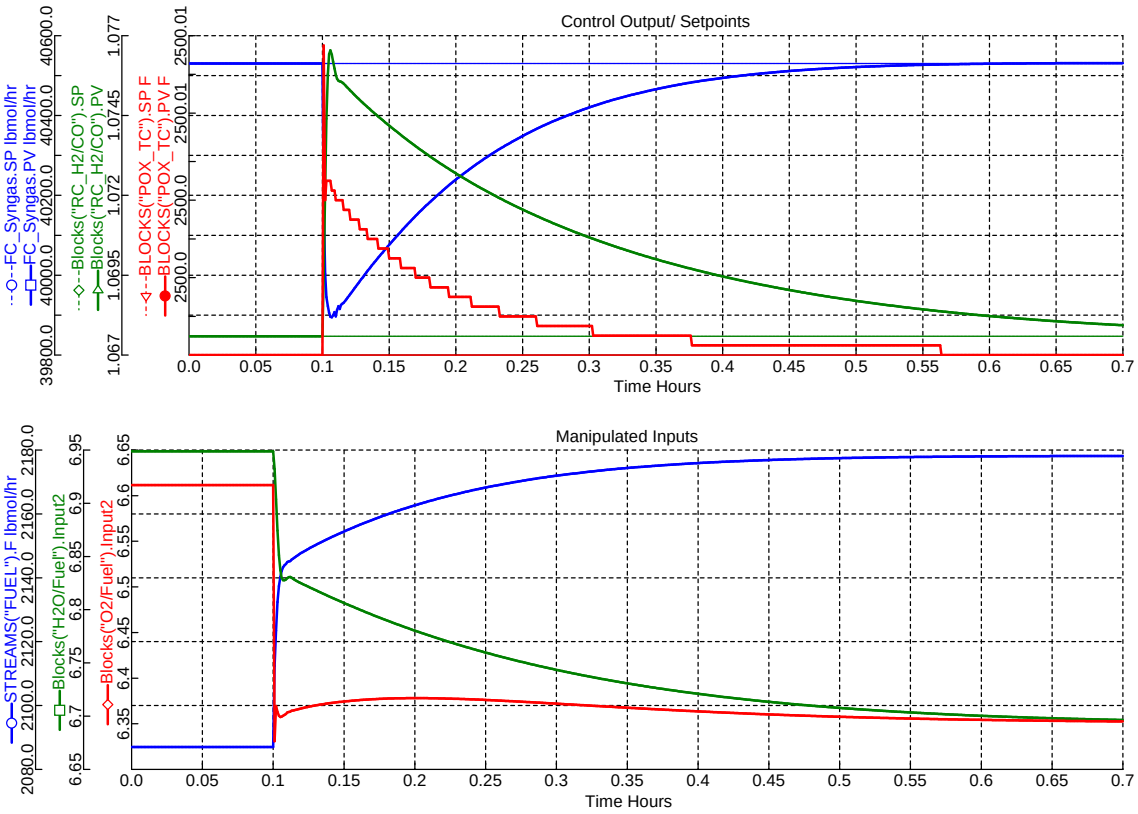

Figure 4.14: Gasifier (Case#2) PID-based multiloop supervisory controller response to disturbance in feed quality (50 lbmol/hr increase in CO, 40 lbmol/hr increase in H_2S and 2 lbmol/hr decrease in $C_{18}H_{20}$) at t = 0.1 hr

shows the controller ability to handle large disturbance in coal quality (small changes in elemental composition percentage of sulfur, carbon and hydrogen in the fuel). The desired operating point is restored within 45 min after the disturbance is provided.

The system has less interaction among the supervisory input-output variables as seen from the RGA matrix for both type of gasifiers. Based on this reasoning along with the fact that this sub-section is significantly "fast" compared to the ASU, a supervisory model predictive control might not add significant benefits in terms of controller dynamics. Instead, focus may be given on devising other controller architecture, including a combination of feedforward–feedback design and/or implement a tighter controller tuning, to improve this subsection's performance.

4.3 Discussion and Conclusion

Chapter 4 provides a detailed discussion on modeling and control of the gasification island, for both carbon capture and sequestration (CCS) equipped IGCC and non-CCS IGCC. A lot of emphasis has been placed on the sub-section's design aspect with suitable approximations for certain proprietary equipments (such as the Selexol units). Due to the limitation of handling solid coal in AspenDyanamics^{TM} (in its current version - V7.1), it has been modeling as a 'pseudofuel' based on its similar dissociation energy and C/H-ratio to coal [102]. The regulatory-layered flow, pressure, temperature and level controllers are placed for various equipment regulation. The overall input-output variables which effect the plant-wide dynamics are identified and the gain and RGA matrices are calculated based on different step-tests. It was found that the coal/fuel flowrate, slurry-water flowrate and oxidant flowrate had a direct impact on the product (syngas) flowrate , H2/CO ratio in syngas (measure of its heating value) and gasifier temperature (at partial-oxidation stage) respectively. Therefore, the corresponding input/outputs were chosen for pairing in a supervisory PID-based control design. It was also realized from the RGA and sensitivity studies (shown in Chapter 8) that unlike the ASU subsection, this unit exhibited low amount of interaction among the overall input/output variables.

CHAPTER 5
DYNAMIC MODELING AND CONTROL OF GAS TURBINE

Most of the literature deals with steady-state modeling of gas-turbine (GT) and compressor. They involve very fast dynamics and the controller design (if any) including sensor-engineering is incorporated within the turbine prototype. Additionally, due to extreme high temperatures involved, the fuel, air and diluent injection required lot of modifications to the conventional natural-gas fired turbines. The dynamic data including the performance curves and surge limits are generally kept proprietary by the developing companies. In this section, we develop a detailed GT dynamic model (pressure driven) based on NETL IGCC Case#2 (with CCS) steady-state data. Later, we implement PID-based control for lower-level loops.

5.1 Steady-State Design

The gas turbine model is based on the GE model 7FB syngas-fired turbine. It consists of a syngas heater (utilizing HP-steam), air compressor, combustor and three stages of expansion and cooling, with the appropriate mixers and splitters (Figure 5.1). The combustor was modeled in Aspen as a stoichiometric reactor (RStoic) with complete conversion of combustion reactions. The flow to the air compressor is calculated via a design specification (T-EXIT) in order to match the vendor-specified exiting flow temperature. The compressor pressure ratio is hard-wired to be 16.4. The air extraction flowrate is set to be 1 lb/hr, essentially zero flow. The combustion air flow is varied via design specification (GT-LOSS) such that it upholds the assumption that 1.5% of the total lower heating value (LHV) of the syngas is lost through the combustor walls. This is given by the following equation

$$\text{Loss} = \left(4347\text{X}_{m,\text{CO}} + 51623\text{X}_{m,\text{H}_2} + 21495\text{X}_{m,\text{CH}_4}\right)\text{F}_{m,\text{syngas}} \times 0.015 \qquad (5.1)$$

where, $X_{m,CO}$, X_{m,H_2} and X_{m,CH_4} are the mass-fractions of CO, H_2 and CH_4 respectively in the syngas stream (before the nitrogen injection). The coefficients give the LHV (or heat of combustion, ΔH_c at 385°F and 460 psia) of corresponding combustible components in Btu/lb. $F_{m,syngas}$ is the total mass-flow of the syngas in lb/hr.

The syngas is diluted with compressed and pre-heated nitrogen product from the ASU until its Lower Heating Value (LHV) is 122 BTU/scf. The nitrogen flow into the syngas is varied via design specification (N2-DIL) in order to achieve this specification.

$$321X_{CO} + 275X_{H_2} + 911X_{CH_4} = 122 \tag{5.2}$$

where, X_{CO}, X_{H_2} and X_{CH_4} are the mole-fractions of CO, H_2 and CH_4 respectively in the resultant nitrogen-diluted syngas stream. The coefficients give the LHV of corresponding combustible components in Btu/ft^3.

The combustor model is configured to generate all combustion reactions and to calculate the heat of reaction. The firing temperature of the turbine is assumed to be 2420°F and the operating temperature of the combustor is assumed to be 2510°F. The pressure drop across the combustor is set at 10% of the inlet pressure, and is calculated by GTPRES.

The air flow split to cool the syngas prior to the first expansion stage is varied via design specification (RTEMP) such that the temperature entering the first stage is 2420°F with no additional heat duty required. A calculator block sets the second and third expansion stage isentropic efficiency equal to that of the first stage in order to meet the vendor specified exhaust temperature. The air flow splits to cool the second and third expansion stages are fixed based on vendor data. All the three turbine stages have a pressure ratio of 0.4.

5.2 Dynamic Design

Many initial attempts to include detailed dynamic gas compressor model through performance curves/tables[31] (at multiple operating speeds) were made. The

[31]Most of these curves were based on typical axial compressors data available in open literature [105]

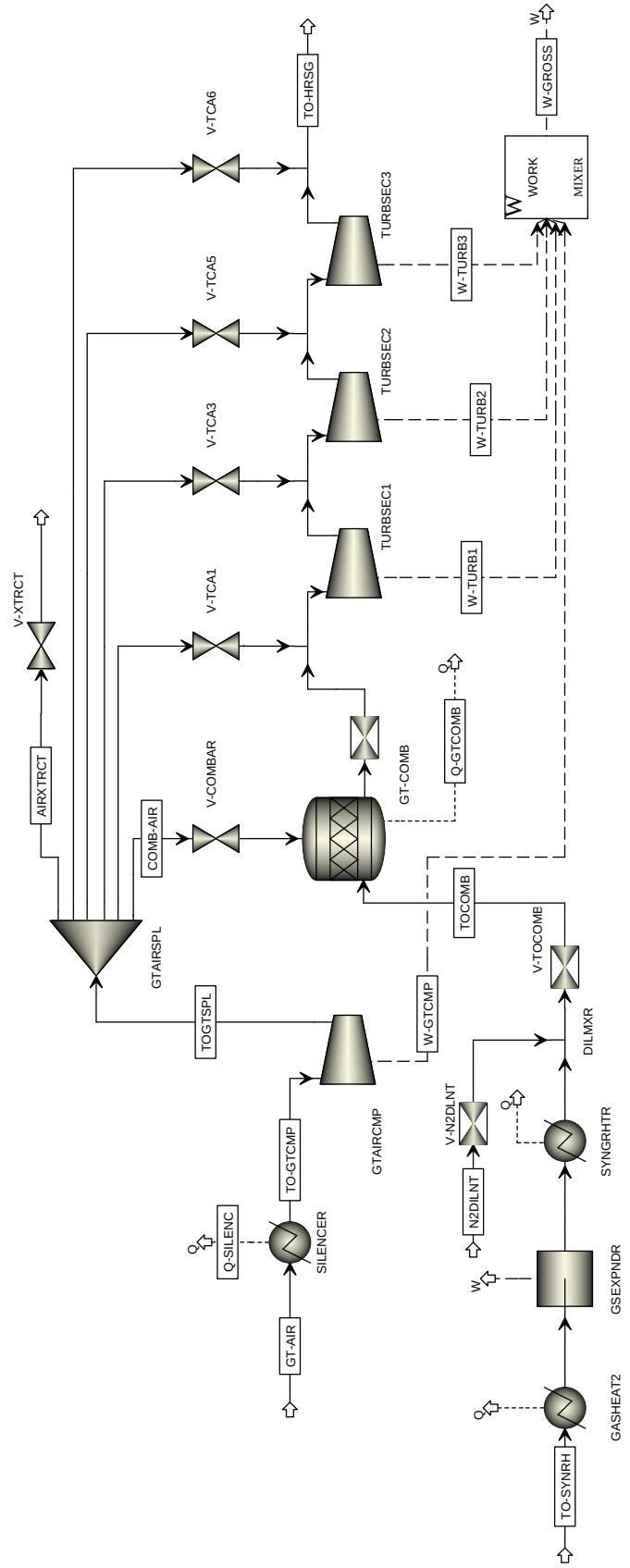

Figure 5.1: Process flowsheet showing GT subsection in AspenPlus™

main idea was to dynamically capture operating limitations such as compressor surge and stonewall, and therefore to use bypass/recycle valves for maintaining operation within "safe" regime. Due to inherent inadequacy of AspenDynamics^{TM}(AD) in handling performance curves[32], we chose an *instantaneous*[33] compressor model for our study. To ensure that we don't reach the surge margins especially during turndown conditions, we monitor the compressor pressure-ratio and flowrates and qualitatively base our judgment for an "acceptable" dynamic response. This approximation of an "instantaneous" model is valid, considering the fast dynamics (order of seconds) for this section, in comparison to slow gasifier dynamics and even slower ASU dynamics.

For dynamic modeling of the combustor, we specified all of the combustion reactions, rather than let AspenPlus^{TM} generate it (since AD cannot handle "auto-generated" reactions). These reactions are given below. We assume a full fractional conversion of each component.

$$2\,CO + O_2 \longrightarrow 2\,CO_2$$
$$C + O_2 \longrightarrow CO_2$$
$$2\,H_2 + O_2 \longrightarrow 2\,H_2O$$
$$CH_4 + 2\,O_2 \longrightarrow CO_2 + 2\,H_2O$$
$$2\,COS + 3\,O_2 \longrightarrow 2\,CO_2 + 2\,SO_2$$
$$2\,H_2S + 3\,O_2 \longrightarrow 2\,H_2O + 2\,SO_2$$

Since the combustion reactions are mostly spontaneous, dynamics of this unit which, in reality take place inside the turbine unit, are ignored and left as an instantaneous block.

We also model the turbine-compressor *operating on a common shaft* in AD. This is a critical step and the following procedure is used

[32] AspenDynamics^{TM} gave persistent errors when interpolating data within curves corresponding to variable speed operation. In addition, the built-in compressor/turbine models had lot of "proprietary" information, which could not be viewed/edited for building user-based models

[33] For process units operating as *instantaneous*, calculations during the dynamic run are based on steady state values, i.e., the derivative term is made zero and only an algebraic equation is solved. Hence, the number of states in the dynamic model is substantially decreased. Equipment details are not needed.

1. The compressor is kept as an instantaneous block
2. Turbine is specified as dynamic
3. The moment of inertia for the turbine is the lumped inertia of the compressor and turbine
4. Turbine brake power (bpower) is made free
5. Compressor outlet work stream power is fixed
6. Compressor shaft speed is made free
7. Compressor gear ratio is fixed

5.3 Regulatory Control Layer

Fixed pressure mode vs. floating pressure mode GT operation have been debated over time. Fixed mode operation offers better controllability and grid frequency modulation. This is a preferred mode when the plant is supplying the work to a grid-based power system. The downside of this operation include a slightly efficiency due to valve throttle losses and the risk of reaching compressor surge limits. Floating pressure mode on the other hand is a self-stabilizing (where lower loads automatically involve lower pressures and flows, without the involvement of external valves for regulating them) and self-optimizing mode operation with high efficiency returns. We design the flowsheet based on a *pseudo*–floating pressure arrangement, where the turbine pressure-ratios instead of absolute pressures have been specified by the controllers given by PRCGT1, PRCGT2 and PRCGT3 in Figure 5.2. The setpoints to these "virtual" controllers, in reality, are directly dependent on the turbine dynamics, but due to simulator limitations have been kept fixed in this study.

It was specified in steady state simulations that 1.5% heating value of syngas mixture entering the turbine is lost as heat (Q-GTCOMB). Since the heating value is not directly measureable in AD, we specify this heat loss as a fixed ratio to the syngas mixture flowrate. This is an admissible approximation as long as the

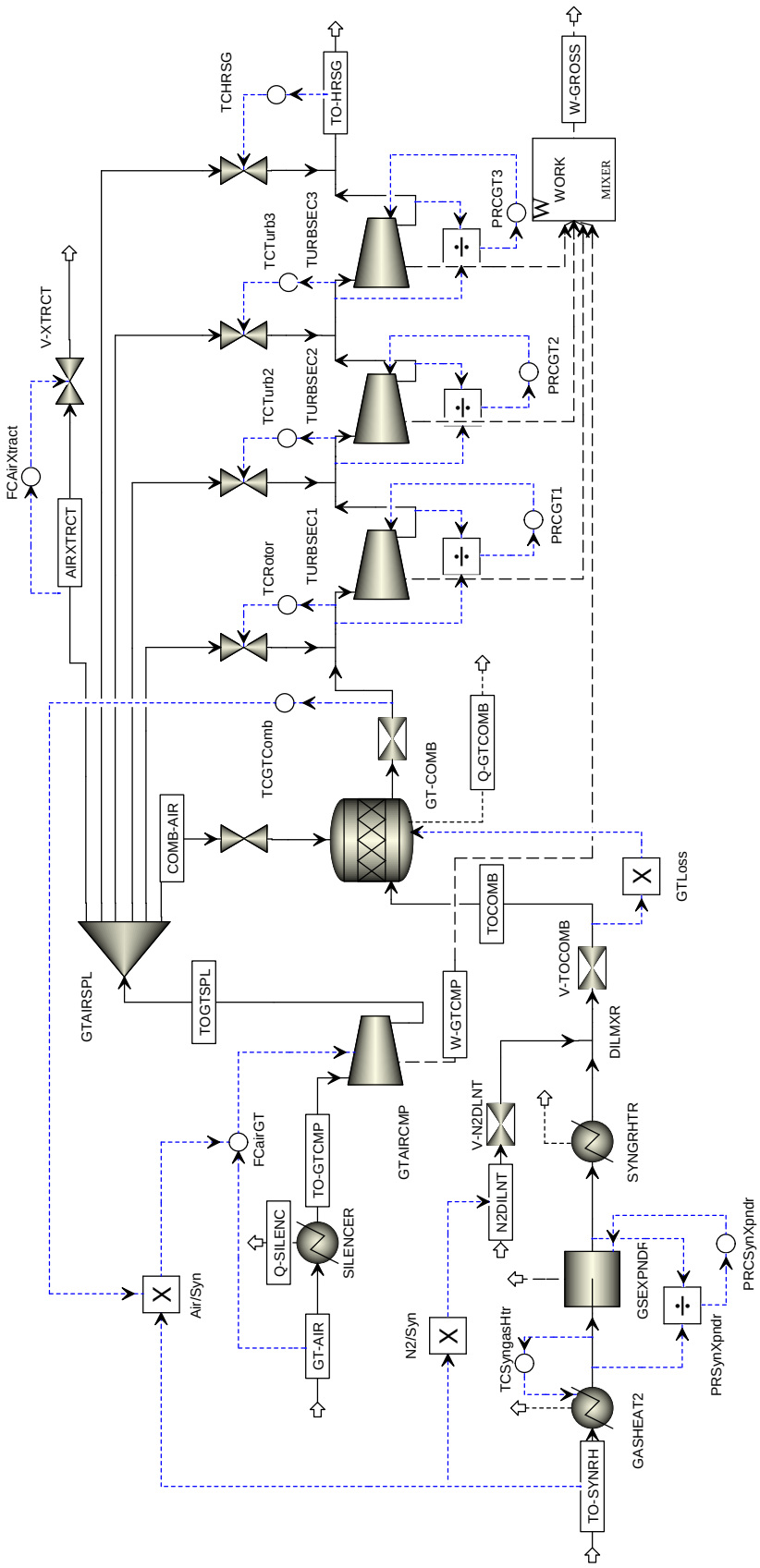

Figure 5.2: Process flowsheet showing GT subsection in AspenDynamics™ with regulatory layer control installed

syngas quality is "near" design value. The post-syngas-heater stream is temperature controlled (TCSyngasHtr) by adjusting heat-duty to the heater (GASHEAT2). In reality, this heat is regulated by HP-steam bypass around the heat exchanger, the dynamics of which can be incorporated here using a "slower" controller to account for thermal-mass delays.

Nitrogen as a diluent from the ASU is added to the gas turbine/compressor unit before it is combusted. This permits more syngas to be consumed, thus increasing the power output of the gas turbine while maintaining optimum firing temperatures as well as reduces the formation of NOx. Since high-pressure nitrogen is extracted from the ASU, which primarily targets to provide oxygen at a certain ratio to the fuel/coal, it makes sense to keep the ratio of the "remaining" nitrogen after separation in a certain ratio to the fuel. For example if the IGCC plant operates at half load, meaning that the amount of coal consumed is halved, the syngas combusted in the turbine is also reduced to 50%. To gasify this reduced quantity of coal, we need half the amount of oxygen as we required when operating at full load. The ASU nitrogen produced will also be reduced by same fraction which now matches with the amount required as diluent for this 50% amount of syngas. If there is a large mismatch in this ratio, the split of the nitrogen vent will be adjusted. In steady-state studies, we had discussed earlier that, to reduce NOX formation the flowrate of nitrogen was determined such that LHV of the resulting syngas-nitrogen mixture is no more than 122 Btu/scf. Again, since the heat value of this mixture cannot be determined during dynamic runs, as long as the LHV of the pure syngas is maintained (which is ensure upstream by the gasifier block controllers), the nitrogen flowrate required is based on a fixed ratio to syngas flowrate.

Feed-forward/ratio control on air flowrate through Air/Syn multiplier block, where air flowrate is calculated affront based on syngas flowrate. Later, based on a measured variable in the process, this ratio amount is corrected using a feedback supervisory layer controller. A flow controller, FCAirXtract, is used to ensure fixed air-extraction to the ASU. A tight tuning for this controller is critical since swings in GT compressor pressure may result in extracted flow variations (if not controlled) leading to fluctuations in air available for GT cooling.

Table 5.1: Primary input-output control variables for GT-subsection

Variable	Description	Nominal
Inputs		
F_syngas	Clean Syngas flowrate	46205 lbmol hr^{-1}
F_airGT	Total air entering gas-compressor	252200 lbmol hr^{-1}
Outputs		
W_GT	Net work (W_{gross} - $W_{compression}$)	656300 hp
T_turb	Gas-turbine firing temperature	2248°F
Disturbances		
T_ambient	Ambient air temperature	59°F
r_H2/CO	Hydrogen to CO ratio in syngas (measure of enthalpy fluctuations)	1.06

5.4 Supervisory Control Layer

The exhaust flue gas is sent to the heat recovery steam generator (HRSG) where most of the heat is extracted to generate steam and drive a steam turbine (ST). An obvious primary output variable is the net turbine work. This work in form of electricity produced by generator (also shafted to the turbine), is supplied to the grid. Feed air flowrate to the gas-compressor can be manipulated using an IGV which acts as one of primary control input. Table 5.1 gives the list of primary inputs-outputs of the GT subsection. It must be noted that the performance of compressor/turbine is highly sensitive to changes in ambient-air temperature, hence this is included as a state-disturbance variable during MPC formulation. In this study, the GT is in reality a "modified" natural gas turbine (meant for handling hot-spots and higher flamability of H_2, using a appropriate distributors), which requires significant amount of air-cooling. Hence, little or no air is available or extracted to the ASU. Based on NETL IGCC Case#2 studies by Parson [3], we consider no air-side integration.

5.4.1 PID-based MV-SISO Design

Figure 5.3 gives us responses of the net GT work, turbine inlet temperature and flue-gas details to 10% step changes in input variables. It can be seen that the process time is of the order of 5–10 min. There are two time-scales involved in the process which can be distinguished by an immediate "jump" in the outputs triggered

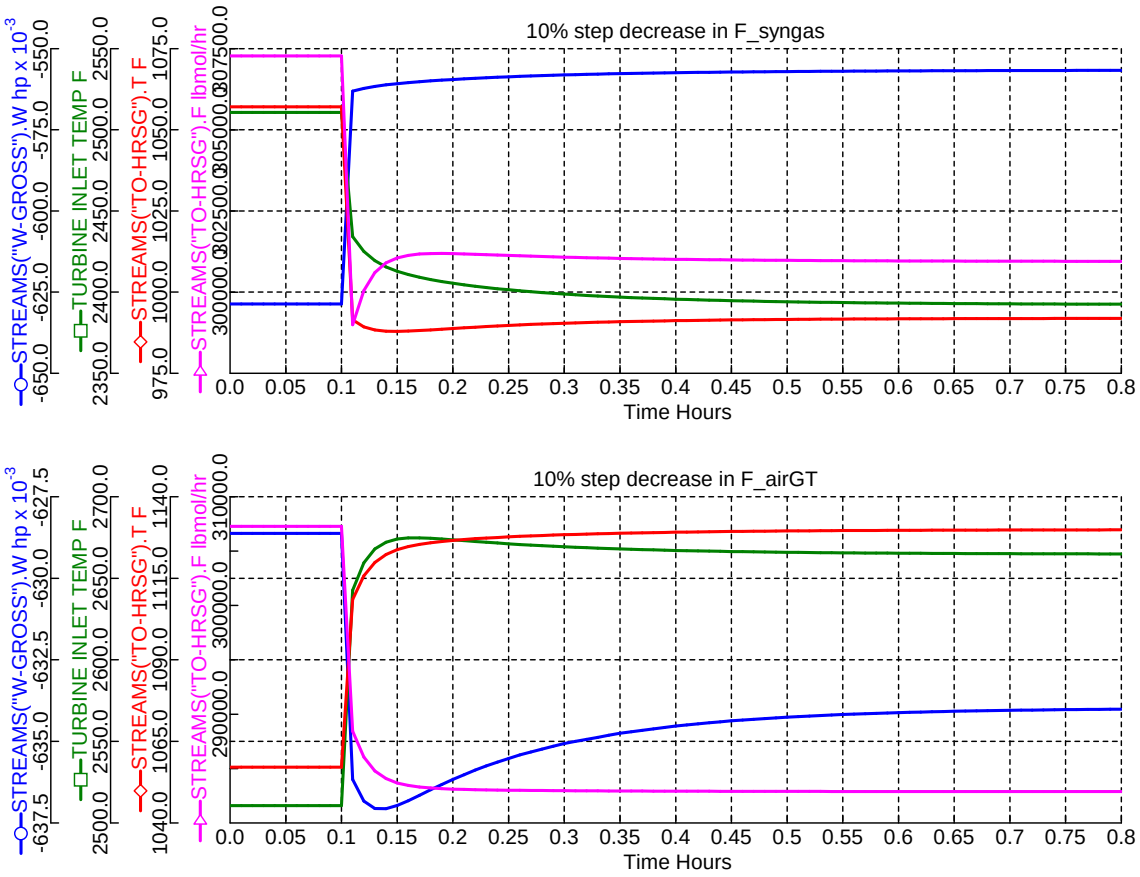

Figure 5.3: Control output responses to (top) 10% step decrease in F_syngas, (bottom) 10% step decrease in F_airGT. All input step changes given at t = 0.1 hr

by the step input change, followed by a gradual attainment of new steady state over a period of the process-time. The first time-scale is associated with pressure changes due to sudden forced flow changes (in case of syngas) or proportional kick by the flow controller (in case of air). The second time-scale involves mechanical and thermal inertia, which for instance in the GT, is the time taken by turbine blades to adapt to the new flow and temperature. It is worth mentioning that during these step tests, the temperature controllers shown by TCGTComb, TCRotor, TCTurb2, TCTurb3 and TCHRSG in Figure 5.2 are kept opened i.e., placed in manual mode.

For determining the overall MV-SISO pairing, we construct the RGA matrix,

when $u = \begin{bmatrix} \mathrm{F_{syngas}} & \mathrm{F_{airGT}} \end{bmatrix}$ and $y = \begin{bmatrix} \mathrm{W_{GT}} & \mathrm{T_{turb}} \end{bmatrix}$ as

$$\Lambda = \begin{bmatrix} \underline{1.0605} & -0.0605 \\ -0.0605 & \underline{1.0605} \end{bmatrix}$$

which clearly shows that W_GT–F_syngas and T_turb–F_airGT are the MV-SISO loops we need to close.

Controller tuning is based on sequentially closing and tuning one loop at a time, starting with the fastest of the loops. As mentioned in previous chapter, we use the AspenDynamics$^{\mathrm{TM}}$ open loop test capability to determine a first order plus time delay model from u to y. Based on the model parameters, we used the SISO-IMC tuning rules [58] to design the PI-controllers.

We test the controller design by providing a 30% step decrease in GT workload. These responses have been shown in Figure 5.4. The GT meets the new work demand in 15–20 min. We see a large increase (40°F) in turbine inlet temperature during the initial transient period, since the air flow is ratio controlled with syngas flow. The correction factor to this ratio is provided after the feedback temperature measurement is made available. We also note that the flue-gas temperature is initially decreased (meaning excess air-cooling), but later the inlet guide throttle valves are closed by temperature controller to bring the flue-gas temperature to vendor specified value.

If interstage temperature measurements are not available, the three turbine inlet valves and aftercooler valve, shown in Figure 5.2, are never throttled. The air gets distributed evenly throughout the turbine stages, since the same turbine pressure ratio is maintained over all the turbine sections during load changes. The temperature at each turbine inlet, in such case, decreases with a load reduction (not shown) due to more amount of air being extracted for cooling than what is required. This prevents the compressor from reaching surge condition during turndown since the flowrate is maintained at a higher level. The downside to this is that the HRSG should be equipped with controllers which can handle flue-gas temperature fluctuations (along with the flow fluctuations). In this study, we throttle the inlet valves

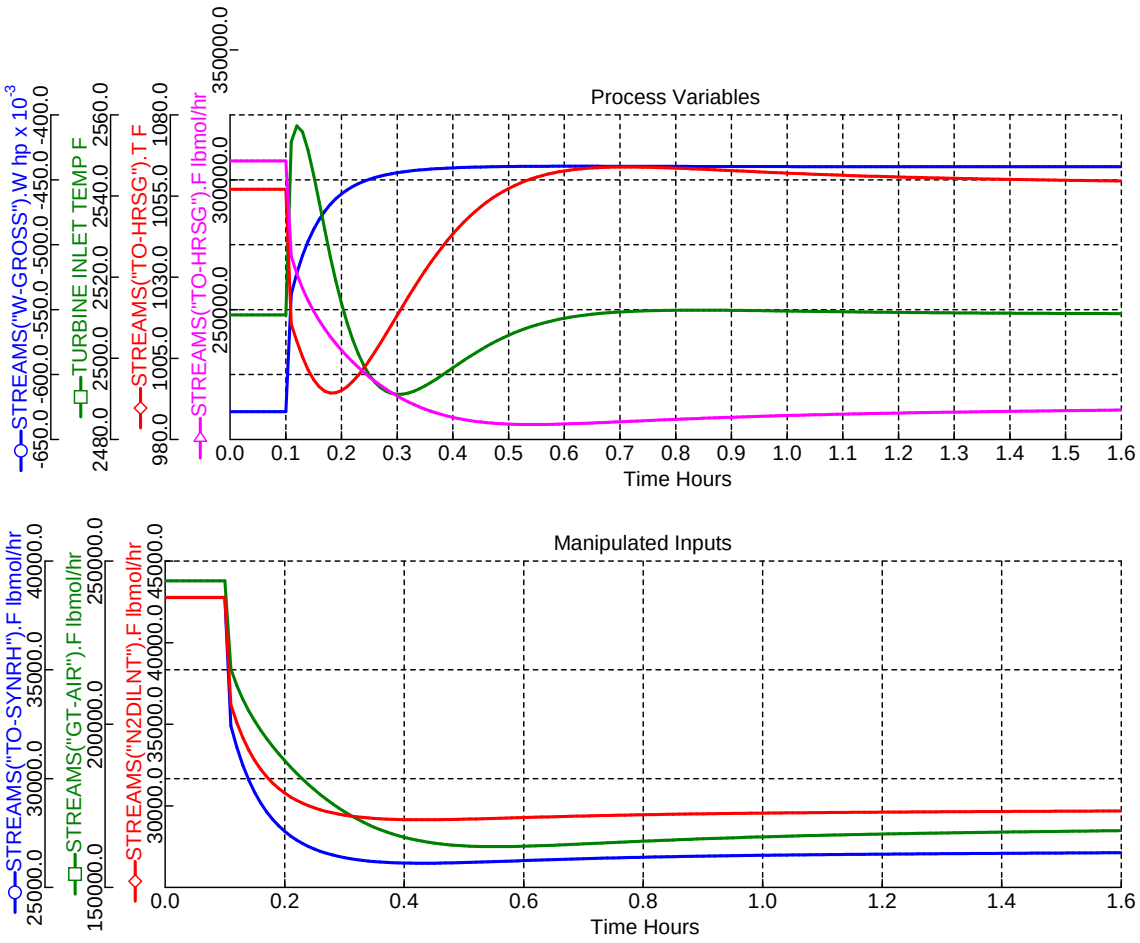

Figure 5.4: Gas Turbine/Compressor PID-based multiloop supervisory controller response to 30% step decrease in gas-turbine work load (W_GT) at t = 0.1 hr

to maintain a constant flue-gas temperature.

5.5 Effect of Ambient Temperature

It is known that variations in temperature of the inlet air feed (i.e., ambient air temperature) can cause substantial variation in the output of an integrated ASU/gas turbine system [106, 107]. More specifically, the outlet temperature of a gas turbine is directly related to its air inlet temperature. This has been shown in Figure 5.5. A very simple realization of a power plant efficiency with regional and climactic variation can be obtained from this response. We notice at at hotter places with an ambient temperature of 90°F, the amount of syngas required to produce the same

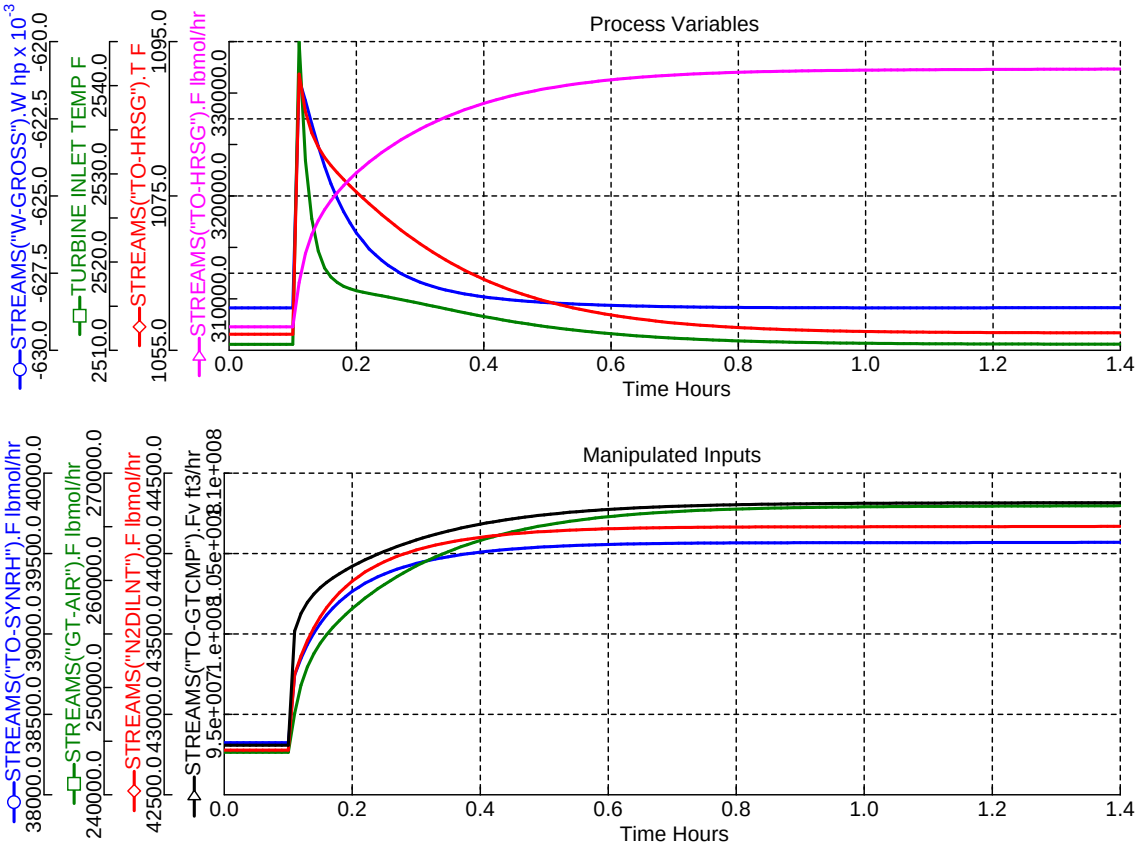

Figure 5.5: Gas Turbine/Compressor PID-based multiloop supervisory controller response to disturbance in ambient-air temperature: step change to 90°F. Note the increase in volumetric flowrate at compressor suction, which is not physically realizable (if the compressor already operates near full load at nominal conditions)

GT-power increases by 3.3%[34]. As will be discussed further, we reach a physical constraint as the ambient temperature rises, due to which we cannot even demand the same GT-power.

Normally, the cold air temperatures which occur in winter enable larger masses of feed air to be supplied. By contrast, when the inlet air temperature rises, such as in the summer, considerable less mass of air is compressed, causing a decrease in overall power output of the system. Hence temperature of air is a relevant disturbance variable. It is also obvious that volumetric flow-rate of air is an important input

[34] Although a slightly higher amount of steam-turbine work can be extracted due to increase in flue-gas flowrate

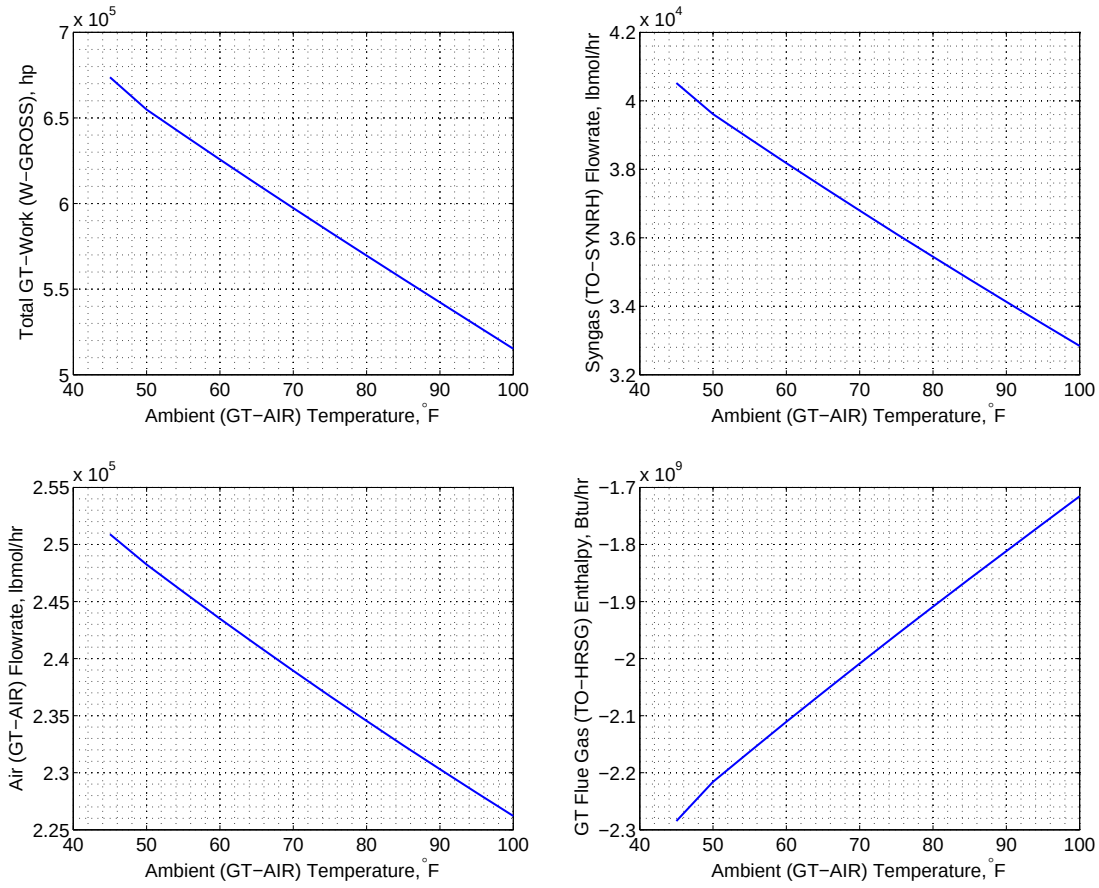

Figure 5.6: Plots showing effect of ambient air temperature on GT performance. All the data are based on an upper limit of compressor suction (TO-GTCMP) volumetric flowrate of 93086700 ft^3/hr

which affects both the turbine inlet temperature and the net work obtained. The volumetric capacity of the compressor, from control and operability point of view, now poses a physical constraint for the maximum amount of air which can be imported. Hence this is a throughput variable which is not being measured/controlled. Plots showing the maximum achievable gross power, along with a few other input variables have been given in Figure 5.6. Any other factor which affects the air-density directly, for instance, elevation of the plant to sea-level[35], will limit the plant's maximum throughput.

[35]IGCC plant in Reno, Nevada found in their demonstration project that the technology would not work in elevations above 300 feet sea level [13], mainly due to abovementioned theoretical reason

5.6 Modifications with new Aspen V7.1 turbine model

All of the study in this chapter up to this point has been based on Aspen Engineering Suite version 2006.0. This section was remodeled in latest version of Aspen (AspenOne V7.1 as of March, 2010). It was found that the 'default' turbine model has been significantly improved and includes the performance curve at the specified frequency/rpm in dynamic simulation (Aspen Plus Dynamics V7.1). Hence, the pressure drop across a turbine and the flow through it are inherently related. Therefore, the work done by a turbine is computed depending on the flow passing through it, and is a calculated, dependent or 'free' variable. In terms of current simulation, this suggests that we cannot (any longer) incorporate pressure controllers across turbines, expanders – shown by PRCGTx and PRCSynXpndr controller blocks in Figure 5.2. This requires us to devise an arrangement which is based on *total*–floating pressure arrangement instead of the *pseudo*–floating pressure scenario earlier.

All of the regulatory controllers except the pressure-ratio and the pressure-ratio controller blocks are kept intact[36] from Figure 5.2. For brevity sake and to keep the flowsheet uncluttered, we removed the interstage temperature controllers – TCRotor, TCTurb2, TCTurb3 and TCHRSG. It must be recalled from earlier, that these controller were inactive and used only for various testing purpose, since in most cases the interstage temperature measurements are not available.

The supervisory layered input-output variables were kept similar to earlier case, i.e., $u = \begin{bmatrix} \mathrm{F_{syngas}} & \mathrm{F_{airGT}} \end{bmatrix}$ and $y = \begin{bmatrix} \mathrm{W_{GT}} & \mathrm{T_{turb}} \end{bmatrix}$. The remaining analysis including controller pairing decision, controller tuning were again similar to earlier case.

The controller design is tested by providing a 30% step decrease in GT workload. These responses have been shown in Figure 5.7. The GT meets the new work demand in ∼5 min. The difference in process time is due to inherent dynamics involved in previous case due to the pressure-ratio controllers (governor-valve dynamics) compared to near-instantaneous operation in the current version. The

[36] In fact, importing the flowsheet from the previous version actually makes the problem over-specified since the brake-power of the turbines is not a 'fixed' variable anymore

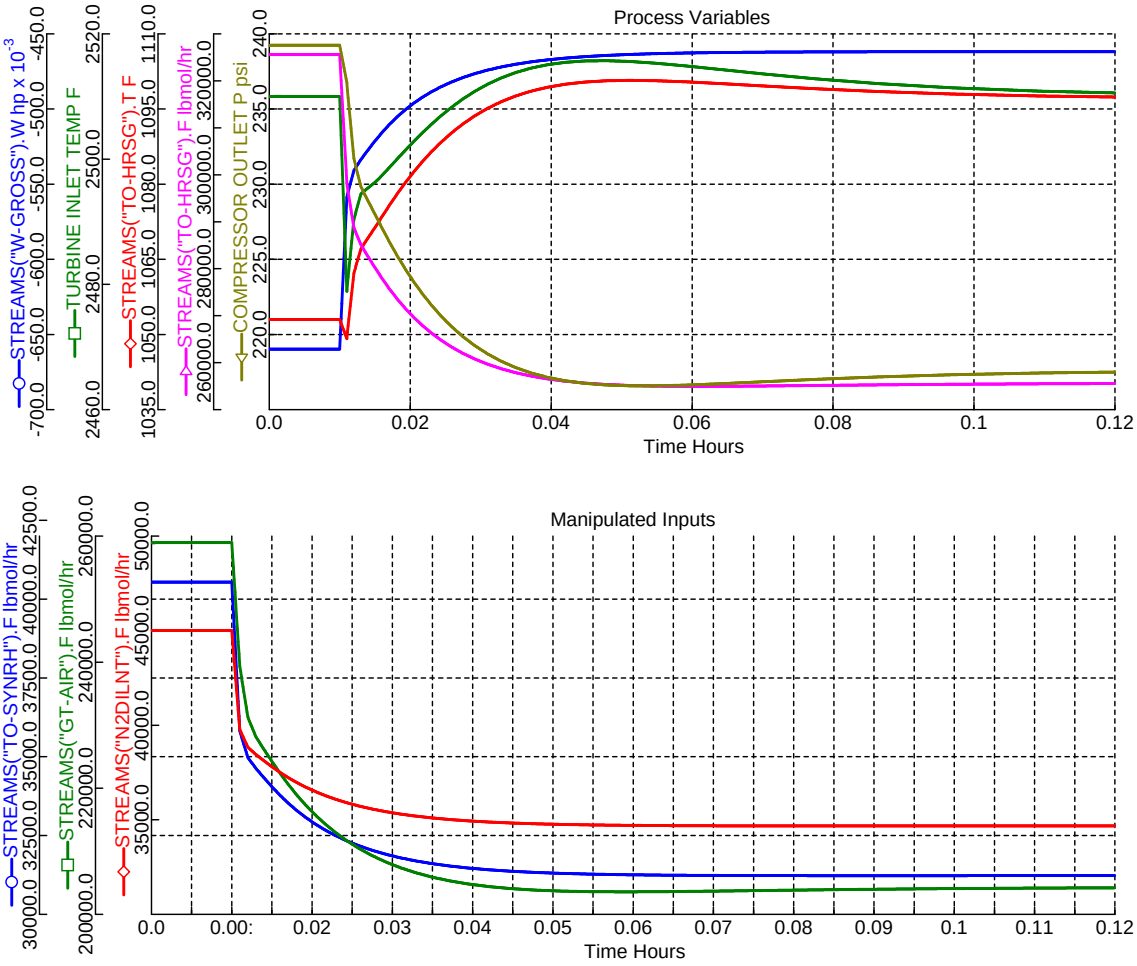

Figure 5.7: Gas Turbine/Compressor PID-based multiloop supervisory controller response using AspenV7.1 turbine model to 30% step decrease in gas-turbine work load (W_GT) at t = 0.01 hr

turbine-inlet temperature naturally tends to decrease (excess cooling) after which the turbine-inlet temperature controller throttles the compressor valve to decrease the flowrate. The most adverse effect of this control structure is noted on the exit flue-gas temperature, which can be seen to rise by ∼40°F, which is far beyond the vendor specified value. An increase in each of turbine-interstage temperature can also be inferred from the abovementioned rising flue-gas temperature.

A structural change in controller design is made based on the above observation where instead of the turbine-inlet temperature, the turbine-outlet flue-gas temperature is chosen as the controlled variable and hence $y = \begin{bmatrix} W_{GT} & T_{flue} \end{bmatrix}$. For

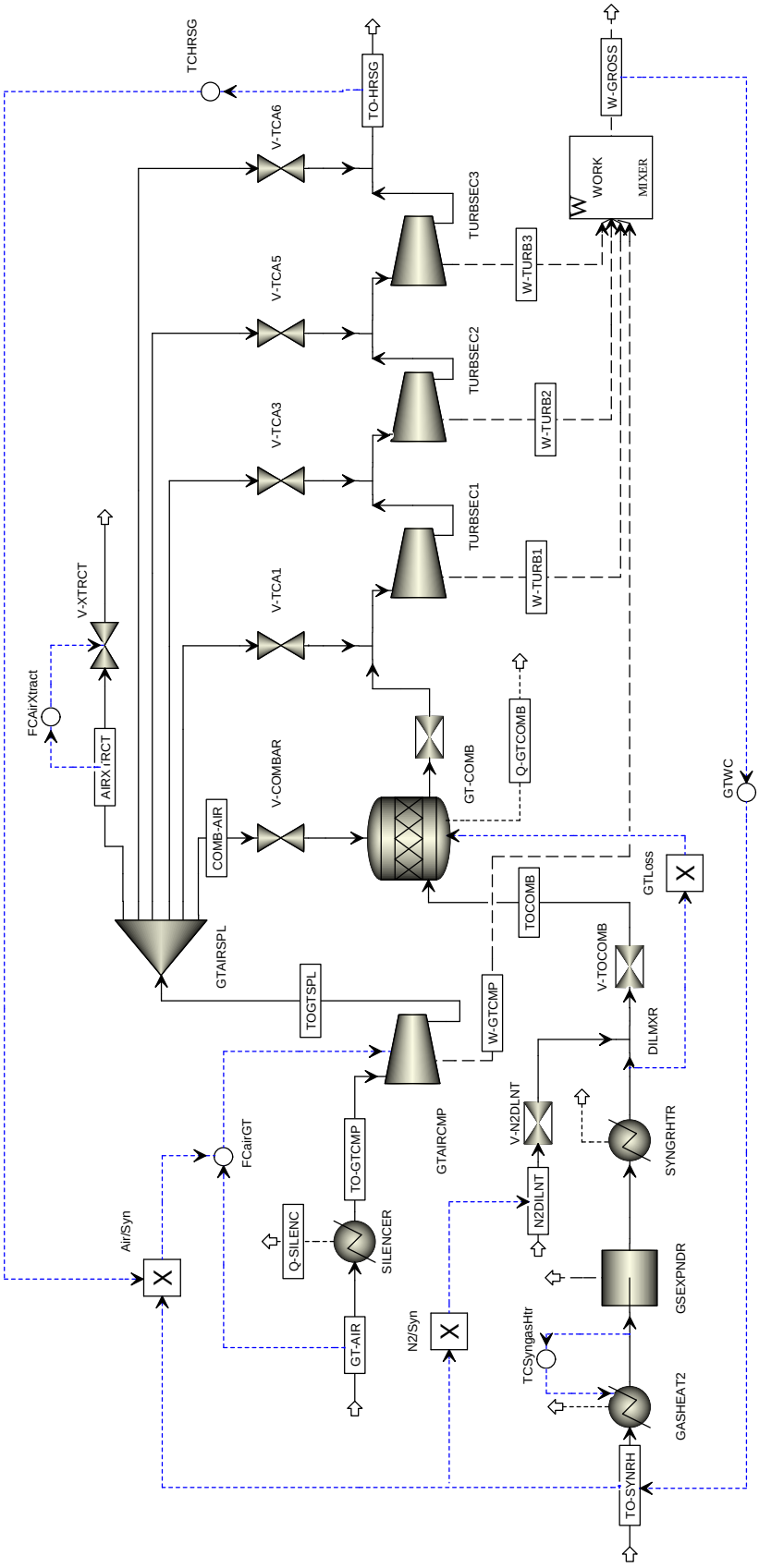

Figure 5.8: Process flowsheet showing GT subsection in AspenDynamics™ with regulatory and supervisory PID layer control using AspenV7.1 turbine model

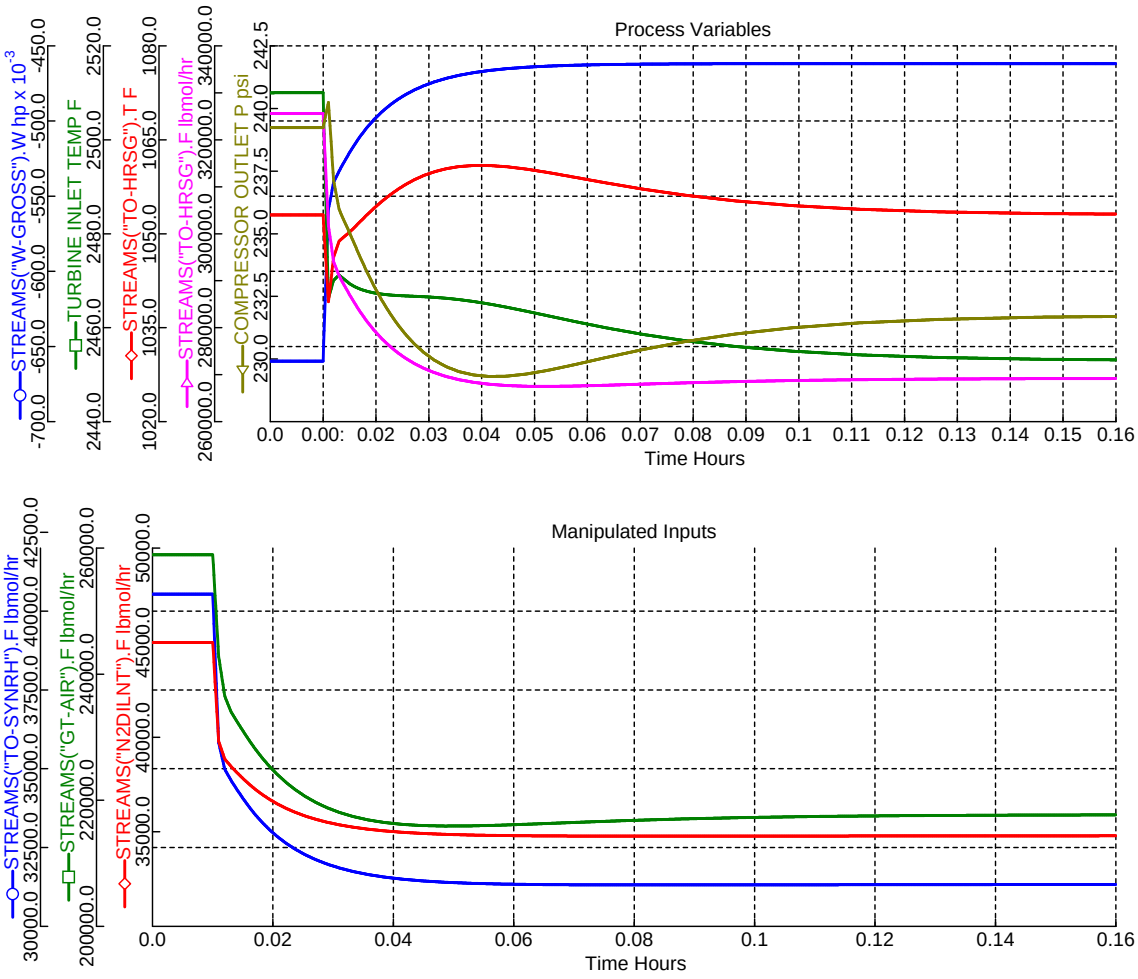

Figure 5.9: Gas Turbine/Compressor PID-based multiloop supervisory controller (modified, see Figure 5.8) response using AspenV7.1 turbine model to 30% step decrease in gas-turbine work load (W_GT) at t = 0.01 hr

these input-output variables, the RGA matrix is constructed to determine the overall MV-SISO pairing

$$\Lambda = \begin{bmatrix} \underline{1.0836} & -0.0836 \\ -0.0836 & \underline{1.0836} \end{bmatrix}$$

which, similar to earlier case, shows that W_GT–F_syngas and T_flue–F_airGT are the MV-SISO loops we need to close.

Figure 5.8 shows the AspenDynamics^{TM} flowsheet with supervisory PID layer controller installed and Figure 5.9 gives the controller responses for 30% step-decrease in GT work load. The flue-gas temperature decrease instantly by ∼15°F

primarily due to air/syngas feedforward-ratio control. The correction factor to this ratio is provided after the feedback of flue-gas temperature measurement is made available. It is also interesting to note that the turbine-inlet temperature is decreased by ∼40°F, leading to a decrease in turbine efficiency, which is commonly noticed in practice, at part-load conditions.

5.7 Discussion and Conclusion

In this chapter, we design and develop a dynamic model and control scheme for the gas-turbine section of IGCC power plant. Using the old turbine model (Aspen v2006.5 and older) with brake-power being an independent variable, we are left with a major operational limitation of determining this extracted work. As a possible workaround, the performance-curve in form of tables or equations are provided. These attempts are unsuccessful due to software's inability to interpolate between the data. Hence an approximation is devised, where the turbine pressure-ratio is used to control its brake-power. Moving forward with the regulatory control design, the air and nitrogen flow are ratio-controlled with the incoming syngas flowrate; the ratio-values being managed by a supervisory layered controller.

With a new turbine model in version 7.1, the internal performance-curve (at a given rpm) makes the pressure-ratio dependent on the flow through the turbine, and hence the entire turbine pressure, including the air and fuel injections nodes, swing with load changes. The most noticeable change from the old model, is the behavior of flue-gas temperature which is observed to increase with a load step-down. A new controller design is proposed, which now controls the flue-gas temperature by manipulating the feed-air flowrate.

To analyze the limitations of ambient air on maximum GT-work, steady-state simulations are run to evaluate the net GT work and syngas-flowrate while maintaining the control objectives (constant turbine inlet/outlet temperature) as well as constraining the upper compressor-suction volumetric flowrate. It is found that with an increase in ambient-temperature from 59°F to 90°F, the maximum GT-work possible decreases by ∼14%, proving the negative effect of the same on IGCC plant performance.

CHAPTER 6
DYNAMIC MODELING AND CONTROL OF HRSG

In most IGCC systems, a Heat Recovery Steam Generator (HRSG) and a steam cycle are combined with a simple cycle gas turbine to form a gas turbine combined cycle (CC). In a combined cycle, the hot exhaust gas is further cooled in the HRSG. The heat is recovered by producing high temperature and high pressure steam. The steam is expanded in a steam turbine to produce shaft work, which is converted into electricity in a generator. Typically, the steam cycle will have several different pressure levels and the steam turbine will have several corresponding stages (Figure 1.4). A portion of steam may be diverted to the gasifier, for example, to be utilized as shift-steam or to other part of the plant for industrial heating. Furthermore, some heat recovered from cooling of hot syngas that exits the gasifier or from other parts of the plant can be used in the HRSG to generate steam. Thus, there is typically some degree of integration between the steam cycle and other components of an IGCC plant. Most of the introductory background and a detailed literature review on HRSG and steam turbine operation has been given in Chapter 1.

It must be emphasized that a HRSG unit, commonly termed as a 'boiler' in a conventional power plant, is a downstream process to the entire IGCC plant. Hence, the primary objective is to maximize the extracted work from heat available from different plant sources, majority of which are the radiant-syngas-cooling unit and GT flue-gas. The amount of extracted steam-turbine (ST) work is not directly regulated unlike that in a conventional power plant, where the amount of fuel maybe directly manipulated to remove the offset between the ST-work generated and the actual load/demand. Here, we have two separate components of work and the control of the total power (GT+ST) as a primary objective requires far more coordination and management among different plant-components by a supervisory-level control layer.

Table 6.1: List of heat-streams entering/leaving HRSG in Parson's IGCC Case#2 flowsheet

Heat Stream	Magnitude (Btu/hr)	Description	Source Name	Sink Name
Heat transferred to HRSG (from flue-gas)				
Q-ECON	622551418	Flue gas to HP economizer	ECONOMZR	HRSGECON
Q-SUPER	505023171	Flue gas to HP superheater	SUPERHTR	HRSGSUPR
Q-HRSGRH	300900209	Flue gas to HP reheater	HRSGREHT	HRSGSUPR
Q-EVAP	141754351	Flue gas to HP evaporator	EVAPRATR	HRSGEVAP
Q-IEVAP	76959925	Flue gas to IP evaporator	IP-EVAP	HRSGIEVP
Q-ECON2	59080802	Flue gas to HP pre-economizer	PREECNZR	HRSGECN2
Q-DEAR	50546555	Flue gas to HRSG deaerator	DEAERATR	HRSGDEAR
Q-FWH	40704392	Flue gas to HRSG feed water heater	FWHEATER	HRSGFWH
Q-IECON	2938379	Flue gas to IE economizer	IP-ECON	HRSGIECN
Heat transferred to HRSG (from sources apart from flue-gas)				
Q-RADCLR	641596506	Gasifier radiant cooler to HP evaporator	RADCLR	EVAP2
Q-WGSC1	245700225	WGS-1 cooler to IP evaporator[37]	WGSC1	RGCLR1
Q-RGCLR4	218608794	Radiant syngas cooler 1 (after shift) to LP evaporator	RGCOOLR4	LPSTEAM
Q-GCLR4	180538489	Radiant syngas cooler 2 (after shift) to HRSG scrubber	RGCOOLR5	SCRUBBER
Q-WGSC2	47729203	WGS-2 cooler to IP evaporator	WGSC2	RGCLR2S
Q-TGCLR1	12805557	Tailgas cooler to HRSG flash	TGCLR-1	FLASH
Q-SCRBCL	6733526	Quench water cooler to LP evaporator	SCRUBCRL	LPSTEAM
Q-AGRX2	14703752	Claus thermal-stage to waste-heat boiler	THRMLSTG	WHBOILER
Q-WHB	13928110	Claus WHBLR stage to waste heat boiler	WHBLR	WHBOILER
Q-SCOND1	4906756	From thermal section sulfur condensor-1	S-COND1	SCOND1
Q-SCOND2	2455276	From thermal section sulfur condensor-2	S-COND2	SCOND2
Q-SCOND3	1138944	From thermal section sulfur condensor-3	S-COND3	SCOND3
Heat extracted/lost from HRSG				
Q-GHEAT2	-99108648	HP water (2000 psi) to syngas heater (prior to GT)	GASHEAT2	HEATER1
N2-HEAT	-51661895	HP water (2000 psi) to N2 heater (before GT injection)	N2HTR1	HEATER1
Q-AGHTR	-2594657	IP-steam (575 psi) for industrial use	AGPREHTR	ACIDGASQ
Q-OX	-549343	-do-	OXHTR	OXIDANTQ
Q-SOUR2	-352954	-do-	SOURHTR	SOURQ
Q-TGHEAT	-1309307	-do-	TGTUHEAT	TGHEATR
Q-REHTR2	-955620	-do-	RE-HTR2	GHEAT1
Q-REHTR3	-700594	-do-	RE-HTR3	GHEAT2
Q-65CND	-294650114	LP steam (65 psi) for industrial use		65COND
Q-250CND	-57404449	Extracted turbine IP-steam (250 psia) for industrial use		250CNDS
Q-HLOSS	-528005	HRSG heat loss to ambient		HRSGLOSS

6.1 Single-pressure boiler operation

This single-pressure study has been done to understand the design and operational limitations in the current simulator especially for the boiler, heat-exchanger and steam turbine units. In addition, the dynamic design methodology and controller implementation can be directly extended to "real" three pressure boiler (or HRSG) unit(s). It is obvious that this involves substantial approximations, which have been highlighted below:

- Net heat transferred to the boiler unit (from sources apart from flue-gas) has been calculated as the sum of different heat streams entering the HRSG unit based on Parson's IGCC Case#2 flowsheet. The complete list has been given in Table 6.1. This has been labeled as Q-IGCC in Figure 6.1. We do not account for temperature differentials required for these heat-transfers.

- The operating pressure of the boiler has been chosen as 2000 psi based on the HP-boiler in Parson's flowsheet. This was chosen reasoning on the fact that equipment size and operation is limited by the highest pressure-level in the HRSG unit.

- The condenser unit has not been modeled and the steam cycle is assumed to be operating as a continuous train starting with the feed-water and ending at the turbine exhaust.

- The deaerator[38] unit has not been modeled and has been assumed part of the economizer unit.

6.1.1 Steady-State and Dynamic Design

The single pressure boiler model consists of economizer, evaporator and superheater blocks operating at around 2000 psi. The economizer and superheater exchanges heat with the flue-gas whereas the evaporator takes heat from the flue-gas as

[38]The deaerator removes oxygen just prior to feedwater entering the boiler economizer section of the HRSG, preventing pitting and reduction of the operating life of steam cycle components. Traditionally, many power plants have relied on a deaerator vessel and storage tank to liberate dissolved oxygen in feedwater by raising its temperature by direct injection of saturated steam. Usually, the steam is provided by an extraction line or by dedicated supplies from a low-pressure source such as the low-pressure (LP) drum in a combined-cycle plant.

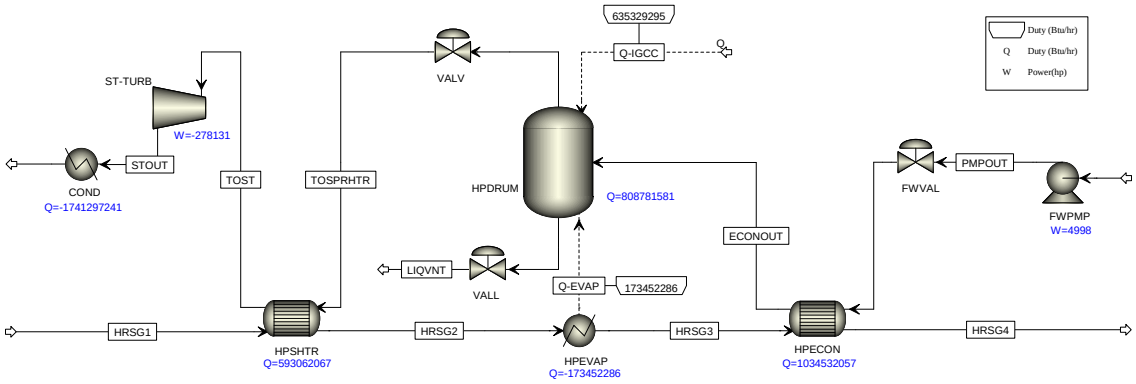

Figure 6.1: Process flowsheet showing a single-pressure boiler operation in AspenPlus™

well as rest of the plant in a single virtual heat-stream (Q-IGCC). The heat distribution in each of these heat-exchangers can be computed by Aspen depending on how we provide the block-specification. This can be done using two methods: (1) specify the hot-stream outlet temperature and (ii) specify the cold-stream outlet temperature. The second approach is much more logical in terms of evaluating the distribution. The economizer, HPECON, is designed such that the cold (or preheated) feed-water is raised to the saturated (bubble) point[39], and hence `vapor-fraction = 0` is specified in AspenPlus™. The evaporator, HPDRUM, is designed to convert all of the liquid to vapor. In Aspen, we specify this by specifying `vapor-fraction = 0.9999` to the drum[40]. This amount of heat is automatically extracted from the HPEVAP cooler on hot-stream side. The superheater, HPSHTR, is designed such that the cold-stream is raised to the vendor-specified turbine-inlet temperature of 1000°F. Figure 6.1 gives the steady-state flowsheet of a single-pressure boiler in AspenPlus™ along with the heat and work amounts. In addition, most of the relevant stream details at steady-state are provided in Table 6.2.

All of these cold-side specifications automatically extract the required heat from the hot flue-gas, depending on the provided feed-water (PMPOUT) flowrate. Obviously it can be inferred that increasing this flowrate promotes more heat ex-

[39] In principle, the temperature is a few degree below the saturated point to prevent HX pipe damage due to sudden 2-phase expansion

[40] A small amount of flowrate must be provided as liquid, since Aspen does not support (or might have robustness issues in dynamic simulation) zero flowrate through a valve (VALL)

Table 6.2: AspenPlus™ steady-state stream results for single-pressure boiler (see Figure 6.1)

Stream Name	**HRSG1**	**HRSG2**	**HRSG3**	**HRSG4**	**PMPOUT**	**ECONOUT**	**TOSPRHTR**	**TOST**	**STOUT**	**LIQVNT**
Temperature (°F)	1052.2	803.0	728.5	269.7	101.5	635.8	635.4	1000.0	211.3	211.3
Pressure (psia)	15.2	15.1	14.9	14.8	2225.0	2000.0	1995.0	1815.0	14.5	14.5
Vapor Fraction	1.00	1.00	1.00	1.00	0.00	0.00	1.00	1.00	0.92	0.51
Mole Flow (lbmol/hr)	307284.6	307284.6	307284.6	307284.6	96300.0	96300.0	96289.4	96289.4	96289.4	9.9
Mass Flow (lb/hr)	8438008.8	8438008.8	8438008.8	8438008.8	1734871.5	1734871.5	1734680.8	1734680.8	1734680.8	178.1
Volume Flow (ft^3/hr)	3.27E+08	2.75E+08	2.62E+08	1.62E+08	27806.71	44491.48	327751.8	760843.3	43306652	2454.054
Enthalpy (MMBtu/hr)	-2132.8	-2725.9	-2899.3	-3933.9	-11781.0	-10746.5	-9936.5	-9343.5	-10051.2	-1.1
Mole Flow (lbmol/hr)										
H_2O	37661.32	37661.32	37661.32	37661.32	96300.00	96300.00	96289.42	96289.42	96289.42	9.89
Ar	2817.52	2817.52	2817.52	2817.52	0	0	0	0	0	0
CO_2	2601.71	2601.71	2601.71	2601.71	0	0	0	0	0	0
O_2	32912.56	32912.56	32912.56	32912.56	0	0	0	0	0	0
N_2	231290.64	231290.64	231290.64	231290.64	0	0	0	0	0	0
SO_2	0.87	0.87	0.87	0.87	0	0	0	0	0	0
Mole Frac										
H_2O	0.123	0.123	0.123	0.123	1	1	1	1	1	1
Ar	0.009	0.009	0.009	0.009	0	0	0	0	0	0
CO_2	0.008	0.008	0.008	0.008	0	0	0	0	0	0
O_2	0.107	0.107	0.107	0.107	0	0	0	0	0	0
N_2	0.753	0.753	0.753	0.753	0	0	0	0	0	0
SO_2	0.000	0.000	0.000	0.000	0	0	0	0	0	0

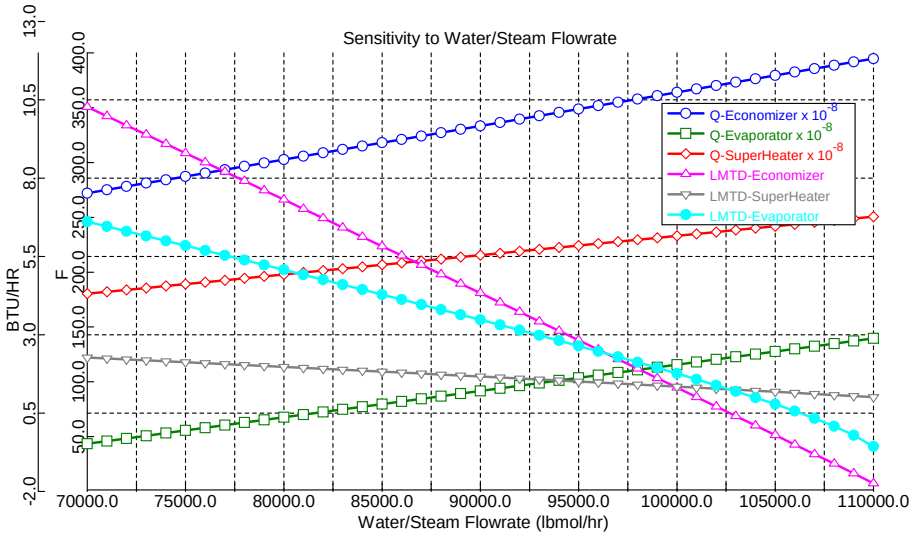

Figure 6.2: Single-pressure boiler heat-duty and LMTD sensitivity to circulation water/steam flowrate

traction resulting in greater steam-turbine work. More importantly, the resulting flue-gas exhaust temperature from each HX is decreased. Therefore, the feed-water flowrate is limited by the pinch point of the system or the minimum temperature approach in these heat-exchangers. Figure 6.2 shows the sensitivity of the heat-duties and the heat-exchanger LMTD to variations in feed-water flowrate. It can be seen that the pinch-point occurs within the economizer for very high feed-water flowrate, showing the exhaust flue-gas temperature quickly approaching the feed-water temperature as we keep increasing the circulation. In this study, we maintain a flowrate (96300 lbmol/hr) which yields an LMTD of $\sim$125°F for each of the HX.

Table 6.3: HX residence-time guide for calculating the volume when exchanger dimensions are unknown

Phase	Shell Side	Tube Side
Liquid/Mixed	15 minutes	5 minutes
Vapor	3 seconds	1 second

For dynamic design, we firstly provide the volumes of hot and cold streams based on volumetric flowrates of corresponding streams. Using Table 6.3 as a guideline, an approximate volume for the inlet and outlet on a given side of the exchanger

can then be calculated from:

$$\text{volume} = (\text{residence-time}) \times (\text{steady-state volumetric flowrate})/2$$

This is also applicable for the evaporator (HPEVAP) block. In addition, we provide a script (see Appendix, page 254) which makes the amount of heat-exchange in the evaporator dependent on medium temperature (in this case, the drum-temperature). This makes the dynamics close to a physical boiler. The drum dimensions are specified based on inlet liquid volumetric flowrate assuming a residence time of $\sim$5 min. The stream turbine is left instantaneous and the default performance curve (at 3600 rpm) in AspenDynamics^{TM} is used.

6.1.2 Controller Design

An obvious controller requirement is to automatically adjust the water flowrate (and hence the steam generation) such that the boiler is capable of extracting industry-generated heat from the relevant units and converting it to work. This is in principle done by the level controller. If the "available heat" increases, either in the gasifier or the flue-gas[41], leading to higher evaporation-rate and lowering of boiler-liquid level. Subsequently, the boiler feed-water valve is opened permitting more water into the cycle, hence higher steam generation and extracted-work.

In this subsection, we study various cases for the controller design for a single-pressure boiler drum. Although this unit does not consist of complex flowsheet structure, including feed splits and recycles, the control structure is nevertheless not trivial. This becomes apparent with different cases we study next.

6.1.2.1 Case I

Here the boiler drum is pressure controlled and steam-turbine operates in floating-pressure mode. The AspenDynamics^{TM} flowsheet with controllers placed is shown in Figure 6.3. The level of the drum-liquid is controlled using a level-controller HPDRUM_LC, which manipulates the inlet feed-water valve (or indirectly

[41] Available heat is only temperature-difference driven and is something very difficult to control. In case of steam as a cooling/heating medium, the steam temperature (limited by its vapor pressure) may be adjusted. Steam/water flowrate, in general, is utilized for level control and is unavailable as a manipulated variable.

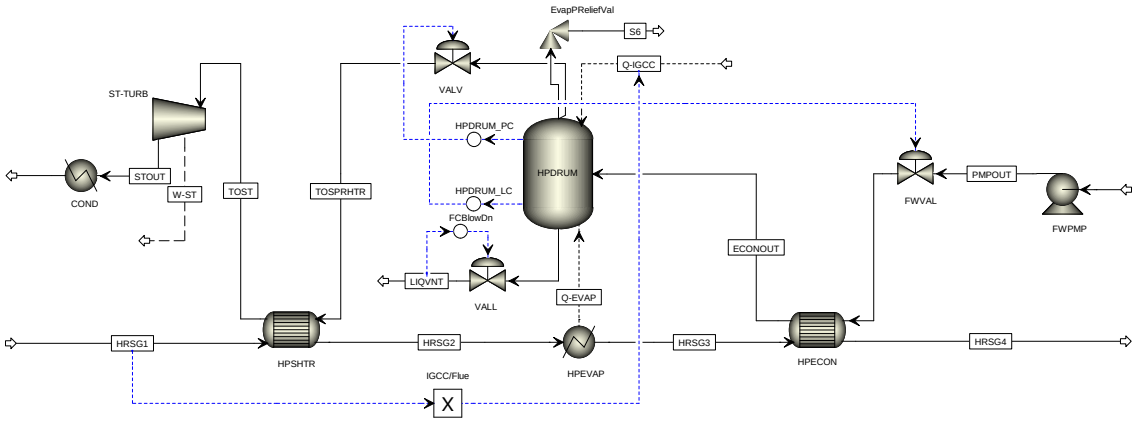

Figure 6.3: Process flowsheet showing a single-pressure boiler (Case I) operation in AspenDynamics™

the feed-water flowrate). The flowrate of blow-down liquid stream is maintained by a flowrate controller FCBlowDn, to ensure the vented liquid amount does not fluctuate with boiler pressure. The boiler pressure (2000 psi) is maintained by a pressure controller HPDRUM_PC, manipulating the valve immediate downstream of the boiler. A pressure relief valve, EvapPReliefVal, is provided to take care of sudden spikes in pressure by opening up the valve beyond 2050 psi drum-pressure.

The heat transferred to the boiler from rest of the plant, especially from the gasifier, is assumed proportional to the flue-gas flowrate. This assumption is valid, close to nominal operating point, when all of the syngas/H_2 generated by the gasifier units is utilized in GT gas-combustion and, henceforth, proportional amount of flue-gas is produced. Hence, a multiplier block (IGCC/Flue) has been placed in the flowsheet to quantify this assumption.

The responses of various variables with step changes in flue-gas flowrate (and heat transferred from the rest of the plant) is shown in Figure 6.4. With a 20% step decrease, the boiler stabilizes to a new steady-state in about 20 minutes. From the heat-duty plot and the simulation results, the percentage decrease in heat extracted from flue-gas in economizer, evaporator and superheater is calculated to be 19.7%, 14.5% and 12.7% respectively. The corresponding steam-turbine work decreased by 22.9%.

Due to sudden decrease (as a step) in heat supplied to the drum, the pressure decreased instantly causing an instantaneous increase in pressure-differential across

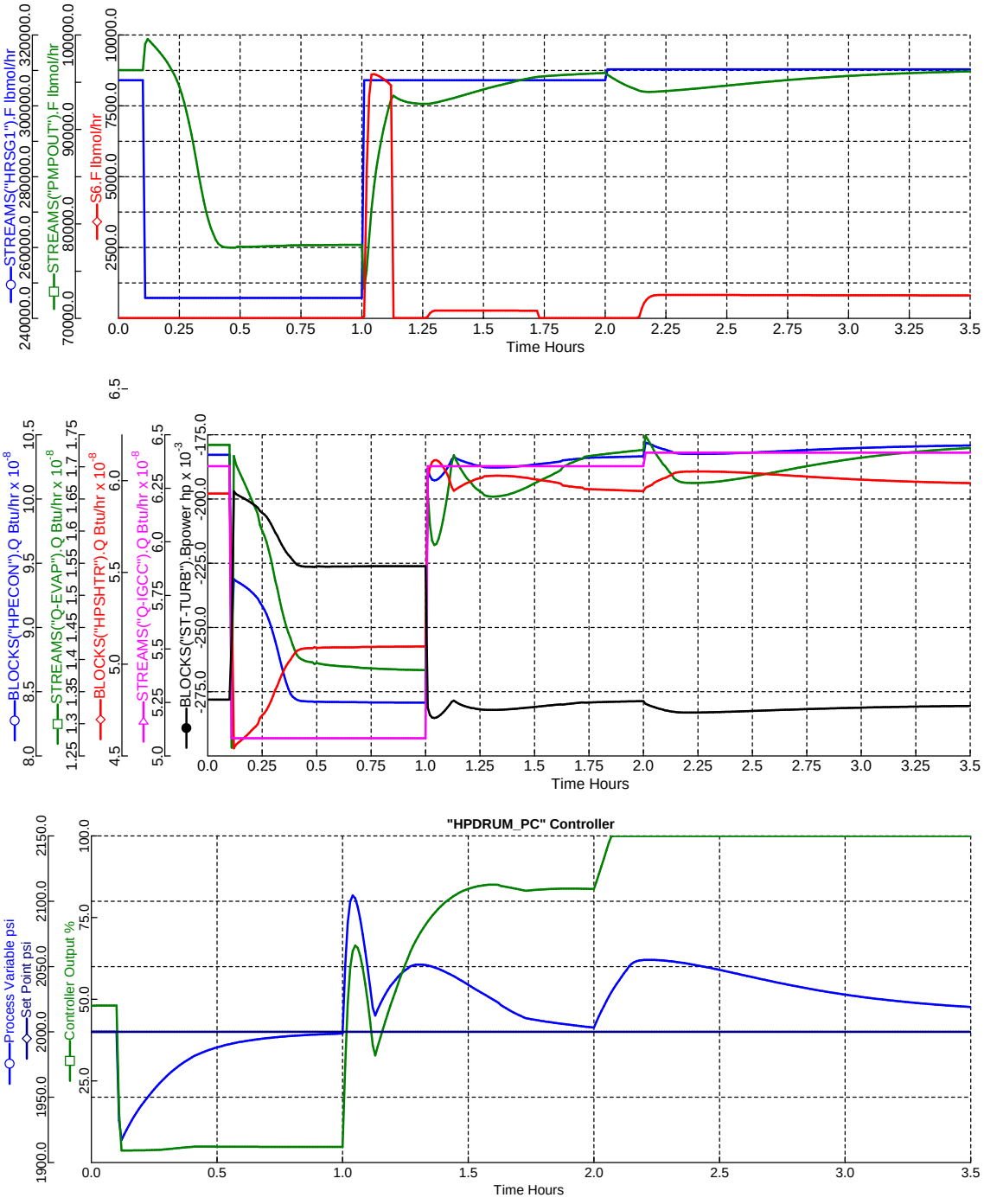

Figure 6.4: Control output responses for Case I to 20% step decrease in flue-gas flowrate at 0.1 hr, returning to nominal value at 1 hr and stepping up 1% at 2 hr; (top) relevant flows, (mid) heat-duties and work and (bot) boiler pressure controller variables

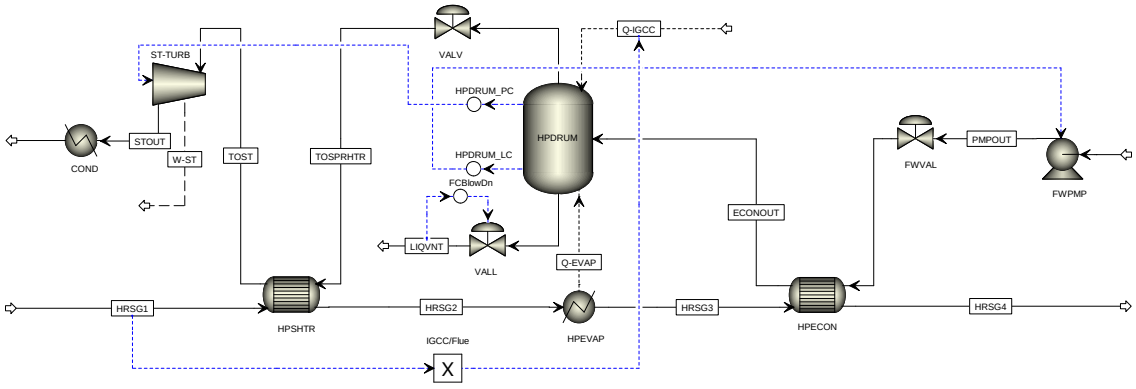

Figure 6.5: Process flowsheet showing a single-pressure boiler (Case II) operation in AspenDynamics™

the valve upstream, due to which more liquid flows into the drum (Figure 6.4 (top)). When the flue-gas is stepped back to nominal-value (at t = 1 hr), we see many unexpected yet interesting responses. The drum-pressure rises very steeply, even though the drum pressure controller opens up the downstream valve. This rise of pressure beyond 2050 psi triggers the pressure relief valve and about 8300 lbmol/hr of steam is bled off for 7 min, bringing the pressure down to a controllable level.

To test the robustness of the system, we provide a step increase in the flue-gas flowrate from the nominal value. The pressure controller valve was observed to saturate (fully open), even for a small flowrate increase. This is illustrated in the plot (Figure 6.4) by giving only a 1% step-up. These simulations were again tried with large valves and higher pressure drops; each showing negligible improvement for the load-increase runs. Upon close observation, it was found that as the flowrate of the steam increased, the steam-turbine inlet pressure increased as well. Due to this back-pressure on the boiler exhaust valve (VALV), the pressure differential decreased leading to valve saturation. Clearly this intuitive design for a single-pressure boiler did not show very promising results for load changes, hence we make a few control-structure changes to study and compare the boiler performance in the next case.

6.1.2.2 Case II

In this case, we focus on maintaining the drum pressure and assume that turbine is capable of handling load-changes, which is in principle done by manipulating the governor valves. In Aspen, we mimic this scenario by directly manipulating the turbine brake-power[42] to control the variable of interest (inlet pressure, outlet pressure, flowrate). Here, we use it to control the drum-pressure (indirectly the turbine suction-side pressure). For brevity sake, we removed the pressure-relief valve. Another modification to improve the robustness of the system in simulations is to use the feedwater pump (FWPMP) electric-power[43] directly instead of feed-water valve (FWVAL) to control the drum level. This is definitely beneficial during load increase where the valve is limited to its full-open point.

As shown in Figure 6.6, we initially make a large (50%) step decrease in flue-gas flowrate at t = 0.1 hr. The boiler stabilizes to a new steady-state in 20 minutes. The percentage decrease in heat extracted from flue-gas in economizer, evaporator and superheater is 45.9%, 43.2% and 44.2% respectively. The corresponding steam-turbine work decreased by 44.6% and the exhaust flue-gas temperature decreased by 80.9°F. The pressure response in Figure 6.6 (bottom) shows a typical dual time-scale behavior, the faster initial response being due to the pressure dynamics and the trailing slower one due to thermal interactions/dynamics. We make a step increase at t = 0.6 hr back to the nominal steady-state. The pressure peaks up to a value of 2100 psi, during which the pressure controller, for a short duration extracts, more work from the ST by utilizing the excess steam. One can see an analogous behavior to the previous case, where the excess steam was purged out. At t = 1.1 hr, the flue-gas flowrate is stepped up by 20%. This design is robust in handling load increases even above the nominal point.

This approach does not pose any equipment constraint on the boiler drum, although it can be realized that the turbine does not operate at its optimized point.

[42]In AspenDynamics™ turbine model, we have to specify `'Use Performance Curves = No'` in Aspen version 7.1 to make BrakePower available for input changes. No change is required in version 2006.0

[43]Similar to the AspenDynamics™ turbine model, we have to specify `'Use Performance Curves = No'` in the pump model to make ElectricPower available for input changes (old and new versions).

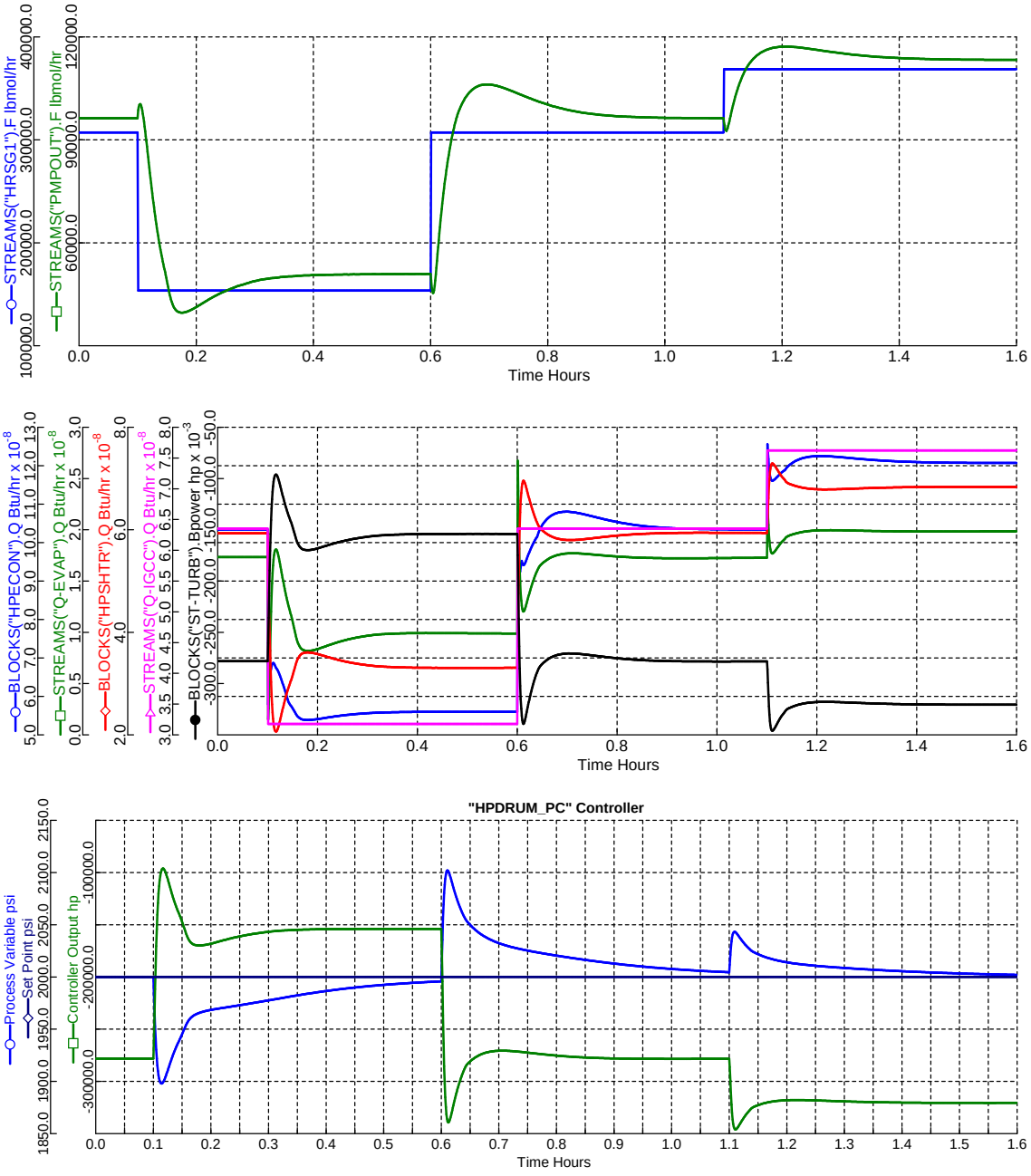

Figure 6.6: Control output responses for Case II to 50% step decrease in flue-gas flowrate at 0.1 hr, returning to nominal value at 0.6 hr and stepping up 20% at 1.1 hr; (top) relevant flows, (mid) heat-duties and work and (bot) boiler pressure controller variables

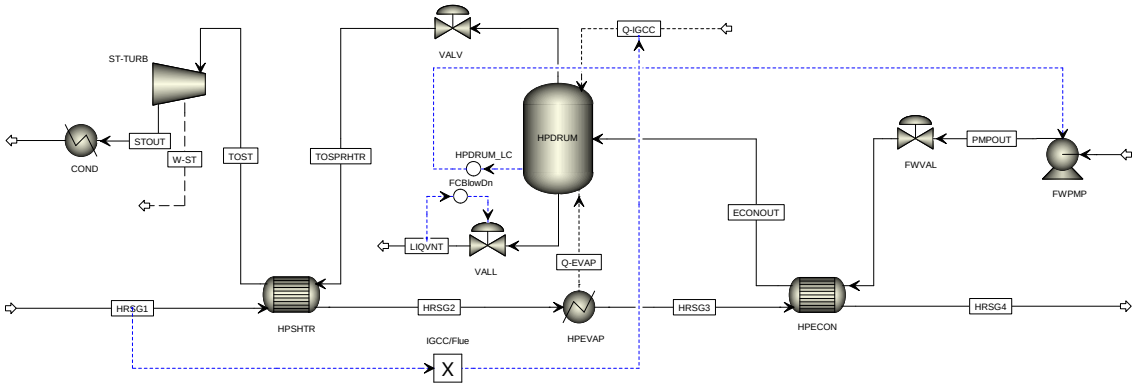

Figure 6.7: Process flowsheet showing a single-pressure boiler (Case III) operation in AspenDynamics™

For instance, at low-load condition and low steam flowrate, the turbine operates at similar pressure ratio as that at full load or design condition. This brings the turbine operation close to surge at a constant 3600 rpm[44]. At the other extreme, i.e., at high flowrates, the turbine deviates from its design condition entering into a stonewall region. In our study, we do not account for detailed turbine modeling and control and hence to mimic a real physical system, we should not choose to simulate a machinery far from its designed operating point. Hence, we take a step back and do not forcefully change the turbine brake-power. Instead we let the simulator handle the dynamics[45] with its in-build performance curve at 3600 rpm.

6.1.2.3 Case III

Here we study the case where there is an inherent relationship between the turbine inlet/outlet pressure and the flowrate, dictated by the performance curve. In this scenario, the turbine operation can be visualized as a simple valve. Higher turbine-inlet pressure (with a near-constant outlet pressure) leads to greater flowrate or, in other words, a greater flowrate through the turbine implies a higher inlet pressure[46]. In terms of boiler operation, it signifies that with load changes the

[44]Throughout this project we maintain the rotor speed as 3600 rpm

[45]Aspen v2006.0 does not handle performance-curve based turbine dynamics and the brake-power is "fixed" by default. To vary the load with flowrate, some criterion such as constant pressure ratio, inlet pressure or outlet pressure has to be chosen.

[46]Large inlet pressure implies a small pressure-ratio (PR) which according to a typical turbine/compressor performance curve indicates a high flowrate

pressure of the turbine inlet and the boiler-drum have to change. Hence we eliminate any drum pressure control and let the pressure float with water/steam flowrate changes. This is shown in Figure 6.7.

The floating-pressure arrangement has always been known to be dynamically more complex and difficult to control. In process units where vapor-liquid equilibrium is involved, this arrangement inherently implies a floating-temperature as well. If these sections exchange heat with other plant components or sections, the temperature-drive and hence the heat-duties will swing. Therefore, unlike the previous two cases, we see a heat transfer imbalance in the economizer, evaporator and superheater units. In this particular example, where we provide a step decrease of 50% in flue-gas flowrate (and Q-IGCC) at t = 0.1 hr, we observe a decrease of 46.7%, **9.4%** and 46.3% in heat-exchange duty for economizer, evaporator and superheater respectively. The corresponding steam-turbine work decreases by 47.4% and the exhaust flue-gas temperature by 115.3°F.

The evaporator drum has a pressure swing of 800 psi (∼55 bar) below nominal point and an equilibrium temperature of 565°F (nominal is 635.8 °F). This results in a higher temperature differential between the flue-gas and drum fluid, and hence a greater heat-exchange duty. This phenomenon is counter-intuitive to the common understanding of heat duties varying proportionally to load-changes.

With load increase beyond the nominal point, the drum-pressure also increases significantly. This is shown in Figure 6.7, where a 10% step-increase is provided at t = 1.1 hr. The steady-state pressure is 250 psi higher than the nominal value causing large mechanical and thermal stress in the drum. Hence, the maximum load (extracted work) is limited by the steam-drum pressure withstanding capacity. This can be altered by shifting the operating 'performance' curve by manipulating the governer valve(s) or altering the operating frequency. These control cases, not being handled elegantly by Aspen (in its current version), is beyond the scope of this research.

In conclusion, after studying the three cases, we understand the operational and control limitations for a single-pressure boiler unit. We realize that implementation of a pressure-control on the boiler drum not only made the dynamics less robust

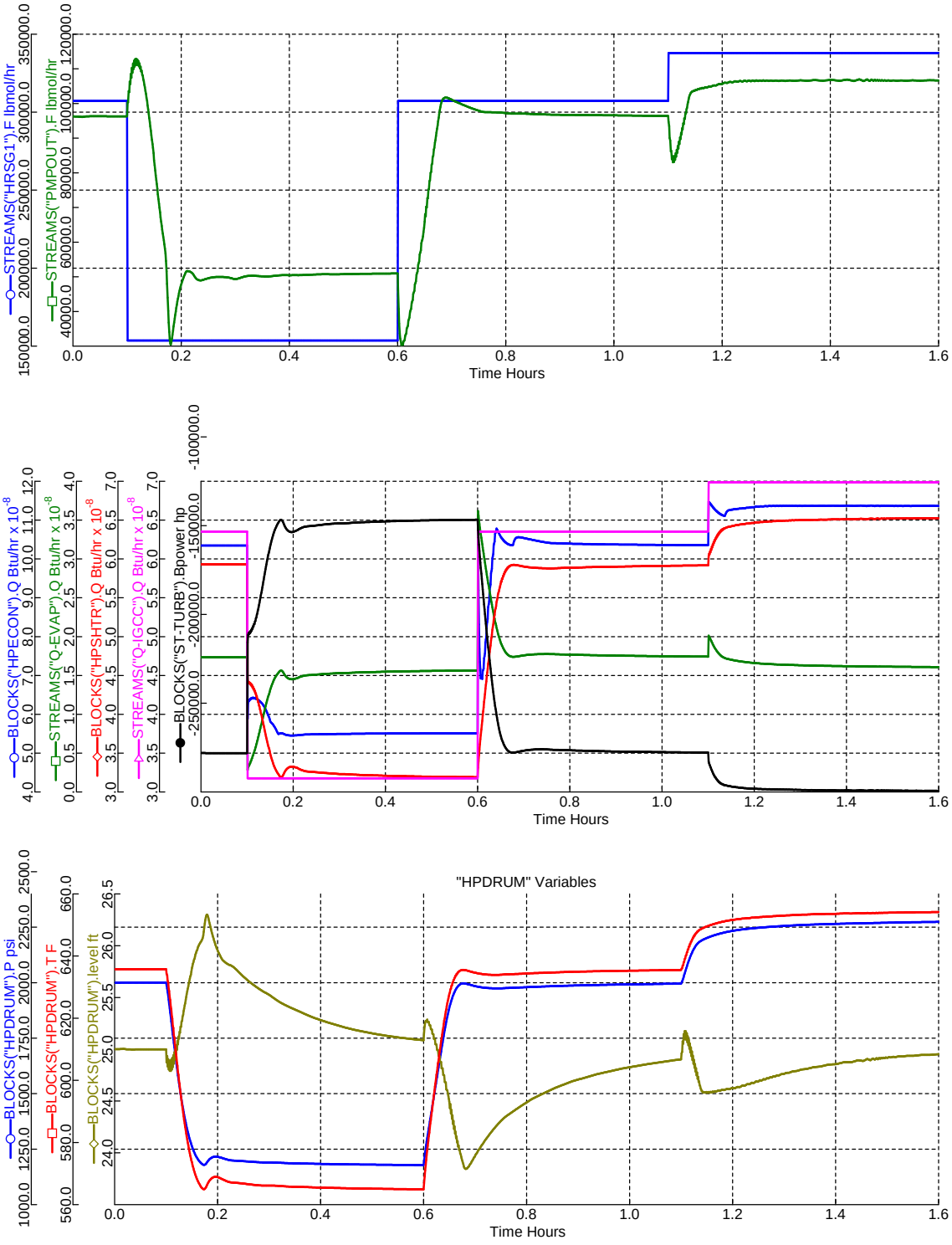

Figure 6.8: Control output responses for Case III to 50% step decrease in flue-gas flowrate at 0.1 hr, returning to nominal value at 0.6 hr and stepping up 10% at 1.1 hr; (top) relevant flows, (mid) heat-duties and work and (bot) boiler variables

but involved installing complex fail-safe devices (pressure-relief valve) for stable operation. In another studied scenario where a possible workaround is possible using the turbine extracted work to control the pressure, we have to incorporate gross approximations in the steam-turbine model, and hence we discard the approach. Finally, after keeping the drum-pressure floating, we obtained a qualitative understanding of the possible load-limitation due to large pressure buildup in the vessel. In the following section, we expand the current ideas to a full-blown HRSG unit with three pressure-level operation.

6.2 Three-pressure level HRSG operation

The three-pressure level operation is characterized by many different heat-exchanger forming a network to maximize the heat recovery from the flue-gas and different portion of the plant, where the source temperature may vary from as high 2500°F to as low as 300°F. Obviously a single pressure (and hence a single equilibrium temperature) cannot provide heat exchange capability for the entire range without loosing considerable amount of entropic efficiency (recoverable heat). In current study, we use boiler pressures of 1995 psi, 580 psi and 79 psi corresponding to high-pressure (HP), intermediate-pressure (HP) and low-pressure (LP) operation. We discuss this at length in the next subsection. Here we highlight some of the assumptions in the current HRSG model:

- The steam-cycle loop has not been closed and is assumed to be operating as a continuous train starting with the feed-water and ending at the condenser unit. Feed-water is the sum of condenser outlet flowrate and fresh makeup water.

- The deaerator unit has not been modeled in detail and has been assumed as a simple heat exchanger, utilizing heat from the tail-end of hot flue-gas stream.

6.2.1 Steady-State and Dynamic Design

The feed-water stream entering the HRSG (MAKEUP) pumped up to a pressure of 135 psi is preheated in FLASCRUB (utilizing heat from tail-gas cooler and

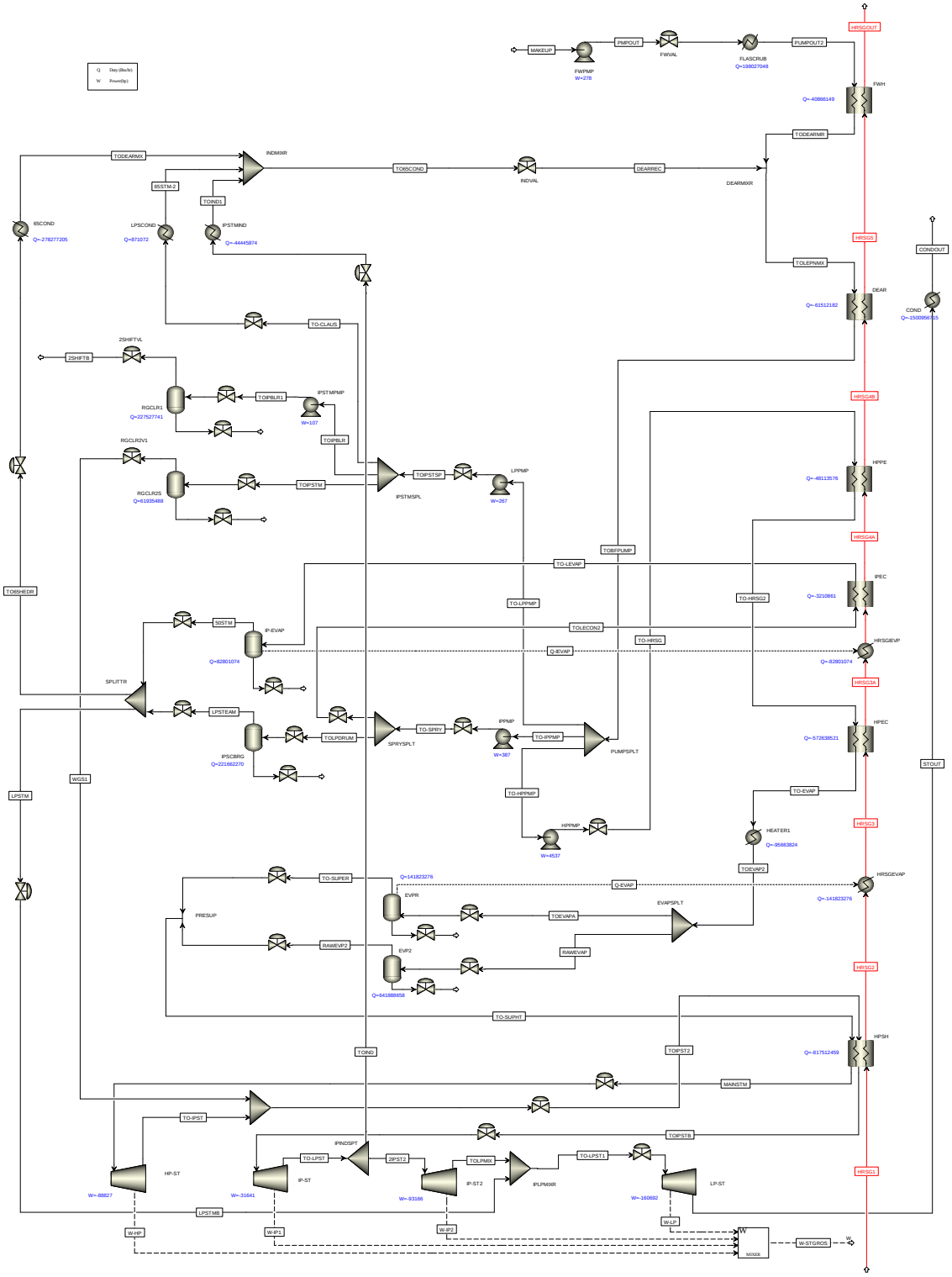

Figure 6.9: Process flowsheet showing HRSG operation in AspenPlus™

radiant syngas cooler) and subsequently in a feed-water heater, FWH (using flue-gas) to a temperature of 235°F. This stream is mixed with the industrial recycled stream and sent to the deaerator, modeled as a single-stream HX (DEAR) taking heat from the flue-gas. The resultant stream, TOBFPUMP (at 45 psi and 275°F) is split towards HP, IP and LP sub-sections of the HRSG in a splitter block (PUMP-SPLT).

The HP portion, constituting of 68.5% of the total flow, is compressed in the high-pressure pump (HPPMP) to a pressure of 2250 psi. This stream is sent to the HP pre-economizer (HPPE) followed by the economizer (HPEC), where it exchanges heat with the flue-gas, to raise its temperature close to bubble-point (635.8°F). The cooler block (HEATER1) provides heat for preheating nitrogen (before GT-injection) and syngas. The resultant HP streams is split into two HP-boiler drums. One boiler (EVPR) accepts heat from the flue-gas and the other (EVP2) takes heat from the gasifier (QGASIFR in Figure 4.9 and 4.11). The saturated steam from both the boilers are mixed and sent to the HP superheater (HPSH) after which it is sent to the high-pressure steam turbine (HP-ST).

The LP portion from the PUMPSPLT (15.5 % of the total flow) is compressed to 875 psi in an intermediate-pressure pump (IPPMP). Part of this stream (27.5%) passes through the spray-valve(pressure reduced to 79 psi) and is sent through the low-pressure economizer (IPEC) to the low-pressure evaporator drum (IP-EVAP), both of which take heat from the flue-gas. The other part, again passing through the spray, enters the low-pressure drum IPSCBRG (modeled separately), which takes heat from radiant syngas cooler and scrubber. A portion of the net LP-steam is sent for industrial use (65 psi header) and the rest is utilized in the low-pressure steam turbine (LP-ST).

The IP-portion after being compressed to 600 psi in a low-pressure pump (LPPMP), is split into three parts. One of them (TO-CLAUS) is used as a LP-water in Claus Plant and other industrial places as a heating/cooling source. This is later mixed with other industry-used water (mentioned above) and recycled back with the feed-water. The second part is further compressed in a pump (IPSTMPMP) to 885 psi and sent to the IP-boiler drum (RGCLR1) which receives heat from

the 1st radiant syngas cooler (after the 1st shift reactor). The steam generated is used in the 1st shift reactor itself. The third part sent to a second IP-boiler drum (RGCLR2S) is evaporated using heat from the 2nd radiant syngas cooler (following the 2nd shift reactor). This evaporated stream (WGS1) is mixed with the HP turbine exhaust steam (TO-IPST) and reheated in a high-pressure superheater (HPSH), before expanding in the IP turbine.

A small portion (∼2.4%) of the IP turbine exhaust steam is bled-off for industrial heating and is eventually recycled back with feed-water. The steam turbine exhaust (STOUT) at a sub-atmospheric pressure (1 psi) is condensed in a condensor block (COND) and cycled back. Figure 6.9 gives the steady-state flowsheet for the HRSG subsection with magnitude of various steady-state heat-duties and work shown. Table 6.4, 6.5, 6.6 and 6.7 gives the steady-state results for relevant streams in the flowsheet.

This is complex network with multiple recycle loops. We ensure fast convergence by specifying the flowrates of streams corresponding to the recycle lines (rather than providing the split fractions). The total work extracted from the turbines is 280 MW which matches very closely with the Parson's IGCC Case#2 flowsheet (280.6 MW). In addition, the exhaust temperature of the flue-gas line (285°F) is also close to the vendor specified value.

In terms of dynamic design, equipment sizing for evaporator drums and HX piping volume have been based on heuristics (∼10 min residence time, see Table 6.3). Instantaneous steam-turbines models and default performance curves[47] for ST corresponding to 3600 rpm (60 Hz) have been used in dynamic simulations. For the evaporator drums, the direction of the heat stream is such that it facilitates the specification on the cold side. After exporting to AspenDynamics^{TM}, this heat stream is deleted and its magnitude is made dependent on the flue-gas evaporator-drum temperature difference. The methodology is highlighted in Appendix, page 254. The dynamic flowsheet, including the regulatory controllers (discussed in the next subsection), consists of 31304 variables, 22337 equations and 895 states. A variable step Gear method (maximum order 5) with default integration tolerances (0.0005

[47]Not available in Aspen Version 2006.0

Table 6.4: AspenPlus™ steady-state stream results for HRSG (see Figure 6.9) - I

Stream Name	HRSG1	HRSG2	HRSG3	HRSG3A	HRSG4	HRSG4A	HRSG4B	HRSG5	HRSGOUT
Total Flow (lbmol/hr)	307285	307285	307285	307285	307285	307285	307285	307285	307285
Total Flow (lb/hr)	8.44E+06	8.44E+06	8.44E+06	8.44E+06	8.44E+06	8.44E+06	8.44E+06	8.44E+06	8.44E+06
Total Flow (ft^3/hr)	3.27E+08	2.54E+08	2.42E+08	1.88E+08	1.81E+08	1.82E+08	1.78E+08	1.73E+08	1.70E+08
Temperature (°F)	1052.2	706.5	644.9	391.2	354.0	352.5	330.8	303.0	284.4
Pressure (psia)	15.24	15.14	15.04	14.94	14.84	14.74	14.64	14.54	14.44
Enthalpy (Btu/lbmol)	-6940.91	-9601.35	-10062.88	-11926.43	-12195.89	-12206.34	-12362.92	-12563.09	-12696.09
Enthalpy (Btu/lb)	-252.77	-349.65	-366.46	-434.32	-444.13	-444.51	-450.22	-457.51	-462.35
Enthalpy (Btu/hr)	-2.13E+09	-2.95E+09	-3.09E+09	-3.66E+09	-3.75E+09	-3.75E+09	-3.80E+09	-3.86E+09	-3.90E+09
Entropy (Btu/lbmol-R)	7.825	5.842	5.448	3.546	3.235	3.236	3.054	2.810	2.647
Entropy (Btu/lb-R)	0.285	0.213	0.198	0.129	0.118	0.118	0.111	0.102	0.096
Density (lbmol/ft^3)	9.39E-04	1.21E-03	1.27E-03	1.64E-03	1.70E-03	1.69E-03	1.73E-03	1.78E-03	1.81E-03
Density (lb/ft^3)	0.0258	0.0332	0.0348	0.0449	0.0467	0.0464	0.0474	0.0488	0.0497
Average MW	27.46	27.46	27.46	27.46	27.46	27.46	27.46	27.46	27.46
Liq Vol 60F (ft^3/hr)	2.42E+05	2.42E+05	2.42E+05	2.42E+05	2.42E+05	2.42E+05	2.42E+05	2.42E+05	2.42E+05
Mole Flow (lbmol/hr)									
H_2O	37661.32	37661.32	37661.32	37661.32	37661.32	37661.32	37661.32	37661.32	37661.32
Ar	2817.52	2817.52	2817.52	2817.52	2817.52	2817.52	2817.52	2817.52	2817.52
CO_2	2601.72	2601.72	2601.72	2601.72	2601.72	2601.72	2601.72	2601.72	2601.72
O_2	32912.56	32912.56	32912.56	32912.56	32912.56	32912.56	32912.56	32912.56	32912.56
N_2	231291.00	231291.00	231291.00	231291.00	231291.00	231291.00	231291.00	231291.00	231291.00
SO_2	0.87	0.87	0.87	0.87	0.87	0.87	0.87	0.87	0.87
Mole Frac									
H_2O	0.123	0.123	0.123	0.123	0.123	0.123	0.123	0.123	0.123
Ar	0.009	0.009	0.009	0.009	0.009	0.009	0.009	0.009	0.009
CO_2	0.008	0.008	0.008	0.008	0.008	0.008	0.008	0.008	0.008
O_2	0.107	0.107	0.107	0.107	0.107	0.107	0.107	0.107	0.107
N_2	0.753	0.753	0.753	0.753	0.753	0.753	0.753	0.753	0.753
SO_2	0.000	0.000	0.000	0.000	0.000	0.000	0.000	0.000	0.000

Table 6.5: AspenPlus™ steady-state stream results for HRSG (see Figure 6.9) - II

Stream Name	CONDOUT	MAKEUP	PMPOUT	PUMPOUT2	TODEARMR	TO65COND	DEARREC	TOLEPNMX	TOBFPUMP
Total Flow (lbmol/hr)	84774.1	98354.4	98354.4	98354.4	98354.4	21095.0	21095.0	119449.0	119449.0
Total Flow (lb/hr)	1527230.0	1771880.0	1771880.0	1771880.0	1771880.0	380032.0	380032.0	2151920.0	2151920.0
Total Flow (ft^3/hr)	24606	28579	28569	29613	29917	6626	7206	36524	37043
Temperature (°F)	94.4	100.0	100.1	212.0	235.0	298.2	298.0	246.2	274.4
Pressure (psia)	0.80	14.50	135.00	110.00	65.00	65.20	65.00	65.00	45.00
Vapor Fraction	0	0	0	0	0	0	2.30E-04	0	0
Enthalpy (Btu/lbmol)	-1.23E+05	-1.22E+05	-1.22E+05	-1.20E+05	-1.20E+05	-1.19E+05	-1.19E+05	-1.20E+05	-1.19E+05
Enthalpy (Btu/lb)	-6803.68	-6798.05	-6797.65	-6685.89	-6662.82	-6598.56	-6598.56	-6651.48	-6622.89
Enthalpy (Btu/hr)	-1.04E+10	-1.21E+10	-1.20E+10	-1.19E+10	-1.18E+10	-2.51E+09	-2.51E+09	-1.43E+10	-1.43E+10
Entropy (Btu/lbmol-R)	-38.392	-38.212	-38.212	-34.931	-34.319	-32.724	-32.724	-34.027	-33.310
Entropy (Btu/lb-R)	-2.131	-2.121	-2.121	-1.939	-1.905	-1.816	-1.816	-1.889	-1.849
Density (lbmol/ft^3)	3.445204	3.441495	3.442702	3.321285	3.287525	3.183738	2.927603	3.270405	3.224629
Density (lb/ft^3)	62.0663	61.9995	62.0212	59.8339	59.2257	57.3559	52.7416	58.9173	58.0926
Average MW	18.02	18.02	18.02	18.02	18.02	18.02	18.02	18.02	18.02
Liq Vol 60F (ft^3/hr)	24511.02	28437.54	28437.54	28437.54	28437.54	6099.27	6099.27	34536.80	34536.80

Stream Name	TO-LPPMP	TOIPSTSP	TOIPSTM	WGS1	TOIPBLR	TOIPBLR1	2SHIFTB	TO-CLAUS	65STM-2
Total Flow (lbmol/hr)	19054.4	19054.4	3590.4	3586.8	13300.0	13300.0	13286.7	2164.0	2164.0
Total Flow (lb/hr)	343271.0	343271.0	64682.5	64617.9	239603.0	239603.0	239364.0	38985.1	38985.1
Total Flow (ft^3/hr)	5909	5899	1111	64443	4117	4114	123635	670	680
Temperature (°F)	274.4	275.3	275.3	459.6	275.3	275.9	528.7	275.3	298.2
Pressure (psia)	45.00	600.00	600.00	465.00	600.00	885.00	875.00	600.00	65.20
Vapor Fraction	0	0	0	0.998906	0	0	0.999769	0	0
Enthalpy (Btu/lbmol)	-1.19E+05	-1.19E+05	-1.19E+05	-1.02E+05	-1.19E+05	-1.19E+05	-1.02E+05	-1.19E+05	-1.19E+05
Enthalpy (Btu/lb)	-6622.89	-6620.91	-6620.91	-5662.64	-6620.91	-6619.78	-5669.50	-6620.91	-6598.56
Enthalpy (Btu/hr)	-2.27E+09	-2.27E+09	-4.28E+08	-3.66E+08	-1.59E+09	-1.59E+09	-1.36E+09	-2.58E+08	-2.57E+08
Entropy (Btu/lbmol-R)	-33.310	-33.306	-33.306	-14.080	-33.306	-33.300	-15.226	-33.306	-32.724
Entropy (Btu/lb-R)	-1.849	-1.849	-1.849	-0.782	-1.849	-1.848	-0.845	-1.849	-1.816
Density (lbmol/ft^3)	3.224629	3.230383	3.230383	0.055659	3.230383	3.233115	0.107467	3.230383	3.183738
Density (lb/ft^3)	58.0926	58.1963	58.1963	1.0027	58.1963	58.2455	1.9361	58.1963	57.3559
Average MW	18.02	18.02	18.02	18.02	18.02	18.02	18.02	18.02	18.02
Liq Vol 60F (ft^3/hr)	5509.27	5509.27	1038.11	1037.07	3845.47	3845.47	3841.63	625.68	625.68

Table 6.6: AspenPlus™ steady-state stream results for HRSG (see Figure 6.9) - III

Stream Name	TO-IPPMP	TO-SPRY	TOLECON2	TO-LEVAP	50STM	TOLPDRUM	LPSTEAM	TO65HEDR	TODEARMX
Total Flow (lbmol/hr)	18500.0	18500.0	5100.0	5100.0	5099.5	13400.0	13132.0	16884.0	16884.0
Total Flow (lb/hr)	333283.0	333283.0	91877.9	91877.9	91868.7	241405.0	236577.0	304170.0	304170.0
Total Flow (ft^3/hr)	5737	5722	1584	1614	507527	4144	1306960	1684400	5303
Temperature (°F)	274.4	275.7	277.3	311.3	311.3	275.7	311.3	311.2	298.2
Pressure (psia)	45.00	875.00	79.40	79.20	79.20	875.00	79.20	79.00	65.20
Vapor Fraction	0	0	0	9.89E-10	1.00E+00	0	1	1	0
Enthalpy (Btu/lbmol)	-1.19E+05	-1.19E+05	-1.19E+05	-1.19E+05	-1.02E+05	-1.19E+05	-1.02E+05	-1.02E+05	-1.19E+05
Enthalpy (Btu/lb)	-6622.89	-6619.94	-6619.94	-6584.99	-5683.69	-6619.94	-5683.69	-5683.69	-6598.56
Enthalpy (Btu/hr)	-2.21E+09	-2.21E+09	-6.08E+08	-6.05E+08	-5.22E+08	-1.60E+09	-1.34E+09	-1.73E+09	-2.01E+09
Entropy (Btu/lbmol-R)	-33.310	-33.303	-33.240	-32.405	-11.345	-33.303	-11.345	-11.341	-32.724
Entropy (Btu/lb-R)	-1.849	-1.849	-1.845	-1.799	-0.630	-1.849	-0.630	-0.630	-1.816
Density (lbmol/ft^3)	3.224629	3.233215	3.220307	3.159977	0.010048	3.233215	0.010048	0.010024	3.183738
Density (lb/ft^3)	58.0926	58.2473	58.0147	56.9279	0.1810	58.2473	0.1810	0.1806	57.3559
Average MW	18.02	18.02	18.02	18.02	18.02	18.02	18.02	18.02	18.02
Liq Vol 60F (ft^3/hr)	5348.97	5348.97	1474.58	1474.58	1474.43	3874.39	3796.90	4881.73	4881.73

Stream Name	TO-HPPMP	TO-HRSG	TO-HRSG2	TO-EVAP	TOEVAP2	TOEVAPA	TO-SUPER	RAWEVAP	RAWEVP2
Total Flow (lbmol/hr)	81895.0	81895.0	81895.0	81895.0	81895.0	14820.0	14818.5	67075.0	67068.3
Total Flow (lb/hr)	1475360.0	1475360.0	1475360.0	1475360.0	1475360.0	266987.0	266960.0	1208380.0	1208250.0
Total Flow (ft^3/hr)	25397	25221	25656	37841	34057	6163	50411	27894	228161
Temperature (°F)	274.4	277.8	310.0	635.8	595.0	595.0	635.5	595.0	635.5
Pressure (psia)	45.00	2250.70	2225.70	2000.70	1998.70	1998.70	1996.70	1998.70	1996.70
Vapor Fraction	0	0	0	0	0	0	1	0	1
Enthalpy (Btu/lbmol)	-1.19E+05	-1.19E+05	-1.19E+05	-1.12E+05	-1.13E+05	-1.13E+05	-1.03E+05	-1.13E+05	-1.03E+05
Enthalpy (Btu/lb)	-6622.89	-6615.07	-6582.45	-6194.32	-6259.16	-6259.16	-5727.91	-6259.16	-5727.91
Enthalpy (Btu/hr)	-9.77E+09	-9.76E+09	-9.71E+09	-9.14E+09	-9.23E+09	-1.67E+09	-1.53E+09	-7.56E+09	-6.92E+09
Entropy (Btu/lbmol-R)	-33.310	-33.291	-32.510	-25.019	-26.105	-26.105	-17.346	-26.105	-17.346
Entropy (Btu/lb-R)	-1.849	-1.848	-1.805	-1.389	-1.449	-1.449	-0.963	-1.449	-0.963
Density (lbmol/ft^3)	3.224629	3.247068	3.192102	2.164176	2.404676	2.404676	0.293951	2.404676	0.293951
Density (lb/ft^3)	58.0926	58.4968	57.5066	38.9882	43.3209	43.3209	5.2956	43.3209	5.2956
Average MW	18.02	18.02	18.02	18.02	18.02	18.02	18.02	18.02	18.02
Liq Vol 60F (ft^3/hr)	23678.57	23678.57	23678.57	23678.57	23678.57	4284.96	4284.53	19393.61	19391.67

Table 6.7: AspenPlus™ steady-state stream results for HRSG (see Figure 6.9) - IV

Stream Name	TO-SUPHT	MAINSTM	TO-IPST	TO-IPST2	TOIPSTB	TO-LPST	TOIND	TOIND1	2IPST2
Total Flow (lbmol/hr)	81886.8	81886.8	81886.8	85473.7	85473.7	85473.7	2047.0	2047.0	83426.7
Total Flow (lb/hr)	1475210.0	1475210.0	1475210.0	1539830.0	1539830.0	1539830.0	36877.3	36877.3	1502950.0
Total Flow (ft^3/hr)	278905	618313	1950150	2014270	3138040	4371290	104688	643	4266600
Temperature (°F)	635.4	1005.0	643.0	634.1	1005.0	897.8	897.8	298.2	897.8
Pressure (psia)	1994.70	1900.00	465.00	465.00	420.00	280.00	280.00	65.20	280.00
Vapor Fraction	0.99968	1	1	1	1	1	1	0	1
Enthalpy (Btu/lbmol)	-103190	-97028.2	-99788.3	-99881.7	-96220.4	-97162.3	-97162.3	-118880	-97162.3
Enthalpy (Btu/lb)	-5727.91	-5385.89	-5539.09	-5544.28	-5341.04	-5393.33	-5393.33	-6598.56	-5393.33
Enthalpy (Btu/hr)	-8.45E+09	-7.95E+09	-8.17E+09	-8.54E+09	-8.22E+09	-8.30E+09	-1.99E+08	-2.43E+08	-8.11E+09
Entropy (Btu/lbmol-R)	-17.345	-12.277	-11.859	-11.944	-8.861	-8.738	-8.738	-32.724	-8.738
Entropy (Btu/lb-R)	-0.963	-0.681	-0.658	-0.663	-0.492	-0.485	-0.485	-1.816	-0.485
Density (lbmol/ft^3)	0.293601	0.132436	0.04199	0.042434	0.027238	0.019553	0.019553	3.183738	0.019553
Density (lb/ft^3)	5.2893	2.3859	0.7565	0.7645	0.4907	0.3523	0.3523	57.3559	0.3523
Average MW	18.02	18.02	18.02	18.02	18.02	18.02	18.02	18.02	18.02
Liq Vol 60F (ft^3/hr)	23676.20	23676.20	23676.20	24713.27	24713.27	24713.27	591.86	591.86	24121.42

Stream Name	LPSTM	LPSTMB	TOLPMIX	TO-LPST1	STOUT
Total Flow (lbmol/hr)	1347.5	1347.5	83426.7	84774.1	84774.1
Total Flow (lb/hr)	24275.4	24275.4	1502950.0	1527230.0	1527230.0
Total Flow (ft^3/hr)	134429	163271	13979500	14143400	479774000
Temperature (°F)	311.2	304.8	566.7	562.4	101.7
Pressure (psia)	79.00	65.00	65.00	65.00	1.00
Vapor Fraction	1	1	1	1	0.94168
Enthalpy (Btu/lbmol)	-1.02E+05	-1.02E+05	-1.00E+05	-1.00E+05	-1.05E+05
Enthalpy (Btu/lb)	-5683.69	-5683.69	-5551.05	-5553.16	-5820.88
Enthalpy (Btu/hr)	-1.38E+08	-1.38E+08	-8.34E+09	-8.48E+09	-8.89E+09
Entropy (Btu/lbmol-R)	-11.341	-10.970	-8.276	-8.313	-6.853
Entropy (Btu/lb-R)	-0.630	-0.609	-0.459	-0.461	-0.380
Density (lbmol/ft^3)	0.010024	8.25E-03	5.97E-03	5.99E-03	1.77E-04
Density (lb/ft^3)	0.1806	0.1487	0.1075	0.1080	0.0032
Average MW	18.02	18.02	18.02	18.02	18.02
Liq Vol 60F (ft^3/hr)	389.60	389.60	24121.42	24511.02	24511.02

relative and absolute) have been used as solver options.

6.2.2 Controller Design

After careful analysis of the previously studied single-pressure boiler operation and extending it to the current flowsheet, a simplified regulatory control layer was devised. The steam turbines are kept in a floating pressure arrangement and consequently the boiler-drum pressures are allowed to swing to avoid any valve saturation (this was one of the problems faced in the single-boiler study). Figure 6.10 shows the HRSG process flowsheet in AspenDynamics^{TM} with various regulatory layer controllers. The pressure controller on each evaporator-drum (flash vessel) is inactive and placed in 'manual' mode. The small amount of blow-down liquid exiting each drum is flow controlled to avoid any fluctuations with the drum-pressure swings.

Furthermore, each of the industrial steam/water line is flow controlled (controllers FC_65CND, FC_65Claus and FC_Ind in Figure 6.10). The pressure of the node where industrial water recycles back and mixes with the feed-water should be maintained to ensure proper recycle operation and avoid pressure buildup. This is done adjusting the feed-water flow by indirectly manipulating the pump electrical power (the use of performance curve in the pump has to be disabled to make the electrical power available for manipulation).

The drum-levels are controlled by the manipulating the inlet water flowrate. This is done by either actuating the valve on the inlet line or varying the pump-power. As was observed in previous case, pump-power as a manipulated input offers a more robust solution in cases where the drum-pressure fluctuates with load changes.

The controller responses were studied for different disturbances rejection cases. In the first case, a step decrease of 25% is made to the flue-gas flowrate (also termed the (GT) load change since the coal/fuel flowrate to the plant is determined based on the total IGCC power demand). This change is done independently of the gasifier heat-extracted/available; in addition, the industrial steam demand is kept con-

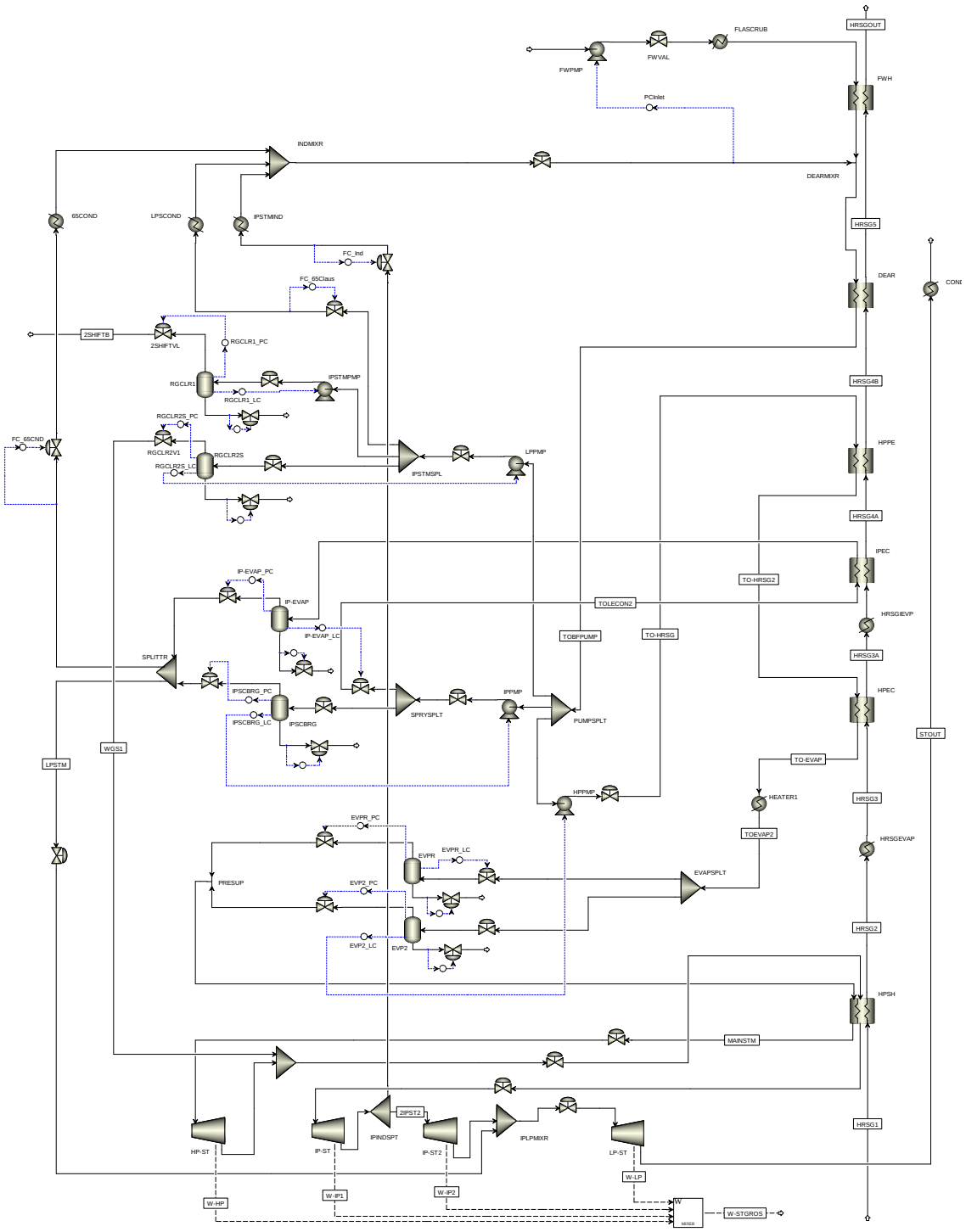

Figure 6.10: Process flowsheet showing heat recovery and steam generator operation in AspenDynamics™ with regulatory layer control installed

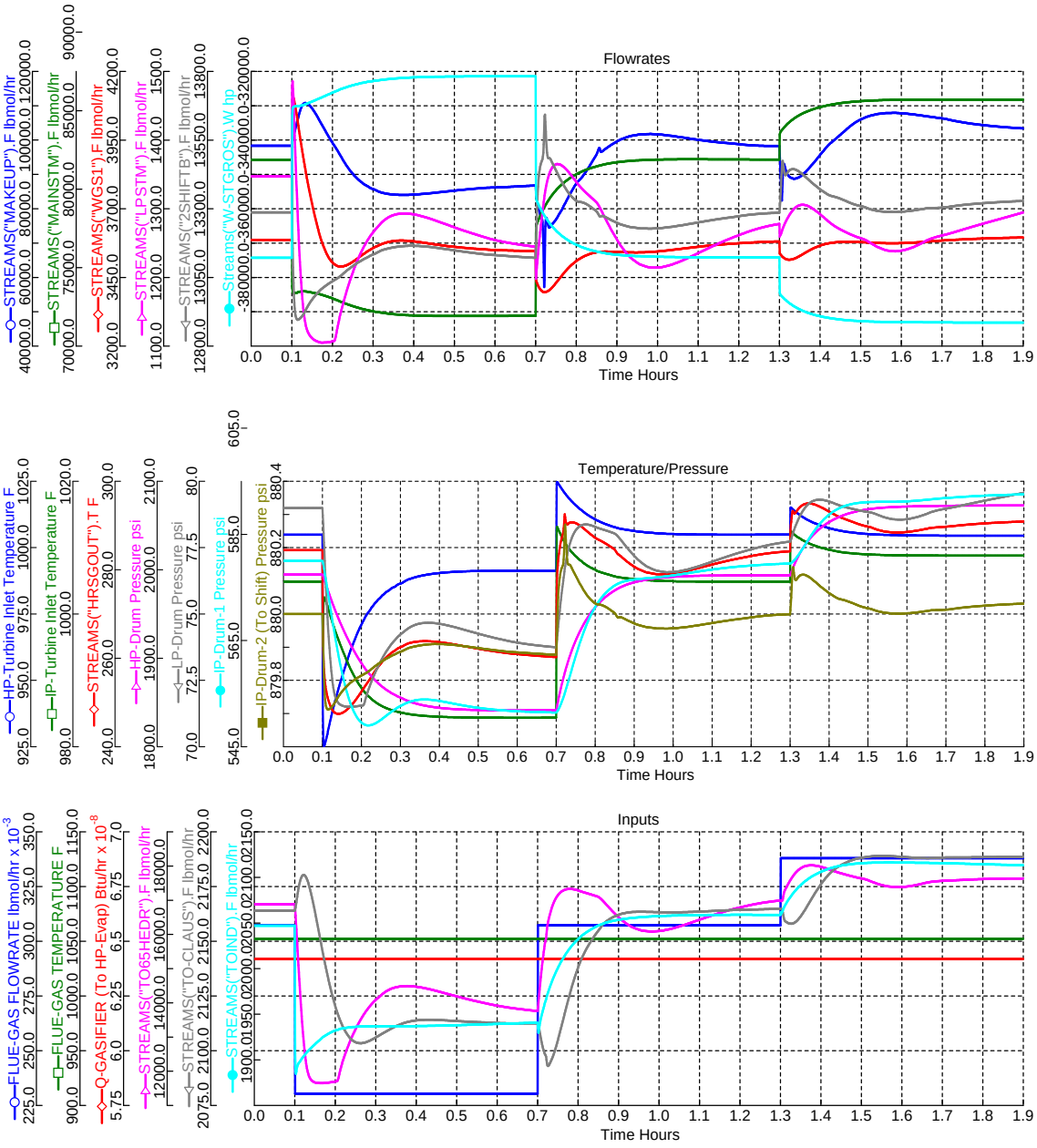

Figure 6.11: HRSG controller responses to 25% step decrease in flue-gas flowrate at 0.1 hr, returning to nominal value at 0.7 hr and stepping up 10% at 1.3 hr; (top) relevant flows, (mid) temperature/pressures and (bot) input variables

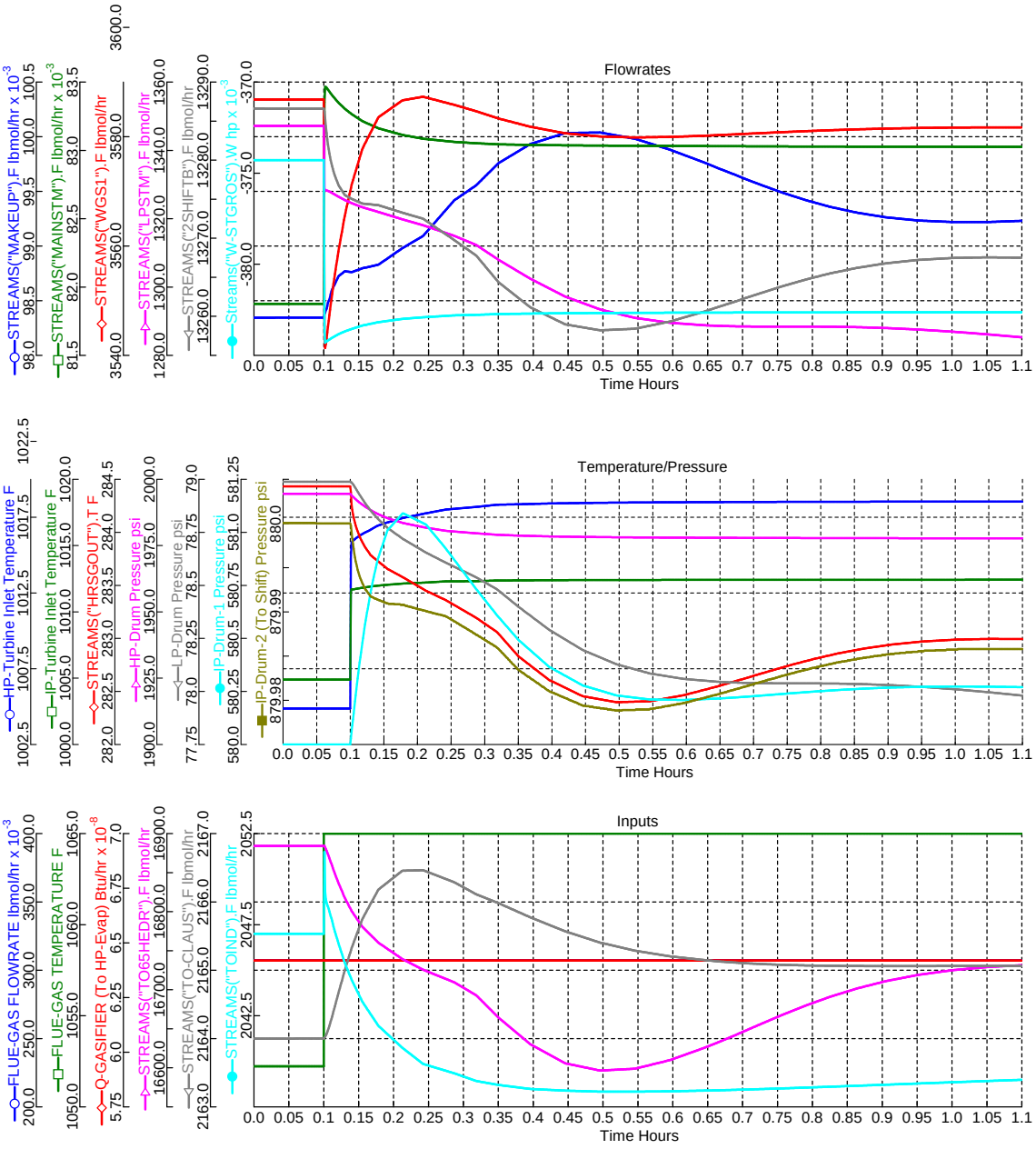

Figure 6.12: HRSG controller responses to step increase in flue-gas temperature (to 1065°F) at 0.1 hr; (top) relevant flows, (mid) temperature/pressures and (bot) input variables

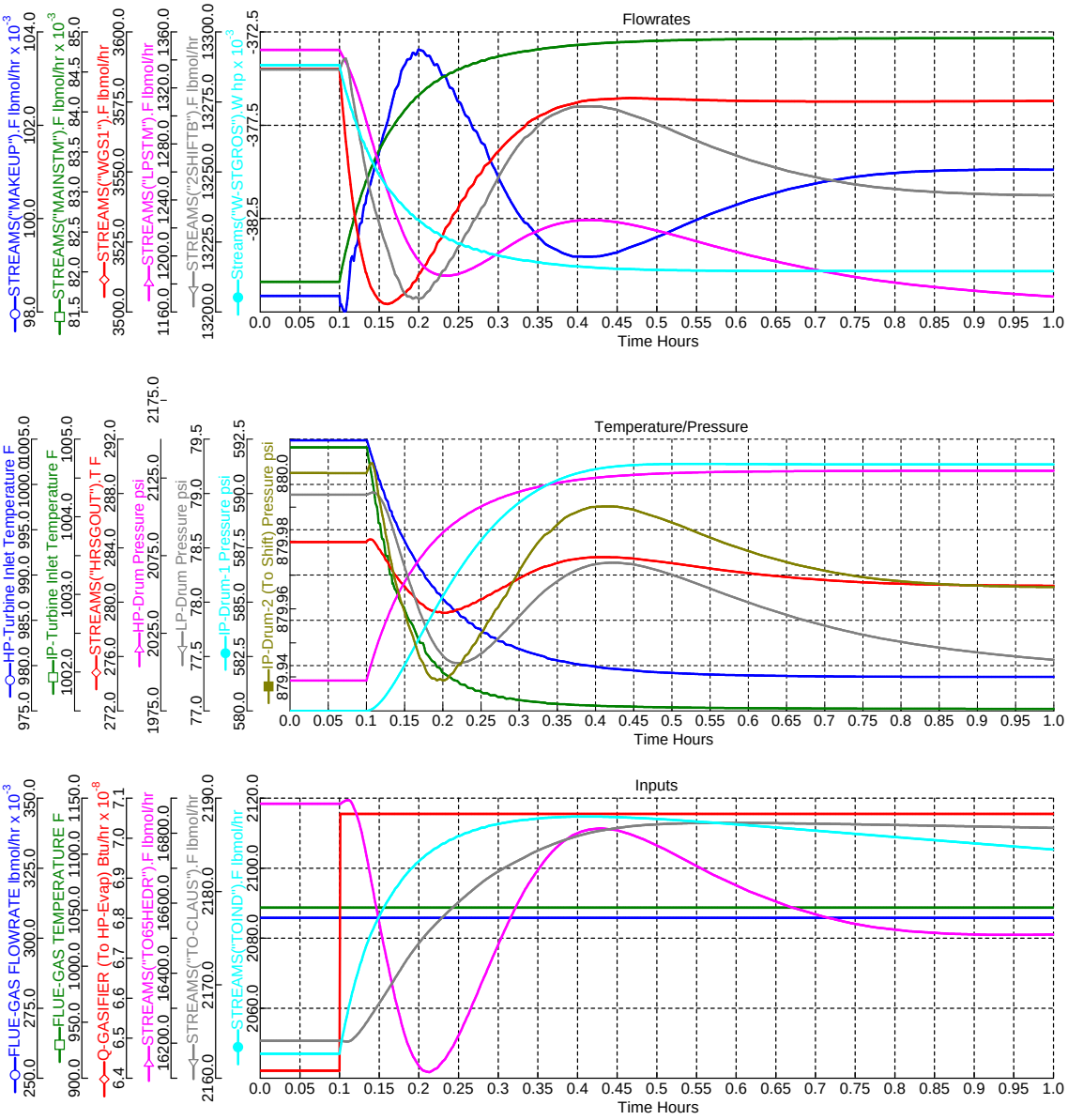

Figure 6.13: HRSG controller responses to 10% step increase in gasifier heating-rate (Q-gasifier) at 0.1 hr; (top) relevant flows, (mid) temperature/pressures and (bot) input variables

stant[48]. The responses have been shown in Figure 6.11. The HP drum-pressure decreases in a first-order fashion and reaches a new steady-state value (150 psi below nominal) in 20 min. The steam-turbine work response also shows an instantaneous jump, reaching the steady-state fairly quickly (20 min).

The industrial heating have slower dynamics and never reach the desired set-point. This is due to the pressure decrease occurring in the upstream drum, while the downstream pressure is maintain constant (PCInlet), leading to flow-control valve saturation. In case of the 65 psi header line (TO65HEDR), an alternative approach to prevent this saturation is to close the valve on the LPSTM line (part of the steam being injected to LP steam turbine) or to implement a split-range controller. During this step load decrease, both the turbine (HP and IP – 1st stage) inlet temperature remain less than the nominal value, requiring no temperature control during shut-down. During load increase (75% to 100%), the temperature bumps up to 1025°F (for ∼10 min) before reaching the full-load nominal temperature of 1000°F. This is not advisable and requires some of the boiler feed-water to be "sprayed" or mixed with the turbine-inlet stream to alleviate the temperature rise.

With step increase in flue-gas temperature shown in Figure 6.12, a fast response for mainsteam and ST-work is observed. The thermal effect on the downstream exchanger is apparent by comparing the response time of the three drum pressures, where the boiler-drum most downstream to the flue-gas (LP drum) has the slowest response. A sharp increase in turbine-inlet temperature is observed, although its adversity can be safely precluded since the GT flue-gas temperature is tightly controlled (Figure 5.9). The makeup water dynamics is sluggish, due to the slow thermal transients in the system. Next, a 10% step increase in available heat from the gasifier is provided to the HRSG while keeping the flue-gas flowrate and industrial heat demand constant (Figure 6.13). A "fast" first order response is seen in the main HP steam and the net ST-work whereas a slower, oscillatory response occurs in the industrial steam lines. Both the HP and IP steam-turbine inlet temperature decreases slightly.

[48]In principle, unless a cogeneration plant is operated, all of the heat-duties and industrial steam/water usage, in long term, swing synchronously with the demand. Here a more stringent condition is imposed, by manipulating these inputs independently.

Upon closely examining the AspenDynamics^{TM} flowsheet (Figure 6.10), it can be seen that the level for each drum corresponding to either HP and LP portions are controlled using a combination of a valve and a pump actuation. For instance, one of the HP evaporator drums (EVPR) is level controlled (EVPR_LC) using the valve immediate upstream to it, and the level for other drum (EVP2) is controlled using the HP feed-water pump (EVP2_LC). In the event of a heat-duty mismatch (for example, if the extracted gasifier-heat increases while the flue-gas flowrate remains relatively constant or decreases, which might occur in case of hydrogen co-production), the direction of the both control actions might conflict with one another, creating oscillatory responses. This phenomenon was ascertained when different values of controller tuning parameters were examined. It was also found that a non-oscillatory behavior became too sluggish and controller performance had to be sacrificed. Furthermore, if the drum corresponding to the pump actuator starts to level-up, requiring low pumping action and leading to a low pressure at the splitter-node, the valve corresponding to the other drum saturates easily. This problem can be countered by one of the following schemes:

- Using a multivariable controller scheme for drum levels, which might lead to added complexity for otherwise daunting plantwide problem
- Using two pumps, one corresponding to each drum. This eliminates the valve saturation problem.
- Modeling both the drums (which operate at the same pressure) as a single physical drum with multiple virtual heat-streams entering. This is closer to the actual physical system.

A modified HRSG design has been given in the next subsection to investigate if the above-mentioned problems can be solved by using a different control scheme.

6.2.3 Modified HRSG controller design

Figure 6.14 provides the dynamic flowsheet with the modified control structure. The two drums in the HP and LP portion of the HRSG have been combined in steady state with the total volume specified as the recalculated value using the

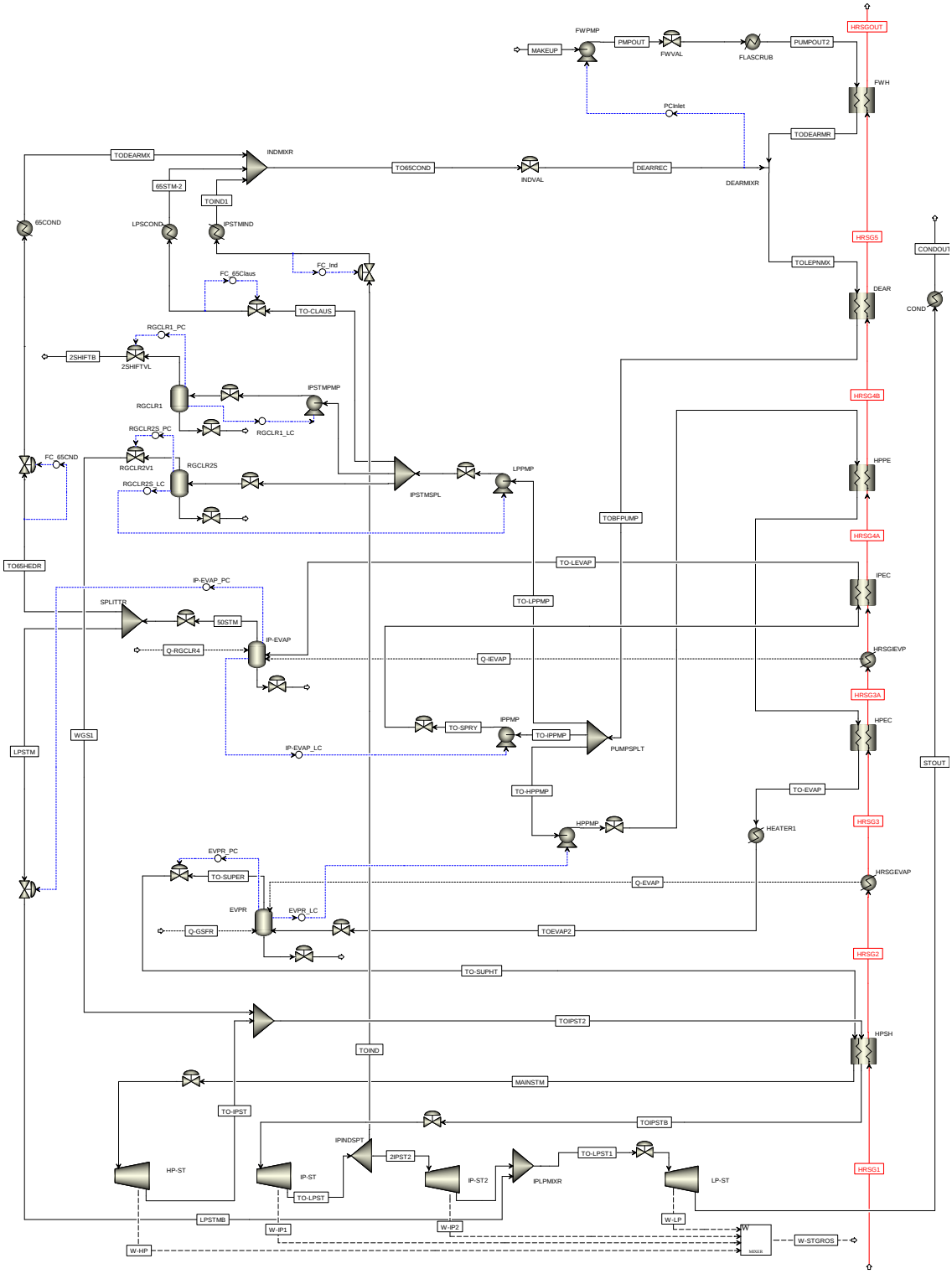

Figure 6.14: Process flowsheet showing heat recovery and steam generator (modified) operation in AspenDynamics™ with regulatory layer control installed

10 min drainage time for combined flowrate. The pressure loop was closed on each drum, using the valves on immediate downstream of the evaporator-drum. An exception to this is the LP-drum (IP-EVAP in Figure 6.14), where major part of the saturated-steam (TO65HEDR) is split and sent for industrial use, whose demand-rate is set by the flow controller, FC_65CND. If this steam is to be made available at a desired pressure, the pressure controller for LP-drum may not manipulate the valve close to the drum, i.e. the valve placed before or upstream to the splitter. Hence, the steam-turbine line (LPSTM) flowrate was used to control this pressure.

It must be realized a-priory that in an event the heat available to LP-drum decreases significantly (for instance during a shutdown), the flow of water/steam evaporating in the drum and hence the steam production decreases simultaneous. Obviously the industrial steam demand cannot exceed this production-rate; in such a case, the valve on LPSTM line will close fully followed by a pressure decrease in the drum, finally leading to valve saturation (fully open) on the TO65HEDR line.

Figure 6.15 provides the controller response for the modified HRSG design to similar disturbance in flue-gas flowrate as investigated in the earlier design (Figure 6.11). The HP and IP drum pressures (and hence the drum temperature) are maintained at nominal values. For a step decrease in flue-gas flowrate, the LP drum pressure is decreased due to the reasons mentioned earlier (note how the LPSTM flowrate drops down to zero). The transients in water circulation rate, steam turbine work generation rate and main HP-steam production rate are settled in less that 10 min showing a marked improvement to the earlier design. The downside of pressure being controlled is the presence of an initial spike in the turbine-inlet temperature during shutdown case, which is primarily due to energy hold-up in the whole process. This mandates the use of bypass spray valves from boiler-feed water for controlling the same. This has been focused in a couple of articles ([34],[42]) in which the authors use first principle CCPP models in MATLAB/Simulink – tuned to mimic a true installation in northern Italy and results of a highly detailed simulator (of the same plant).

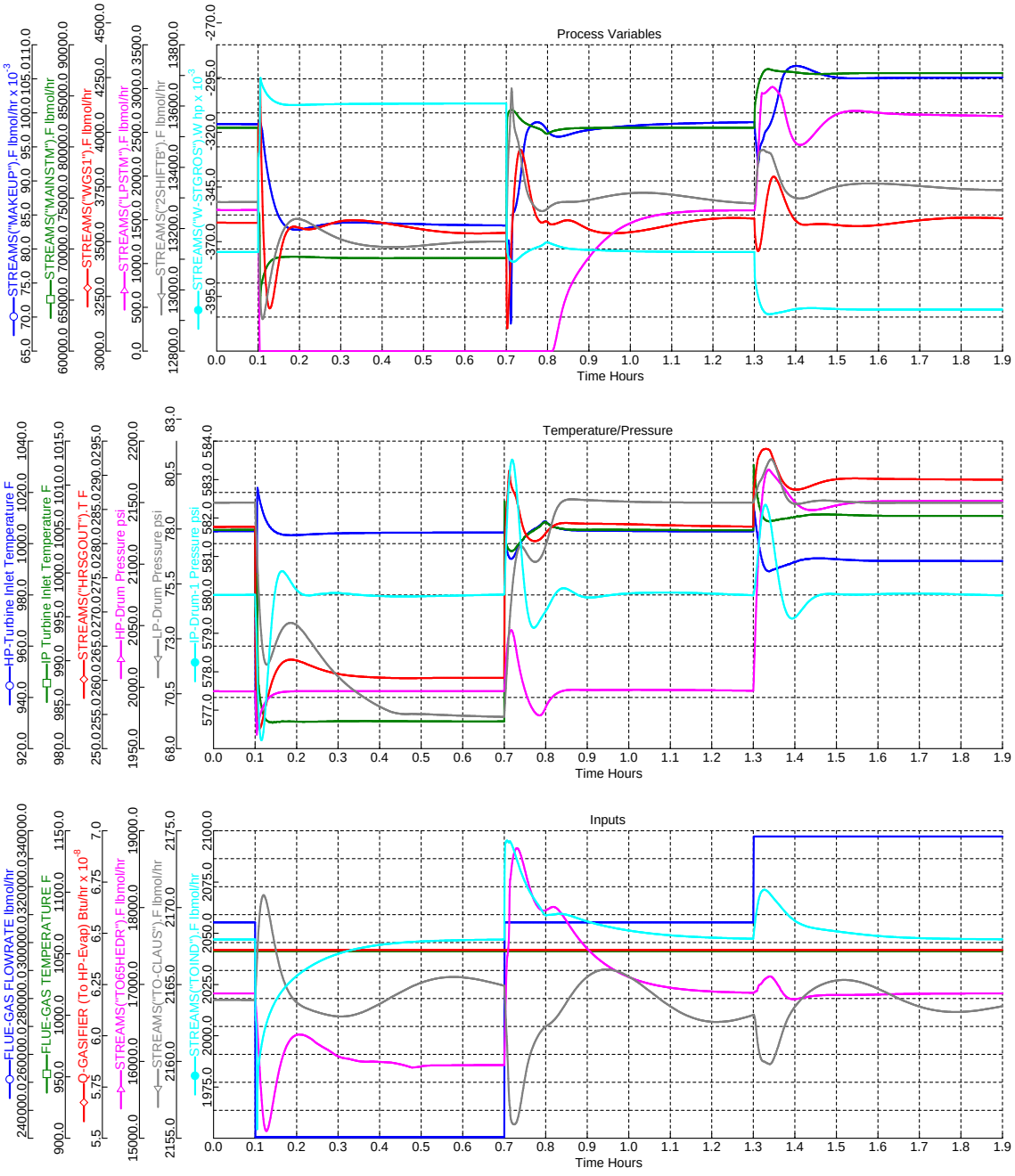

Figure 6.15: HRSG (modified) controller responses to 25% step decrease in flue-gas flowrate at 0.1 hr, returning to nominal value at 0.7 hr and stepping up 10% at 1.3 hr; (top) relevant flows, (mid) temperature/pressures and (bot) input variables

6.3 Discussion and Conclusion

In this chapter, the heat recovery steam generator (HRSG) as a part of IGCC plant is studied. Due to the flowsheet complexity involving many heat-exchangers, recycle streams, bypass streams, turbine steam extraction and injection lines etc., an understanding of the pressure dynamics as a first step is required (especially with the new AspenV7.1 turbine models). To achieve this, a rigorous pressure-driven model of a single-pressure boiler operation is designed, which includes proper temperature-dependent heat-integration specification for the boiler drum. After a close inspection of the flow, temperature and pressure dynamics involved in this subsection, various regulatory-layered control structures have been proposed and studied which might ensure maximum operational flexibility and robustness, especially with respect to load changes and flue-gas temperature disturbances. It was found that a floating-pressure boiler operation displayed better performance in terms of lower settling-time and storage/release of energy.

The concepts developed in the single-pressure boiler study is thereafter extended to a full-blown HRSG unit, with a regulatory-layered control structure placed to handle drastic fluctuations. It was found during simulations, involving the Aspen's new performance-curve based turbine models (a more realistic model), that the feed-pressure on the industrial-steam line decreased with IGCC load decrease. This precluded the possibility of any additional steam co-generation without saturating the feed-valves. In addition, the presence of separate evaporator-drum corresponding to each (major) heat-source led to oscillations due to conflicting pump/valve actuations. An improved controller design based on fixed drum-pressure is proposed and implemented after identifying these limitations; the resultant responses show improved performance and faster settling time.

CHAPTER 7
PLANTWIDE CONTROLLER DESIGN

In this chapter, we initially focus on modeling the entire plant, especially the dynamically "faster" process units, and building section-wide regulatory and supervisory layered controller around it, similar to the ASU section in previous chapters. The later part of the chapter focuses on proposing and designing two plantwide control design for the main power-loop (Gasifier–GT–ASU) in IGCC plants. This chapter of the report is based on the paper presented in [108].

7.1 Plantwide Dynamic Model

For studying the operability and controllability of the plant configuration and to develop an efficient control strategy, a plant-wide dynamic model is required. This plantwide control study involves major power-cycle subsections: the gasification island which includes the gasifier, RSC, WGS, water quench; gas-turbine section (which includes the gas-turbines, combustor, compressor (mounted on a common shaft with turbine), inlet guide valves (IGV) to vary flowrate of air; and the ASU (partially integrated with gas-compressor). These three subsections are subjected high material transfer swings during varying load conditions and disturbances (coal quality, ambient air temperature etc.). A semi-rigorous pressure driven Aspen Dynamic model for each of these plant subunit blocks as well as for the combined plant have been developed as focused in detail in the previous chapters. Here we merge all these process sub-units into a single flowsheet. Figure 7.1 shows this flowsheet as it appears in AspenPlus^{TM}.

7.2 Plantwide Regulatory Control Layer

The oxygen flowrate is regulated by actuating the oxygen compressor brake power or suction side pressure. The setpoint to this controller is given at a fixed ratio (provided by the higher layer) to the coal flowrate. This arrangement proves advantageous in cases where there is substantial feedback signal time-delay. A sim-

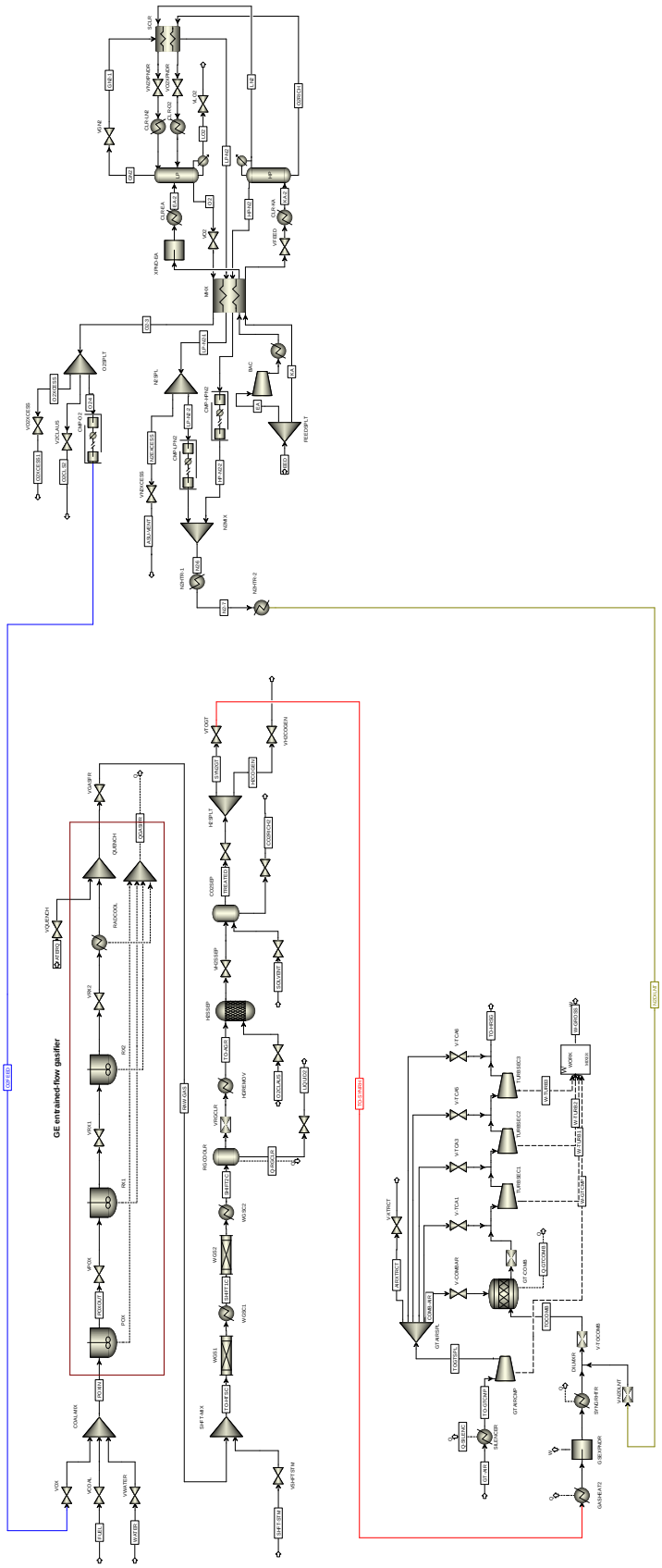

Figure 7.1: Process flowsheet showing ASU-GT-Gasifier subunits in AspenPlus™

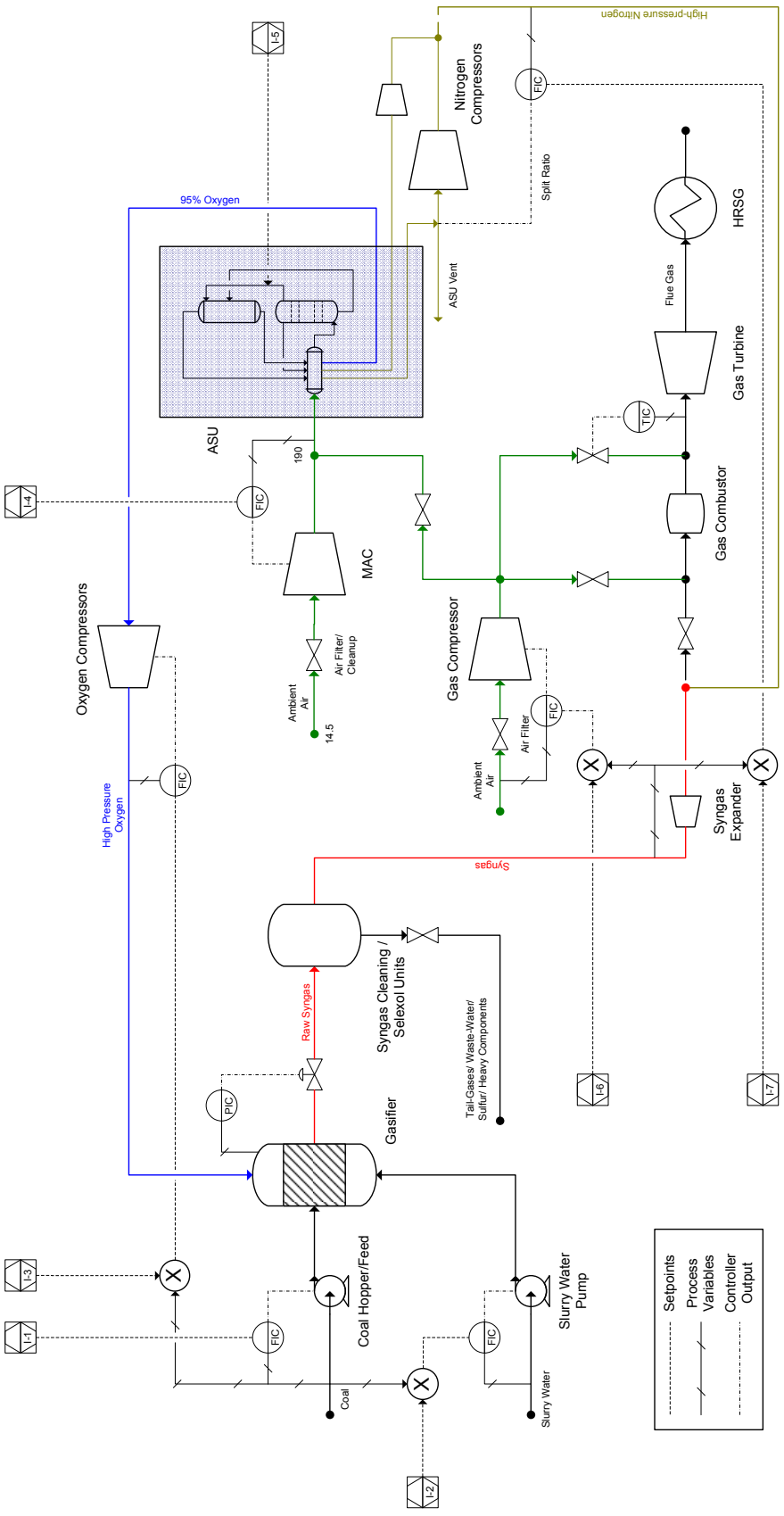

Figure 7.2: Simplified IGCC process flowsheet with regulatory layer control installed. Note: Detailed regulatory-layer control design within each subsection (relevant ones) have been discussed earlier.

ilar kind of ratio control is implemented for most of the other controllers including slurry water feedrate (ratioed to coal flowrate), GT-air and diluent N_2 flowrate (both ratioed to syngas flowrate). The flowrate of each of these streams is controlled by using valves, compressors or other pressure changers.

For controlling the nitrogen stream (which is required depending on how much of HP nitrogen we want to inject to the gas turbine), we can vent out some of the nitrogen as ASU waste stream and this gives the split ratio of the vented nitrogen to the injected nitrogen as an available manipulated variable. This control architecture is shown in Figure 7.2[49]. At the lowest hierarchy are the inventory level controllers which are not shown in the figure. The process instrumentation block shown by 

, denotes the main computer which sends setpoint signals to relevant controllers which have been shown. These controller effect plantwide flows/ net energy outputs etc. and serve as the overall inputs for any higher supervisory layer controller. Here, these values will be used as manipulated variables for the plantwide decentralized and centralized MPC design.

7.3 Plantwide Decentralized MPC Design

In a decentralized controller design each individual sub-section has its own controller/MPC structure which pass setpoint (but not state) information among each other. Once a setpoint signal is obtained from another subsection, the controller tries to meet the setpoint by measuring/estimating states and manipulating input variables (which might have a cascaded lower level controller to meet this manipulation demand) within the subsections. Due to this reason, simplified linear step response models has been used for developing the controllers in this study. In general, these responses can be fitted to a first order (with some numerator dynamics) or, at best without loss of simplification, second-order dynamics. An additive output disturbance assumption (similar to dynamic matrix control) in appended-state Kalman Filter formulation is utilized in the linear MPC study for individual

[49]A simplified version of flowsheet (for brevity sake) with relevant inputs/outputs has been shown. The Aspen Dynamics flowsheet has not been shown here as the number of process units and controller blocks if fitted onto one page renders each of these units visible as tiny dots, which make their identification and determination of flowsheet connectivity practically impossible

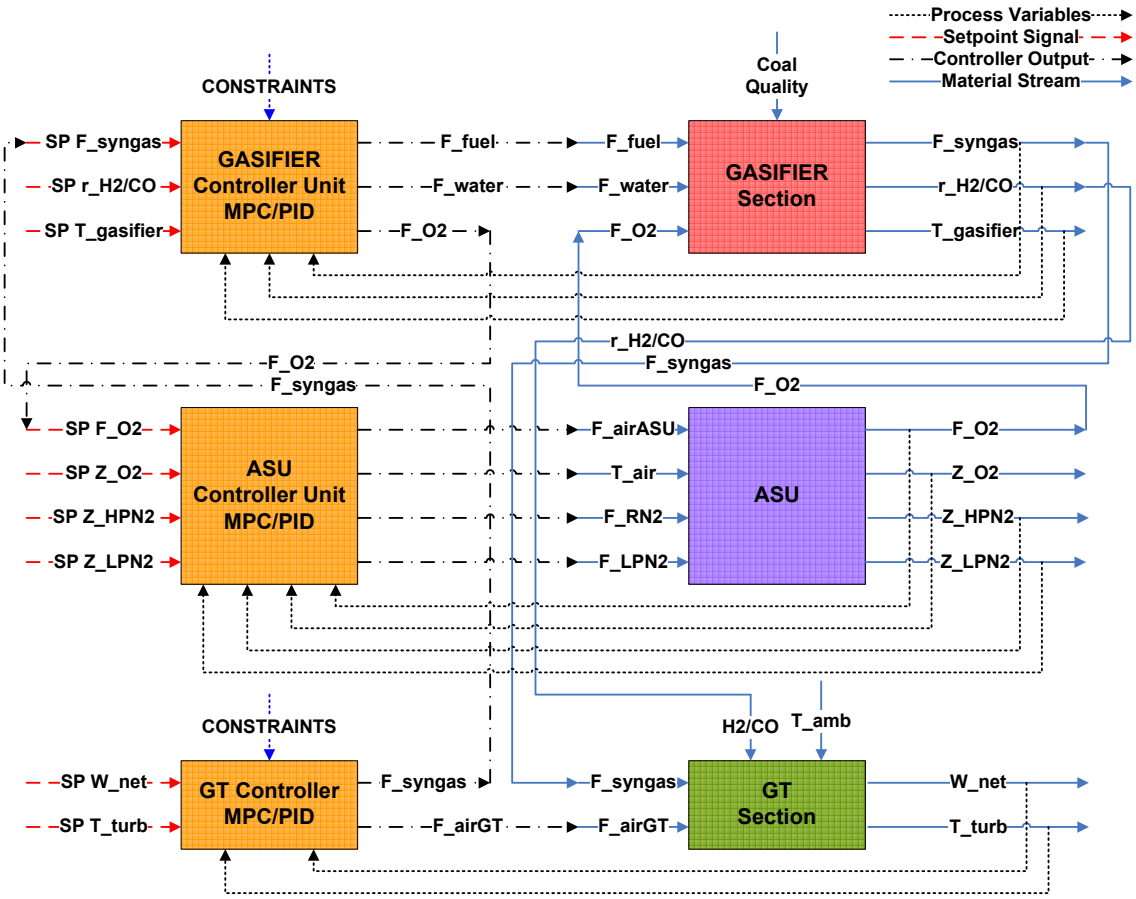

Figure 7.3: Block diagram showing decentralized controller design

subsections. Figure 7.3 shows the plantwide decentralized controller block diagram (for primary control inputs/outputs) used in this study.

7.4 Plantwide Centralized MPC Design

Moving from decentralized to centralized design

In a centralized controller design, we measure and control all the relevant inputs/outputs spanning across all subsections through a single centralized controller. Most of the measurements and states which were used by the decentralized controller within a subsection are now made available to the central computer/controller (Figure 7.5). With respect to current plantwide applicability of centralized control on entire IGCC plant, we must determine what is needed to control. What loops should be left for the secondary/inventory controllers to handle? When we move

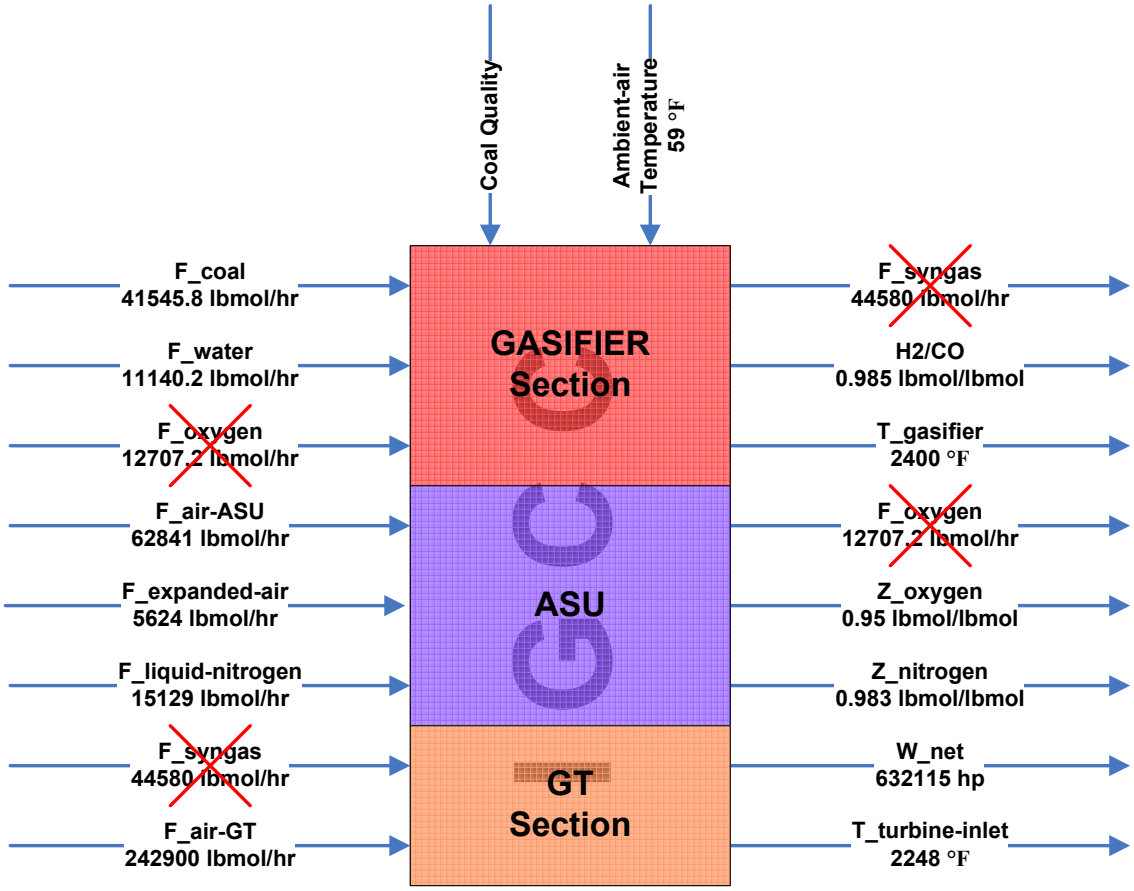

Figure 7.4: Block diagram for (de)centralized MPC showing subsections and nominal values

to centralized design, we eliminate the setpoint signals which were passed from one subsection to another (see Figure 7.5) and consider the overall inputs/outputs (and not the intermediate stream values); these values are used as measured disturbances for improving/stabilizing the controller performance in a feed-forward fasion. At present, step response models (similar to decentralized case), imported directly from AspenDynamics^{TM} have been used to estimate linear parametric state-space models. Since first-principle models have not been used in this study, we only control the state associated with the measured output (including the intermediate streams). Hence, an additive output disturbance assumption, similar to dynamic matrix control, in an appended-state formulation is utilized in the linear MPC study. It is worth mentioning that the open loop response is stable for each input-output pair showing effective control at secondary level.

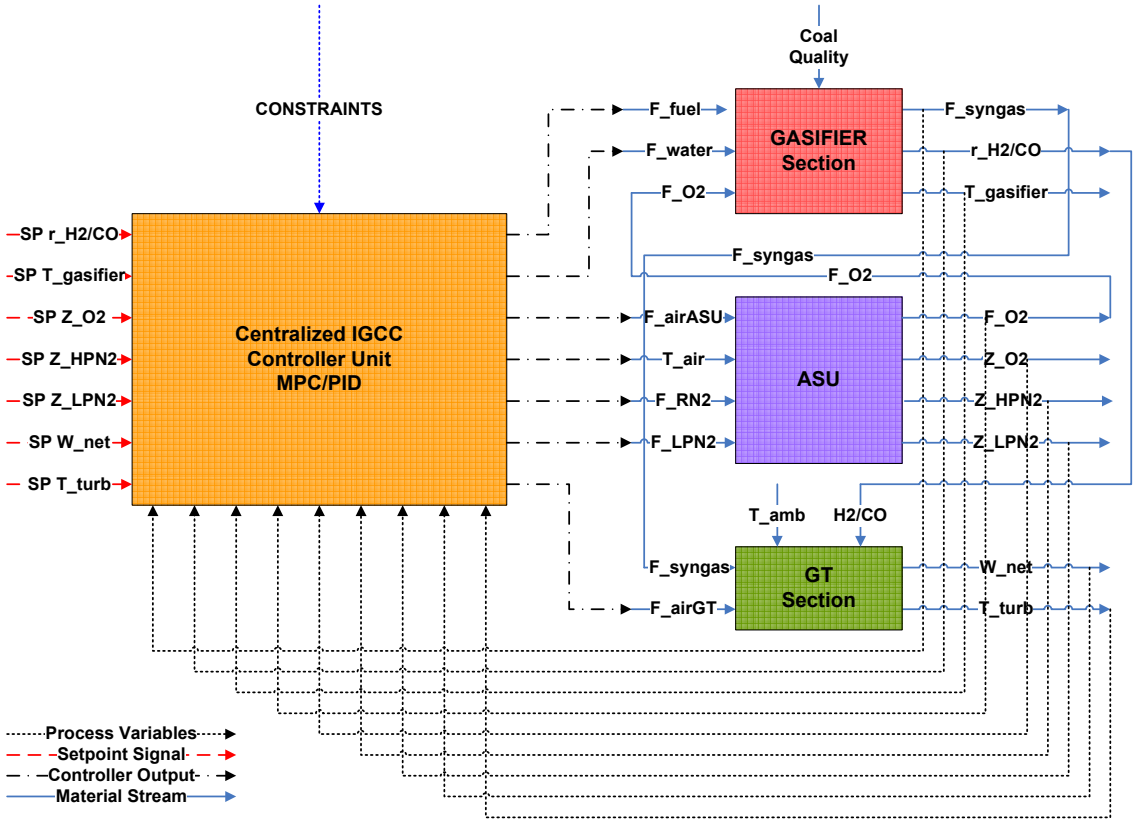

Figure 7.5: Block diagram showing centralized controller design

7.5 Simulation Results

A comparison between decentralized and centralized controller responses have been shown in Figure 7.6 for a 20% step decrease in the net GT output work setpoint (W_net). The centralized controller, reaches the new setpoint value in a much smoother fashion, especially with the gasifier and GT control variables. It is interesting to note that the ASU output stream purities, behave more aggressively for the centralized case. This shows that implementing a local subsection control for ASU might be more effective and can be moved to a more lower level heirarchy. The controller also performs adequately within the absolute and rate of change input-output constraints.

Another set of simulation (Figure 7.7) shows comparison between the two control strategies for 10% step increase in H/C ratio of coal (perturbation in coal quality). We again see a smoother response in case of the centralized controller for gasifier and GT control variables, compared to the ASU variables.

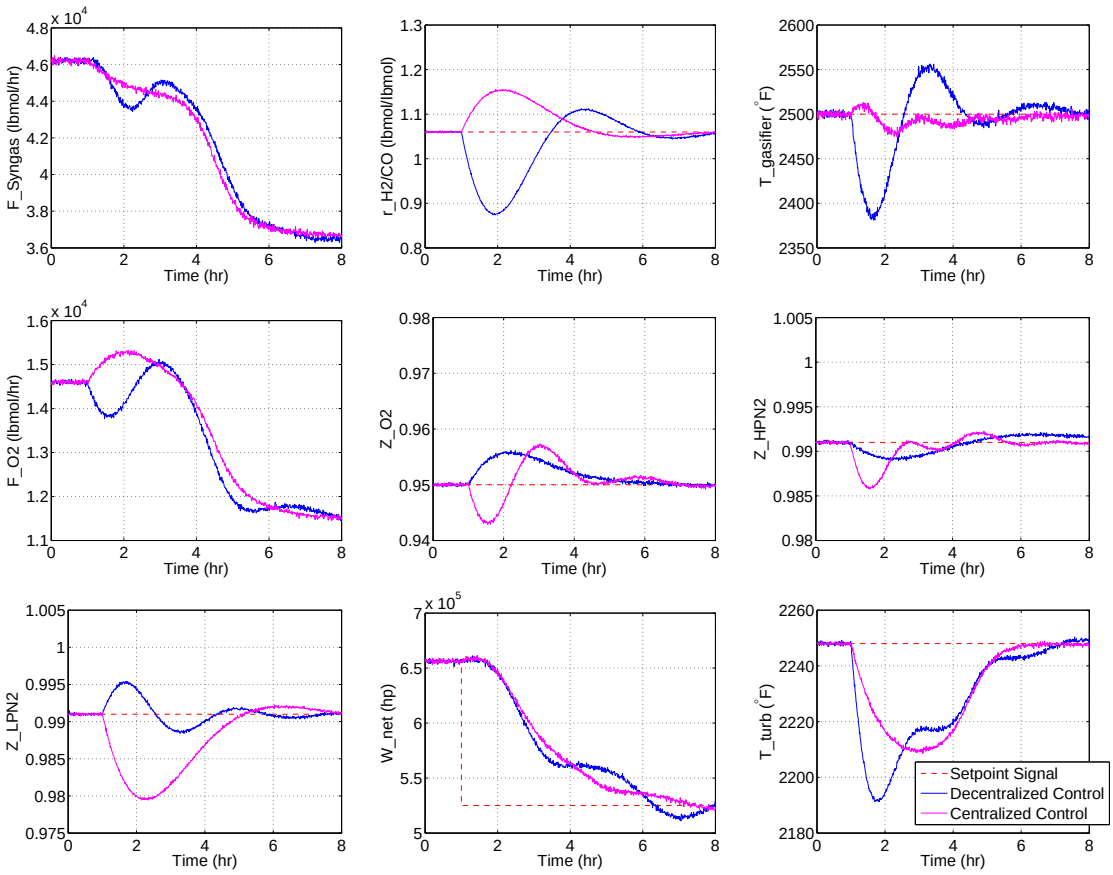

Figure 7.6: Simulation results showing decentralized and centralized controller responses (outputs only) for 20% step load decrease

The computational time is increased by approximately 1.5 times as compared to decentralized design. This limitation is on the MATLAB end and largely due to large number of states (34) involved when the transfer functions are converted to the corresponding state-space form. As stated earlier, the delay due to transfer of data from MATLAB to Aspen and vice versa, at every integration step (instead of each time-step), is the main bottleneck. As the responses become increasingly steeper, Aspen cuts down the integration steps, causing more number of integration performed (and hence increased data transfer) within a certain time step causing additional delays. The simulation results shown later consumed 15 hrs on a personal computer with 2.4 GHz Intel Core 2 Duo processor.

As discussed earlier, the ASU internal flows/compression work are responsible for controlling the ASU purities more effectively and the input variables do not have

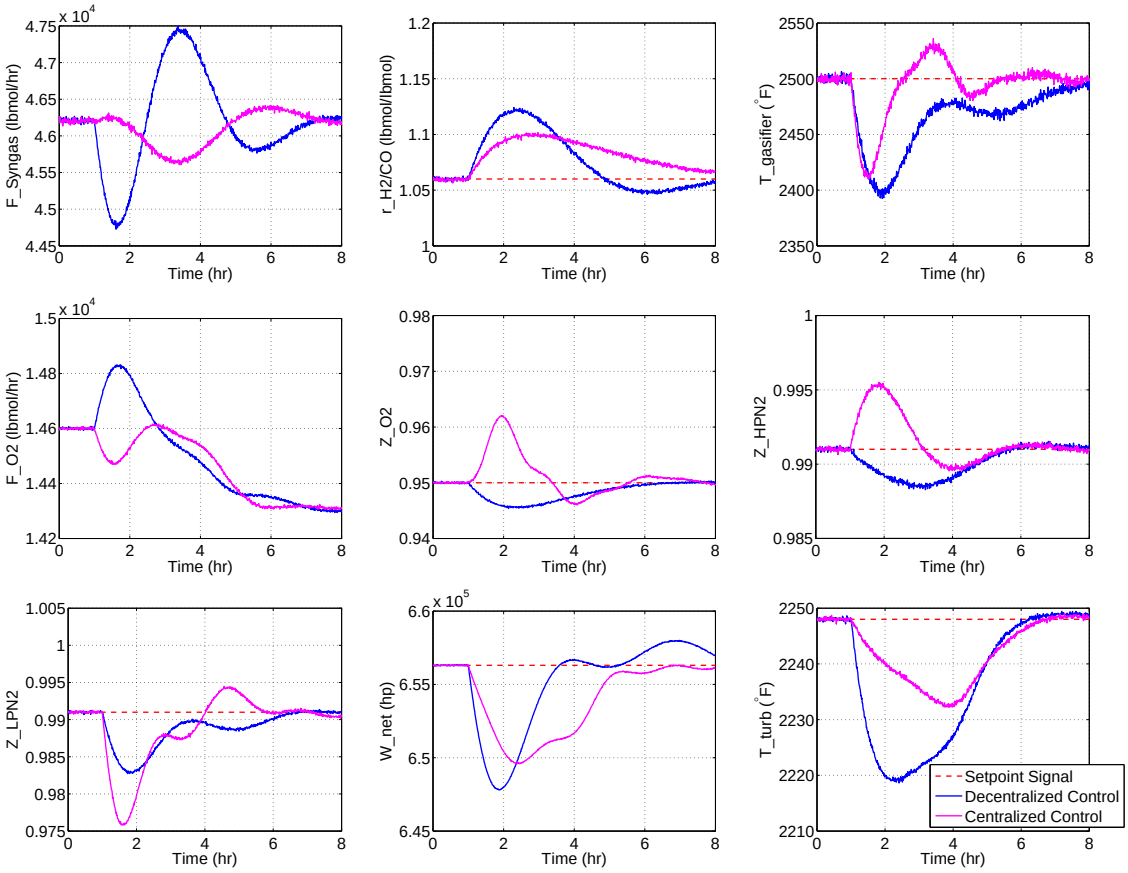

Figure 7.7: Simulation results showing decentralized and centralized controller responses (outputs only) for 10% step H/C ratio increase in coal

significant effect on remaining plant outputs, which is what is expected. An obvious question arises: why do we care to incorporate ASU purity control in the centralized design when most of the other inputs outside ASU do not have much effect on these variables? In addition, the manipulated variables internal to ASU, do not affect output of variables outside ASU.

7.6 Discussion and Conclusion

Clearly this is a highly nonlinear, multivariable process requiring very accurate process model. The absence of immediate syngas flowrate and oxygen flowrate control could introduce significant process delays and rapid mass flow fluctuations, unless these measurements are used for updating the states. The advantage of using

this architecture is that the complete plant model would be incorporated in the controller. Hence depending on how well developed the MPC algorithm is; it can take care of multi-rate and multiple time-scale scenarios. These cases will certainly occur here as we see the control variables vary from fast responding turbine inlet temperature to slow dynamics of oxygen/nitrogen product compositions. Developing an accurate model at present is not feasible given the intrinsic complex of the flowsheet. Another issue that should be considered is the range of manipulated inputs. These ranges do not remain similar to single-input step response ranges when we start making simultaneous changes to the inputs leading to many numerical integration problems reported by Aspen. Hence for this 7-input 7-output problem we have to span a 7-D space of possible input combination which is extremely difficult. In addition, rate of input changes/ input direction is also important. For instance, if we change flowrate of recycled nitrogen, F_RN2, by stepping down 10% (keeping other inputs unchanged), Aspen reports an "integration failure" message within a few integration steps; whereas making a ramp decrease of 0.5% every 15 seconds upto a final value of 10% change does not report any error. This problem is greatly amplified, when we perturb multiple inputs simultaneously. One of the limitations of this analysis is that the sample-time of all the units have been taken as 0.1 hrs. This acts as a major bottleneck for fast-dynamic subunits such as gasifier and gas-turbine. As a scope of future research, multisample and multirate control architecture may be studied within the framework of single centralized design, where sampling frequency of measured data for fast-dynamic sub-units will be higher, and will update the corresponding state information.

CHAPTER 8
OPERABILITY ANALYSIS

In this chapter, an operability analysis study has been done on individual sub-units of the NETL IGCC (Parson's) Case#1 flowsheet. Each of these sub-units is directly or indirectly correlated to other sub-units of the flowsheet through material and energy streams and various AspenPlus^{TM} flowsheeting options such as 'Design Specs' and 'Calculators'. The following sections show analysis of relevant sub-units and in-depth operability studies.

8.1 Gasifier Subsection

This subsection has three input streams (material) and one output stream which are listed below. Figure 8.1 shows the gasifier sub-unit separated from the entire flowsheet.

Input Stream	**Description/Specifications**
WET-COAL	Wet coal feed given to plant, T = 60°F, P = 14.4 psi, Total flowrate = 489690 lb/hr
SLRY-WATER	Slurry water feed to be mixed with coal, T = 60°F, P = 14.7 psi, Total flowrate = 201165 lb/hr
OXIDANT	95% oxygen supplied from the ASU, T = 90°F, P = 125 psi, Total flowrate = 409900 lb/hr
Output Stream	**Description/Specifications**
PRODUCTS	Raw Syngas products from gasifier, T = 2400°F, P = 814.7 psi, Total flowrate = 1100755 lb/hr

In addition, following design-specifications were inherently provided as flowsheeting options in the original flowsheet

- Total flowrate of WET-COAL is varied such that gross power generated from the gas-turbines (after complete flowsheet simulation) equals 631710 hp.
- Total flowrate of SLRY-WATER is made equal to 41.08% of total flowrate of WET-COAL

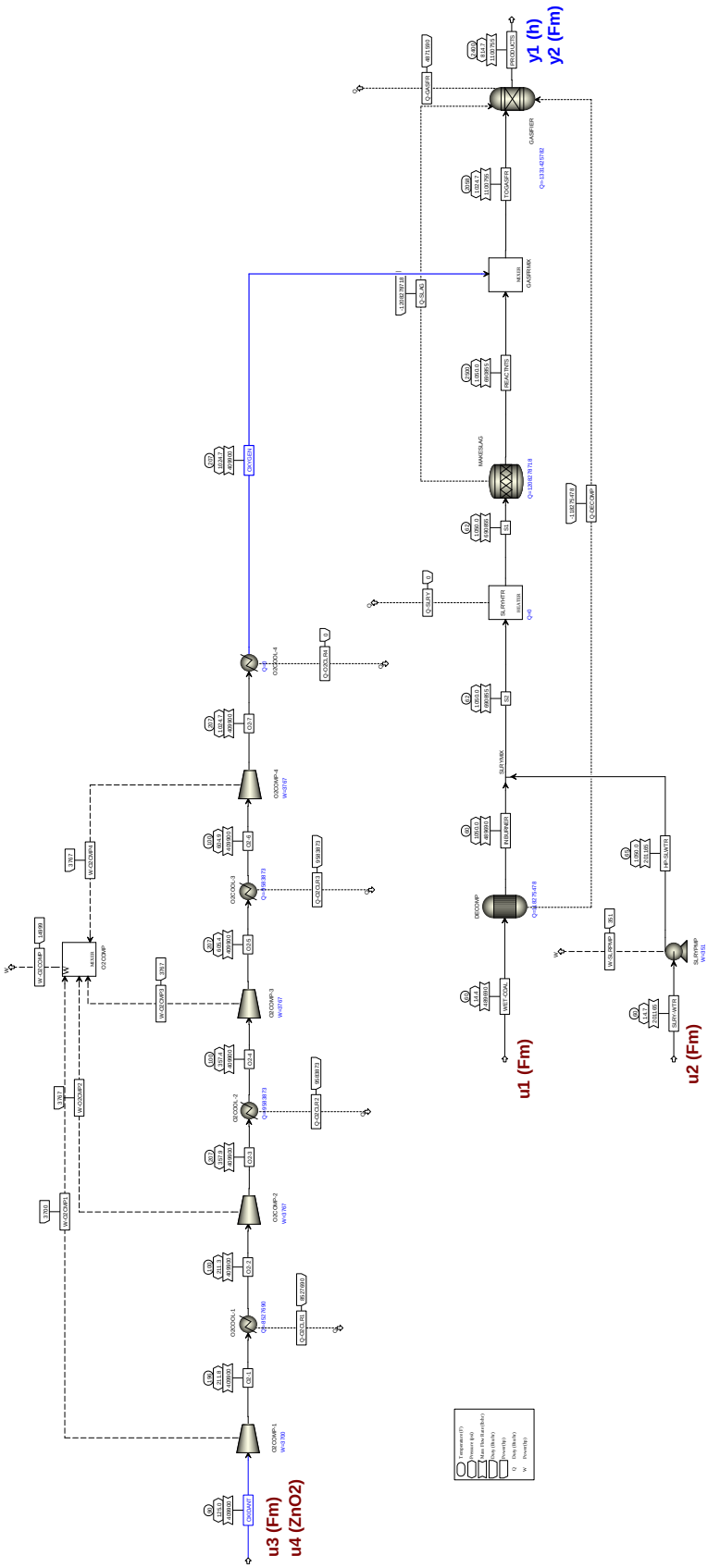

Figure 8.1: AspenPlus flowsheet of gasifier sub-section (separated from complete Parson's IGCC NETL flowsheet) with control input/output variables shown

- Total flowrate of OXIDANT is made equal to 83.706% of total flowrate of WET-COAL

All these design-specs were deactivated in the separated flow-sheet and inputs were made equal to the final values of integrated-flowsheet steady-state simulation. It was made sure that results from both flowsheets were consistent. The following input-output variables were chosen for operability and control studies

Input	**Description/Nominal-Value/Range**
u_1	Total mass flowrate of coal feed (WET-COAL, NC substream), 489690 lb/hr, ±20%
u_2	Total mass flowrate of slurry water feed (SLRY-WATER), 201165 lb/hr, ±20%
u_3	Total mass flowrate of oxygen supplied from ASU (OXIDANT), 409900 lb/hr, ±20%
u_4	Mole fraction of oxygen in OXIDANT stream, disturbance input, 0.95, 0.93 to 0.97
Output	**Description/Nominal-Value/Range**
y_1	Enthalpy of gases in gasifier-product stream (PRODUCTS), -1810 Btu/lb, ±20%
y_2	Mass flowrate of gases in gasifier-product stream (PRODUCTS), 1047000 lb/hr, ±20%

Step changes of ±1% in flowrates and ±0.01 in mole fraction input variables were made and changes in output variables were noted to obtain the following gain matrix.

$$K = \begin{bmatrix} 0.0046\frac{\text{Btu-hr}}{\text{lb}^2} & -0.0028\frac{\text{Btu-hr}}{\text{lb}^2} & -0.0041\frac{\text{Btu-hr}}{\text{lb}^2} & -2422\frac{\text{Btu}}{\text{hr}} \\ 0.89 & 1 & 1 & 0\frac{\text{Btu}}{\text{hr}} \end{bmatrix} \tag{8.1}$$

Following shows the scaled gain matrix and its singular value decomposition

$$K_{scaled} = \begin{bmatrix} 1.2441 & -0.3125 & -0.9312 & -0.1338 \\ 0.4164 & 0.1921 & 0.3915 & 0 \end{bmatrix} =$$

$$\underbrace{\begin{bmatrix} -0.9991 & -0.0430 \\ -0.0430 & 0.9991 \end{bmatrix}}_{\text{left singular vector matrix}} \underbrace{\begin{bmatrix} 1.5920 & 0 & 0 & 0 \\ 0 & 0.5996 & 0 & 0 \end{bmatrix}}_{\text{singular value matrix}} \underbrace{\begin{bmatrix} -0.7920 & 0.6046 & 0.0578 & 0.0625 \\ 0.1909 & 0.3425 & -0.9188 & -0.0443 \\ 0.5738 & 0.7191 & 0.3895 & -0.0448 \\ 0.0840 & 0.0096 & -0.0270 & 0.9961 \end{bmatrix}}_{\text{right singular vector matrix}} \tag{8.2}$$

The condition number 2.6551 shows that this is not an ill-conditioned system. The first column of left singular vector matrix indicates that the most sensitive output direction is a change in gasifier-product-stream enthalpy (y_1). The first column of the right singular vector matrix indicates that the strongest input direction is to simultaneously change slurry water flowrate (u_2), oxidant flowrate (u_3) by three times and coal flowrate (u_1) by four times (approx.) but in opposite direction.

For controlling the output variables, we must choose two manipulated inputs. Among the four input variables, mole fraction of oxygen in OXIDANT stream (u_4) is a disturbance input and coal feed flowrate (u_1) should be used to control the plant's gross power generated. This leaves us with two manipulated input. The gain matrix and RGA matrix for the remaining two inputs and outputs variables are shown below

$$K = \begin{bmatrix} -0.0028 \frac{\text{Btu-hr}}{\text{lb}^2} & -0.0041 \frac{\text{Btu-hr}}{\text{lb}^2} \\ 1 & 1 \end{bmatrix} \tag{8.3}$$

$$\Lambda = \begin{bmatrix} -2.1626 & \underline{3.1626} \\ \underline{3.1626} & -2.1626 \end{bmatrix} \tag{8.4}$$

This shows that u_3-y_1 and u_2-y_2 pairing should be used, i.e., gasifier product enthalpy should be controlled by varying oxidant flowrate and gasifier-product amount should be controlled by varying slurry-water flowrate.

$$K_{scaled} = \begin{bmatrix} \text{-}0.3125 & \text{-}0.9312 \\ 0.1921 & 0.3915 \end{bmatrix}$$

$$= \underbrace{\begin{bmatrix} \text{-}0.9149 & 0.4038 \\ 0.4038 & 0.9149 \end{bmatrix}}_{\text{left singular vector matrix}} \underbrace{\begin{bmatrix} 1.0734 & 0 \\ 0 & 0.0527 \end{bmatrix}}_{\text{singular value matrix}} \underbrace{\begin{bmatrix} 0.3386 & 0.9409 \\ 0.9409 & \text{-}0.3386 \end{bmatrix}}_{\text{right singular vector matrix}} \tag{8.5}$$

Singular value analysis shows that the condition number has increased 20.3673, which means that the system is slightly difficult to control as compared to when coal stream was available as manipulated input. Also the most sensitive output direction is a change in product flowrate and a simultaneous change (opposite direction) in product enthalpy by ∼2 times. The strongest input direction is to change slurry-water flowrate and oxidant flowrate (by 3 times magnitude) in same direction.

8.2 Gas-Turbine/Compressor Subsection

This subsection has four input streams and three output streams (two material and one energy) which are listed below. Figure 8.2 shows the gas-turbine/compressor subsection separated from the entire flowsheet.

Input Stream	**Description/Specifications**
TO-SYNRH	Syngas (after cleaning) as fuel feed to gas turbine combustor, T = 343.55°F, P = 700 psi, Flowrate = 953260.6 lb/hr
GT-AIR	Ambient air to main air compressor (MAC), T = 59°F, P = 14.696 psi, Flowrate = 7065198.2 lb/hr
N2DILNT	N_2 from ASU to be injected as gas-turbine diluent, T = 385°F, P = 460 psi, Flowrate = 795682.1 lb/hr
SNGHP	Intermediate stream from gas-cleaning section, T = 150.64°F, P = 460 psi, Flowrate = 135823.2 lb/hr
Output Stream	**Description/Specifications**
TO-HRSG	Combusted flue-gas products to heat recovery, T = 1116.1°F, P = 15.23 psi, Flowrate = 8663904.15 lb/hr
AIRXTRCT	Compressed air from MAC to ASU, T = 798.64°F, P = 262.58 psi, Flowrate = 286060 lb/hr
W-GROSS	[Energy stream] Gross power generated, -631627.59 hp

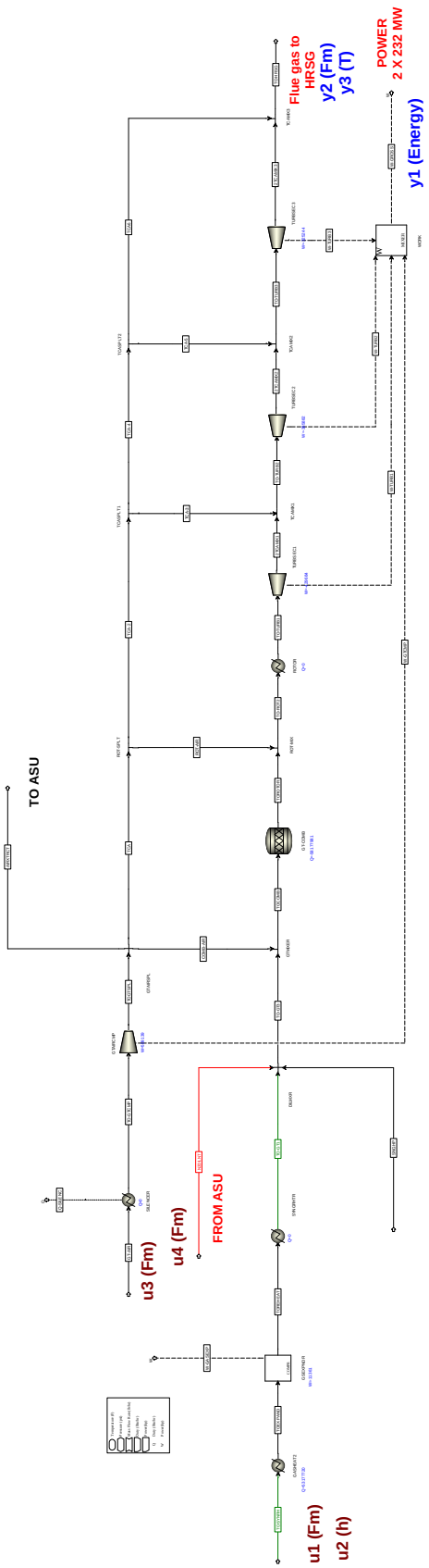

Figure 8.2: AspenPlus flowsheet of gas-turbine sub-section (separated from complete Parson's IGCC NETL flowsheet) with control input/output variables shown

In addition, following design-specifications were inherently provided as flow-sheeting options in the original flowsheet

- GT-COMB (gas turbine combustion reactor) temperature is varied such that heat loss in the reactor is 1.5% enthalpy value (Btu/hr) of syngas stream entering the reactor
- Split-fraction of bypass air to GT-COMB is varied such that temperature of turbine-feed = 2450°F
- N2DILNT mass flowrate varied such that (321 Zn(CO) + 275 Zn(H_2) + 911 Zn(CH_4)) in GT-COMB feed = 128
- GT-AIR mass flowrate varied such that temperature of flue gas (TO-HRSG) = 1116°F

The first two design-specs are essential and pertain to equipment design requirement (heat loss of reactor, temperature of turbine feed). The other two design-specs were deactivated in the separated flow-sheet and inputs were made equal to the final values of integrated-flowsheet steady-state simulation. It was made sure that results of both flowsheets were consistent. The following input-output variables were chosen for operability and control studies

Input	**Description/Nominal-Value/Range**
u_1	Mass flowrate of syngas (TO-SYNRH), 953260.619 lb/hr, ±20%
u_2	Enthalpy of TO-SYNRH stream, -2715.9505 lb/hr, ±20%
u_3	Mass flowrate of ambient air to MAC (GT-AIR), 7065198.24 lb/hr, ±20%
u_4	Mass flowrate of diluent N2 from ASU (N2DILNT), 795682.114 lb/hr, ±20%
Output	**Description/Nominal-Value/Range**
y_1	Gross power generated, -631627.59 hp, ±20%
y_2	Mass flowrate of flue-gas (TO-HRSG), 8663904.15 lb/hr, ±20%
y_3	Temperature of TO-HRSG stream, 1116.1F, ±10%

Step changes of ±1% in input flowrates and enthalpy were made and changes in output variables were noted to obtain the following gain matrix.

$$K = \begin{bmatrix} -0.883\ \frac{\text{hp}}{\text{lb/hr}} & -1149\ \frac{\text{hp}}{\text{Btu/lb}} & 0.034\ \frac{\text{hp}}{\text{lb/hr}} & -0.0115\ \frac{\text{hp}}{\text{lb/hr}} \\ 1 & 0\ \frac{\text{lb/hr}}{\text{Btu/lb}} & 1 & 1 \\ 0.0006\ \frac{^\circ\text{F}}{\text{lb/hr}} & 0.867\ \frac{^\circ\text{F}}{\text{Btu/lb}} & -7.3 \times 10^{-5}\ \frac{^\circ\text{F}}{\text{lb/hr}} & -8.9 \times 10^{-5}\ \frac{^\circ\text{F}}{\text{lb/hr}} \end{bmatrix} \tag{8.6}$$

Following shows the scaled gain matrix and its singular value decomposition

$$\begin{aligned} K_{scaled} &= \begin{bmatrix} \text{-1.3332} & \text{-4.9408} & 0.3817 & \text{-0.0145} \\ 0.1100 & 0 & 0.8155 & 0.0918 \\ 1.0377 & 4.2197 & \text{-0.9231} & \text{-0.1270} \end{bmatrix} \\ &= \underbrace{\begin{bmatrix} \text{-0.7563} & 0.3316 & 0.5640 \\ \text{-0.0121} & \text{-0.8690} & 0.4946 \\ 0.6542 & 0.3672 & 0.6612 \end{bmatrix}}_{\text{left singular vector matrix}} \underbrace{\begin{bmatrix} 6.7728 & 0 & 0 & 0 \\ 0 & 0.9476 & 0 & 0 \\ 0 & 0 & 0.0489 & 0 \end{bmatrix}}_{\text{singular value matrix}} \\ &\quad \underbrace{\begin{bmatrix} 0.2489 & \text{-0.1653} & \text{-0.2321} & \text{-0.9257} \\ 0.9593 & \text{-0.0937} & 0.0729 & 0.2564 \\ \text{-0.1332} & \text{-0.9720} & 0.1686 & 0.0955 \\ \text{-0.0108} & \text{-0.1385} & \text{-0.9552} & 0.2613 \end{bmatrix}}_{\text{right singular vector matrix}} \end{aligned} \tag{8.7}$$

The condition number 138.425 shows that this is an ill-conditioned system. The first column of left singular vector matrix indicates that the most sensitive output direction is a simultaneous change in gross power (y_1) and flue-gas temperature (y_3) in opposite direction. The first column of the right singular vector matrix indicates a strong impact of syngas quality/enthalpy (u_2) on the outputs. Syngas quality is a disturbance input to this subsection and its effect on gross-power is high. From this analysis it is recommended to effectively control this variable upstream.

We have three manipulated inputs (u_1, u_3, u_4) and three outputs (y_1, y_2, y_3) for this system. The gain matrix now reduces to

$$K = \begin{bmatrix} -0.883\ \frac{\text{hp}}{\text{lb/hr}} & 0.034\ \frac{\text{hp}}{\text{lb/hr}} & -0.0115\ \frac{\text{hp}}{\text{lb/hr}} \\ 1 & 1 & 1 \\ 0.0006\ \frac{^\circ\text{F}}{\text{lb/hr}} & -7.3 \times 10^{-5}\ \frac{^\circ\text{F}}{\text{lb/hr}} & -8.9 \times 10^{-5}\ \frac{^\circ\text{F}}{\text{lb/hr}} \end{bmatrix} \tag{8.8}$$

The following RGA matrix is obtained

$$\Lambda = \begin{bmatrix} \underline{0.3114} & 0.5180 & 0.1705 \\ 0.0845 & \underline{1.8675} & -0.9520 \\ 0.6041 & -1.3855 & \underline{1.7815} \end{bmatrix} \tag{8.9}$$

Following shows the scaled gain matrix and its singular value decomposition

$$\begin{aligned} K_{scaled} &= \begin{bmatrix} \text{-1.3332} & 0.3817 & \text{-0.0145} \\ 0.1100 & 0.8155 & 0.0918 \\ 1.0377 & \text{-0.9231} & \text{-0.1270} \end{bmatrix} \\ &= \underbrace{\begin{bmatrix} \text{-0.6800} & 0.4768 & 0.5570 \\ \text{-0.1851} & \text{-0.8467} & 0.4988 \\ 0.7094 & 0.2361 & 0.6640 \end{bmatrix}}_{\text{left singular vector matrix}} \underbrace{\begin{bmatrix} 1.9434 & 0 & 0 \\ 0 & 0.8803 & 0 \\ 0 & 0 & 0.0471 \end{bmatrix}}_{\text{singular value matrix}} \\ &\quad \underbrace{\begin{bmatrix} 0.8348 & \text{-0.5497} & 0.0301 \\ \text{-0.5482} & \text{-0.8252} & 0.1362 \\ \text{-0.0500} & \text{-0.1302} & \text{-0.9902} \end{bmatrix}}_{\text{right singular vector matrix}} \end{aligned} \tag{8.10}$$

The condition number is 41.29. The best possible pairing observed from RGA matrix is u_1-y_1, u_3-y_2 and u_4-y_3. This implies that syngas flowrate should be varied for controlling gross-power, ambient air (to MAC) flowrate should be changed to control amount of hot flue-gas product and nitrogen injection should be used to control flue-gas temperature.

8.3 Air Separation Unit Subsection

This sub-section has two input streams and four output streams. Figure 8.3 shows this sub-section separated from the entire flowsheet

Input Stream	**Description/Specifications**
AMBNTAIR	Dedicated air for ASU (not from MAC), T = 59°F, P = 14.4 psi, Flowrate = 1529931.76 lb/hr
GT-AIR1	Compressed air from GT-MAC, T = 811°F, P = 235 psi, Flowrate = 286060 lb/hr
Output Stream	**Description/Specifications**
O2GASIF	95% pure oxygen sent to gasifier section, T = 90°F, P = 125 psi, Flowrate = 409899.7 lb/hr
O2CLAUS	95% pure oxygen sent to Claus Sulfur removal section, T = 90°F, P = 125 psi, Flowrate = 6781.64 lb/hr
N2-8	Pure nitrogen stream sent as gas-turbine diluent, T = 385°F, P = 460 psi, Flowrate = 795682.10 lb/hr
ASU-VENT	Waste nitrogen being vented, T = 56.37°F, P = 16.4 psi, Flowrate = 603628.25 lb/hr

In addition, following design-specifications were inherently provided as flow-sheeting options in the original flowsheet

- AMBNTAIR mass flowrate is varied such that O2GASIF flowrate matches with OXIDANT flowrate (= 83.7% WET-COAL flowrate)
- GT-AIR1 is varied to equal AIRXTRCT (GT section) mass flowrate
- N2SPL block split fraction is varied for making N2-8 mass flowrate equals N2DILNT (nitrogen diluent stream in GT section)
- O2SPLT varied to match O2CLAUS to the oxygen demand in Claus cycle (O2TOCLAS)

All these design-specs were deactivated in the separated flow-sheet and inputs were made equal to the final values of integrated-flowsheet steady-state simulation. The following input-output variables were chosen for operability and control studies

Note: we do not have oxygen or nitrogen purity as our controlled output here, because the main separator block is very simplistic and specifies the composition

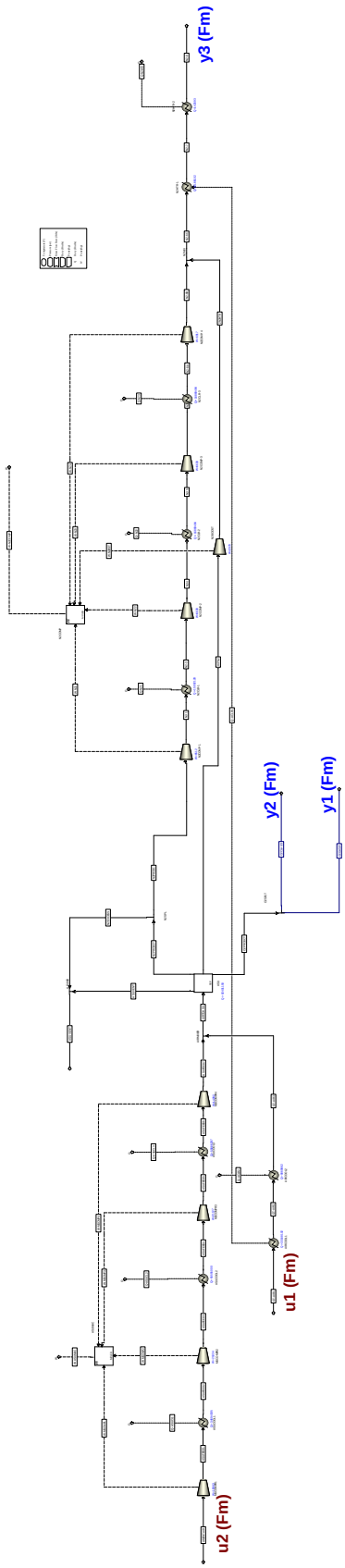

Figure 8.3: AspenPlus flowsheet of air separation unit sub-section (separated from complete Parson's IGCC NETL flowsheet) with control input/output variables shown

Input	**Description/Nominal-Value/Range**
u_1	Mass flowrate of GT-AIR1 (TO-SYNRH), 286060 lb/hr, ±20%
u_2	Mass flowrate of AMBNTAIR stream, 1523391.76 lb/hr, ±20%
Output	**Description/Nominal-Value/Range**
y_1	Mass flowrate of O2GASIF, 409899.75 lb/hr, ±20%
y_2	Mass flowrate of O2CLAUS, 6781.6 lb/hr, ±20%
y_3	Mass flowrate of N28, 795682.12 lb/hr, ±20%

using fixed component split fraction. So the purities always remain constant irrespective of input flow changes. Step changes of ±1% in input flowrates and enthalpy were made and changes in output variables were noted to obtain the following gain matrix.

$$K = \begin{bmatrix} 0.2257 & 0.2257 \\ 0.00373 & 0.00373 \\ 0.4381 & 0.4381 \end{bmatrix} \tag{8.11}$$

As can be noted, changes in inputs affect the outputs in a similar way and hence nothing can be done from control point of view. In fact, the separator model is as simple as a splitter block. More rigorous model for the separator block (having distillation vessels and/or other separator blocks) need to be developed for predicting control structure and operability, rather than a working on a simplistic model which forces a certain output stream composition.

A double column heat-integrating cryogenic model for ASU has been developed. Replacing the simplified separator block in the current flowsheet with the newer detailed model so as to adapt completely into the NETL integrated flowsheet is a challenging task.

8.4 Claus-Burner/Sulfur-Removal Section

This subsection has three input streams and two output streams which are listed below. Figure 8.4 shows the gas-turbine/compressor subsection separated from the entire flowsheet.

Input Stream	**Description/Specifications**
TOCLAUS	Sour-gas feed to Claus Unit for sulfur removal, T = 120°F, P = 30 psi, Flowrate = 31089.6 lb/hr
O2TOCLAS	Oxygen stream from ASU to Claus Unit, T = 90°F, P = 125 psi, Flowrate = 6781.64 lb/hr
SWS-VAP	Additional sour stream extracted from middle of gas cleaning, T = 247°F, P = 35 psi, Flowrate = 8839.12 lb/hr
Output Stream	**Description/Specifications**
SULFUR	Recovered sulfur from the sour-gas in Claus Unit, T = 360.5°F, P = 24.9 psi, Flowrate = 12248.76 lb/hr
TAILGAS	Product stream after sulfur is removed, T = 450°F, P = 24.8 psi, Flowrate = 34461.57 lb/hr

In addition, following design-specifications were inherently provided as flowsheeting options in the original flowsheet (See Figure 8.4)

- AG-BYPSS mass flowrate is varied such that TOAGMIX stream temperature is 2400°F
- AG-RXTR temperature is varied such that AG-RXTR heat-duty = 0.01123 × 7097× (H_2S-flowrate in 2CLAUSRX)
- O2TOCLAUS mass flowrate varied such that ratio of H_2S flowrate in 2AG-RXT2 to SO_2 flowrate in 2AG-RXT2 is 1.8609

The first two design-specs are essential and pertain to equipment design requirement (heat loss of reactor, temperature of turbine feed). The third design-spec was deactivated in the separated flow-sheet and inputs were made equal to the final values of integrated-flowsheet steady-state simulation. It was made sure that results of both flowsheets were consistent. The following input-output variables were chosen for operability and control studies

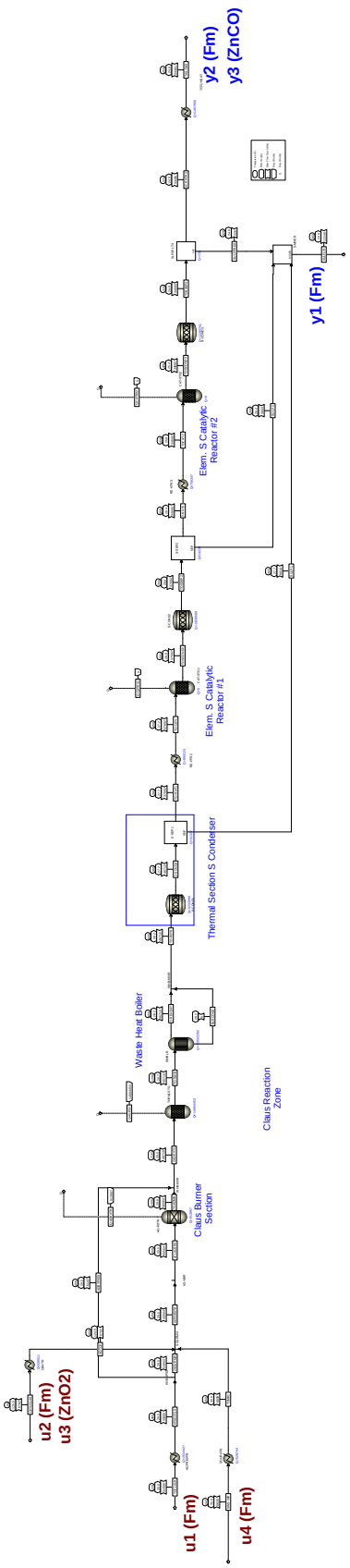

Figure 8.4: AspenPlus flowsheet of Claus-Plant/ Sulfur removal sub-section (separated from complete Parson's IGCC NETL flowsheet) with control input/output variables shown

Input	**Description/Nominal-Value/Range**
u_1	TOCLAUS mass flowrate, 31089.56 lb/hr, ±20%
u_2	O2TOCLAS mass flowrate, 6781.64 lb/hr, ±20%
u_3	Oxygen mole fraction in O2TOCLAS (disturbance), 0.95, 0.93 to 0.97
u_4	SWS-VAP mass flowrate, 8839.11 lb/hr, ±20%
Output	**Description/Nominal-Value/Range**
y_1	SULFUR mass flowrate, 12248.76 lb/hr, ±20%
y_2	TAILGAS mass flowrate, 34461.57 lb/hr, ±20%
y_3	CO mole fraction in TAILGAS stream, 0.138, ±0.1

It must be noted that CO mole fraction in the tailgas stream is chosen as another output variable since tail-gas cleaning section involves substantial reduction in CO mole fraction and hence is an important variable for downstream process. Step changes of ±1% in input flowrates and 0.01 in mole fractions were made and changes in output variables were noted to obtain the following gain matrix.

$$K = \begin{bmatrix} 0.0135 & 2.267 & 14897\ \frac{\text{lb}}{\text{hr}} & -0.394 \\ 0.9865 & -1.2673 & -14897\ \frac{\text{lb}}{\text{hr}} & 1.394 \\ -3.1 \times 10^{-6} \frac{1}{\text{lb/hr}} & 1.1 \times 10^{-5} \frac{1}{\text{lb/hr}} & 0.107 & 2.51 \times 10^{-6} \frac{1}{\text{lb/hr}} \end{bmatrix} \tag{8.12}$$

Following shows the scaled gain matrix and its singular value decomposition

$$K_{scaled} = \begin{bmatrix} 0.0342 & 1.2554 & 0.1216 & -0.2844 \\ 0.8900 & -0.2494 & -0.0432 & 0.3576 \\ -0.1931 & 0.1494 & 0.0214 & 0.0444 \end{bmatrix}$$

$$= \underbrace{\begin{bmatrix} -0.8987 & - & - \\ 0.4192 & - & - \\ -0.1293 & - & - \end{bmatrix}}_{\text{left singular vector matrix}} \underbrace{\begin{bmatrix} 1.3709 & 0 & 0 & 0 \\ 0 & 0.9069 & 0 & 0 \\ 0 & 0 & 0.1316 & 0 \end{bmatrix}}_{\text{singular value matrix}} \underbrace{\begin{bmatrix} 0.2679 & - & - & - \\ -0.9133 & - & - & - \\ -0.0950 & - & - & - \\ 0.2916 & - & - & - \end{bmatrix}}_{\text{right singular vector matrix}} \tag{8.13}$$

The condition number 10.4 shows that this is not an highly ill-conditioned system. Oxygen mole fraction quality is a disturbance input and its directional

sensitivity is lower as compared to other inputs. Therefore fluctuations in oxygen purity in ASU do not pose serious problems to Claus Unit (as compared to gasifier unit).

We have three manipulated inputs (u_1, u_2, u_4) and three outputs (y_1, y_2, y_3) for this system. The gain matrix now reduces to

$$K = \begin{bmatrix} 0.0135 & 2.267 & -0.394 \\ 0.9865 & -1.2673 & 1.394 \\ -3.1 \times 10^{-6} \frac{1}{\text{lb/hr}} & 1.1 \times 10^{-5} \frac{1}{\text{lb/hr}} & 2.51 \times 10^{-6} \frac{1}{\text{lb/hr}} \end{bmatrix} \tag{8.14}$$

The following RGA matrix is obtained

$$\Lambda = \begin{bmatrix} 0.0136 & \underline{0.8381} & 0.1484 \\ 0.5378 & -0.0819 & \underline{0.5441} \\ \underline{0.4487} & 0.2438 & 0.3076 \end{bmatrix} \tag{8.15}$$

$$K_{scaled} = \begin{bmatrix} 0.0342 & 1.2554 & -0.2844 \\ 0.8900 & -0.2494 & 0.3576 \\ -0.1931 & 0.1494 & 0.0444 \end{bmatrix}$$

$$= \underbrace{\begin{bmatrix} 0.8981 & - & - \\ -0.4205 & - & - \\ 0.1291 & - & - \end{bmatrix}}_{\text{left singular vector matrix}} \underbrace{\begin{bmatrix} 1.3646 & 0 & 0 \\ 0 & 0.9068 & 0 \\ 0 & 0 & 0.1314 \end{bmatrix}}_{\text{singular value matrix}} \underbrace{\begin{bmatrix} -0.2700 & - & - \\ 0.9171 & - & - \\ -0.2931 & - & - \end{bmatrix}}_{\text{right singular vector matrix}} \tag{8.16}$$

The condition number is 10.38. The best possible pairing observed from RGA matrix is u_1-y_3, u_2-y_1 and u_4-y_2. This implies that sour-gas flowrate should be varied for controlling CO molefraction in tail-gas, oxygen flowrate should be paired up with extracted sulfur stream amount and SWS-VAP flowrate should control tail-gas flowrate.

8.5 Discussion and Conclusion

Operability analysis studies based directly on NETL IGCC Case#1 integrated flowsheet provides a generic although not very conclusive result related to controller structuring and design. One of the main reason is that some of the units are not rigorously modeled to capture behavior of important process variables. The flowsheet is full of design specifications and calculators which change certain variables values to satisfy some physical requirement. This serves as an internal controller (design-specs as feedback control and calculators as feed-forward control) which makes the corresponding input-output pair unavailable for external pairing. Although the use of Aspen flowsheeting option has been minimized, certain internal specifications cannot be undone with, which might in-turn lead to incorrect results.

CHAPTER 9
SUMMARY AND FUTURE DIRECTIONS

The research topic is very open ended and depending on the increasing level of modeling details involved, the control architecture becomes more and more complex and challenging. Unfortunately, modeling each and every piece of equipment in a full-blown IGCC plant is beyond the scope of a three-year dissertation project. Due to lack of such detailed models, we have tried to identify and build semi-rigorous models of dynamically important sub-processes within the whole plant before implementing plantwide controller design on the entire IGCC plant. The following chapter summarizes the work covered in this report, provides a general conclusion and highlights/proposes a general scope for possible future research.

9.1 Summary

To summarize this research, we pause and look back at various limitations that were posed at the beginning of this report (see Research Contributions on page 23). The lack of rigorous dynamic model not only makes the in-silico understanding of plant dynamics unrealizable and/or inaccurate, it limits testing and validation of newly developed control algorithms only to a real existing plant. Since these plants, especially those equipped with CCS, are non-existent in the world, a rigorous and accurate plantwide dynamic model is only way to perform any kind of operability and control studies. Furthermore, the control-models (for example, the state-space models fitted to "plant" step-test data) are only as accurate as the "plants" themselves.

In this report, we address this real-plant plant-model mismatch problem, as a first step. All the units identified as playing an important role in IGCC plant dynamics, are carefully modeled by providing as much equipment details as possible within Aspen. The overall flowsheet structure including placement of various equipments have been based on steady-state NETL IGCC Case#1 or Case#2 flowsheets. The beauty of using Aspen for developing a possible "mirror-image" of the

real plant is because of its ability to incorporate extremely complex thermodynamic calculations with ease and speed.

Upon taking motivation from gaps and limitations in the existing literature, we realized that most of the models available are not pressure-driven, i.e., the flowrate in a stream is not dependent on the pressure difference but is mostly specified independently. For a full-blown process flowsheet with more than 200 process units, this work is not trivial and will need to carefully specify the exit-pressure, pressure-differences of each block as well as incorporate valve, pump and compressor at places where pressure mismatch occurs. In addition, further equipment details need to be provided when moving from flow-driven to pressure-driven mode operation.

Apart from these steps involved in dynamic modeling, there are many additional details specific for the type of process unit block. At many places, we take the opposite approach of simplifying the specifications rather than detailing it, mostly as a workaround to software limitations. The above steps, in their full rigorousness, have been the focus of first part (dynamic modeling) in all the chapters; where limitations, additional detailing and suitable assumptions have been identified and provided.

As a second step, these dynamic models (which may now be visualized as "plants") need to be stabilized and ensured that each equipment is working at their nominal operating point. This task is done by providing regulatory controllers, on every process equipment (except in certain cases). These controllers placement and the choice of input-output variables are generally based on equipment proximity and various other heuristics. We call this the 'lower-level' or the 'regulatory-layered' controller and used PID-based control blocks within the AspenDynamics^{TM} simulator. Depending on control objectives for the overall section or plant, the setpoint to some of these lower-level controller are determined by a higher-level control, which essentially is responsible for overall plant-coordination, dynamic response and sometimes optimized response (optimization layered control). The regulatory-controller design has also been focused in all of the chapters, as an essential step for plantwide controller design.

We then move towards developing the abovementioned 'higher-level' or the

'supervisory-layered' controller. These controllers are designed using a PID-based multiloop architecture or a multivariable model predictive control architecture. The PID-based approach involves controller placement within the simulator, with pairing decision and controller tuning parameter calculations shown. The MPC-approach is more complex, and in absence of Aspen's dynamic optimization and dynamic matrix control (DMC) module, has been designed using MATLAB/Simulink environment with much more flexibility. The control-model used was developed in state-space form by providing small perturbations around the nominal point, with multiple combination of step-inputs, and thereafter using system identification methods.

For slower and highly interactive ASU section, both these approaches are taken and the responses are compared. The benefits of using multivariable MPC approach are shown and analyzed. In addition, a pure feed-forward controller is designed and a better response is shown for longer sampling time (or delayed measurements). For faster and non-interacting systems, including the gasifier and the GT, the MPC approach is not taken and PID-based scheme providing sufficient controllability in terms of faster and robust response for large load changes, is justified. Similarly, the HRSG section is shown to provide sufficient controllability, using a regulatory-layered control structure.

In the final step, a section-wide regulatory and supervisory layered controller is designed around the 'clubbed' plant sections. Initially, plantwide pressure swings were analyzed to identify controllable pressure nodes in the plant, based on which a plantwide regulatory design was provided. For a supervisory layered design, two variations of plantwide MPC was studied and compared: a decentralized MPC design where each individual sub-section has its own controller/MPC structure passing setpoint information among each other and a centralized MPC design where a single centralized controller is used to measure and control all the relevant inputs/outputs spanning across all subsections. The centralized design was proved slightly advantageous, both during the load-following and disturbance-rejection scenarios.

An operability analysis study was also done on individual sub-units of the NETL IGCC (Parson's) Case#1 flowsheet which provided a generic yet inconclusive results related to controller operability and input-output directionality due to

substantial approximation in the steady-state flowsheet.

9.2 Future Research Directions

While the research in this report makes significant contributions to both dynamic modeling and advanced control implementation for plantwide IGCC, there still remain research issues in this field that are unexplored in open literature. For the benefit of future graduate students and researchers in these fields, it is important to highlight several of the most promising and intriguing potential areas of future research. This section discusses some of the potential research topics that may serve as a scope for future research.

9.2.1 Temperature-based Control of ASU

Chapter 2 and 3 illustrated that composition control loops provided good dynamic performance in the face of feed flow rate. However, online composition analyzers are expensive, require high maintenance, and can introduce long time delays. This problem became very apparent with our studies with large dead-time (Figure 3.16). Temperature measurements are inexpensive and reliable and provide rapid responses. However, they only provide an estimation of composition. In a binary system at constant pressure, knowing the temperature fixes the composition. However, in systems which operate at floating pressures, we cannot control a single temperature but use differential temperature control method within a single column and between the LP and HP-column.

Although not extensively focused within the scope of this research, the preliminary idea (motivated by references [109, 110]) was to start by studying the sensitivity of differential tray locations on product purities and try to control the differential tray temperatures as a cascaded loop within a slower composition loop. Some of the current studies covering this aspect [111], do not consider drastic load-following scenarios where pressure changes are significant (as observed in an IGCC plant). Hence this topic presents itself as a challenging future research.

9.2.2 Controller Design for IGCC with co-production of Hydrogen and External Steam

The proposed controller design for co-production of hydrogen and external steam has been given in Figure 9.1. For sake for brevity, the feedback process variable signals have not been shown. All of them (excluding the coal quality disturbance) are measured either directly or indirectly and sent to the respective controllers.

As the total power demand signal is obtained from the grid, the setpoint to the GT-work is calculated, using information of current steam-turbine work generated, i.e., W-GT = W-demand – W-ST. The localized GT-controller, comprising air flow (IGV) regulation, fuel-flow regulation (FFS) and injected N2/moisture regulation, generates the appropriate signals - F_syngasGT (sent to the local gasifier controller), F_airGT (sent to the IGV actuator) and F_N2 (sent to the local ASU controller). The frequency (related to turbine rpm) is an important parameter to be regulated especially at part load conditions. Aurora and Colombo (2004), have given energy storage exploitation (comparing operation with and without pressure swings) and using HP-turbine bypass system to improve frequency regulation for CCPP. In our study, frequency regulation is absent due to inherent difficulty in Aspen Dynamics (AD) turbine/compressor modules to model rotational speed corresponding GE-7FB turbines clearly.

Hydrogen co-production can be handled by adding the external syngas demand, SP_external_H2/syngas (calculated from the quantity of co-generated H2 required) to the GT-syngas demand (F_syngasGT generated by the local GT controller) which gives a total syngas amount. This signal (SP F_tot_syngas) along with other setpoint signals (gasifier temperature, syngas quality) are sent to gasifier controller which manipulate the flow of coal (F_coal), water (F_water) and oxygen (F_O2). In case the syngas quality is unmeasured, we use a ratio/feed forward control for F_water/F_coal or less commonly F_O2/F_coal.

The oxygen flowrate (demanded by the local gasifier control), may be adjusted directly using a valve/compressor operating on the oxygen stream/pipeline. In such a scenario, the upstream ASU purity/pressures/levels are regulated using total feed

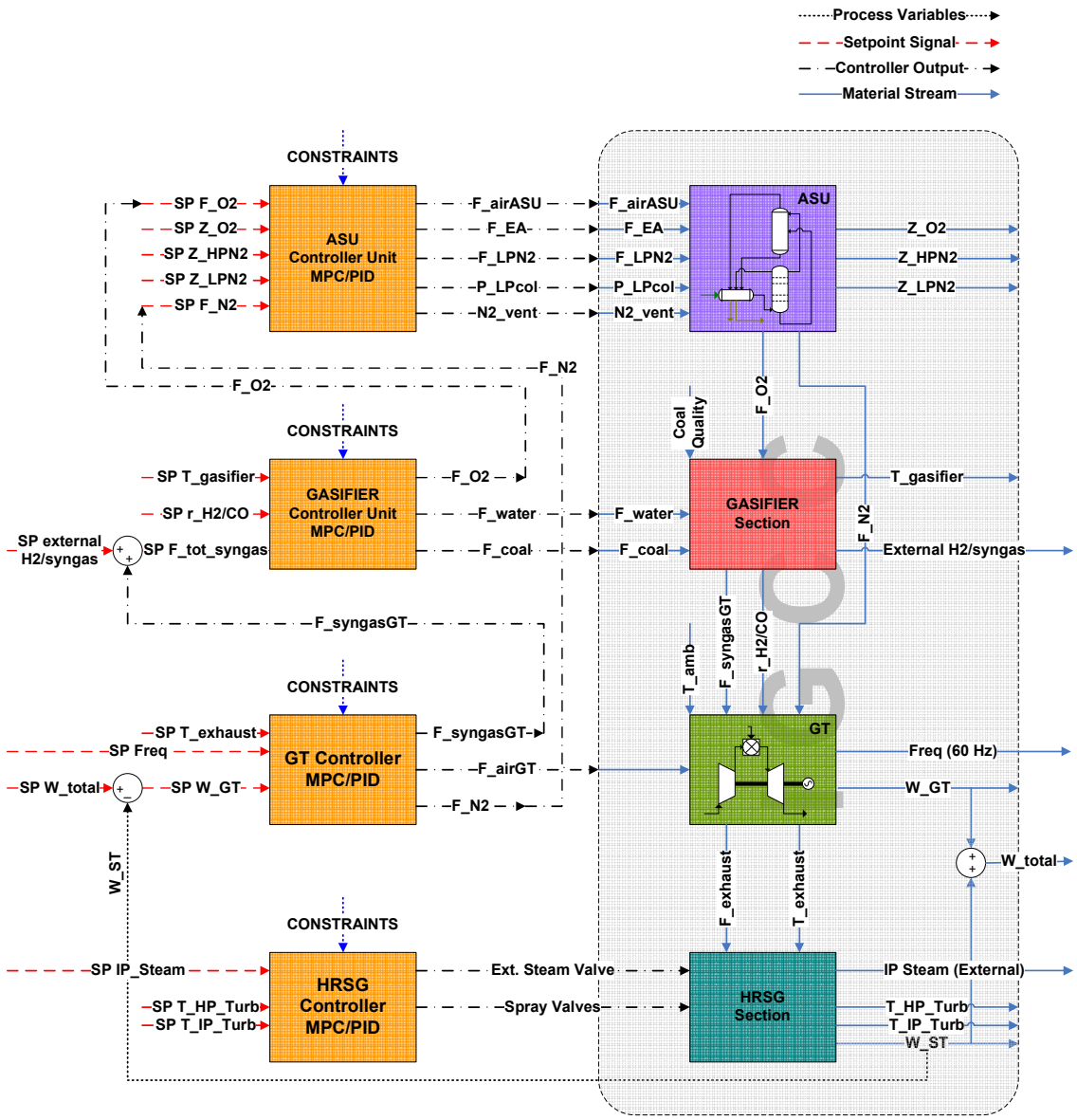

Figure 9.1: Block diagram showing controller design for co-production of hydrogen and IP-steam

air flowrate as one of the manipulated input. As shown in previous report, direct O2-flowrate manipulation caused huge pressure swings on the suction side of the compressor, leading to sudden purity loss and other undesired transients (in addition to simulator convergence issues). Instead, here the oxygen stream is responsible for maintaining the level in the LP-column reboiler. The desired oxygen flowrate is met by adjusting the total air feed (along with other variables predominantly responsible for maintaining the purities). For instance, if the total air flowrate increase, the

pressures and purity regulators adjust the internal flowrates such that the level in the reboiler drum rises, this increases the oxygen flowrate by actuating the downstream valve. Since the actual oxygen flowrate signal is fed-back to the controller, the air-flowrate is kept changing till any offset between actual and demanded oxygen flow is removed.

Similar to the oxygen flowrate, the nitrogen injection amount (from GT-control) is provided as a setpoint signal to the ASU-controller. The N2-vent or split-fraction of nitrogen to be sent to the GT as compared to the total produced by ASU is being calculated. Since this is a straightforward input-output correlation, a simple PID-based controller is used, which manipulates the vent/waste-N2 valve depending on the N2 demand/set-point. It should be noted that there is an upper-cap to the quantity of nitrogen demanded, due to the primary purpose of ASU serving the gasifier for oxygen production. If more dilution is needed, water-vapor or CO2 is used. This is rarely the case; the amount of nitrogen required for adequate dilution (NOx control) is, in general, less than the total nitrogen produced by ASU. If the plant requires cogeneration of H2/syngas, even lower amount of nitrogen injection is needed. In such cases, venting is done before nitrogen compression to reduce operating costs (unless storage of nitrogen is done).

The HRSG is a newly added section to our previous flowsheet analysis and controller design. To further generalize the control problem, co-production of IP-steam which may serve as localized home heating needs or other steam inventory storage/needs, external to the plant. It should be noted that this does not refer to the internal heating requirements provided by HRSG, for instance, to the WGS reactors or syngas pre-heating etc., since the total amount of heat availability and temperatures directly depends on these internal energy transfers and should be incorporated in the dynamic model.

Since HRSG is responsible for extracting the maximum “waste” heat energy and produce work / provide external steam, there is no concept of “work demand” from the steam turbine (ST), although we do pose a demand for the external steam needs. If there is no external steam demand, all of the available heat is converted to steam-turbine work. Increasing the work extracted from ST, poses lower load-

demand to the GT (to meet the same total grid load) and hence less coal/fuel. Since, most of the extracted heat for ST is directly related to the GT-exhaust flowrate (assuming GT-exhaust temperate is maintained at maximum limit), lower GT-work directly implies lower ST-work and hence significant lowering of total-work. In addition, due to slower thermal transients, the effect of lowering exhaust flowrate (enthalpy) and hence the ST-work is seen much slower than the GT-work; this demands a tight HRSG control for meeting the total grid-power demand in a robust fashion.

The request of a greater external steam flowrate, for a given power production, can be satisfied through an increase of the coal load only if the turbine combustion temperature is below the maximum operating limit and if the oxygen ramp can be accomplished by the oxygen plant (this is actually a limit on the system velocity in achieving the new setpoint). If one of the previous conditions is not satisfied, the power setpoint will be decreased, so reducing the steam fed to the turbine, according to the increased external needs. Such a control strategy is referred to as "steam demand" to highlight that, in this case, the steam required by the refinery becomes crucial. This study is currently in progress and is in its premature stage (due to recently added HRSG section). Hence, any study pertaining this has not been provided here, but can serve as a future research possibility.

9.2.3 Multiple Model Predictive Control

The multiple model predictive control strategy is based on the use of n models in the model bank that have the general form given in equation (9.1)

$$\begin{aligned} {}^{i}\hat{x}_{k+1} &= {}^{i}\Phi\,{}^{i}\hat{x}_{k} + {}^{i}\Gamma u_{k} + {}^{i}\Gamma^{F} d_{k}^{F} \\ {}^{i}\hat{y}_{k+1} &= {}^{i}C\,{}^{i}\hat{x}_{k+1} + {}^{i}D u_{k} \end{aligned} \tag{9.1}$$

The left superscript i denotes the model number, with i ranging from 1 to n models. Although the plant being controlled in practice is likely nonlinear, the models in (9.1) are all linear. Each linear model is chosen to represent a discrete subspace of the overall nonlinear operating space. When all n models are combined,

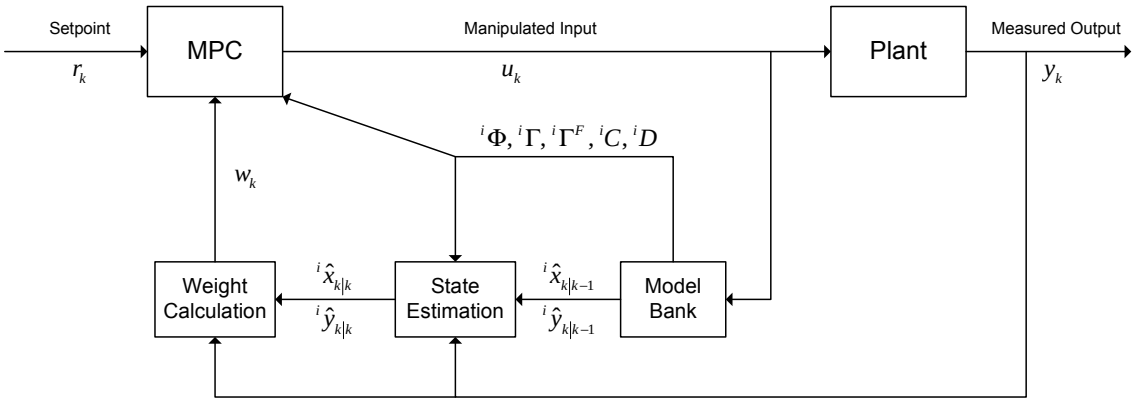

Figure 9.2: Control block diagram of multiple model predictive control strategy

the resulting bank of linear models spans the entire nonlinear operating space. As Figure 9.2 shows, the models in the model bank are updated in parallel with the plant.

In our previous control study on LP-ASU, non-linearity was observed (Figure 3.13) even for operation close to nominal operating point. At part-load conditions, for instance at 50% of full-load operation, predictions using a single linear model may deviate from the plant-outputs by a large extent. Therefore, separate models corresponding to various 'plant' operating points may be stored in the model bank. If the plant operates at a fixed discrete load point at any given time, for example, only at 100%, 80%, 60% or 40% of the full-load, it is very natural to find linear models around these points. Rather than switching among these models once the operation "approaches" a discrete load-point value, MMPC structure naturally and continously adapts by promoting the corresponding model, based on the plant measurements only. This dynamically gives an advantage, say, in case of 70% load where a combination of 80% and 60% models (each weighted equally) might give better model-predictions compared to each model individually.

9.2.4 Using "ideal" plant in Aspen as control-model

It has been mentioned earlier, within the context of system-identification procedures, that Aspen provides an option (called the Control Design Interface, CDI) to directly obtain state-space model (from the differential equation) around the cur-

rent operating point. The more rigorous and realistic a plant becomes, higher the number of states exist in the system. For instance, the rigorous gasifier subsection model consists of more than 230 states, which if used in MPC design (using the CDI approach) would lead to huge computational time. An alternative approach is to devise a parallel Aspen flowsheet using approximations such as ideal thermodynamic properties and "instantaneous" dynamics specification for unit-operations possessing very fast dynamics. This may significantly reduce the number of states involved in the system while maintaining similar flowsheet model structure. The control-model using CDI approach, now based on this "ideal" plant serves as a good candidate for control-model.

LITERATURE CITED

[1] Energy Information Administration. Annual Energy Outlook 2009 – With Projections to 2030. Technical Report DOE/EIA-0383, U.S. Department of Energy, March 2009.

[2] U.S. Department of Energy, Clean Coal Technology. Clean Coal Power Initiative. (`http://www.fe.doe.gov/programs/powersystems/cleancoal/`), November 2009.

[3] U.S. Department of Energy. Cost and Performance Baseline for Fossil Energy Plants, Volume 1: Bituminous Coal and Natural Gas to Electricity. Technical Report DOE/NETL-1281, National Energy Technology Laboratory, August 2007.

[4] L.F. O'Keefe and K.V. Sturm. Clean Coal Technology Options – A Comparison of IGCC vs. Pulverized Coal Boilers. In *2002 Gasification Technologies Conference, San Francisco, California*, October 28-30 2002.

[5] Gasification Technologies Council (GTC). Gasification: Redefining Clean Energy. (`http://www.gasification.org/Docs/Final_whitepaper.pdf`), 2008 [accessed Sept 21, 2008].

[6] O. Maurstad, J. Deutch, A.D. Ellerman, S.J. Friedmann, and H. Herzog. An Overview of Coal based Integrated Gasification Combined Cycle (IGCC) Technology. Technical Report MIT LFEE 2005-002 WP, Massachusetts Institute of Technology (MIT), September 2005.

[7] S. Ansolabehere, J. Beer, J. Deutch, A.D. Ellerman, S.J. Friedman, and H. Herzog. The future of coal. An interdisciplinary MIT study, Massachusetts Institute of Technology (MIT). (`http://web.mit.edu/coal/`), 2008 [accessed Sept 19, 2008].

[8] M.J. Mudd. IGCC's Chasm – What Drives Technology Choices? In *2003 Gasification Technologies Conference*, October 12-15 2003.

[9] U.S. Department of Energy. Tampa Electric Polk Power Station - Integrated Gasification Combined Cycle Project: Final Technical Report. Technical Report DE-FC-21-91MC27363, Prepared for the U.S. Department of Energy, Office of Fossil Energy, National Energy Technology Laboratory (NETL): Morgantown, West Virginia, August 2002.

[10] J.S. Falsetti, R.A. De Puy, D. Brdar, A. Anand, and Paolino J. From Coal or Oil to 550 MWe via 9H IGCC. In *2000 Gasification Technologies Conference*, October 19 2000.

[11] W.E. Preston. Texaco Gasification 2001 Status and Path Forward. In *2001 Gasification Technologies Conference, San Fransisco, California*, October 2001.

[12] Electric Power Research Institute. Evaluation of the British Gas Corporation/Lurgi Slagging Gasifier in Gasification-Combined-Cycle Power Generation. Technical Report EPRI AP-3980, Prepared by Ralph M. Parsons Company, British Gas Corporation and Lurgi, GMBH for Electric Power Research Institute, Palo Alto, California, 1985.

[13] U.S. Department of Energy. Pinõn Pine IGCC Power Project: A DOE Assessment. Technical Report DOE/NETL-2003/1183, National Energy Technology Laboratory, December 2002.

[14] D. Simbeck and H. Johnson. World Gasification Survey: Industry Trends & Developments. In *2001 Gasification Technologies Conference, San Fransisco, California*, October 2001.

[15] U.S. Environmental Protection Agency. Texaco Gasification Process. Technical Report EPA 540/R-94/514a, Center for Environmental Research Information, Cincinnati, Ohio, April 1995.

[16] H.C. Frey and N.V. Akunuri. Probabilistic Modeling and Evaluation of the Performance, Emissions and Cost of Texaco Gasifier-based Integrated Gasification Combined Cycle Systems using ASPEN. Technical report, Prepared by North Carolina State University for Carnegie Mellon University and U.S. Department of Energy, Pittsburgh, PA, January 2001.

[17] Electric Power Research Institute. Cost and Performance for Commercial Applications of Texaco gasifier-based Gasification-combined-Cycle Plants, Volume 2: Design Details. Technical Report EPRI AP-3486, Prepared by Fluor Engineers, Inc. for Electric Power Research Institute, Palo Alto, CA, 1984.

[18] Electric Power Research Institute. Coal Gasification Systems: A Guide to Status, Applications and Economics. Technical Report EPRI AP-3109, Prepared by Synthetic Fuel Associates, Inc. for Electric Power Research Institute, Palo Alto, CA, 1983.

[19] F.J. Brooks. GE Gas Turbine Performance Characteristics. Technical Report GER-3567H, GE Power Systems, Schenectady, NY, October 2000.

[20] U.S. Department of Energy. The Turbines of Tomorrow. (`http://fossil.energy.gov/programs/powersystems/turbines/`), November 2009.

[21] D.M. Todd. Gas Turbine Improvements Enhance IGCC Viability. In *2000 Gasification Technologies Conference*, 2000. GE Power Systems, Schenectady, NY.

[22] R.D. Brdar and R.M. Jones. GE IGCC Technology and Experience with Advanced Gas Turbines. Technical Report GER-4207, GE Power Systems, Schenectady, NY, 2000.

[23] R.K. Matta, G.D. Mercer, and R.S. Tuthill. General Electric Power Systems for the 21^{st} Century – "H" Gas Turbine Combined-Cycles. Technical Report GER-3935B, GE Power Systems, Schenectady, NY, October 2000.

[24] U.S. Department of Energy. Gasification Plant Cost and Performance Optimization: Task 1 Topical Report, IGCC Plant Cost Optimization. Technical Report DE-AC26-99FT40342, Prepared by Bechtel Corp., Global Energy Inc., and Nexant Inc. for the U.S. Department of Energy, National Energy Technology Laboratory, Morgantown, West Virginia, 2002.

[25] W.I. Rowen. Simplified mathematical representations of heavy-duty gas turbines. *Journal of Engineering for Power*, 105:865–869, October 1983.

[26] W.I. Rowen. Simplified mathematical representations of single shaft gas turbines in mechanical drive service. *Turbomachinery International*, pages 26–32, July/August 1992.

[27] O. Bolland and P. Mathieu. Comparison of two CO_2 removal options in Combined Cycle Power Plants. *Energy Conversion and Management*, 39(16-18):1653–1663, 1998.

[28] A. R. Smith and J. Klosek. A review of air separation technologies and their integration with energy conversion processes. *Fuel Processing Technology*, 70(2):115–134, 2001.

[29] R. Prasad, J. Chen, B.V. Hassel, J. Sirman, J. White, P. Apte, and E. Aaron, T.and Shreiber. Advances in OTM Technology for IGCC. In *Nineteeth Annual International Pittsburgh Coal Conference, Pittsburgh, PA*, September 23-27 2002.

[30] Farina, G.L. and Bressan, L. Optimizing IGCC Design. Technical report, Foster Wheeler, Autumn 1999.

[31] A. R. Smith, J. Klosek, and D. W. Woodward. Next-generation integration concepts for air separation units and gas turbines. *Journal of Engineering for Gas Turbines and Power*, 119(2):298–304, 1997.

[32] John G. Wimer, Dale Keairns, Edward L. Parsons, and John A. Ruether. Integration of Gas Turbines Adapted for Syngas Fuel With Cryogenic and Membrane-Based Air Separation Units: Issues to Consider for System Studies. *Journal of Engineering for Gas Turbines and Power*, 128:271–280, April 2006.

[33] U.S. Department of Energy. Market-Based Advanced Coal Power Systems. Technical Report DOE/EIA-0400, Office of Fossil Energy, May 1999.

[34] C. Aurora, C. Paolo, F. Pretolani, and R. Scattolini. Supervisory and dynamic control optimization of Combined Cycle Power Plants. In *Bulk Power Systems Dynamics and Control, VI, Cortina dÁmpezzo, Italy*, August 22-27 2004.

[35] Thomas D. Younkins and Joe H. Chow. Multivariable Feedwater Control Design for a Steam Generator. *Control Systems Magazine*, 8(2):77–80, April 1988.

[36] Working Group on Prime Mover and Energy Supply Models for System Dynamic Performance Studies. Dynamic Models for Combined Cycle Plants in Power System Studies. *IEEE Transactions on Power Systems*, 9(3):1698–1708, 1994.

[37] Takao Akiyama, Hiroshi Matsumoto, and Kazuyasu Asakura. Dynamic Simulation and its applications to Optimum Operation Support for Advanced Combined Cycle Plants. *Energy Conversion and Management*, 38(15-17):1709–1723, 1997.

[38] Q Zhang and P.L. So. Dynamic Modelling of a Combined Cycle Plant for Power System Stability Studies. *IEEE Power Engineering Society, Winter Meeting*, 2:1538–1543, 2000.

[39] P. Colonna and H. van Putten. Dynamic modeling of steam power cycles.: Part I–Modeling paradigm and validation. *Applied Thermal Engineering*, 27(2-3):467–480, 2007.

[40] H. van Putten and P. Colonna. Dynamic modeling of steam power cycles: Part II - Simulation of a small simple Rankine cycle system. *Applied Thermal Engineering*, 27(14-15):2566–2582, 2007.

[41] Zygfryd Domachowski and Marek Dzida. Specific Problems of Combined Cycle Power Plant Control. In *Proceedings of 2000 International Joint Power Generation Conference, Miami Beach, Florida*, July 23-26 2000.

[42] C. Aurora, M. Diehl, P. Kuehl, L. Magni, and R. Scattolini. Nonlinear Model Predictive of Combined Cycle Power Plants. In *2005 IFAC World Congress, Prague, Czech Republic*, 2005.

[43] Gillian Lalor and Mark O'Malley. Frequency control on an island power system with increasing proportions of combined cycle gas turbines. In *Power Tech Conference Proceedings, 2003 IEEE Bologna*, volume 4, page 7, 23-26 June, 2003.

[44] Giancarlo Ferrari-Trecate, Eduardo Gallestey, Paolo Letizia, Matteo Spedicato, Manfred Morari, and Marc Antoine. Modeling and Control of Co-generation Power Plants: A Hybrid System Approach. *IEEE Transactions on Control Systems Technology*, 12(5):694–705, September 2004.

[45] D. Sáez, R. Zúñiga, and A. Cipriano. Adaptive hybrid predictive control for a combined cycle power plant optimization. *International Journal of Adaptive Control and Signal Processing*, 22:198–220, 2008.

[46] Rongrong Zhai, Yongping Yang, Liqiang Duan, and Qin Yan. Modelling and simulating of GTCC system with CO_2 removal plant using Aspen Plus. *International Journal of Modelling, Identification and Control*, 7:365–370, 2009.

[47] Ligang Zheng and Edward Furimsky. ASPEN simulation of cogeneration plants. *Energy Conversion and Management*, 44(11):1845–1851, 2003.

[48] A.L. Polyzakis, C. Koroneos, and G. Xydis. Optimum gas turbine cycle for combined cycle power plant. *Energy Conversion and Management*, 49(4):551–563, 2008.

[49] U.S. Department of Energy. Major Environmental Aspects of Gasification-based Power Generation Technologies. Technical report, Prepared by Science Applications International Corporation for Gasification Technologies Program, NETL and DOE, December 2002.

[50] N.A.H. Holt. IGCC Power Plants EPRI Design & Cost Studies. In *1998 Gasification Technologies Conference, San Francisco, California*, October 6 1998.

[51] N.A.H. Holt. Operation experience and improvement opportunities for coal-based IGCC plants. *Material at High Temperature*, 20(1):1–6, 2003.

[52] H.C. Frey and E.S. Rubin. Stochastic Modeling of Coal Gasification Combined Cycle Systems: Cost Models for Selected Integrated Gasification Combined Cycle (IGCC) Systems. Technical Report DOE/MC/24248-2901, Prepared by Carnegie-Mellon University for U.S. Department of Energy, Morgantown, West Virginia, June 1990.

[53] H.C. Frey and E.S. Rubin. Development and Application of a Probabilistic Evaluation for Advanced Process Technologies. Technical Report DOE/MC/24248-3015, Prepared by Carnegie-Mellon University for U.S. Department of Energy, Morgantown, West Virginia, April 1991.

[54] H.C. Frey and E.S. Rubin. Probabilistic Evaluation of Advanced SO_2/NO_x Control Technology. *Journal of Air & Waste Management Association*, 41(12):1585–1593, 1991.

[55] H. Cristopher Frey and Yunhua Zhu. Improved System Integration for Integrated Gasification Combined Cycle (IGCC) Systems. *Environmental Science & Technology*, 40(5):1693–1699, 2006.

[56] G. Ordorica-Garcia, P. Douglas, E. Croiset, and L. Zheng. Technoeconomic Evaluation of IGCC Power Plants for CO_2 Avoidance. *Energy Conversion and Management*, 47(15-16):2250–2259, 2006.

[57] M. Pérez-Fortes, A.D. Bojarski, E. Velo, J.M. Nougués, and L. Puigjaner. Conceptual model and evaluation of generated power and emissions in an IGCC plant. *Energy*, 34(10):1721–1732, 2009.

[58] B. Wayne Bequette. *Process Control – Modeling, Design and Simulation*. Prentice-Hall, Inc., Upper Saddle River, NJ, 2003.

[59] E.F. Camacho and C. Bordons. *Model Predictive Control*. Springer, London, 2004.

[60] J.A. Rossiter. *Model-based Predictive Control: A Practical Approach*. CRC Press, London, 2003.

[61] J.M. Maciejowski. *Predictive Control with Constraints*. Prentice-Hall, Inc., Upper Saddle River, NJ, 2003.

[62] C.R. Cutler and B.L. Ramaker. Dynamic matrix control a computer control algorithm. In *Proceeding of Joint Automatic Control Conference*, 1980. Paper WP5-B.

[63] Sigurd Skogestad. Control structure design for complete chemical plants. *Computers & Chemical Engineering*, 28(1-2):219–234, 2004.

[64] Sigurd Skogestad. Plantwide control: The search for the self-optimizing control structure. *Journal of Process Control*, 10:487–507, 2000.

[65] P.S. Buckley. *Techniques of process control*. John Wiley and Sons, NY, 1964.

[66] R.C. Hicks, G.R. Worrell, and R.J. Durney. Atlantic seeks Improved Control; Studies of Analog-Digital Models. *Oil and Gas Journal*, 24:97, 1966.

[67] W. Lee and V.W. Weekman. Advanced Control Practices in the Chemical Process Industry: A View from Industry. *AIChE Journal*, 22(1):27–38, 1976.

[68] Y. Arkun and G. Stephanopoulos. Studies in the Synthesis of Control Structures for Chemical Processes: Part IV. Design of Steady-State Optimizing Control Structures for Chemical Process Units. *AIChE Journal*, 26(6):975–991, 1980.

[69] R. Shinnar. Chemical Reactor Modeling for purposes of Controller Design. *Chemical Engineering Communications*, 9:73–99, 1981.

[70] M. Hovd and S. Skogestad. Procedure for Regulatory Control Structure selection with application to the FCC Process. *AIChE Journal*, 39(12):1938–1953, 1993.

[71] J.W. Ponton and D.M. Laing. A Hierarchical Approach to the Design of Process Control Systems. *Trans IChemE*, 71 (Part A):181–188, 1993.

[72] R.M. Price and C. Georgakis. Plantwide Regulatory Control Design procedure using a Tiered Framework. *Industrial & Engineering Chemistry Research*, 32:2693–2705, 1993.

[73] R.M. Price, P.R. Lyman, and C. Georgakis. Throughput Manipulation in Plantwide Control Structures. *Industrial & Engineering Chemistry Research*, 33:1197–1207, 1994.

[74] L.T. Narraway and J.D. Perkins. Selection of Process Control Structure based on Economics. *Computers & Chemical Engineering*, 18:S511–S517, 1994.

[75] W.L. Luyben, B.D. Tyréus, and M.L. Luyben. *Plantwide Process Control*. McGraw-Hill, USA, 1998.

[76] G. Stephanopoulos and C. Ng. Perspectives on the Synthesis of Plant-wide Control Structures. *Journal of Process Control*, 10:97–111, 2000.

[77] J.A. Heath, I.K. Kookos, and J.D. Perkins. Process control structure selection based on economics. *AIChE Journal*, 46:1998–2016, 2000.

[78] D. Wang. *Elimination Methods – Texts and Monographs in Symbolic Computation*. Springer, New York, 2001.

[79] S. Skogestad and I. Postlethwaite. *Multivariable Feedback Controller: Analysis and Design*. John Wiley & Sons, Chichester, UK, 2005.

[80] A. Koggersbøl, B.R. Andersen, J.S. Nielsen, and S. Bay Jørgensen. Control Configurations for an Energy Integration Distillation Column. *Computers & Chemical Engineering*, 20, Suppl.:S853–S858, 1996.

[81] W. F. Castle. Air separation and liquefaction: recent developments and prospects for the beginning of the new millennium. *International Journal of Refrigeration*, 25(1):158–172, 2002.

[82] Beate Seliger, Richard Hanke-Rauschenbach, Frank Hannemann, and Kai Sundmacher. Modelling and dynamics of an air separation rectification column as part of an IGCC power plant. *Separation and Purification Technology*, 49(2):136–148, 2006.

[83] Richard Hanke, Frank Hannemann, and Kai Sundmacher. Dynamic Simulation of a Low-Temperature Rectification Column as Part of an IGCC Power Plant. *Chemical Engineering & Technology*, 26(11):1126–1130, 2003.

[84] P. Mahapatra and B. Wayne Bequette. Modeling and Control of an Air Separations Unit for an IGCC Power Plant. In *2007 AIChE Annual Meeting, Salt Lake City, UT*, November, 2007.

[85] P. Mahapatra and B. Wayne Bequette. Effect of Gas–Turbine ASU Integration in Dynamics and Control of IGCC Power Plants. In *2008 Pittsburgh Coal Conference, Pittsburgh, PA*, September, 2008.

[86] P. Mahapatra and B. Wayne Bequette. Dynamics and Control of Air Separations Unit–Gas Turbine–Gasifier Integrated Power Cycle in IGCC Power Plants. In *2008 AIChE Annual Meeting, Philadelphia, PA*, November, 2008.

[87] P. Mahapatra and B. Wayne Bequette. Oxygen Purity Control in the Air Separation Unit of an IGCC Power Generation System during rapid production fluctuation. In *Annual International Pittsburgh Coal Conference 2009 CDROM Proceedings*, 20-23 Sept, 2009.

[88] P. Mahapatra and B. Wayne Bequette. Process design and control studies of Elevated-Pressure Air Separation Unit for IGCC power plants. In *2010 American Control Council Annual Meeting, Baltimore, DC*, June, 2010.

[89] K.B. Wilson, A.R. Smith, and A. Theobald. Air Purification for Cryogenic Air Separation Units. *IOMA Broadcaster*, Jan-Feb 1984.

[90] F.G. Kerry. Front-ends for air separation plants – The cold facts. *Chemical Engineering Progress*, pages 48–54, August 1991.

[91] B. Roffel, B. H. L. Betlem, and J. A. F. de Ruijter. First principles dynamic modeling and multivariable control of a cryogenic distillation process. *Computers & Chemical Engineering*, 24(1):111–123, 2000.

[92] Shoujun Bian, Michael A. Henson, Paul Belanger, and Lawrence Megan. Nonlinear State Estimation and Model Predictive Control of Nitrogen Purification Columns. *Industrial & Engineering Chemistry Research*, 44(1):153–167, 2005.

[93] R.H. Perry and D.W. Green. *Perry's Chemical Engineers' Handbook*. McGraw-Hill, seventh edition, 1997.

[94] N.P. Lieberman and E.T. Lieberman. *A Working Guide to Process Equipment*. McGraw-Hill, second edition, 2003.

[95] E.A. Avallone and T. Baumeister. *Marks' Standard Handbook for Mechanical Engineers*. McGraw-Hill, third edition, 1996.

[96] David R. Vinson. Air separation control technology. *Computers & Chemical Engineering*, 30(10-12):1436–1446, 2006.

[97] Yu Zhu and Carl D. Laird. Optimal Load Scheduling for Efficient Operation of Air Separation Systems Under Uncertain Costs and Demands. In *2009 AIChE Annual Meeting, Nashville, TN*, November 2009.

[98] Guang-Yan Zhu, Michel A. Henson, and Lawrence Megan. Low-order dynamic modeling of cryogenic distillation columns based on nonlinear wave phenomenon. *Separation and Purification Technology*, 24(3):467–487, 2001.

[99] W.L. Luyben. *Distillation Design and Control using Aspen Simulation*. John Wiley and Sons, NY, 2006.

[100] Charles E. Baukal. *Oxygen-Enhanced Combustion*. CRC Press LLC, 1998.

[101] Aspen Technology, Inc.: Cambridge, MA. *Aspen Plus 2004-1, Getting Started: Modeling Processes with Solids*, 2004.

[102] Patrick J. Robinson and William L. Luyben. Simple Dynamic Gasifier Model that runs in Aspen Dynamics. *Industrial & Engineering Chemistry Research*, 47(20):7784–7792, 2008.

[103] Debangsu Bhattacharyya, Richard Turton, and Steve E. Zitney. Plantwide dynamic simulation of an IGCC plant with CO_2 capture. In *Annual International Pittsburgh Coal Conference 2009 CDROM Proceedings*, 20-23 Sept, 2009.

[104] Yongtaek Choi and Harvey G. Stenger. Water gas shift reaction kinetics and reactor modeling for fuel cell grade hydrogen. *Journal of Power Sources*, 124(2):432–439, 2003.

[105] Earl Logan and Ramendra Roy. *Handbook of Turbomachinery*. Marcel Dekker, Inc., NY, 2003.

[106] Felipe R. Ponce Arrieta and Electo E. Silva Lora. Influence of ambient temperature on combined-cycle power-plant performance. *Applied Energy*, 80(3):261–272, 2005.

[107] Cheng Yang, Zeliang Yang, and Ruixian Cai. Analytical method for evaluation of gas turbine inlet air cooling in combined cycle power plant. *Applied Energy*, 86(6):848–856, 2009.

[108] P. Mahapatra and B. Wayne Bequette. Decentralized vs. centralized control of IGCC power cycles. In *Annual International Pittsburgh Coal Conference 2009 CDROM Proceedings*, 20-23 Sept, 2009.

[109] Hao Ling and William L. Luyben. New Control Structure for Divided-Wall Columns. *Industrial & Engineering Chemistry Research*, 48:6034–6049, 2009.

[110] Hao Ling and William L. Luyben. Temperature Control of the BTX Divided-Wall Column. *Industrial & Engineering Chemistry Research*, 49:189–203, 2010.

[111] Kejin Huang, San-Jang Wang, Koichi Iwakabe, Lan Shan, and Qunxiong Zhu. Temperature control of an ideal heat-integrated distillation column (HIDiC). *Chemical Engineering Science*, 62(22):6486–6491, 2007.

APPENDIX A
PRESSURE SWING STUDY

In full-blown plant structure, very less emphasis is given to pressure dynamics in open literature when a floating pressure arrangement is considered. In IGCC power plants (or in case any combined cycle plants), this arrangement is very common and implemented to minimize pressure losses encountered in constant pressure mode especially when plant is operating at low load (far from design value). In simplified terms, if we want to maintain a constant pressure at relevant pressure nodes in the plant during a lower flowrate, it would involve closing of a control valve which in turn increases resistance to the flow hence higher pressure losses. Alternatively, for decreasing flow rates we could decrease the power supplied to the drive units in the plant (compressor, pumps) which saves significant amount of energy not only by cutting down on the compression power but also by not increasing the flow resistances; at the cost of pressure fluctuations at node points. Hence effective control design is required for maintaining the flowrate and purity fluctuations which are inherent to floating pressure arrangement. Conventionally, a pressure-fluctuating operation is used in power cycle loops or in units where pressure differences across valves are not significant and easy saturation of control valves are observed. In process units such as distillation, reaction or absorption-desorption columns where the states are highly sensitive to operating pressure, a fixed operating pressure mode is preferred (at a certain cost to energy-loss).

In IGCC, certain portions of the plant like the gasification island including the Selexol units are operated at fixed controlled pressure irrespective of the power load demands. Gas turbine/compressor and ASU operate at floating pressure mode to minimize the energy losses across valves in the high pressure interconnecting streams which significantly affects the total power output. Due to this dual-mode operation, pressure dynamics are not intuitive and may lead to incorrect or infeasible controller design.

Figure A.1 shows the simplified process flowsheet with pressure values in ac-

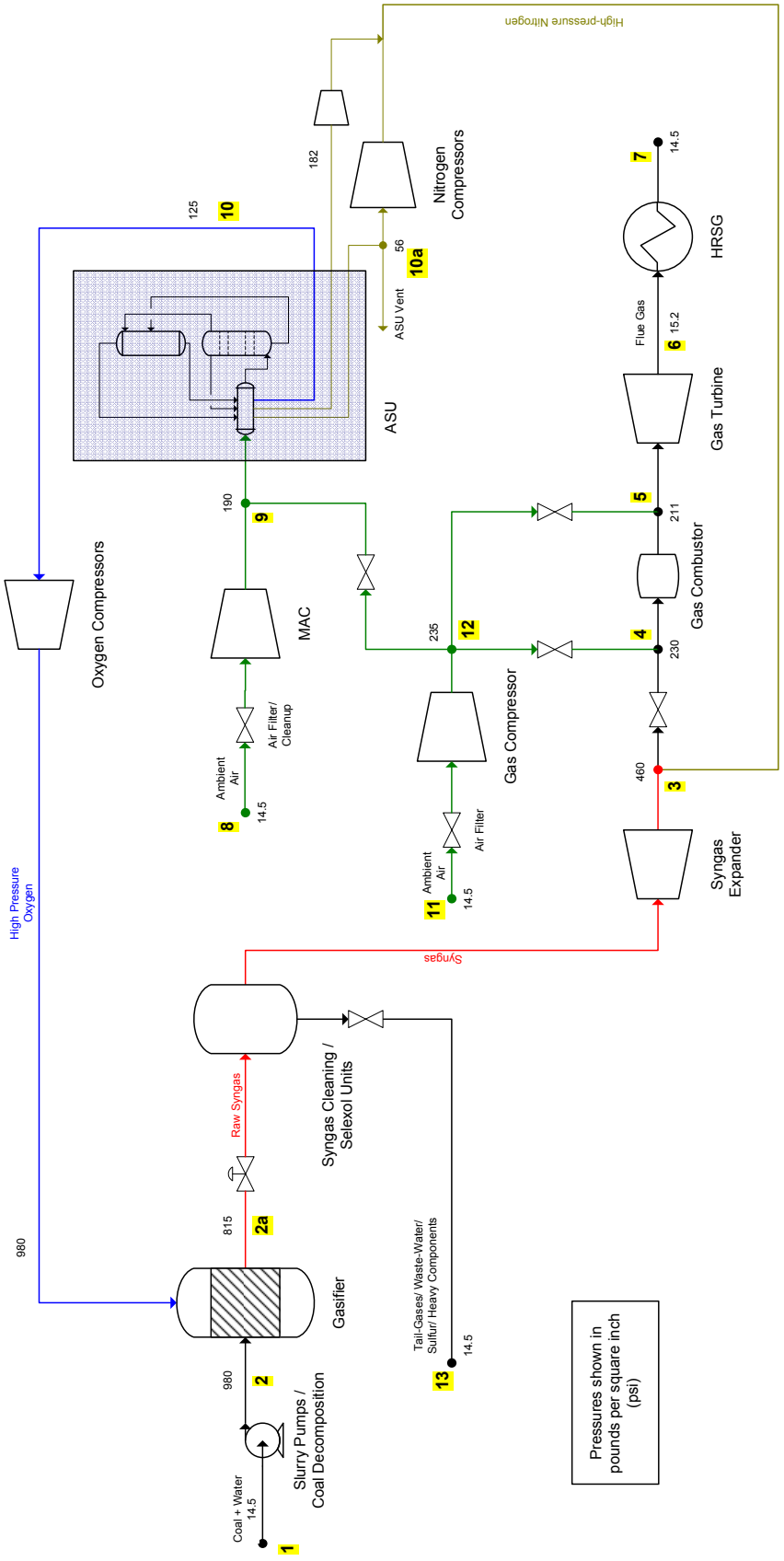

Figure A.1: IGCC flowsheet showing relevant pressure nodes (highlighted in yellow)

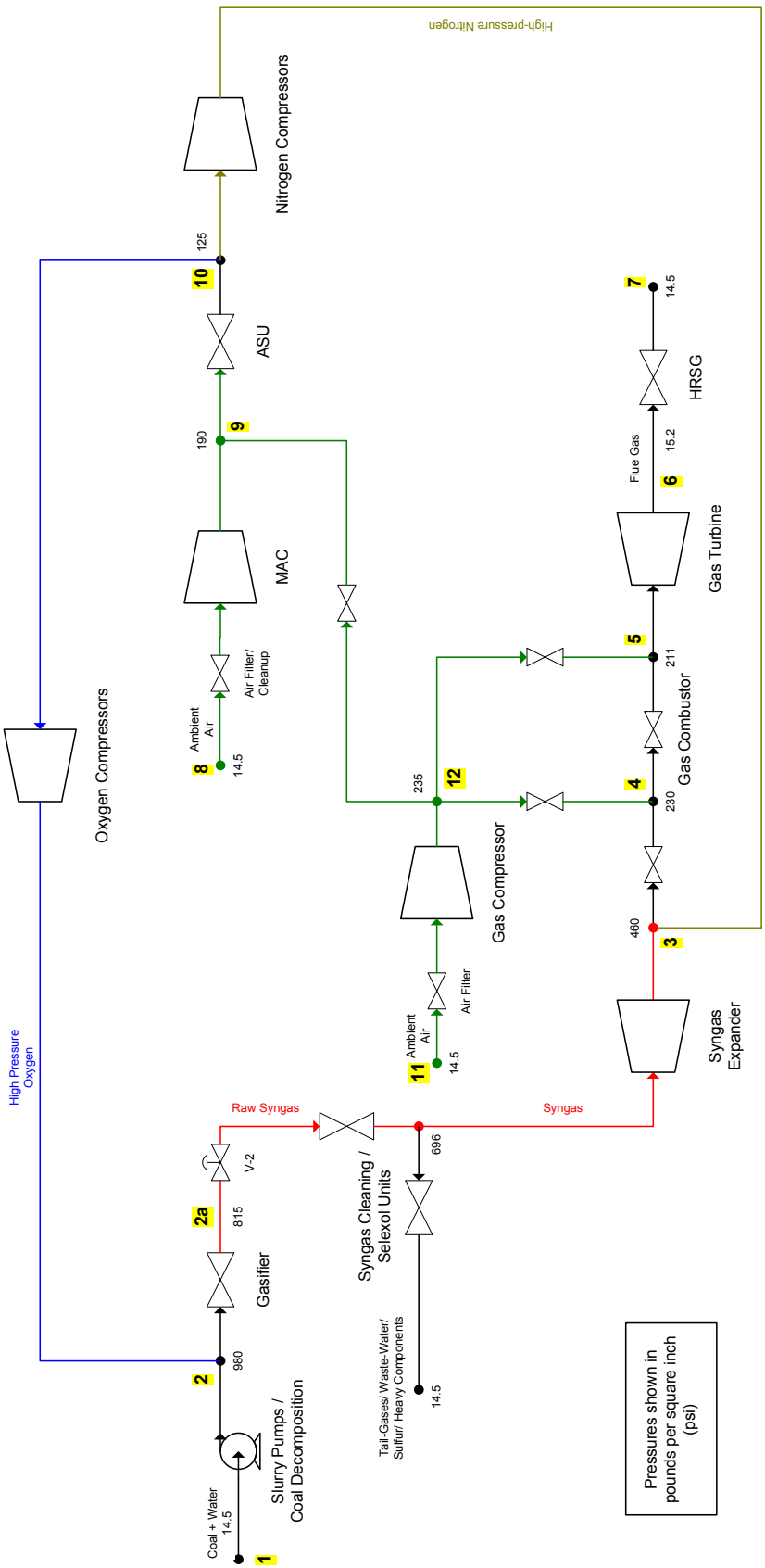

Figure A.2: Simplified IGCC flowsheet showing relevant pressure nodes (highlighted in yellow) for studying pressure dynamics

cordance to Parsons IGCC steady state Aspen flowsheet (IGCC003v2.apt). The relevant pressure nodes in the plant are focused in this figure shown as highlighted numbers. Many process units have been clubbed together into a single block, for example the unit block shown between the streams marked "raw-syngas" and "syngas" involves hundreds of process units in reality including syngas-quench, COS shift reactor, NH_3 condensor, flash drums and Selexol units.

As mentioned earlier, to closely understand the trend of pressure changes and more importantly to devise a control configuration, we assume that each unit or combination of units between relevant pressure nodes be separated by atleast one "pressure changer" block. These blocks may be valves, pumps, compressors or turbines. This transformed flowsheet is shown in Figure A.2.

Node 1, 8, 11, 7 are fixed pressure nodes at atmospheric conditions. The relevant power cycle (excluding the steam cycle which is not shown) takes material (coal, water, air) from these node points or throws off/ purges material (flue gases, nitrogen vent) to them. If the complete flow (analogous to currents in electrical circuits) is driven by compressors and pumps without closing/opening the valve (i.e. no change in any resistance), each individual node points excluding ones mentioned above will change their pressures. The unit operations which are pressure sensitive, an upstream or downstream pressure controller can be installed which will change the corresponding resistances (in direction opposite to the flowrate) such that the node or unit pressure remains the same. This is analogous to increasing/decreasing resistance when a decrease/increase of current is demanded such that the voltage across the circuit remains the same.

Most pertinent among the node points are mentioned as follows:

- Node 9 - feed pressure to the ASU
- Node 12 - which has a major role to play in ASU feed flow disturbances and also as an input to the turbine combustor
- Node 5 - the pressure of this node a play a direct role in GT power generation
- Node 2a - the gasifier pressure, which has a role to play on net power generated both from the amount of syngas transferred downstream and also as a exhaust

pressure for oxygen compressor

- Node 10 - suction side pressure for the oxygen compressor, playing direct role on net power usage
- Node 10a - suction side pressure for nitrogen compressor, again playing a major role on net power usage

A.1 AspenPlus^{TM} Specifications

For floating pressure nodes downstream to these units, the specification is given as follows:

- Valves – 'Rating' procedure is used where C_v is specified and outlet pressure is calculated. This value is generated by first running the simulation for desired pressure drop
- Compressors – Power required is specified. This value is generated by first running the simulation for desired pressure ratio/difference or outlet pressure.
- Pumps – Similar specifications as compressors
- Turbines – Power generated (as a 'negative' power required) is specified. Again this value is obtained by running the simulation for desired pressure ratio, pressure difference or outlet pressure specification

For fixed pressure nodes (which follow the below-mentioned units), the specifications are simple as given below:

- Valves – Either simple 'Adiabatic Flash' or a 'Design' procedure is adapted
- Compressors – The pressure difference, discharge pressure or pressure ratio
- Pumps – Similar specifications as compressors
- Turbines – Similar specifications as compressors

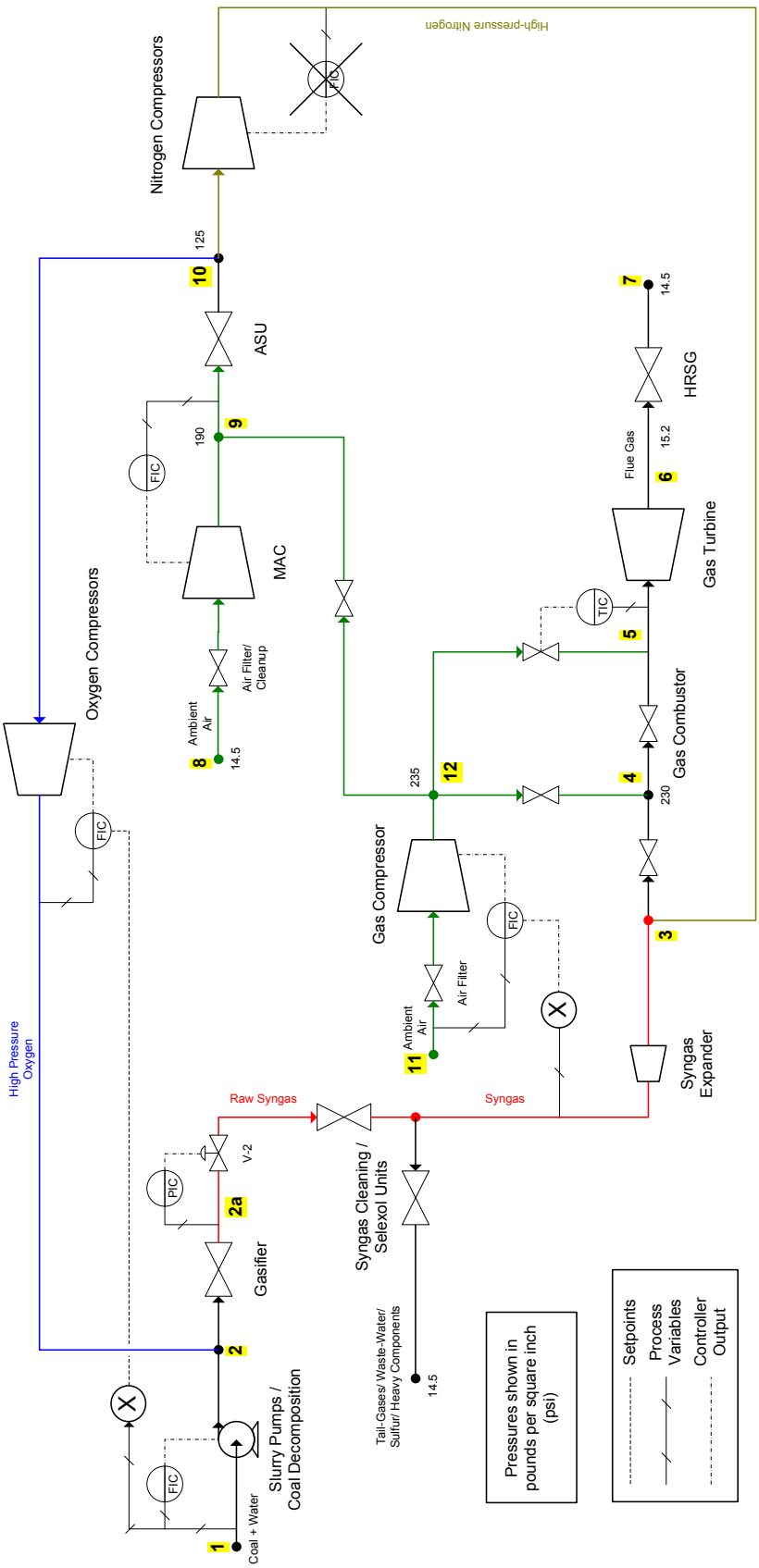

Figure A.3: Simplified IGCC flowsheet with controllers showing relevant pressure nodes (highlighted in yellow) for studying pressure dynamics

Since complex blocks which do involve pressure drops like reactors, distillation columns, heat exchangers, the floating pressure analysis cannot be done in steady state (Aspen Plus) because the blocks require either discharge pressure or pressure drop to be specified. Based on these during simulations, relevant unit design sizing parameters are automatically calculated by AspenPlus^{TM}. There are hardly any options to keep the pressure requirement open i.e. a truly dynamic model even when dynamic option is switched on and the flowsheet is configured to be completely pressure-driven. Analysis related to pressure behavior on important node points such as those shown in Figure A.1 or Figure A.3, involving process units more than simple valves, compressors, pumps and turbines have to be run in Aspen Dynamics even for SS analysis because Aspen internally passes all the relevant equipment parameters and coefficients it calculated after the SS run into AspenDynamics^{TM}.

A.2 AspenDynamics^{TM} Specifications

After export to Aspen Dynamics there are certain changes which have to be made to make it agree with what is needed. These are listen down as follows for both floating pressure mode and fixed pressure modes. Most of the units are inherently designed to operate at floating pressure arrangement.

For floating pressure nodes downstream to these units, the specification is given as follows:

- Valves, Compressors, Pumps, Turbines – No change is required
- Distillation Columns (RADFRAC) – No change is required (no pressure controller installed)
- Reactors – Outlet pressure is made free and pressure-drop is made fixed

For fixed pressure nodes (which follow the below-mentioned units), the specifications are simple as given below:

- Valves – Pressure-controller (PC) installed at the node to change valve-position
- Compressors – BP is made free and P is fixed; or PC is installed to change BP

- Pumps – Similar specifications as compressors
- Turbines – Similar specifications as compressors
- Reactors – No change required
- Distillation Columns – PC (which measures pressures at some stage and manipulates a relevant input variable, most commonly the condenser heat-duty) is installed
- Heat Exchangers – Here always pressure-drop is fixed, there is no option of fixing the discharge pressure. Generally this is not required because if we want to operate pressure mode the upstream and downstream units will be operating at fixed pressure and hence the node following the heat exchanger will be at fixed pressure.

Running the simulation in steady state mode with simplistic flowsheet, where every unit or network of units across relevant pressure nodes is approximated with a single pressure drop unit or valve, helps us determine whether our chosen part-fixed part-floating pressure mode is feasible or not. Additionally complex systems such as ASU which pose significant convergence problems during large pressure swings would not pose any hindrance in determining the pressure dynamics behavior during SS simulations.

A.3 Dynamic Perturbation Studies

As discussed in previous section, the simplified IGCC flowsheet is given in Figure A.2 and Figure A.3. Since we are concerned with only the pressure dynamics, the only component involved is air, even though different stream colors represent different components (fuel, oxygen, nitrogen, air) in the actual flowsheet. Here we wish to observe how a pressure control on valve V-2 (Figure A.2) immediately downstream of the gasifier block (variable being controlled is the pressure of gasifier) affects the net dynamic response, and what how the response of the important node points listed above looks like for simplified flowsheet in Figure A.2 and control structure shown in Figure A.3. The two X blocks represent multipliers used to supply

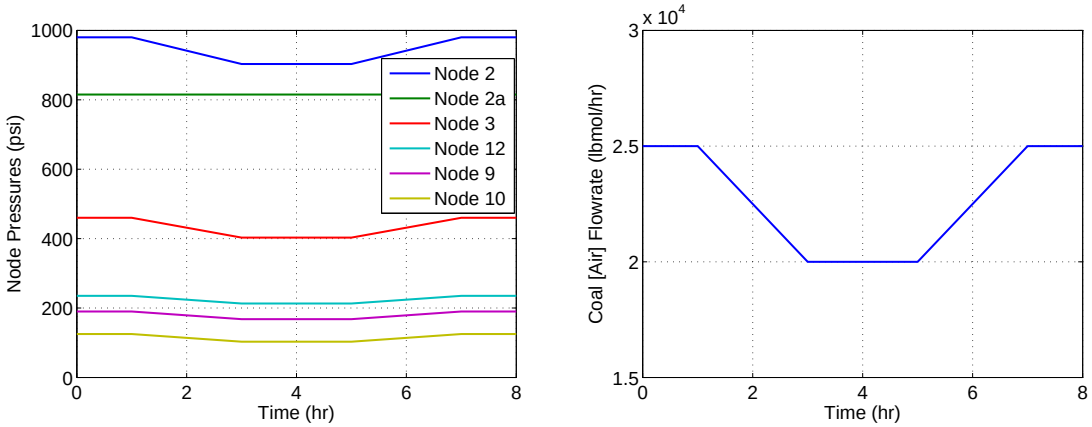

Figure A.4: Response of individual nodes pressures with ramp changes in coal input feed-line. Note: all the node pressures are floating in accordance with flowrates except the gasifier node where a pressure-controller is installed.

oxygen flowrate setpoint as a fixed ratio to the coal flowrate (0.84), and the air to syngas ratio (6.29). Note independent flow controller on nitrogen stream is infeasible as mass-balance around node 10 is violated. These are the kind of inconsistencies we are looking for in this analysis, and AspenDynamics^{TM} immediately reports integration errors upon encountering such problem, although the exact detection of the problem is a challenging task. Upon careful investigation of each stream, it can be observed that for the provided set of flow controller all flow-rates can be determined except the streams joining node 9 and 12 as well as those joining 8 and 9 (out of which finding one determines the other). This means that the flow of the air from Gas Compressor and ASU can be independently set and this flow actually determines the degree of integration between the GT-ASU in IGCC power plants. Now, once the gas-turbine and gas-compressor are mounted on common shaft, we loose this degree of freedom too. This is because the shaft speed of compressor becomes same as that of the turbine and brake power of the compressor becomes free. Figure A.4 shows this response for ramp input changes in coal feed line

APPENDIX B
'PSEUDO' HEAT-EXCHANGER IMPLEMENTATION IN ASPEN

In a full-blown IGCC power plant, we encounter numerous heat exchangers transferring energy within various sections, predominantly to/from the HRSG unit. Detailed equipment-level modeling for each of them not only enlarges the steady-state structural complexity but leads to manifold increase in computational time during dynamic simulations (due to significant increase in state variables). Here we highlight a method for modeling a heat-exchanger which is structurally simple yet detailed enough to capture thermal interactions and process dynamics.

B.1 Temperature control using HX bypass

In our attempt to model and control a single-pressure boiler operation, initially, a more realistic approach involving a heat exchanger (HeatX) blocks in Aspen, corresponding to superheater, evaporator and economizer processes was taken. The temperature of the hot-stream outlet was controlled using a HX bypass, as shown in Figure B.1, for an economizer HX example. The bypass is indirectly implemented by manipulating the flow through the exchanger (FCThruHX). The pressure controller on the bypass valve (BYPVAL) ensures that the pressure upstream is maintained. This setup behaves as a *split-range controller*, where, if the through-flow is decreased (by closing valve FCThruHX), creating a back-pressure upstream, the bypass-flow is increased simultaneously (by opening valve BYPVAL), to decrease this pressure, hence implementing a split of flows.

It can be seen from Figure B.2 that heat-exchange duty (and exhaust flue-gas temperature) is insensitive to the amount of bypass, till as large as 80% of the total flowrate; whereas a sudden decrease in heat-duty is observed at bypass values approaching ∼85%. This abrupt behavior, in the particular example, can be rationaled to a 2-phase system exiting the HX, which maintains near-constant LMTD (and hence heat-duty) even with varying flowrate. After the bypass flow exceeds a

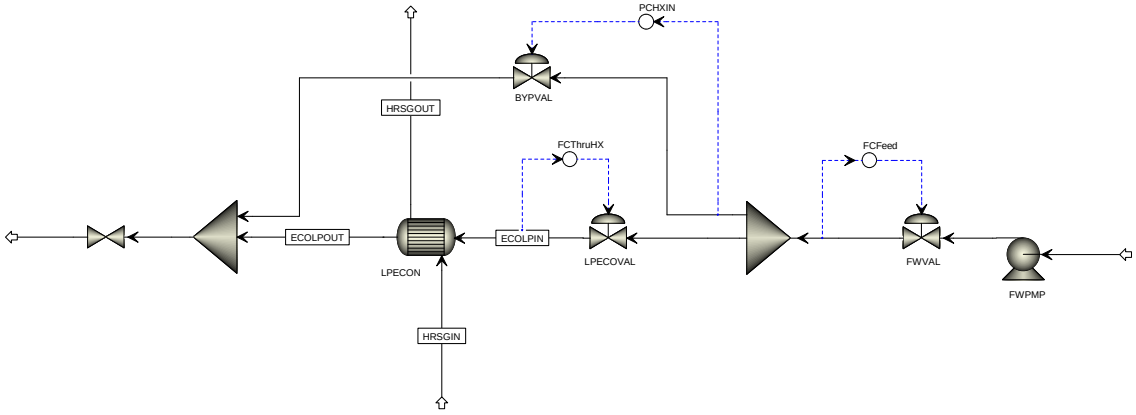

Figure B.1: AspenDynamics block diagram showing implementation of HX bypass for controlling the hot stream outlet

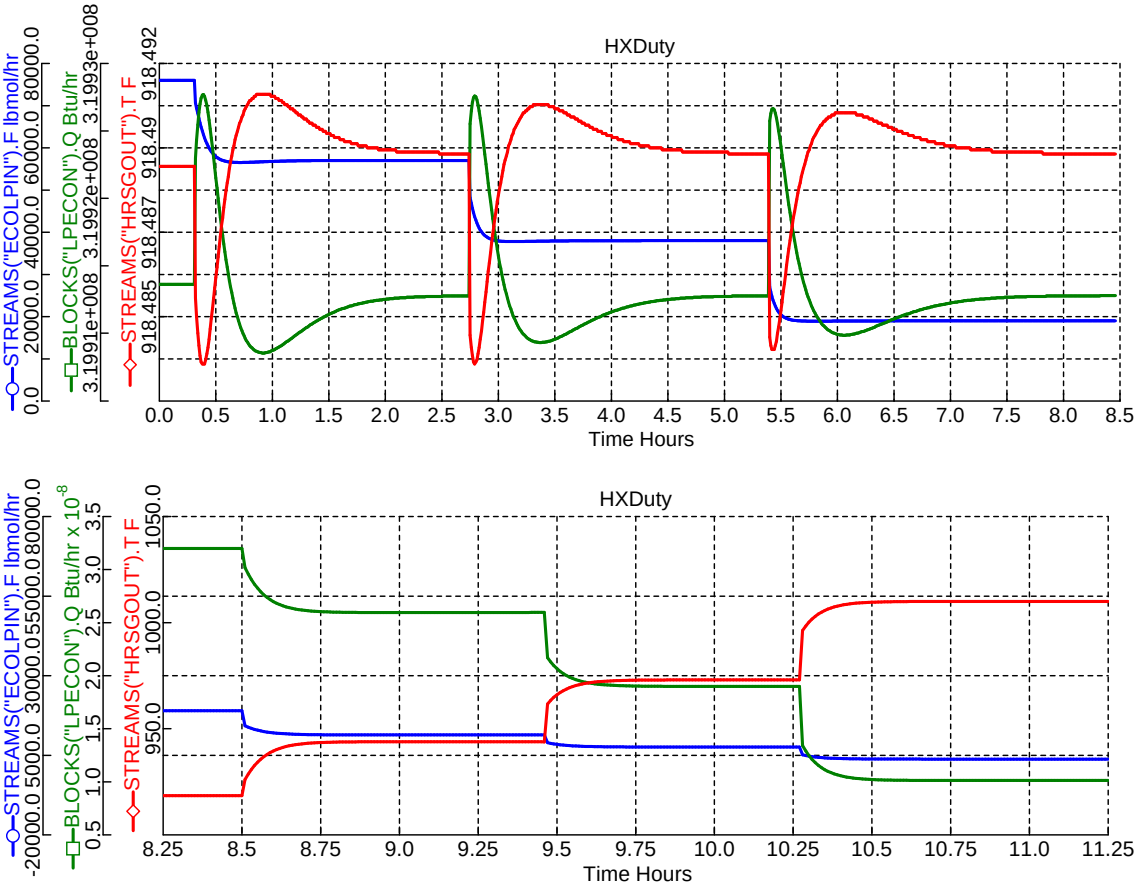

Figure B.2: Plots showing the response of HX-bypass flowrate, on the heat exchanger heat duty for 25%, 50% and 75% bypass (top); continued w/ 85%, 90% and 95% bypass (bottom)

certain value (or the thru-HX flow goes below a certain value), a superheated vapor phase exits the HX. This is when the LMTD and the heat-duty starts varying and responding to bypass valve. In terms of system controllability, this poses significant difficulty when a simple feedback temperature controller is used to control the hot-stream outlet temperature by "indirectly" varying this heat-duty, since input variable (bypass amount) has insignificant effect on output variable (hot outlet temperature). In most of the cases, the flow-through valve is almost fully closed for even slight increase in HX hot-stream outlet temperature setpoint. Alternate design is to use a hot stream bypass, where the possibility of the hot-stream "condensing" or entering a 2-phase regime, is absent.

Many complex control structure has been devised in the existing literature for temperature control of either hot or cold exit streams (and in some cases, both simultaneously). All these design carefully assay the possibility of any stream entering a multiphase region. A "perfect" controller design of a single HX is highly circumstantial and requires significant experience and multiple simulated runs. In a highly heat-integrated system, such as an IGCC plant, where number of heat-exchangers (both small and large sized) exceeds 50, we use an alternative simplified approach to dynamically model and control them.

B.2 Simplified HX design in Aspen

To proceed with controller design for a large scale boiler unit, a suitable approximation has been devised for implementation of these heat-exchangers in Aspen. A set of heater and cooler blocks connected via a virtual heat stream has been used to mimic a real two-stream HX. More importantly to counter the problem we faced earlier, we directly manipulate the heat-exchange coefficient (UA) to simulate a heat-exchanger bypass scenario. The slower bypass dynamics have been induced by using a large integral time constant in the corresponding temperature controller.

The following summarizes all the steps involved *when the hot-stream exit temperatures are known*:

1. The cooler-blocks are placed on the hot-streams, where the temperature and pressure specifications are provided.

2. These blocks are made dynamic, with inlet and outlet volume specified (this corresponds to the hot stream inlet/outlet volume specified in the HX block in earlier attempts)

3. The heater blocks, corresponding to economizer and superheater, are placed on cold streams.

4. Similar to the cooler blocks, the heater blocks are made dynamic and inlet/outlet volumes are specified.

5. A virtual heat stream is provided which connect from the cooler block to the heater block (and not vice-versa). The values of the virtual heat streams (or the cooler heat duties) are calculated based on the outlet temperature specification of the cooler blocks. Since the heater and cooler are connect via this heat stream, it automatically matches the corresponding heat duties.

6. Only the pressure (or pressure drop) specification is provided in the heater blocks.

7. For economizer and superheater cooler blocks, which exchange heat with a continuous stream of cold liquid/vapor, LMTD type of heat exchange is chosen and temperature of the medium is specified as the temperature of the inlet cold stream. For evaporator, which exchanges heat with a medium with constant temperature, a 'constant temperature' mode is chosen, and the medium temperature is specified as the temperature of the evaporator drum.

8. In the heat transfer option, a constant duty mode is chosen for both the heater blocks.

9. In AspenDynamics^{TM}, to mimic a real heat exchanger, the values of these virtual heat stream must depend on the temperature differential of the cold and hot streams and hence a Fortran Script is written in AspenDynamics flowsheet, which makes the medium temperature of the cooler blocks same as the temperature of the inlet cold streams (Note: the type of heat exchange,

constant T or LMTD had been specified earlier). An example of script for economizer, evaporator and superheater HX is given as follows:

```
Blocks("ECON-Cooler Name").T_med_in = Streams("ECON-Heater Inlet Name").T;
Blocks("SHTR-Cooler Name").T_med_in = Streams("SHTR-Heater Inlet Name").T;
Blocks("EVAP-Cooler Name").T_med = Blocks("EVAP-Drum Name").T;
```

In HX modeling where the temperature of cold-stream has to be specified, the methodology is very different. This is the case in boiler units where the heat inputs to the cold-stream are defined, for example, the economizer is designed such that exit cold-stream is exactly at saturated liquid (vapor fraction is zero) and the evaporator accepts the precise amount of heat which is required to boil the water to saturated vapor. We let the simulator calculate this heating value and extract this heat from the corresponding cooler blocks. Hence, direction of the virtual heat stream (from the heater unit to the cooler unit) is opposite to the previous case. This leaves only the pressure (or pressure drop) in the cooler blocks to be specified. The following summarizes the steps *when the cold-stream exit temperatures are known*. Steps 1 to 4 remain the same as earlier:

5. A virtual heat stream is provided which connect from the *heater block to the cooler block*.

6. Only the pressure (or pressure drop) specification is provided in the cooler blocks.

7. In the heat transfer option, a constant duty mode (default) is kept for all heater–cooler blocks.

8. Once exported to AspenDynamics^{TM}, we perform the following steps:

   (a) Remove the heat streams (one at a time for each heater–cooler pair to avoid encountering initialization problems).

   (b) In the cooler block, change constant duty to constant temperature (for evaporator) or LMTD (economizer/superheater) in the cooler `Configure` form. This gives the medium temperature a default value of 77°F.

(c) For the cooler, make Q 'fixed'[50] and UA 'free'. Make an initialization run.

(d) Change the medium temperature to the drum temperature (evaporator) or heater inlet-stream temperature (economizer/superheater) and make an initialization run again.

(e) Make the cooler UA 'fixed', T 'free' and Q 'free'. On the drum/heater side, make specified heat-duty, Qr 'free'. This leaves the simulation underspecified by two.

(f) We provide the following scripts (one at a time for each heater–cooler pair), and compile the flowsheet to make the system completely specified or 'square'. For the evaporator,

```
Blocks("Drum Name").Qr = -Blocks("Cooler Name").Q;
Blocks("Cooler Name").T_Med = Blocks("Drum Name").T;
```

For the economizer/superheater heater–cooler pair,

```
Blocks("Heater Name").Qr = -Blocks("Cooler Name").Q;
Blocks("Cooler Name").T_med_in = Streams("Heater Inlet Name").T;
```

In majority of the cases, which do not involve any phase changes within the exchanger, a temperature control across a heat-exchanger is not needed and a "we get what we get" approach is used (i.e., we do not have a variable 'UA' in principle or a HX-bypass in practice). In such cases, a simple Multistream HX block from Aspen model library is sufficient, as used throughout Chapter 6. This is uncontrolled HX is acceptable for the economizer[51] and superheater blocks, whereas an evaporator block involves heat-exchange with a 2-phase boiling liquid and hence, writing the above scripts is the only method to involve correct temperature dependent heat-exchange.

[50] This is not trivial. We first view the results by double-clicking the block and then choose to display 'Specs' in the view properties (by right clicking on the column name)

[51] An economizer, in comparison to the superheater, runs the risk of cold-stream reaching the saturation point within the HX, which may be catastrophic for the equipment. In such cases, the HX is either designed for exiting liquid to remain in subcooled region, or a HX-bypass on the hot-stream, to control the exiting cold-stream temperature, is installed

APPENDIX C
SYSTEM-IDENTIFICATION FROM ASPEN DYNAMICS DATA

C.1 MIMO step-response models

We estimate linear parametric state-space models from MIMO step-response data, imported directly from AspenDynamics^{TM}. We make extensive use of System Identification Toolbox (v7.3) in MATLAB for this process. As shown in Figure 3.12, different combination of simultaneous step-changes are provided (either in Aspen or Simulink), around the nominal operating point, to generate sequence of output responses[52]. These input-output data is then imported into the System Identification Toolbox as a Time-Domain Data. The time-domain data is imported into MATLAB workspace as the following variables:

- For single-input/single-output (SISO) data, the output must be a column vector.
- For a data set with N_y outputs and N_T samples (measurements), the output is an $N_T \times N_y$ matrix.

The state-space model with free parameterization is estimated in the System Identification Tool GUI by first selecting the model-order[53]. An estimation method is thereafter selected between two inbuilt algorithms – N4SID (subspace method) and PEM (iterative prediction-error method). In current work, both of these methods using different model-order are tried and the best-fit estimation is selected.

The disadvantage of state-space model based on step-responses (over the 'CDI-method' given next) is that the states do not carry any physical significance, and hence state estimation cannot be used for correcting/observing the "physical" states.

[52]The responses within AD are imported into MATLAB workspace via a textfile or a direct 'copy-paste' into a matrix

[53]This choice is on a trial-and-error basis. Matlab also provides a 'Order Selection' menu where singular values for different model-orders are compared and a default is suggested.

This limits our MPC studies to processes with open-loop stability[54] and to those which do not possess large non-linearities.

Another approach is the use of SISO step-response models using a two-step process. In the first-step, for each input-output pair, step responses are obtained corresponding to many step changes in the input variable (usually within the range of ±20% nominal value). In general, sets of +5% and -5% are used for model-estimation and +10% and -10% sets are used for model-validation. Model estimation uses MATLAB's System Identification Toolbox to generate SISO transfer function (process model); the choice of model-order is provided therein. In the second step, after transfer functions are obtained for all input-output pair (n×m transfer functions for m-inputs and n-outputs), they are converted to state-space form using LTI-model conversion functions/tools in MATLAB (for e.g. `tf2ss`). In this approach, the number of states obtained are moderately high, although the matrices obtained are sparse.

C.2 State space models from differential equations using CDI

The AspenDynamics™ flowsheet simulator offers an option, the so-called Control Design Interface (CDI) to get the dynamic model of the process. The CDI determines the differential equation system in the form of state space representation around the operating point of the system to be investigated. Moreover, the results obtained with CDI can be directly processed and evaluated with the help of the Matlab software package.

Determination of the state space representation is made with the help of the Control Design Interface module of Aspen Dynamics. To do this, a short VisualBasic™ script is needed to be written in Aspen Custom Modeler™ in which we give the input variables and output variables, and call the appropriate functions to calculate the matrices A, B, C, D of the state space model. An example of this

[54] If an open-loop instability exists, in most cases steps may be taken at a lower-level controller hierarchy to counter it, either by adding an additional regulatory controller or by restructuring the existing design. An instance of this was shown while discussing the regulatory control of LP-column drum.

script for the LP-ASU supervisory inputs/outputs is given below. It is important that the specifications of the input variables always have to be "fixed" and the output variables have to be "free".

```
Set Doc = ActiveDocument
Set LINEARISE = Doc.CDI
LINEARISE.Reset
LINEARISE.AddInputVariable "Streams(""FEED"").F"
LINEARISE.AddInputVariable "Blocks(""FCLN2"").SPRemote"
LINEARISE.AddInputVariable "Blocks(""FCGOX"").SPRemote"
LINEARISE.AddInputVariable "Blocks(""FCHPN2"").SPRemote"
LINEARISE.AddOutputVariable "Streams(""O2"").Zn(""O2"")"
LINEARISE.AddOutputVariable "Streams(""HP-N2"").Zn(""N2"")"
' Set tags for CDI variables. These will be used in
' generating the step response DMCPlus (mdl) file
Streams(""FEED"").F.Tag="F_airASU"
Blocks(""FCLN2"").SPRemote.Tag="F_LN2"
Blocks(""FCGOX"").SPRemote.Tag="F_O2"
Blocks(""FCHPN2"").SPRemote.Tag="F_HPN2"
Streams(""O2"").Zn(""O2"").Tag="Z_O2"
Streams(""HP-N2"").Zn(""N2"").Tag="Z_HPN2"
LINEARISE.StepResponseTimeInterval=0.1
LINEARISE.GenerateStepResponse
LINEARISE.Calculate "CDI_LINEARISE"
```

In order to use the script, the simulation has to be started and then stopped when steady state is reached. The system will be linearized around this point. If a system is considered with a set point change in a given range, then this study should be repeated at several possible set points. From this investigation, we can conclude how linear the system is and how much the results can be generalized. When the simulation is stopped, the script can be run. There are many output files of the script. One contains basic summarizing information about the results: name, number, and steady state value of the input, output and state variables as well as the time of linearization and the number of nonzero elements of the A, B,

C, D matrices. The other files contain the A, B, C, D matrices (in a sparse matrix representation), gain and RGA matrices.

APPENDIX D
NOTES ON INTERFACING ASPEN DYNAMICS WITH SIMULINK

D.1 Methodology

Instructions for associating the AspenDynamics^{TM} (`.dynf`) file with MATLAB/Simulink (`.mdl`)

1. Open the `.mdl` file in Matlab.
2. Double click on the "`AMSimulation`" block(s). Browse to the respective `.dynf` file(s) provided.
3. Wait till the model(s) opens up in Aspen Dynamics. Make sure "Dynamic" type simulation is selected inside AD.
4. Save the Simulink (`.mdl`) file.
5. When closing the Simulink model file, NEVER close the AD model which Simulink opened. This might lead to data corruption. Instead just close the Simulink model and the (linked) AD model should close automatically.

The re-association of `.dynf` and `.mdl` has to be done by double-clicking the `AMSimulation` block inside Simulink everytime the following event occurs:

- The `.dynf` file corresponding to the "plant" changes its name.
- The `.dynf` file's absolute location is changed. For example, if the folder containing the `.mdl`, `.dynf`, `.appdf`, `AMSimulation.m` and other `.m` files, '`D:\Documents\PM_Gasifier`' is moved to another folder, '`D:\PM_Gasifier`'. This shows that the reference to the `.dynf` in the `mdl` file is not relative.

D.2 Solver options

For fast simulation, the solver should be chosen as type 'Fixed Step Discrete' (`Simulation/Configuration Parameters...`) inside Simulink. The fundamental sample time determines the resolution of the "plant", i.e. how smooth the plant plot should be. Increasing this number does not mean the results will be inaccurate, since within Aspen a variable step-size method is implemented. This definitely speeds up the net simulation time (since the data transfer b/w Simulink and AD is reduced) at the cost of lower plot-resolution. NEVER select 'Variable Step', as it is extremely slow (and sometimes inaccurate).

D.3 File Distribution

When distributing these files, the following should be considered:

1. When last saving the `.dynf`, make sure "Dynamics" is selected and NOT "Initialization" or "Steady State".

2. There is no need to provide the `AMSimulation.m` and `AM_*` 'history' folder(s). These will be created automatically. The essential files are `.dynf`, `.appdf` and `.mdl`. Which `.appdf` file is being used by the `.dynf` can be found by opening the `.dynf` in any text-editor and search for "Properties".

3. Specific instructions on how to link the `.dynf` to the `mdl` must be given. These are discussed next

Instructions for associating the Aspen Dynamics (.dynf) file with Matlab/Simulink (.mdl)

- Open the `.mdl` file in Matlab.

- Double click on the "`AMSimulation`" block(s). Browse to the respective `.dynf` file(s) provided.

- Wait till the model(s) opens up in Aspen Dynamics. Make sure "Dynamic" type simulation is selected inside AD.

- Save the Simulink (`.mdl`) file.
- When closing the Simulink model file, NEVER close the AD model which Simulink opened. This might lead to data corruption. Instead just close the Simulink model and the (linked) AD model should close automatically.